UNIVERSITY *of the* WESTERN CAPE

FUNCTIONALISATION OF POLYMER NANOFIBRES AND TRACK-ETCHED MEMBRANE FOR REMOVAL OF ORGANIC AND INORGANIC POLLUTANTS FROM WATER

By

Chris Ademola Bode-Aluko

MSc Inorganic Chemistry (Ibadan)
BSc (Hons) Industrial Chemistry (Ado-Ekiti)

A thesis submitted in fulfilment of the requirements for the degree of
Doctor of Philosophy in Chemistry
in the

Department of Chemistry
Faculty of Natural Sciences
University of the Western Cape

Supervisor: Prof. Leslie Petrik

Co-supervisor: Prof. Catherine Branger

December, 2017

Declaration of Authorship

I declare that "***Functionalisation of Polymer Nanofibres and Track-etched Membrane for Removal of Organic and Inorganic Pollutants from Water***" is my own work, and that it has not been submitted for any degree or examination in any other university. All the resources I used or quoted have been indicated and acknowledged by in-text citations and complete reference list.

Chris Ademola Bode-Aluko

December, 2017

Signature…………………....

UNIVERSITY *of the*
WESTERN CAPE

Keywords

Electrospinning

Nanofibres

Polyacrylonitrile

Polyamide 6

Track-etched membrane

Polyethylene terephthalate

Surface modification

Immobilisation

2-pyridine amidoxime

Adsorption

Rhodamine 6G

Lead

Abstract

Abstract

Organic and inorganic pollutants are two broad classes of pollutants in the environment with their main sources from waste waters that are indiscriminately dumped from chemical related industries. Among the organic pollutants are dyes that come as effluents from the textile industries. Toxic metals are the main inorganic pollutants with their sources from industries such as mining, electroplating, batteries etc. The presence of both classes of pollutants in the aquatic environment poses a serious threat to aquatic organisms and humans who depend on these waters for domestic purpose. Therefore, this research focused on the fabrication of materials and designing of methods for removal of both classes of pollutants from their aqueous solutions.

For organic pollutants, the research focused on the use of improved nano-filtration methods for the removal of dye rhodamine 6G (RD) from water. Five membranes were fabricated and were studied for the adsorption-filtration of RD in a continuous flow process. Polyacrylonitrile (PAN) and polyamide 6 (PA6) were electrospun into nanofibres in dimethyl formamide (DMF) and formic acid respectively, via electrospinning process. The average fibre diameters (AFD) for polyamide 6 nanofibres (PA6-nfs) and polyacrylonitrile nanofibres (PAN-nfs) at optimum concentrations of 14 wt% (PA6) and 8 wt% (PAN) as measured from the HRSEM images were 52 ± 9.8 nm and 354 ± 40 nm, respectively. Further characterisations such as TEM, ATR-FTIR, TGA and BET analyses were also performed on PA6-nfs and PAN-nfs. Their TEM results showed that the internal images of both nanofibres were clear with no dark areas. Their ATR-FTIR spectra confirmed that the nanofibres were not chemically affected during electrospinning process. TGA analysis of the nanofibres followed similar profiles reported in the literature. The BET surface area of PA6-nfs and PAN-nfs were 25.57 m^2/g and 10.93 m^2/g, respectively.

Polyethylene terephthalate track-etched membrane (PET-TM) was fabricated via ion-irradiation method followed by chemical etching and subsequently coated with TiO_2 via magnetron sputtering method. PET-TM was coated with TiO_2 in order to make the membrane conductive and subsequently be used as collector in the

Abstract

electrospinning process. The pore size and pore length of PET-TM were 3.5 ± 0.36 μm and 17 μm, respectively. PA6-nfs or PAN-nfs was combined with PET-TM through electrospinning process to produce composite membranes of PET-TMPA6 or PET-TMPAN, with respective nanofibres thickness of ≈0.5 mm. The composite membranes were confirmed with HRSEM analysis.

PAN-nfs, PA6-nfs, PET-TM and their composites membranes, PET-TMPAN and PET-TMPA6, were used to adsorb RD from aqueous solution. The highlight of the results was that the composite membranes, PET-TMPAN and PET-TMPA6, gave better results when compared with the initial membranes, PAN-nfs, PA6-nfs or PET-TM. The adsorption of RD by these membranes could be best achieved for 2 mL of 10 mg/L of RD when the initial pH was 10 and at a flow rate of 1 mL/min using 0.0026 g of each membrane with 12 mm diameter, and the adsorption capacity of each membrane at these conditions were; PET-TMPAN, 6.32 mg/g (91.27%), PET-TMPA6, 4.89 mg/g (70.66%), PAN-nfs, 4.56 mg/g (65.97%), PA6-nfs 2.55 mg/g (36.80%) and PET-TM 1.70 mg/g (24.53%). From the adsorption results, PET-TMPAN gave the best result. The adsorption patterns of RD onto PET-TMPA6 and PET-TMPAN were well fitted to the Langmuir isotherm. Furthermore, all the membranes were regenerated by flowing through the membranes 2 mL deionised water of pH 1.85, adjusted with 1 M H_2SO_4, to overcome the fouling effect. The regenerated membranes were reused again and the results showed the following reduction in the adsorption capacities of each membrane; PET-TMPAN 17.26%, PET-TMPA6 12.29%, PAN-nfs 14.62%, PA6-nfs 28.17% and PET-TM 8.042%.

For inorganic pollutants, the study focused on the use of polymer nanofibres for adsorption of Pb^{2+} from aqueous solution. 8 wt% polyacrylonitrile nanofibres of AFD 354 ± 40 nm was fabricated via electrospinning. 2-pyridine amidoxime (PyAMI) was synthesised through the reaction between 2-pyridine carbonitrile and hydroxylamine hydrochloride and was subsequently characterised using NMR, FTIR and TGA techniques. Subsequently, PyAMI was immobilised on PAN-nfs surfaces via two reaction pathways; the base-catalysed immobilisation reaction using NaOH and the acid-catalysed immobilisation reaction using $AlCl_3.6H_2O$. A preliminary

Abstract

characterisation on the products from the two reaction pathways using HRSEM showed that the nanofibres surfaces were smooth for the acid-catalysed pathway but disintegrated in the base-catalysed reaction pathway. Therefore the base-catalysed immobilisation reaction pathway was discontinued. The acid-catalysed immobilisation reaction pathway was used to fabricate PAN-PyAMI (PyAMI immobilised on PAN-nfs). The resultant PAN-PyAMI was further characterised using TEM, ATR-FTIR, XRD, BET and TGA analyses. The ATR-FITR spectrum of PAN-PyAMI showed that PyAMI was immobilised on PAN-nfs at optimum reaction time of 60 minutes at 60°C with the presence of peaks such as 1654 cm^{-1} (C=N), 1605 cm^{-1} (N-H bending vibration) and 968 cm^{-1} (N-O) which are attributed to the peaks of PyAMI. The peak at the range of 3181 cm^{-1}—3030 cm^{-1} was also assigned to CH stretching of pyridine ring. Also a peak at 1145 cm^{-1} (C-N) was assigned to be the new bond formed. The TEM result showed that the internal image of PAN-PyAMI became dark. The XRD result of PAN-PyAMI showed decrease in intensity of diffraction peaks of pristine PAN-nfs. The TGA results showed that PAN-PyAMI started losing stability at temperature of about 200°C due to the loss of organic ligands on the nanofibres. From the TGA results, it was estimated that for 1 g of PAN-nfs, 0.111 g of PyAMI was immobilised. The BET surface area gave 2.44 m^2/g which was a drastic reduction compared to the pristine PAN-nfs. The stability of PAN-PyAMI was tested in different pH solutions and it was found according to ATR-FTIR spectra that the material was only stable at pH higher than 4.5 and less stable at pH lower than 4.5. 0.1 M HNO$_3$ and 0.1 M EDTA were used to test for the regeneration of PAN-PyAMI. The ATR-FTIR results after the test showed that PAN-PyAMI could only be regenerated using 0.1 M ETDA, as all the peaks attributed to PyAMI was retained but disappeared with 0.1 M HNO$_3$.

PAN-nfs and PAN-PyAMI were used to adsorb Pb^{2+} in aqueous solution as batch experiment. The results showed that PAN-PyAMI could adsorb Pb^{2+} far better than the PAN-nfs at the same conditions, 0.1 g weight of adsorbent, pH 4.9, concentration 200 mg/L and contact time 60 minutes, at 25°C with maximum adsorption capacity of 4.70 mg/g (22.5%) for PAN-PyAMI and 1.54 mg/g (8%) for PAN-nfs. The experimental data were fitted with the Langmuir isotherm and the kinetic rate was best described as pseudo second-order. PAN-PyAMI was

Abstract

regenerated using 0.1 M EDTA after each adsorption experiment and was subsequently reused for 4 times. The adsorption capacities of PAN-PyAMI decreased from 5.65 mg/g to 1.45 mg/g as the number of regeneration increased from 1 to 4. The ATR-FTIR analysis after every regeneration showed that the ligand peaks on PAN-PyAMI were gradually disappearing and that only 3 regeneration cycles could be done on PAN-PyAMI.

Overall, this research is reporting for the first time the fabrication of ultrafast nano-filtration membrane from the combination of nanofibres and track-etched membrane via electrospinning process. Likewise a new metal nanofibres adsorptive membrane was also synthesised from the immobilisation of ligands on nanofibres. The ultrafast nano-filtration membrane and the metal nanofibres adsorptive membrane have shown great potential in adsorption-filtration of contaminants from water.

UNIVERSITY *of the*
WESTERN CAPE

Publications from the thesis

Bode-Aluko, C.A., Pereao, O., Ndayambaje, G. and Petrik, L. (2017). Adsorption of toxic metals on modified polyacrylonitrile nanofibres: A Review, *Water, Air, & Soil Pollution,* 228: 35, DOI: 10.1007/s11270-016-3222-3 (Published).

Bode-Aluko, C.A., Pereao, O., Fatoba, O. and Petrik, L. (2017). Surface-modified polyacrylonitrile nanofibres as supports, *Polymer Bulletin*, Vol. 74, pp. 2431-2442, DOI: 10.1007/s00289-016-1830-0 (Published).

Pereao, O. K., **Bode-Aluko, C.**, Ndayambaje, G., Fatoba, O. and Petrik, L.F. (2016). Electrospinning: Polymer nanofibres adsorbent applications for metal ion removal, *Journal of Polymers and the Environment*, DOI: 10.1007/s10924-016-0896-y (Published).

Bode-Aluko, C.A., Pereao, O., Petrik, L. and Branger, C. (2017). Electrospinning and chemical surface modification of polyacrylonitrile nanofibres, *Polymer Bulletin* (manuscript).

Bode-Aluko, C.A., Pereao, O., Petrik, L., Kochnev, Y., Nechaev, A.N. and Apel, P.Y. (2017). Removal of rhodamine 6G from water using ultrafast nano-filtration membranes, *Desalination* (manuscript).

Bode-Aluko, C.A., Pereao, O., Petrik, L.F., Musyoka, S. and Sone, B.T. (2017). Key points on electrospinning process, *Polymer Bulletin* (manuscript).

Bode-Aluko, C.A., Pereao, O., Petrik, L.F. and Branger, C. (2017). Adsorption and separation of toxic metals using functionalised polymer nanofibres, *Journal of Hazardous Materials* (manuscript).

Bode-Aluko, C.A., Pereao, O., Petrik, L.F. and Branger, C. (2017). Removal of toxic metals using amidoxime chelating adsorbents, *Colloid and Interface Science Communications* (manuscript).

Dedication

This thesis is dedicated to the memory of my late mother, Esther Moyoade Aluko (Nee Okedele). Continue to rest in the bosom of the Almighty God till we meet to part no more.

Acknowledgements

Firstly, my deepest gratitude goes to my supervisor; Prof. Leslie Felicia Petrik, the group leader, Environmental and Nano Sciences group, whom without prior knowledge of me consent to supervise my PhD study. Thank you for this life time opportunity. On behalf of the entire family of Bode-Aluko, we say thank you so much, *ese adupe pupo*. I would like to appreciate my co-supervisor, Prof. Catherine Branger for her contribution to my research from her wealth of experience. So also, I am grateful to the staffers of Environmental and Nano Sciences group; Averil Abbott (administration), ILse Wells (ICP-OES, administration), Rallston Richards (instrumentations) and Mama Vanessa Kellerman (administration), thank you all.

I would like to appreciate the immediate past and the present H.O.D of the department of Chemistry, Prof. Ameer and Prof. Baker, respectively, for the admission to this prestigious department. I am also grateful to other staffs of the university and the research institutes who helped me with analysis; Mr. Josephs Adrian (HRSEM), Dr. Edith Beukes (NMR), Mr. Yunus Kippie (TGA and ATR-FTIR), Ms. Natasha Peterson (TEM), Ms. Winnie Monama (BET, PhD student, PetroSA), Sensor Lab. Staffs (UV-vis), Mr. Martin Makombe (ICP-OES, Scientific services), Dr. Sone B.T (electrospinning set-up, iThemba Labs) and Mrs. Miranda Waldron (HRSEM, University of Cape Town). My appreciation also goes to the funder of my research, Water Research Commission, South Africa.

To my friends and colleagues at ENS; Omoniyi Pereao, Emmanuel Ameh, Cosmas Uche, Kassim Badmus, Bulelani Sidawu, Emile Massima, Mero-Lee Cornelius, Jean-Luc Mukaba, Emmanuel Omoniyi, Anthony Okotie, George Ndilowe, Mr. and Mrs. Abegunde, Miyelani Maluleke, Deborah Kalume, Cecilia Sanusi, Dr. Jimoh Tijani, Dr. Guillaume Ndayambaje, Dr. Roland Missengue (Postdoctoral), Dr. Bernardus Barnard (Postdoctoral), Dr. Olanrewaju Fatoba (Postdoctoral), Dr. Olushola Adeniyi (Postdoctoral) and Dr. Stephen Musyoka (Postdoctoral), I say thank you all.

Special thanks go to Prof. Pavel Apel, Prof. Alexander Nechaev and Dr. Yuri Kochnev, all of the Joint Institute for Nuclear Research (JINR) Dubna, Russia, for

Acknowledgements

their contributions to my research. Thanks for the opportunity to visit your laboratory and for the provision of TiO_2 coated PET track-etched membrane.

I also appreciate all my past employers; De-shalom pharmaceuticals, Ilesa; St. Johns Comprehensive Academy, Ilesa; Atani Community Secondary School, Atani, Anambra State, and the department of Science Laboratory Technology, Osun State College of Technology, Esa-Oke, Osun State, Nigeria.

I will also like to thank my past academic supervisors; Bsc (Hons): Dr. A.A Azeez (University of Ado-Ekiti) and Dr. Afolabi (University of Agriculture, Abeokuta); Msc: Dr A.J Odola (University of Ibadan) and Prof. J.A Obaleye (University of Ilorin) and my secondary school chemistry teacher, Mr. I. Makanjuola.

I am grateful to Dr. Damian Onwudiwe (Department of Chemistry, North-West University, Mafikeng Campus) and Mr. Adegboyega Daramola for their help while searching for PhD supervisor and admission.

I would like to thank my Dad and my late Mum for given me the best support parents could give a child, I love you so much. To my siblings, Tolu and Toyosi, thank you. I will not forget those you became part of the big family; Mr. Jacobs Ajayi, Engr. Femi Asaolu, Akin Asaolu, Funmbi Ogbara, Timileyin Fawale and Aderonke Adebanjo. Thank you so much for all your supports.

Special thanks go to the pastorate and the members of The Redeemed Christian Church of God (RCCG), Household of God Parish, Belhar, Western Cape, South Africa.

Finally, my utmost gratitude goes to the Almighty God, the giver of life and knowledge.

Table of Contents

Table of Contents

http://etd.uwc.ac.za/

Table of Contents

Table of Contents

http://etd.uwc.ac.za/

Table of Contents

Table of Contents

Table of Contents

http://etd.uwc.ac.za/

Table of Contents

Table of Contents

UNIVERSITY *of the*
WESTERN CAPE

http://etd.uwc.ac.za/

List of Figures

List of Figures

List of Figures

List of Figures

List of Figures

http://etd.uwc.ac.za/

List of Figures

http://etd.uwc.ac.za/

List of Tables

List of Schemes

http://etd.uwc.ac.za/

List of Equations

List of Equations

http://etd.uwc.ac.za/

Abbreviations

Abbreviations

AFD	Average fibres diameter
APD	Average pore diameter
ATR-FTIR	Attenuated total reflectance Fourier transform infrared spectroscopy
BET	*Brunauer, Emmett and Teller* analysis
DEPT	Distortion enhancement by polarisation transfer
DMF	Dimethyl formamide
DMSO-d_6	Deuterated dimethyl sulfoxide
D_2O-d_6	Deuterium oxide (Deuterated water)
DTG	Derivative of thermal gravimetry profile
EDTA	Ethylenediaminetetraacetic acid
EDS	Energy disperse X-ray spectroscopy
HRSEM	High resolution scanning electron microscopy
ICP-OES	Inductively coupled plasma-optical emission spectroscopy
JINR	Joint institute for nuclear research
MSDS	Materials safety and data sheet
^{13}C NMR	Carbon 13 nuclear magnetic resonance
^1H NMR	Proton nuclear magnetic resonance
PA6	Polyamide 6
PA6-nfs	Polyamide 6 nanofibres
PAN	Polyacrylonitrile
PAN-nfs	Polyacrylonitrile nanofibres
PAN-PyAMI	2-pyridine amidoxime immobilised on polyacrylonitrile nanofibres
PET	Polyethylene terephthalate
PET-TM	TiO_2 coated polyethylene terephthalate track-etched membrane
PET-TMPA6	Polyamide 6 nanofibres polyethylene terephthalate track-etched composite membrane
PET-TMPAN	Polyacrylonitrile nanofibres polyethylene terephthalate track-etched composite membrane
PyAMI	2-pyridine amidoxime

Abbreviations

RBF	Round bottom flask
RD	Rhodamine 6G
rpm	Revolution per minute
TEM	Transmission electron microscopy
TGA	Thermal gravimetry analysis
TM	Track-etched membranes
UV-vis	Ultraviolet-visible spectrometry
XRD	X-ray diffraction

1   Introduction

This chapter is a synopsis of this research. It presents the background, problem statement, aims and objectives, research questions, research approach and hypothesis of this work. The background briefly discussed the key aspects of this research such as environmental pollution, dyes and toxic metals as pollutants and the existing methods for the removal of these pollutants from water. The background further discusses the salient areas such as electrospinning, nanofibres and track-etched membranes. The research approach is presented as a brief discussion and in schematic form. Thereafter, the scope and delimitation of the study are highlighted and the latter part of this chapter presents the summary of each chapter in this thesis.

1.1   Background

1.1.1   Organic water pollutants and remediations

The textile industry has been recognized globally as one of the most chemically intensive industries, and has contributed significantly to environmental pollution (Shah, 2014; Gupta and Suhas, 2009). It is a major threat to potable water in recent years. The textile industry is associated with enormous quantities of complex substances, especially dyes, as unused and waste materials which come out as wastewater during textile production (Bae and Freeman, 2007). Dyes are classified as organic pollutants which are visible to the naked eye because of their colour. However, their presence in water bodies is not desired because of the health hazards associated with these compounds. When dyes are discharged into streams, they move with the water current and get diluted along the way.

Dyes get into the human body through oral ingestion and inhalation and can cause skin and eye irritations and most dangerously, some dyes could be classified as carcinogenic (Rai et al., 2005; Hatch and Maibach, 1999). Dyes also interfere with transmission of light and upset the biological metabolism process thereby affecting aquatic organisms (Shah, 2014; Christie, 2007). Furthermore, dyes have the propensity to sequester metal ions and may cause micro-toxicity to fish and other aquatic species (Gupta and Suhas, 2009; Christie, 2007).

The methods for removal of dyes from water have received great attention over the past few decades. The existing methods include; sedimentation (Cheremisinoff, 2002), filtration (Avlonitis et al., 2008), chemical treatments (Zhou et al., 2008), electrochemical methods (Faouzi et al., 2007), advanced oxidation processes (Bandala et al., 2008; Ghorai et al., 2007; Namboodri and Walsh, 1996), biological treatments (Barragan et al., 2007; dos Santos et al., 2007; Frijters et al., 2006), adsorption (Bansal and Goyal, 2005; Imamura et al., 2002) and ion exchange (Liu et al., 2007; Raghu and Ahmed-Basha, 2007). Although these methods have been reported to remove various types of dyes; two or more of them have to be combined for better removal results (Gupta and Suhas, 2009).

In domestic water treating systems, filtration technologies are the most common and large scale method for water purification. Most communities make use of this process to purify water for domestic use. Filtration processes can include micro-filtration, ultra-filtration, nano-filtration and reverse osmosis. Filtration is considered efficient for tertiary treatment of dye wastewater so as to avoid frequent clogging of the membrane pores in the process (Avlonitis et al., 2008). Adsorption techniques are widely known to remove colour and non-biodegradable pollutants from waters and therefore have wide applicability in wastewater treatment (Fu and Wang, 2011). Dyes that are difficult to breakdown via biological means can often be removed by using adsorbents (Bansal and Goyal, 2005; Imamura et al., 2002). For adsorption purposes, adsorbents should generally possess high surface area (pores as additional advantage) and the time taken for adsorption equilibrium to be established should be as small as possible for the removal of pollutants from water (Saeed et al., 2008).

Some of the adsorbents that have been used for dye wastewater treatment include; alumina, silica gel, zeolite and activated carbon (Gupta and Suhas, 2009).

1.1.2 Inorganic water pollutants and remediations

Contamination of water by toxic metals has steadily increased over the last decades as a result of over population and expansion of industrial activities (Barakat, 2011). Toxic metals could also originate from natural sources (contaminations from the bedrock) or from anthropogenic sources. The anthropogenic source of toxic metals in the soil and water can be as a result of mining activities, smelting and aerosol deposition (Fu and Wang, 2011; Tutu et al., 2008; Fergusson, 1990). The source can also be an outcome of working on the soil such as the application of fertilizer (agriculturally induced), which can in turn pollute the soil and water bodies close by (Topolska et al., 2004). Mining is arguably the largest anthropogenic source of toxic metal contamination into the environment (Tutu et al., 2008). Geochemical processes acting upon mining wastes initiate the process of transporting toxic metals from contaminated areas and redistributing them to the surrounding soils, streams and groundwater (Yin, 2010; Winde, 2006; Winde and Sandham, 2004). Toxic metals in their aqueous solutions behave the same way in the natural aquatic environment (Akcay et al., 2003). They can be transported via sorption, dissolution and precipitation and can even form complexes with organic molecules present in the water. Toxic metals also respond to changes in physicochemical variables such as pH, redox conditions or ionic strength and hydrodynamic effects (which are responsible for sediment transportations) (Akcay et al., 2003; Dassenakis et al., 1998). Because of their high solubility in the aquatic environments, toxic metals can be absorbed by living organisms either by direct intake or through the food chains (Islam et al., 2015; Meena et al., 2008). Once they find their way into the food chain, these toxic metals may accumulate in certain organs of the human body and if the metals are ingested beyond the permitted concentration, they can cause serious health problems such as poisoning and cancer (Islam et al., 2015; Meena et al., 2008; Sin et al., 2001; Deniseger et al., 1990). Therefore, it is necessary to treat metal contaminated wastewater prior to its discharge to the environment; at least this will substantially reduce their discharge to the environment from human activities.

As mentioned, several techniques have been used to remove toxic metals from contaminated water. These techniques include; ion-exchange, chemical precipitation, coagulation-flocculation, flotation, membrane filtration, electrochemical treatment, reverse osmosis and adsorption (Fu and Wang, 2011; Kurniawan et al., 2006). Among these techniques, adsorption is arguably the simplest and most effective technique and its efficacy largely depends on the fabrication of high capacity adsorbents (Fu and Wang, 2011). Adsorption has been used to remove toxic metal ions from various aqueous solutions even at low concentrations (Bode-Aluko et al., 2017a; Pereao et al., 2016). The performance of these adsorbents largely depends on their physical and chemical properties. It is noteworthy that adsorption is a surface phenomenon and therefore the efficiency of adsorbents largely depends on their ability to adsorb metal ions from solution onto their surfaces in order to remove the metal ions from the solution. However, the purpose of adsorption is not to permanently keep the metal ions (chemisorption) on the adsorbents, since adsorbents should be able to give away the metals afterwards (desorption). This is important for the purpose of recovery of metals and regeneration of adsorbents (Eldridge et al., 2015; Hong et al., 2015; Kampalanonwat and Supaphol, 2014).

In recent years, the use of chelating agents for the selective extraction and concentration of toxic metal ions has been on the rise especially from dilute industrial waste waters (Ndayambaje et al., 2016; Nilchi et al., 2008a; Bilba et al., 1998). The selectivity of an adsorbent could be used to separate different metals in the same solution (Nilchi et al., 2008b; Bilba et al., 1998). This has led researchers to grafting chelating ligands on hydrophilic supports for extraction of metal ions in a solid-liquid system (Ndayambaje et al., 2016; Nilchi et al., 2008a; Jal et al., 2004; Bradshaw et al., 1989). The supports can be organic (polymer, resins, fibres) or inorganic materials (silica gel) (Ndayambaje et al., 2016; Jal et al., 2004; Bilba et al., 1998). The surface of adsorbents can either be chemically activated through direct chemical reactions on them or can serve as a support for the chelating ligands (Ndayambaje et al., 2016; Horzum et al., 2012). The performance of these chelating adsorbents therefore depends on the chelating group they are carrying which would bring about the selective metal-ligand complexes (Eldridge et al., 2015).

Among organic chelating groups such as imidazole, carboxylic and amidoxime, adsorbent surfaces with amidoximes chelating group have shown strong interaction with toxic metals (Chi et al., 2013; Chen et al., 2012; Horzum et al., 2012; Egawa et al., 1979), thus their use as extractant for several decades. Amidoxime are chemically introduced onto the surfaces of adsorbents that contain nitrile groups (Chen et al., 2012; Horzum et al., 2012; Zhang et al., 2005a; Bernasek, 1957). Amidoxime resin has been studied for extraction of toxic metals with promising results (Hubicki and Kolodyńska, 2012; Choi et al., 2003; Kago et al., 1992; Egawa et al., 1988; Egawa et al., 1987; Astheimer et al., 1983; Egawa et al., 1979). These metals include; U, Cd, Pb, Cr, Hg, Ag etc. Likewise, polymer fibres with amidoxime chelating groups have also been extensively studied for extraction of various toxic metals (Huang et al., 2013; Horzum et al., 2012; Feng et al., 2011; Simon et al., 2011; Kago et al., 1992; Morooka et al., 1991; Takeda et al., 1991; Kobuke et al., 1990).

1.1.3   Electrospinning process

Electrospinning has been recognised as an efficient technique for the fabrication of polymer nanofibres (Baji et al., 2010) that could be used as support for functional ligands or chelating groups (Bode-Aluko et al., 2017b). The electrospinning set-up comprises; a high voltage source, spinneret (polymer solution holder) and a collector. In the absence of an external electrical field, an ionic polymer solution has an equal number of positive and negative ions present within each volume unit. Upon the application of a high voltage, an electrical potential field is created between the droplet of a polymer solution held at the end of a spinneret tip and a grounded collector. As the intensity of the electric field is increased, the induced charges on the polymer solution surface repel each other thereby creating shear stresses, hence, the charge repulsion within the solution. At this point, a "Taylor cone" is formed at the tip of the spinneret which eventually results in the ejection of an unstable charged jet of polymer from the tip of the Taylor cone. The charged jet moves as a rapid whipping jet in the space between the spinneret tip and collector which leads to evaporation of the solvent. The jet travels by following the vector path of the electric field leaving the electrospun nanofibres deposited on the collector (Adomaviciute and Milasius, 2007; Taylor, 1969).

In recent years, various polymers have been successfully electrospun into ultrafine nanofibres in a solvent solution and some in melt form. These polymers include; polyamide 6, polyacrylonitrile, polyethylene terephthalate, polystyrene etc. (Bhardwaj and Kindu, 2010; Huang et al., 2003). The diameters of these polymer fibre materials are in the nano-meter range (Bhardwaj and Kindu, 2010). At these diameters, nanofibres exhibit characteristics such as high surface area to volume rate (which allows fast and high adsorption capacities), flexibility in surface functionalities and superior mechanical performance (e.g. stiffness and tensile strength) (Bhardwaj and Kindu, 2010). Furthermore, the surface of some nanofibres such as polyacrylonitrile can be functionalised (by surface modifications) to introduce certain functional groups. Functionalisation binds chelating groups such as amine and hydroxide to the surface of the fibres (Saeed et al., 2008; Deng and Bai, 2003). Also, functionalisation could be achieved by immobilisation of ligands upon nanofibres to enhance their affinity towards extraction of toxic metals. Ndayambaje et al. (2016) immobilised 2-(1H-imidazol-2-yl)pyridine through chemical reaction on PAN nanofibres for removal of nickel ion from aqueous solution. Meanwhile, in an effort to immobilise ligands on polymers, an emphasis must be laid on covalent bonds between the ligands and the polymer surface to avoid detachment of the ligands during regeneration (Neghlani et al., 2011).

1.1.4 Track-etched membranes

Track membrane technology has become an establish industry in the field of membrane filtration. The membranes are made by irradiation of polymer films with fragments from fission of heavy nuclei such as uranium (Lueck et al., 1990; Flerov et al., 1989; Fleischer et al., 1975). The process creates damage to the polymer films to give latent tracks which would later be modified using a chemical etchant to form controllable pores in the polymer films, so-called track-etched membrane. The track etching provides a way for the simple and effective production of asymmetrical nano-pores with controllable longitudinal path (Apel, 2013). The control of pore size, shape, pore distribution, transport and retention properties of track-etched membranes (TM) give it advantages over conventional membranes (Ferain and Legras, 2003). Typical areas where the use of TMs has been successful are in general filtration, air monitoring, blood filtration, templates for nanowires etc. (Apel, 2013).

Polymer films that have been made into track-etched membranes include; polyethylene terephthalate, polycarbonate, polyester etc. (Apel, 2013).

1.2   Problem statement

South Africa has been classified as a water stressed country. The looming *El Niño* effect is ravaging the Southern African countries. The shortage of potable water is increasing day by day. Owing to the increase in industries and expansion of rural areas, most of the available water has been polluted due to the disposal of organic and inorganic waste. Manufacturing industries have greatly contributed to the pollution of water and have thereby made potable water scarce for consumption. There are no existing portable water purification techniques that can be used for quick removal of dyes and toxic metals as the existing water treatment technologies are cumbersome and complex. Therefore, there is a need to design equipment to salvage this situation, especially in this time of water scarcity. This research will be looking into the use of nano-materials such as nanofibres for the removal of both organic pollutant (dye, rhodamine 6G) and inorganic pollutant (toxic metal, Pb^{2+}). For removal of dyes, the study will combine two removal technologies (adsorption and filtration) for efficiency. The use of nanofibres would increase the rate at which pollutants will be removed from water before being filtered by the track-etched membrane. This will at the same time reduce the work done by the track etched membrane and overcome the drawback of quick pore blockage and fouling of the membrane during filtration. Furthermore, the amidoxime chelating ligand will be immobilised on polyacrylonitrile nanofibres for the extraction of the toxic metal. Meanwhile, a proper ligand immobilisation reaction pathway will be investigated to prevent the displacement of the ligand from the support during regeneration and to assure the reusability of the adsorbent.

1.3   Aims and objectives of the research

The aims of this research are; to use electrospinning process to produce polymeric nanofibres; to use electrospinning process to combine nanofibres and track-etched membranes to form composite nanofibres track-etched membranes, and to immobilise the chosen ligand upon nanofibres to produce metal adsorptive

membrane. Furthermore, the electrospun nanofibres, the track-etched membrane and the composite nanofibre track-etched membranes will be used for adsorption-filtration of dye. Also, the metal adsorptive membrane will be used for extraction of toxic metal.

The overall objectives of this study are summarised as follow:

- ➢ To produce polyamide 6 nanofibres (PA6-nfs) and polyacrylonitrile nanofibres (PAN-nfs) via electrospinning process.

- ➢ To optimise the polymer concentrations of polyamide 6 (PA6) and polyacrylonitrile (PAN) to achieve bead free PA6-nfs and PAN-nfs respectively via electrospinning process.

- ➢ To functionalise the surface of PAN-nfs with 2-pyridine amidoxime to produce adsorptive membrane (2-pyridine amidoxime immobilised on polyacrylonitrile nanofibres (PAN-PyAMI)).

- ➢ To formulate composite nanofibres track-etched membranes using polyethylene terephthalate track-etched membrane (PET-TM) combined with PA6-nfs or PAN-nfs via electrospinning process.

- ➢ To design adsorption-filtration experiments suitable for dye removal.

- ➢ To determine the adsorption-filtration capacity of initial materials (polyamide 6 nanofibres, polyacrylonitrile nanofibres and polyethylene terephthalate track-etched membrane (PET-TM)) on dye (rhodamine 6G solution).

- ➢ To determine the adsorption-filtration capacity of the composite membranes on dye (rhodamine 6G solution).

- ➢ To determine the adsorption capacities of PAN-nfs and PAN-PyAMI on Pb^{2+} in aqueous solution.

- ➢ To check the regenerability of PAN-PyAMI after Pb^{2+} adsorption.

1.4   Research questions of the study

The research questions of this study are summarised as follow:

- ➢ Can nanofibres be combined with track-etched membrane through electrospinning process?

- ➢ Can PA6-nfs and PAN-nfs remove rhodamine 6G from aqueous solution?

➢ Can composite nanofibre track-etched membranes remove rhodamine 6G from its aqueous solutions?

➢ Can 2-pyridine amidoxime ligand be immobilised on the surface of PAN-nfs?

➢ Can PAN-PyAMI adsorb Pb^{2+} better than PAN-nfs?

➢ Can PAN-PyAMI be regenerated after Pb^{2+} adsorption?

1.5 Research approach

In order to achieve the aims and objectives of this research, background studies of electrospun polyamide 6 and polyacrylonitrile nanofibres were first reviewed. Some electrospinning parameters of both polymers were optimised to produce bead free nanofibres using Al foil as the collector. The optimised polymer solutions and the polyethylene terephthalate track-etched membrane were the initial materials used towards the formation of composite nanofibres track-etched membranes via electrospinning. Instead of the usual Al foil covering the collector screen during electrospinning process, TiO_2 coated polyethylene terephthalate track-etched membrane collectors were used while the respective polymer solution was electrospun.

The surface of PAN nanofibres were modified using 2-pyridine amidoxime. The immobilisation process was investigated in two reaction pathways namely acidic and basic. The acidic pathway was by the use of $AlCl_3.6H_2O$ while the basic used KOH as catalyst.

All the electrospun nanofibres and their composite track-etched analogues were characterised for a better understanding of their physical and chemical properties. For physical characterisation, the techniques used are high resolution scanning electron microscopy (HRSEM), transmission electron microscopy (TEM), thermal gravimetry analysis (TGA), Nitrogen adsorption–desorption measurement (BET) and X-ray diffraction (XRD) analysis. Attenuated total reflectance Fourier transform infrared spectroscopy (ATR-FTIR) and nuclear magnetic resonance spectroscopy (NMR) were used to monitor the chemical changes of functionalised samples and the synthesised ligand.

Figure 1.1 is the schematic of the experimental plan of this study. The experimental is basically carried out in 3-step process. Step 1 is the production of adsorbents. Step 2 discussed the functionalisation of PAN-nfs and characterisation of the sample membranes produced in step 1 while the step 3 is the application experiments.
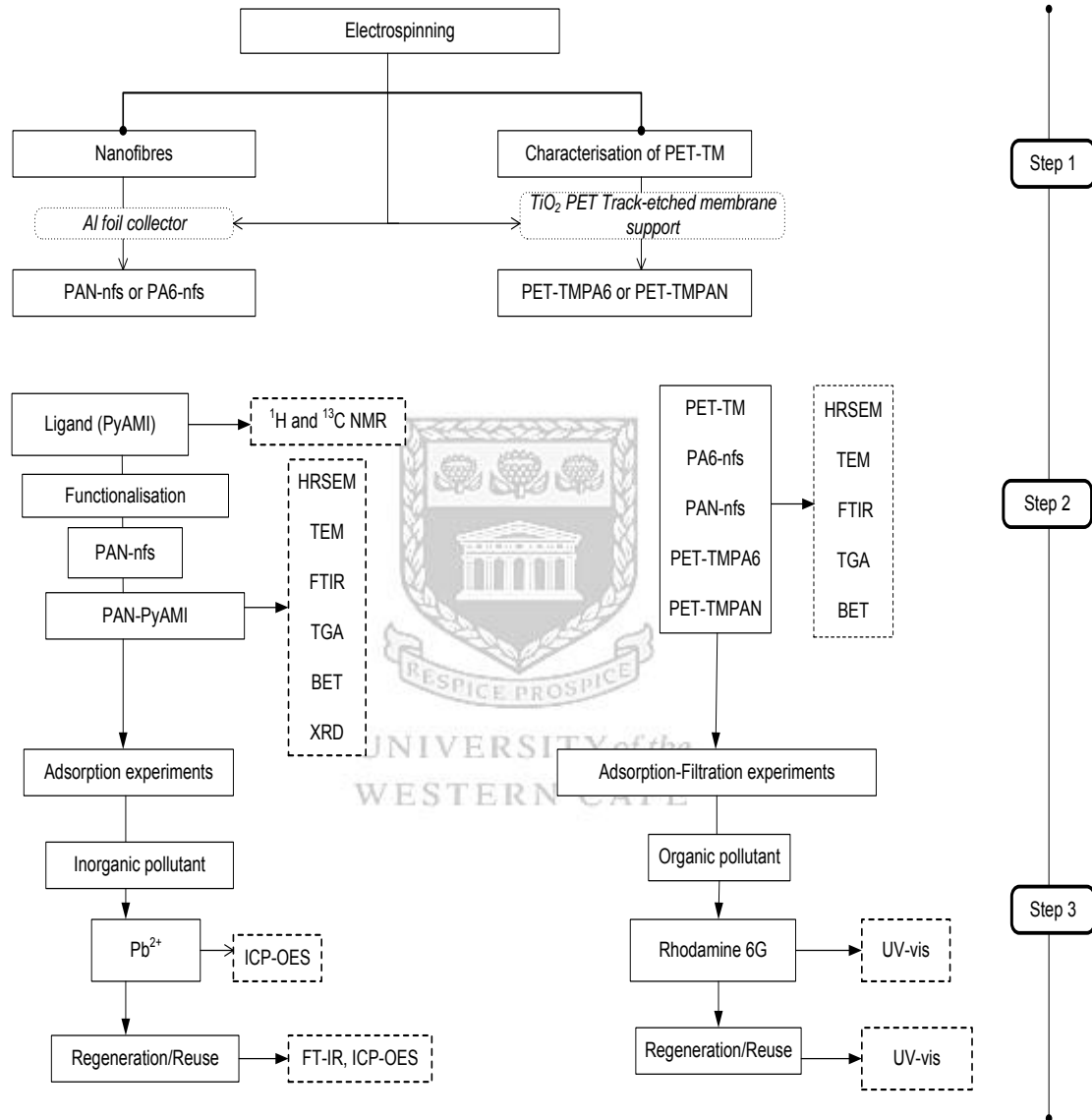
Figure 1.1: The schematic illustration of the experimental protocol of the study.

The PA6-nfs, PAN-nfs and the composite membranes were used for adsorption-filtration of rhodamine 6G in continuous modes. A certain volume of known concentration of rhodamine 6G was allowed to pass through each sample membrane and the decrease in concentration of the effluent was monitored by UV-vis

10

spectrophotometry after each batch. The effect of pH, initial concentration and flow rate on the adsorption-filtration of rhodamine 6G was also looked into. PAN-PyAMI was also used for the adsorption of Pb^{2+} from aqueous solution. The quantity adsorbed was monitored by inductively coupled plasma-optical emission spectroscopy (ICP-OES). The effects of initial pH, initial concentration and the contact time on the adsorption of Pb^{2+} were also studied. For every adsorption experiment, the quantity and percentage adsorbed were calculated to determine the adsorption capacities of respective membrane.

1.6 Hypothesis

Nanofibres and track-etched membranes can be combined using the electrospinning process and the resultant composite nanofibre track-etched membranes are good for the removal of organic dyes from aqueous solution. PAN-nfs can be functionalised by immobilising amidoxime chelating ligand on it for adsorption of Pb^{2+} from aqueous solution.

1.7 Scope and delimitations of the study

The behaviour and characteristics of materials at nano-level have given many researchers great insights to solving various problems facing the human race. Electrospinning of polymer solutions into nanofibres and the creation of nano-pores by heavy ion irradiation are no doubt two processes for creating materials at the nano-level and the combination of the material products of these two processes would be an innovation; hence, the motivation for this research.

It is important to note that many polymers have been electrospun into nanofibres, however, polyamide 6 and polyacrylonitrile were chosen for this research. The two polymers can be easily electrospun into bead free nanofibres of small diameters. Likewise, the two polymers are cheap and readily available. In addition, PAN was chosen because of easy surface chemical modification. For the electrospinning process, parameters such as polymer concentration, voltage applied, distance between spinneret and collector, temperature, type of collector, etc. have been reported to affect the spinnerbility and diameter of polymer nanofibres, however,

because of time constraints, only the polymer concentration parameter was studied for spinning the two polymers.

For ion-tracking process, the facilities required are sophisticated and are in-fact huge and required expert handling. The only facility accessible for the research is located at the Joint Institute for Nuclear Research (JINR), Dubna, Russia. Therefore, the production of ion-tracking of membrane could not be carried out in the laboratory. The PET track-etched membrane (PET-TM) was made available by the JINR collaborator. Ordinarily, PET-TM was not conductive enough; therefore, it was advised at JINR that the membrane should be coated with TiO_2 which was done via magnetron reactive sputtering method. PET-TM of 3.5 micron pore size was chosen as micro-filter to overcome the high pressure challenge involved in other lesser membranes pore sizes.

Owing to the time consuming nature of immobilisation of 2-pyridine amidoxime (PyAMI) on PAN-nfs, only time experiments were investigated. In addition to that, the use of NMR techniques to prove the immobilisation reaction proved abortive due to the inability of the machine to properly characterise the polymer solution.

1.8   Thesis outline

This thesis is divided into seven chapters (including this one; Chapter one). The following presents the synopsis of each chapter.

Chapter one: This chapter serves as the introduction to the whole study. It presents the problem statement, the aims and objectives of the study and the hypothesis. The chapter also provides an insight to the research approach and various questions of which the study is expected to answer. A brief overview of the background as well as the general literature review of the various aspects this research would look into is also discussed.

Chapter two: This chapter presents the literature review covering relevant aspects of the research. It starts with a brief introduction into water scarcity followed by organic and inorganic pollutants. The target organic pollutant "dyes" and inorganic pollutants

"toxic metals" are discussed. Dyes are discussed in-terms of their use in textile industries, their structure and their different classifications. The literature proceeds to describe various methods that have been used to remove dyes from wastewater. Meanwhile, out of the methods discussed, filtration and adsorption processes are further elaborated. In the same vein, toxic metals are discussed in relation to their sources, toxicity and methods of removal. Electrospinning, being the key part of the research was extensively reviewed. The review pointed out important areas of the process such as, the history, the set-up and various parameters that affect the electrospinning process. Also, various characterisation techniques of electrospun nanofibres were discussed. Furthermore, the two polymers that have been chosen for this research, PA6 and PAN, were reviewed based on their electrospinning parameters, their physical and chemical characterisations as well as their applications in various fields. Again, PAN-nfs are further discussed based on various chemical surface modification procedures. Ion track technology, being another important aspect of this research is discussed in relation to the production of track-etched membranes, the magnetron sputtering method of coating membranes and a brief application of track-etched membranes. This chapter also discussed the amidoxime chelating groups; the type of reactions amidoxime can undergo and how the ligand can be attached to a support. Finally, a critical review was presented on the use of surface modified PAN-nfs on the adsorption of toxic metals. A summary of this chapter is presented at the end.

Chapter three: This chapter presents all the materials and equipment used for this study. Also included are the experimental procedures in detail. The chapter also discussed the principles and the science behind all the instruments used for the characterisations of the initial materials and the products of this research.

Chapter four: This chapter presents the characterisation results from various instrumental techniques of all the materials synthesised in chapter three which include; PA6-nfs, PAN-nfs, PET-TM, PET-TMPA6, PET-TMPAN, PyAMI and PAN-PyAMI. A summary of the chapter is presented at the end of the chapter.

Chapter five: This chapter presents the results and discussion of the removal of rhodamine 6G from its aqueous solution using the electrospun nanofibres, PET-TM and the composite nanofibres track-etched membranes. A summary of the findings is presented at the end of the chapter.

Chapter six: This chapter presents the results and discussions of the adsorption of Pb^{2+} from its aqueous solution using PAN-nfs and PAN-PyAMI. It also discusses desorption and the regeneration of PAN-PyAMI. A summary of the findings is presented at the end of the chapter.

Chapter seven: This chapter is a summary of the main findings of the whole study. It includes the consideration of research questions from chapter one, the novelty of this study, the recommendations and the future work in line with this research. The list of references and appendices are presented after this chapter.

2   Introduction

This chapter presents the literature review relating to this research. It covers critical areas such as water pollution, including organic and inorganic pollutants, and the existing methods for removal of these pollutants from their aqueous solutions. The important background of this research topic is highlighted including; filtration, adsorption, nanotechnology, electrospinning, nanofibres, surface modification of nanofibres and ion track technology. Overall, the literature cogently provides the basic links of all these areas towards the development of composite adsorptive membranes and the functionalised nanofibres for the treatment of dye and toxic metal wastewaters, respectively.

2.1   Water pollution

"Water", arguably the most essential commodity in life without which there would be no life, is seriously under attack. Water safety could be the most critical element in-terms of saving human kind. The topic "water pollution" has been trending for a few decades and will remain a problem if the causes are not addressed. Unfortunately, water pollution might not soon be resolved; this is due to the fact that, the negligence and lackadaisical attitude humans have shown to the environment for decades is now overwhelming and difficult to deal with. Even with a high level of alertness, a lot of water pollution is still on going. Now, due to the emergence of industrialisation and advancement in technology, and the fact that the world economy largely depends on increasing growth of both, water pollution has come to stay.

Water covers 70% of the earth, however, out of this 70%, the following breakdown is noteworthy. 98% of the water is salty, and only 2% is fresh water (Figure 2.1). Moreover, out of this fresh water, 87% is constantly in ice, 12% is classified as underground water while the remaining 1% is found in rivers and lakes. This is a clear indication that there is not enough water to support the rapidly growing population. It is therefore not surprising that some pundits have predicted that the struggle for water might be the beginning of the third world war.
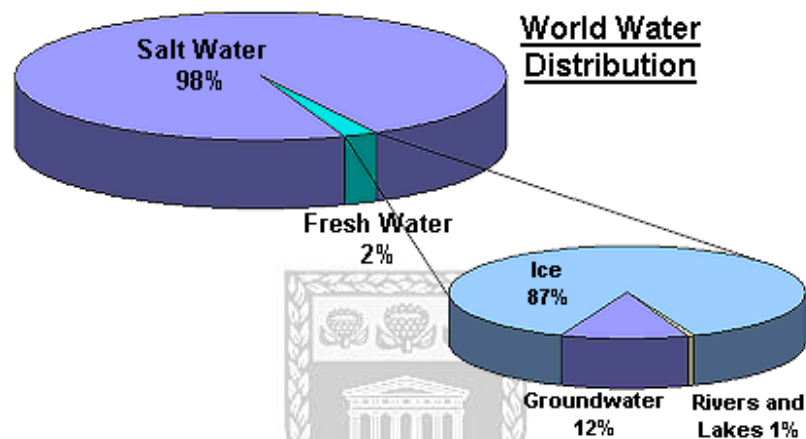
Figure 2.1: World water distribution.
(**Source:** http://snr-1349.unl.edu/navigation/waterdistribution.aspx).

South Africa has been classified as a water stressed country (Figure 2.2), because of its inability to meet growing human and ecological water demand (Department of water affairs, 2010). It can basically be linked to water scarcity. A lot of water stressed areas lack fresh waters, especially, surface and ground waters. South Africa is critically located in an area affected by the *El Niño* effect. *El Niño* affected areas are characterised by drought due to a rise in oceanic temperature in the southern Pacific ocean which affects the weather patterns. Considering all these factors, the imminent danger facing the future of water in South Africa cannot be over emphasised.
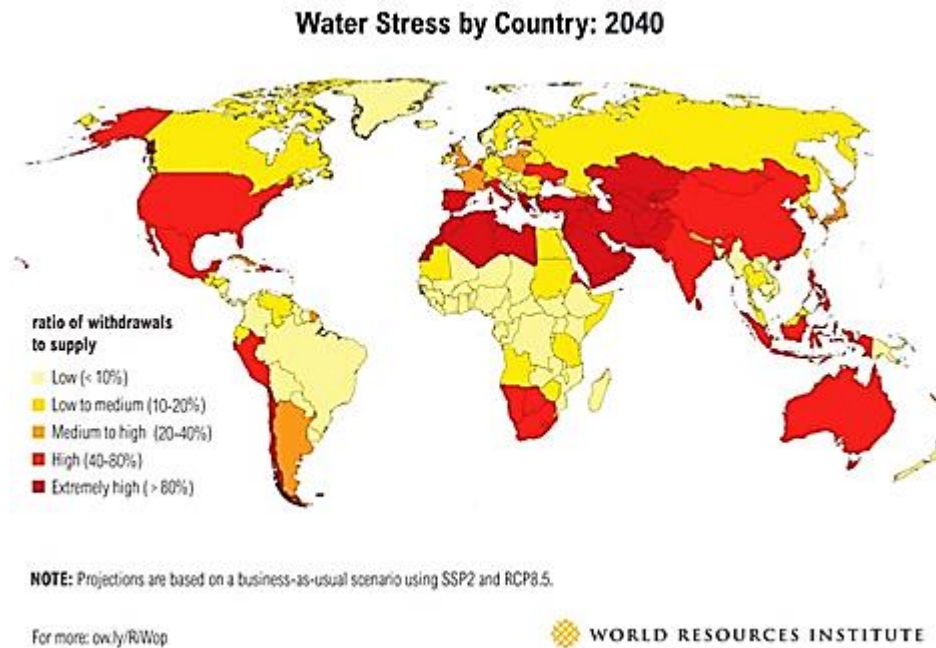
Figure 2.2: Water stress map 2040 projection.
(**Source:** http:// www.wri.org/blog/2015/08/ranking-world's-most-water-stressed-countries-2040).

Considering the breakdown of water use in South Africa, over 70% in total go to economic sectors such as agriculture, mining and industries (Figure 2.3). This shows that huge competition is on-going between the economic sector and domestic use for the available water; hence, political pronouncements would not stop water pollution. It is generally accepted that water that goes into industries does not come out clean and their effluents are subsequently being pumped back into fresh water bodies (Hai et al., 2007; Husain, 2006). It is worrisome that these wastewaters are released into the environment without proper quantification of the pollutants present. Even though some pollutants are visible to the naked eye (such as dyes), many more are not visible and the immediate effect most times are not noticeable, but in the long run, can affect aquatic organisms and even humans through ingestion (Christie, 2007; Walsh et al., 1980).

Wastewater can come from different sources (Figure 2.4) containing organic or inorganic pollutants or both. Organic pollutants can go into solution and becoming undetectable except for chemical analysis while some are tangible and can be seen (Bae and Freeman, 2007; Christie, 2007).

17
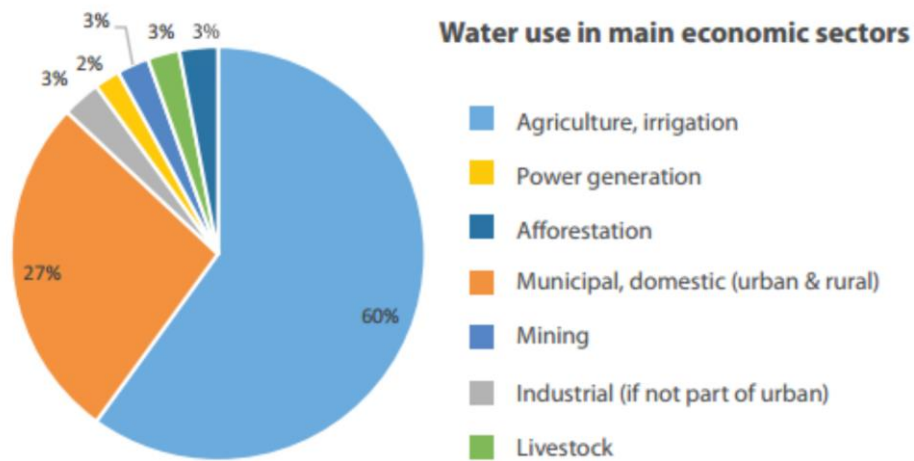
Figure 2.3: Percentage of water use in main economic sectors in South Africa. (**Source:** http://www.moneyweb.co.za/news/industry/the-drought-will-impact-your-investments/).
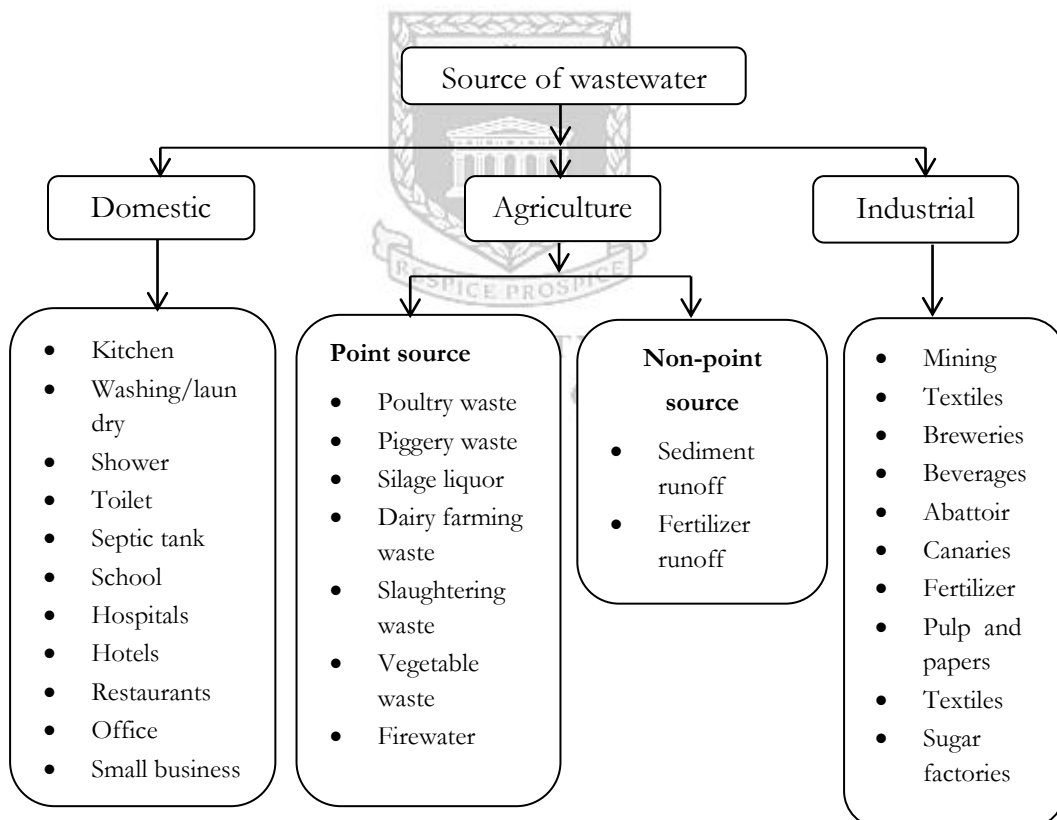
Figure 2.4: Sources of wastewater (Matheyarasu et al., 2015).

http://etd.uwc.ac.za/

South Africa is a developing country and the growing economy largely depends on industries such as mining, textile, electroplating, paints etc., in other words, more polluted waters are expected to be discharged into rivers, lakes etc. Chemical pollutants can enter the human food chain as they tend to contaminate and accumulate in micro-organisms, fauna and aquatic flora (Fu and Wang, 2011).

A lot of human and animal health issues have been associated with water quality problems (Armitage et al., 2007; Sin et al., 2001; Deniseger et al., 1990). Many pollutants in the aquatic environment can travel many miles through mechanisms such as dissolution, sorption, precipitation and compelxation (Fu and Wang, 2011). The chemical reactions in polluted water are complicated because the process responds to changes in physicochemical variables such as pH, ionic strength or redox conditions and hydrodynamic processes that affect sediment transport, formation of authigenic particles and pollutant sorption on particles (Akcay et al., 2003; Dassenakis et al., 1998).

2.2   Dyes as organic pollutants

Organic compounds are compounds having carbon atoms as the major elements in their structures. However, some carbon containing compounds such as oxides and cyanides are classified as inorganic compounds. Organic compounds can occur naturally or can be synthesised in the laboratory. Organic compounds with chromophores such as dyes are characterised by bright colour, visible to the naked eyes. These compounds have been in existence for several millenniums and have generally been used as colourants and decorations (Gupta and Suhas, 2009). Some dyes are natural and can be isolated from insects, plants and mollusks (Gordon and Gregory, 1983). Apart from chromophores (responsible for the colour), dyes also contain auxochromes which are responsible for their dissolution in water and also serves as bonding agent. For this reason, dyes have been one of the main substances used in textile industries (Gupta and Suhas, 2009).

Dyes can be classified by either their chemical structures (macromolecule unit) or their usage. They can also be classified based on their solubility (Hunger, 2003).

Chemical classification using chemical structures is the most convenient way of classifying dyes for chemists; however, classification based on application is easier for the lay man who would not understand the complexity of the structures and nomenclature of the dyes. The following sub-sections are eight classes of dyes based the combination of chemical structures and their general applications.

Acidic dyes: These are salts of sulfuric, carboxylic and phenolic organic acid dyes. They are water soluble dyes used in the textile industry for nylon, wool and silk. They also find applications in the paper, food and cosmetic industries. Acidic dyes can contain azo, anthraquinone, xanthene (Figure 2.5 (a)), rhodamine 6G), nitro- or nitroso- group in their chemical structures.

Basic dyes: Basic dyes give colour cations in solution; hence, can be called cationic dyes, and therefore react with materials with a negative charge. They are used as colourant for paper, polyacrylonitrile, polyester, silk and wool. They are also used in medicine as stain. Their chemical structures can contain diazahemicyanine, triarylmethane, cyanine, thiazine (Figure 2.5 (b), methylene blue) or oxamine.

Disperse dyes: Disperse dyes are characterised by water in-soluble, non-ionic in nature and generally used for hydrophobic fibres such as polyester, nylon, acrylic fibres and cellulose. Their chemical structures are the smallest among dyes and can contain azobenzene (Figure 2.5 (c), Disperse yellow 26), anthraquinone, nitro or benzodifuranone.

Reactive dyes: Reactive dyes are characterised by forming covalent bonds with fibres using their chromophores, hence, their application for dying cotton and cellulose. They have simpler structures with brighter colour. Their chemical structures can contain chromophore units such as formazan (Figure 2.5 (d)), azo, phthalocyanine, anthraquinone or oxazine.
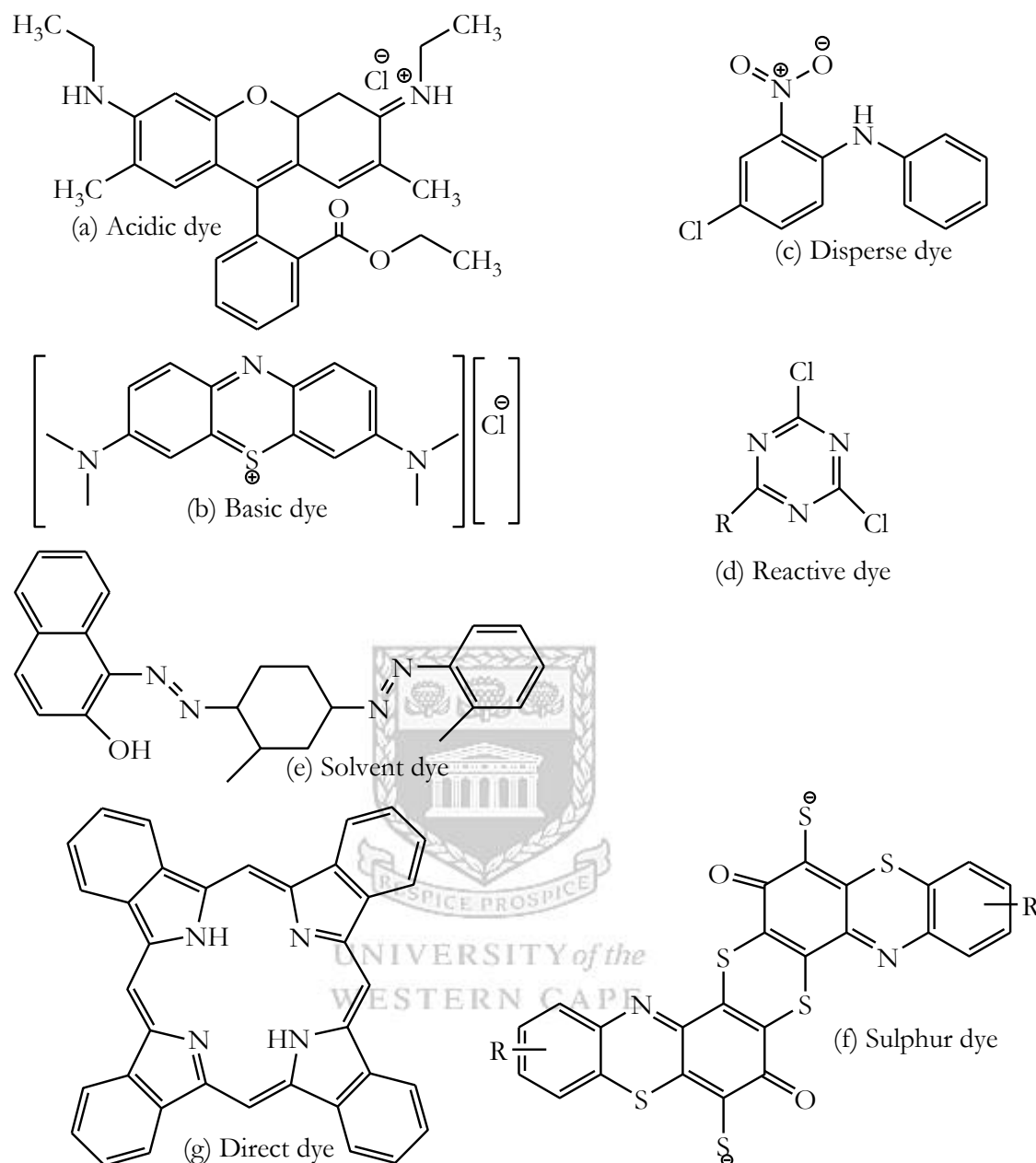
Figure 2.5: Structures of common dyes.

Solvent dyes: These dyes are soluble in organic solvent but insoluble in water. They are predominantly used for plastics, oils, waxes, gasoline and lubricants. They can contain chromophores such as azo (Figure 2.5 (e), sudan IV), phthalocyanine, anthraquinone etc.

Sulphur dyes: Sulphur dyes are the most commonly used dyes for cotton. They are characterised as water insoluble and having intermediate structures with sulphur in their structure (Figure 2.5 (f), Sulphur black 1). Sulphur dyes are low cost type of dyes with good wash fastness. They are also used for paper, wood and leather dyeing.

Direct dyes: Direct dyes are molecules that can adhere to fabric without chemical help. They are water soluble anionic dyes. They are characterised by having a high affinity for cellulose fibres such as cotton and also for nylon. They also find applications in paper industries. Their chemical structures can contain phthalocyanines (Figure 2.5 (g)), stilbenes or oxazines.

Vat dyes: Vat dyes can be said to encompass all types of dyes, so far the dye can be used in a vat or bucket. However, vat dyes are generally classified as dyes that can be used for cellulose fibres.

More than 100,000 dyes are commercially available (Christie, 2007; Husain, 2006; Hunger, 2003). Dyes are hugely used in industries such as textile, paper and paints. The textile dyeing industry consumes large quantities of water and produces large volumes of wastewater from different steps in the dyeing and finishing processes (Babu et al., 2007). The huge quantities of wastewater coming out of these industries contribute mostly to organic pollutants in fresh water (Bae and Freeman, 2007; Christie, 2007). It is reported that 10 to 15% of these dyes are being discharged into the environment as wastes (Hai et al., 2007; Jin et al., 2007; Husain, 2006). These compounds are difficult to treat because of their synthetic origin and can also form complex molecular structures which make them difficult to degrade. This is why dye pollutants are regarded as dangerous and persistent in water bodies (Rai et al., 2005; Forgacs et al., 2004).

Their health implications when ingested include; eye and skin irritation and skin sensitisation (Christie, 2007; Rai et al., 2005; Hatch and Maibach, 1999). Azo dyes for example are known to have an effect on aquatic photosynthesis, ability to deplete dissolved oxygen, and have high toxicity to flora, fauna and humans. Moreover, the breaking down of azo dyes generates aromatic amines, which are carcinogenic and

mutagenic (Shah, 2014). Dyes wastewaters are also characterised for having high biological oxygen demand (BOD) and chemical oxygen demand (COD) values. Dyes can also sequester metal ions; hence, leading to accumulation of metals in aquatic animals which may in turn cause toxicity to humans when ingested (Christie, 2007). It is worthy of note that not only dyes come out as pollutants from textile and industrial wastewater but also other chemical compounds (Table 2.1) (Dey and Islam, 2015).

Table 2.1: Textile wastewater effluent composition.

Process	Effluent composition	Pollutant nature
Sizing	Starch, waxes, carboxy methyl cellulose (CMC), polyvinyl alcohol (PVA), wetting agents	High in BOD, COD
Desizing	Starch, CMC, PVA, fats, waxes, pectins	High in BOD, COD, dissolved solids (DS)
Bleaching	Sodium hypochlorite, Cl_2, NaOH, H_2O_2, acids, surfactants, sodium phosphate, $NaSiO_3$	High alkalinity
Mercerizing	Sodium hydroxide, cotton wax	High pH, low BOD, high DS
Dyeing	Dyestuffs urea, reducing agents, oxidizing agents, acetic acid, detergents, wetting agents	Strong coloured, high BOD, DS, heavy metals
Printing	Pastes, urea, starches, gums, oils, binders, acids, thickeners, cross-linkers, alkali	Highly coloured, high BOD, slightly alkaline

(**Source;** Dey and Islam, 2015), Note: BOD; Biochemical oxygen demand, COD; Chemical oxygen demand.

2.3 Toxic metals as inorganic pollutants

Toxic metals are classified as inorganic pollutants. Toxic metals are known to be recalcitrant and persistent inorganic pollutants in our natural environment (Barakat, 2011; Fu and Wang, 2011; Kisku et al., 2011). These are the reasons why toxic metal pollutions are considered as one of the most serious environmental problems to deal with at present as well as in the nearest future (Fu and Wang, 2011), and another reason is not far-fetched when considering the discharge of large amounts of metal contaminated effluents from industries into the natural eco-system over decades (Barakat, 2011). Unlike organic contaminants, toxic metals such as Cd, Cr, Sr, Ni, As, Pb, Sr and U are not biodegradable and tend to accumulate (Fu and Wang, 2011; Argun and Dursun, 2008). Toxic metals effluents are directly or indirectly discharged into the environment from industries such as metal plating facilities, mining operations, fertilizer industries, tanneries, batteries, paper industries, pesticides etc., especially in the developing countries (Fu and Wang, 2011; Tutu et al., 2008). Due to high solubility of toxic metals in the aquatic environments, toxic metals can easily be ingested by humans either by direct intake or through food chains (Islam et al., 2015; Meena et al., 2008; Deniseger, et al., 1990).

South Africa has a rich diversity of mineral deposits and many of them are either toxic themselves or associated with toxic elements (Winde, 2006). The country has one of the most sophisticated and developed mining industries in the world (Akcil and Koldas, 2006). In South Africa, water is used in mining and heavy industries for cooling, creating slurries, separation processes, etc. The results of the research conducted by Rosner, (1999) showed the presence of toxic metals such as Cr, Pd, U and As in five difference gold mine tailings in Rand area of Gauteng, South Africa (Table 2.2).

Table 2.2: Average trace elements concentration of five different gold mine tailings dam in the East Rand area (Rosner, 1999).

Trace elements (mg/kg)	Site 1	Site 2	Site 3	Site 4	Site 5
As	109.0	82.7	103.5	112.5	123.4
Co	13.1	4.8	4.0	18.6	20.5
Cu	27.0	14.0	17.5	22.7	25.1
Cr	462.4	395.8	347.3	445.5	553.1
Ni	71.6	34.5	33.6	73.1	88.4
Pb	46.4	20.8	36.3	125.0	23.1
Zn	45.4	27.8	17.6	94.5	21.4
Th	<3.0	<3.0	<3.0	3.5	4.0
U	17.9	9.7	9.5	46.4	13.7

Acid mine drainage (AMD) is arguably the main source of environmental pollution in South Africa (Tutu et al., 2008). Characterised by low pH and high concentrations of toxic metals and other toxic elements, AMD can severely contaminate surface and groundwater as well as soils (Peppas et al., 2000). Acid mine drainage is produced when sulfide-bearing material is exposed to oxygen and water. Although this process occurs naturally, mining promotes AMD formation simply by increasing the quantity of sulphides exposed to air and water (Akcil and Koldas, 2006).

The following subsections will briefly discuss some sources of specific toxic metals alongside their health implications.

> **Lead**

The major sources of lead in the environment especially in the third world countries are mainly from petrol, lead-acid batteries, paint, water pipes etc. (Tong et al., 2000). Lead can cause damage to body organs such as the kidneys, liver and brain as well as body systems such as the central nervous system and reproductive system (Naseem and Tahir, 2001).

> ➤ **Cadmium**

Cadmium is commonly found in the metallurgical processing as a by-product of metals such as copper, lead and zinc (Gupta et al., 2001). It is still being used extensively in electroplating, metallurgical products as well as pigments and batteries. Even at low concentration, cadmium is considered to be one of the most toxic metal elements (Rodríguez et al., 2005). The entry of cadmium into the body can occur through skin contact, inhalation or via ingestion (MSDS). Cadmium can cause lung, blood and kidney diseases. It is also considered carcinogenic (MSDS).

> ➤ **Chromium**

Chromium exists in two stable oxidation states in aquatic environment, Cr^{3+} and Cr^{6+}. The Cr^{3+} state is considered one of the essential elements for living organisms; on the other hand, Cr^{6+} state is toxic. Chromium is being used in motor manufacturing, electroplating, leather tanning, cement industries and photography (Khezami and Capart, 2005) and it dissolves easily in water thereby finding its way into water bodies. Cr^{3+} causes damage to the kidneys, liver, gastrointestinal tract, the upper respiratory track, skin and eyes (MSDS). It also causes birth defects (Khezami and Capart, 2005).

> ➤ **Mercury**

Mercury contamination can be considered a threat to humans because when ingested, it can be transferred through secretion into the maternal milk of mammalians (MSDS). It is widely known that mercury has a tendency to accumulate in fish and shellfish and this can be catastrophic considering the Minamata bay incidence. Mercury is very toxic to the kidneys, lungs and central nervous system (MSDS; Namasivayam and Kadirvelu, 1999).

> ➤ **Radionuclides**

Radionuclide elements such as uranium and thorium occur in nature while radionuclides such as strontium are a by-product of nuclear fission reactions. In

South Africa, the presence of radionuclides such as UO_2^{2+} and Sr^{2+} in water are inevitable because of gold mining activities and the presence of a nuclear reactor (Winde, 2006; Winde and Sandham, 2004). Uranium has been reported to be present in sea water in large amounts (Madrakian et al., 2007; Pekel et al., 2000). Strontium removal and recovery from nuclear wastewater has also received a lot of attention in recent years (Tian et al., 2005). Radionuclides elements are generally toxic and they cause serious damage to kidneys. They are also carcinogenic in bone and may even cause mutagenic effects (Gorden et al., 2003).

2.4 Methods for removal of dyes from water

Several treatment methods have been adapted for removal of dyes from water, however, it should be noted that no single standard treatment has been confirmed for total removal of dyes from water. The following sub-sections are overview of various dye removal methods that have been reported in the literature.

Sedimentation: Sedimentation is the basic and most common primary treatment of municipal and industrial wastewater. It requires leaving the wastewater to settle under gravity especially the suspended particles. This method would obviously not work for treatment for dyes as it would take forever to settle organic molecules under gravity (Cheremisinoff, 2002). Meanwhile for such a method, other treatments such as chemical flocculants can be combined for efficiency.

Chemical treatment: Chemical treatment involves the use of coagulating/flocculating agents for the removal of dyes (Zhou et al., 2008; Shi et al., 2007). Agents such as calcium, ferric ions have been reported to induce flocculation (Yue et al., 2008; Mishra et al., 2006). The combination of two or more of these agents can also enhance the process of flocculation. This process is considered economical but sometimes the high cost of the agents and the amount needed might be a disadvantage especially when treating disperse, sulfur and vat dyes (Fu and Viraraghavan, 2001). The flocculation process is also associated with concentrated sludge in large quantities and the removal is largely pH dependent (Lee et al., 2006).

Oxidation process: The oxidation process is simply the use of oxidizing agents for the treatment of dye wastewater. The method involves the use of chlorine (Omura, 1994), hydrogen peroxide (Hage and Lienke, 2006), Fenton's reagent (Wang, 2008; Meric et al., 2003), and ozone (Perkins et al., 1996; Wu et al., 2008a). The oxidation process is applied for treating the product water coming from primary treatment methods such as sedimentation. The oxidation process is considered as the most effective for decolourisation of dyes (Bandala et al., 2008), this is because; the process partially or completely degrades dyes especially for low molecular weight compounds. Theoretically, the dyes are expected to break down into CO_2 and water, even though this has not been 100 per cent achieved (Bandala et al., 2008). The oxidizing agents at times are assisted by the use of ultraviolet radiation (Bandala et al., 2008), and this led to the advanced oxidation processes.

Advanced oxidation processes: Advanced oxidation processes (AOP) are the use of more than one oxidation process to accomplish a better result. The main goal of the AOP process is to generate the reactive hydroxyl free radical (Tijani et al., 2014). This technique includes the combination of Fenton's reagent/oxidation (Namboodri and Walsh, 1996), UV-photolysis (Bandala et al., 2008) or sonolysis (Hong et al., 1999). The AOP system can work at ambient temperatures and pressure, and the main idea is to convert all these organic pollutants to CO_2. The chemical oxidation process involves the combination of ozone/ hydrogen peroxide. The UV based systems include; the combining of UV/hydrogen peroxide, UV/Ozone and UV/wet air oxidation. The photo-Fenton process is the combination of UV-light and Fenton's reagent. Photo-catalysis is another process which involves combining light energy and a catalyst for the degradation of dyes in water (Ghorai et al., 2007; Behnajady et al., 2006; Aguedach et al., 2005). Various chalcogenide oxides such as TiO_2, ZnO, ZrO_2 etc. have been used in photo-catalysis (Kansal et al., 2007). This process is capable of removing a wide range of dyes with the variation of parameters such as pH and catalyst concentration. The main drawback of AOP is the production of undesirable secondary metabolites as by-products which may be toxic themselves. Also, the decolourisation depends on pH and complete mineralisation has not often been achieved (Shah, 2014; Robinson et al., 2001), moreover inorganic contaminants are not removed.

Electrochemical treatment: This is a tertiary treatment of dye wastewater (Gupta et al., 2007; Lin and Peng, 1994). The decolourisation is achieved by electro oxidation with non-soluble anodes (Faouzi et al., 2007; Oliveira et al., 2007; Dogan and Turkdemir, 2005). Anodes such as iron, conducting polymer and boron doped diamond have been used for electro-degradation of dyes. It should be noted that the rate of decolourisation largely depends on the anode material and the working potential (Faouzi et al., 2007; Chen, 2004). The main drawback is the high electricity consumption of the system and the high risk involved in the process.

Biological treatment: This is the commonest and most readily available technique for treatment of dye wastewater (Barragan et al., 2007; dos Santos et al., 2007; Frijters et al., 2006). Numerous biological materials have been used for the decolourisation of dyes (Gupta and Suhas, 2009). The method is considered relatively inexpensive. The process can be aerobic or anaerobic or combined. Aerobic treatment (in the presence of oxygen) involves the use of micro-organisms such as bacteria and fungi (Rai et al., 2005; Sani and Banerjee, 1999). The enzymes created by these micro-organisms break down the organic pollutants. Research to identify and isolate these bacteria and fungi responsible for the break down has been on-going for the past few decades (Rai et al., 2005). Various parameters such as pH, concentration and temperature also play important roles in the process. Anaerobic treatment (absence of oxygen) has been used to treat dye waste water (Rai et al., 2005; Forgacs et al., 2004; Delee et al., 1998). This process is considered cheap because the cost of aeration is excluded. The two biological methods have been combined and found effective for the removal of dyes (Stolz, 2001). For example, the reduction of the azo bond can be achieved under anaerobic conditions and the post treatment with aerobic treatment would further break down and decolourise the compounds (Brown and Hamburger, 1987; Brown and Laboureur, 1983). The main drawback of biological treatment is that most dyes are non-biodegradable. Also this method is less organised, occupying large areas and cannot be made into a continuous flow system. Furthermore, the time required for the fermentation-decolourisation processes is extensive and therefore not suitable for quick production of potable water for domestic use (Crini, 2005; Bhattacharyya and Sarma, 2003; Robinson et al., 2001).

2.5 Filtration

The filtration process for water purification is a technique that has been in existence for ages. The method is being used for various purposes such as separation of materials, purification, identification and many more. It is the easiest method for treating drinking water (Machenbach, 1998). Filtration is divided into four depending on the membrane materials; namely; microfiltration, ultrafiltration, nano-filtration and reverse osmosis (Avlonitis et al., 2008; Cheremisinoff, 2002). The filtration process is considered as tertiary treatment of dye wastewater. The choice of membrane is the most important part of the filtration system. The choice of membrane and its effectiveness is reflected by the product of the process (Figure 2.6).
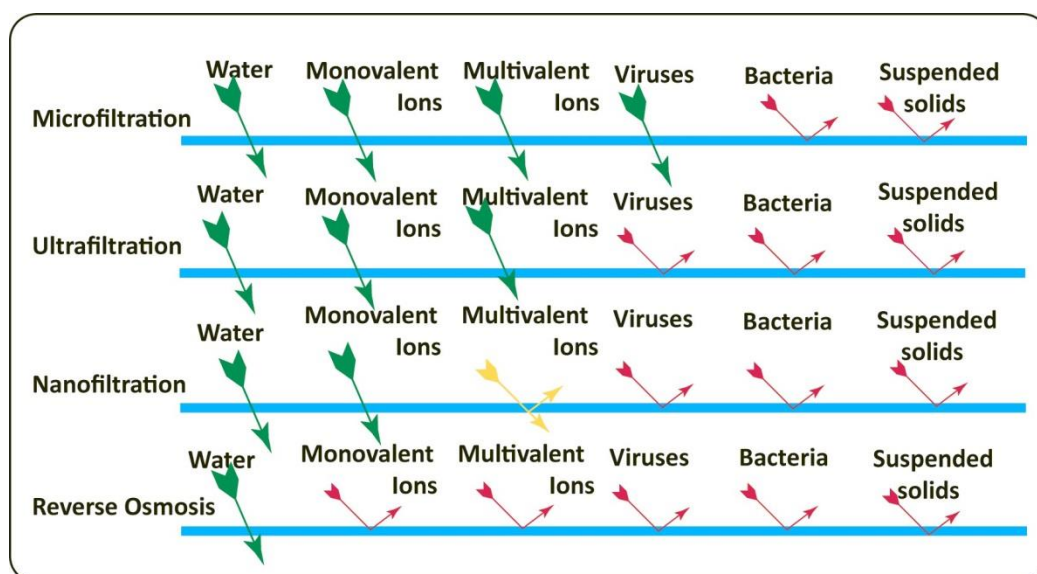
Figure 2.6: Permeability of membranes.
(**Source:** http://www.aquafieldservices.com/index.php/technologies/membrane-filtration).

Processes using membranes provide very interesting possibilities for the separation of hydrolysed dye-stuffs and dyeing auxiliaries and simultaneously reduce colouration and BOD/COD of the wastewater (Babu et al., 2007).

2.5.1 Membranes

Membranes offer semipermeable barriers that selectively allow the passage of some compounds but restrict others. Membranes have a wide range of separation

applications. For example, they are used in biomedical sciences for separation of blood components, cells, the controlled release of drugs and pharmaceutics into patients (Gupta and Suhas, 2009; Rothman and Orci, 1990; Sergent-Engelen et al., 1990). They have also been used for removal of bacteria, micro-organisms, particulates and organic materials (Gupta and Suhas, 2009). Membranes are also used for removal of colour, tastes and odour (Gupta and Suhas, 2009). All these applications have contributed to the rapid growth of membrane industries and the decrease in cost of membrane production. The main advantage of membrane filtration compared to others is the easy scalability and integration into other separation methods (Apel, 2013). Table 2.3 presents the classes of membranes and their pore sizes.

Table 2.3: Pore sizes of membranes.

	Symbol	Pore size µm	Operating pressure psi
Microfilter	MF	1.0-0.01	<30
Ultrafilter	UF	0.01-0.001	20-100
Nanofilter	NF	0.001-0.0001	50-300
Reverse osmosis	RO	<0.0001	225-1,000

Microfiltration (MF): The membrane used for micro filtration process has pore sizes of approximately 1.0-0.01 microns. This type of membrane can be used to remove substances such as sand, silt, clays, algae and some bacteria. Microfiltration is considered best for treatment of dye baths containing pigment dyes (Al-Malack and Anderson, 1997). This is to separate the chemical in the dye bath from the other substances. Microfiltration can also be used as pre-treatment for reverse osmosis and nano-filtration to decrease fouling (Ghayeni et al., 1998).

Ultrafiltration (UF): The membranes used for ultrafiltration have pore sizes of approximately 0.01- 0.001 microns and can be used to remove microbiological materials. Ultrafiltration can remove macro molecules and particles; however, the

removal of dyes is mostly an average of 55% (Watters et al., 1991), this is why ultrafiltration is also often considered as a pre-treatment for reverse osmosis and nano-filtration treatment of dyes (Ciardelli and Ranieri, 2001; Mignani et al., 1999).

Nano-filtration (NF): The membranes used for this process have pore sizes between 0.0001 to 0.001 microns. Pushing water through such small pores requires higher pressure compared to MF and UF (Table 2.3). The nano-filtration process is often preceded by adsorption in textile industries in order to decrease the concentration of dyes before the final filtration (Chakraborty et al., 2003; Freger et al., 2000; Rossignol et al., 2000). Nano-filtration membranes are capable of removing low molecular weight organic compounds, dyes and divalent ions.

Reverse osmosis (RO): This method is used to remove nearly all inorganic materials from water. The membrane pores are less than 0.0001 microns and the process can remove ions and dissolved non-ions as well as pesticides and bacteria. However, RO requires more pressure which is tantamount to high energy for separation (Table 2.3). Reverse osmosis membranes do have a retention rate of about 90% with high quality of permeate (Ghayeni et al., 1998; Treffry-Goatley et al., 1983). The removal of colour and chemicals in textile wastewater can be done by reverse osmosis. It has been particularly used for removal of mineral salts and reactive dyes (Sostar-Turk et al., 2005; Al-Bastaki, 2004; Marcucci et al., 2001).

Most membranes are made of synthetic polymers, though other forms such as ceramics and metallic membranes are also available. However, membranes for domestic use are often in polymeric form. They are less expensive and are easy to fabricate. Polymeric membranes do have surface charges and this helps in removing materials of opposite charge due to electrostatic attraction (Apel, 2013). Among polymers that have been used for membranes are polyacrylonitrile, polyethylene terephthalate, polypropylene, polysulfone, polyethersulfone and polyvinylidene fluoride (Apel, 2013; Apel, 2001).

2.5.2 Track-etched membranes

The ion tracking process is simply the damage done to solid materials (mostly polymer membrane) by swift heavy ion irradiation. The method allows the production of materials of micro- and nano- pores of various shapes with high aspect ratio (Apel, 2013; Ferain and Legras, 2003; Apel, 2001).

Basically, track-etched membranes are produced in two steps (Figure 2.7); in the first step, the swift heavy ion penetrates through the solid and this leads to damaging the materials, producing what is termed "latent ion tracks". This process is also called ion-irradiation. The second step is called the chemical etching. This involves the use of chemical etchants such as NaOH, which then convert the latent ion tracks into pores.
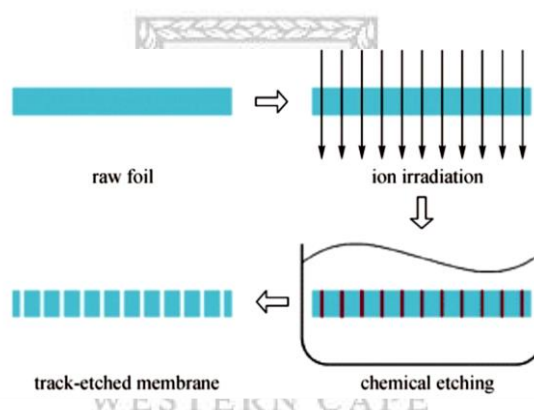
Figure 2.7: Schematic diagram of production of track-etched membrane (Wang et al., 2012a).

Etching is carried out at a controlled temperature with sodium hydroxide, hydrogen peroxide or acetic acid solutions. The pH of the solution can also affect the etching of the polymer. In-between these two steps mentioned above, there can be intermediate steps such as thermal treatment or UV light sensitization. The treatment with UV plays an important role as it affects the final pore size and shape of the pores. Overall, the strength of the modification of the polymer films depends on the deposited energy density, radiation sensitivity of the material, and the storage conditions of the polymer after the ion irradiation, as environmental conditions such as gases, temperature and light can affect the polymer film (Apel, 2001; Vilensky and Tolstikhina, 1999).

The morphology of the track-etched membrane is important in order to know the distribution of pores (pore density) on the membrane. Pores can be cylindrical (polyethylene terephthalate) (Figure 2.8) or tooth pick-like in shape as in the case of polycarbonate and polyester. Other polymers that have been track-etched include; polyvinylidene fluoride and polyimide (Apel, 2013).
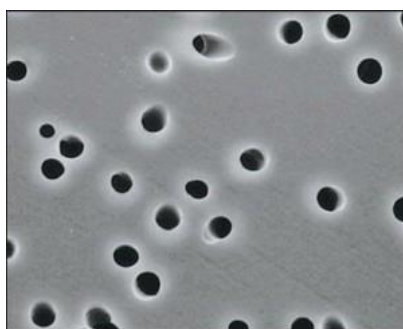
Figure 2.8: SEM image of PET track-etched membrane (Source; Apel, 2013).

Track-etched membranes have been used for several applications. The story of track-etched membrane has been encouraging in separation technologies. They are used in filtration, biomedical applications, templates for nanowires and as diode-like apertures (Apel, 2013).

Membranes (including track-etched) could also be used as support for catalyst via coating/immobilisation mechanisms (Barnes et al., 2004; Safi, 2000). A classical method known as magnetron reactive sputtering has been used for this type of coating (Barnes et al., 2004). Magnetron reactive sputtering can be defined as the sputtering of elemental targets in the presence of chemically reactive gases that mass react with both the ejected target material and the target surface (Safi, 2000). The method has become a classical technique in search for new and improved material properties. The process is considered complex and non-linear because it involves many inter-dependent parameters such as the pumping speed, the target-to-substrate distance, pulsed reactive gas flow, plasma emission monitoring and voltage control (Barnes et al., 2004; Safi, 2000). This method has widely been used for the deposition of compounds and alloy thin films including nitrides, oxides, carbides, fluorides etc. (Safi, 2000). Among these compounds, TiO_2 has been the most compound coated on

membranes through this method (Barnes et al., 2005). This is due to 3 facts; the various applications of TiO_2 which include the breaking down most organic pollutants such as dyes, pesticides and herbicides under UV light irradiation; magnetron reactive sputtering can as such coated membranes in industrial scale (Zhang et al., 2003a) and to overcome the challenge of recovering the powder from the treated water after TiO_2 has been used (Zheng et al., 2004; Zhang et al., 2003a).

2.5.3 Membrane fouling

Membranes can be hydrophilic (water loving) or hydrophobic (water-repulsing). This determines the wettability of the surface of the membrane and the ability to resist fouling, which is the main challenge in industrial separation. The performance of polymer membranes is often measured by the hydrophilicity of the membranes which can be measured using the contact angle. Hydrophilicity is preferred because it reduces fouling with negatively charge molecules and increases water permeability. Membrane fouling is also influenced by the surface chemistry of the membranes and colloidal particles, as well as the ionic environment (Lawrence et al., 2006; Salgin et al., 2006).

2.6 Adsorption and Ion-exchange

The adsorption process is considered the most used method for treating dyes wastewater (Bansal and Goyal, 2005; Imamura et al., 2002). In fact, adsorption can deal with a wide range of target pollutants (inorganics and organics in wastewater treatment) with high capacity and fast kinetics (Fu and Wang, 2011). The performance of the adsorption process largely depends on the type of adsorbents used. A good adsorbent is required to have pores and a large surface area which allow fast and high adsorption capacities (Saeed et al., 2008; Deng and Bai, 2003). It is noteworthy that adsorption is a surface phenomenon and therefore the efficiency of the adsorbent largely depends on its ability to adsorb solutes from the solution onto its surface. It is well known that adsorbents have generally been used in dye wastewater systems. Examples of adsorbents that have been used for removal of dyes include; alumina (Adak et al., 2005), silica gel (Alexander and McKay, 1977; Allingham et al., 1958) and zeolite (Alpat et al., 2008; Wang and Ariyanto, 2007; Nur

et al., 2005). Activated carbon, arguably the oldest adsorbent, has not only been used to remove dyes, but also taste and odour (Al-Degs et al., 2001; Pelekani and Snoeyink, 2000; Walker and Weatherley, 1999). Other adsorbents in circulation include clay minerals, oxide minerals, resins, TiO_2 and polymeric materials (Fu and Wang, 2011; Gupta and Suhas, 2009).

Ion exchange (IE) is defined as the exchange of ions between the immobilised solid particle and the medium in which the substrate is. Adsorption and IE are grouped as sorption process because both share common features such as batch and fixed bed processing (LeVan et al., 1997). However, IE is a reversible reaction and the ion exchanger can be reused many times, which is sometimes difficult to achieved via adsorption. Ion exchangers are mostly resins which are insoluble in aqueous and organic solvents. They are usually made of a cross linked polymer matrix with functional groups covalently bonded on them (Sherrington, 1998). Ion exchangers can be cationic or anionic depending on the counter-ions they carry. Resins vary in particle size distribution between 20-50, 50-100, 100-200 and 200-400 mesh. The particle sizes below 100 mesh are used when complexing agents are attached on the surface (Hubicki and Kołodyńska, 2012). IE has been used to remove dyes (Wu et al., 2008b; Liu et al., 2007; Delval et al., 2005). For instance, Delval et al. (2005) used starch based polymer cross linked with epichlorohydrin in NH_4OH, to remove various dyes from solutions.

2.7   Electrospinning process

Electrospinning is one of the processes in nanotechnology designed by researchers to fabricate nanoscale materials (Huang et al., 2003). It is generally defined as a process by which polymer nanofibres with diameters lower than 100 nm can be produced using an electrostatically driven jet of polymer solution (or polymer melt) delivered through a millimeter-scale nozzle (Bhardwaj and Kundu, 2010; Huang et al., 2003; Reneker et al., 2000). The idea of electrospinning, also known as electrostatic fibre processing method, came about when electrical forces were used to produce polymeric filaments as far back as 1934 (Formhals, 1934). The process occurs as the result of applying an electrical field to a highly conducting polymer

solution, which drives the formation of an electrically driven polymer solution jet (Taylor, 1969).

Electrospun nanofibres have interesting properties, such as a high porosity, small inter-fibre pore sizes, high gas permeability, high surface area to volume ratio, tuneable porosity and the ability to manipulate nanofibres' composition in order to get the desired properties and functions (Bhardwaj and Kundu, 2010; Huang et al., 2003). Electrospun fibres have been employed for several applications such as, high-performance air filters (Gopal et al., 2007; Hajra et al., 2003), protective textiles (Schreuder-Gibson et al., 2002), sensors (Zhao et al., 2012; Aussawasathien et al., 2011, Liu et al., 2004), advanced composites (Kim and Reneker, 1999), photovoltaic cells (Drew et al., 2002), wound dressings (Khil et al., 2003; Verreck et al., 2003), as scaffolds in tissue engineering (Fouad et al., 2013; Gautam et al., 2013; Pham et al., 2006) and in adsorptive membranes (Neghlani et al., 2011; Saeed et al., 2008; Zuwei et al., 2005).

2.7.1 Preparation and electrospinning of polymer solution

The electrospinning process is considered to start from the dissolution of the polymer to be electrospun. Before a polymer can be electrospun, it must completely dissolve in a suitable solvent to form a homogenous solution. This is the main challenge to overcome before polymers can be successfully electrospun. Many times, a mixture of solvents would be required to give the best result (Bhardwaj and Kundu, 2010). Dissolution is essentially carried out at room temperature and atmospheric condition; however, some polymers and even solvents may emit unpleasant or even harmful smells, so it is advised to carry out the processes in a ventilated chamber (Chronakis, 2005; Huang et al., 2003). Solvents chosen for electrospinning are usually volatile and are expected to dry up during the travelling of the polymer jets towards the collector (Nataraj et al., 2012; Yu et al., 2006). Therefore, solvent peaks are not expected on the ATR-FTIR spectra of nanofibres.

To make the electrospinning process more benign (free of solvents), some polymers have also been electrospun in molten form. Instead of bringing the polymer into solution, the powdered polymer is introduced into a syringe followed by the

application of heat to melt the polymer. The electrospinning process for a polymer melt is usually carried out in vacuum (Lyons et al., 2004). The vacuum is advantageous because higher electric field strength over large distances and higher temperatures can be used compared to when carried out in a ventilated chamber. Copolymerization, melt-blending or incorporation of fillers can also be part of polymer solution preparation in order to manipulate some properties such as mechanical strength, morphology, structure, pore size and distribution, biodegradability, thermal stability and barrier properties (Wang et al., 2005).

Polymer solution concentrations are prepared in weight percentage (wt%). After the appropriate solvent has been determined, the following must be known before the preparation; the weight percentage of polymer (g) to be dissolved in the solvent, the volume of solvent to be prepared (mL) and the density of the solvent (g/cm^3). The mass of polymer (solute) (g) is the only unknown. From equations 2.1 and 2.2, equation 2.3 can be derived; then substituting equation 2.4 into 2.3, equation 2.5 can be derived.

$$Wt\% = \frac{mass\ of\ Solute}{mass\ of\ Solution} \times 100 \dots\dots\dots\dots\dots\dots\dots\dots\dots equation\ 2.1$$

$$Mass\ of\ Solution = mass\ of\ Solute + mass\ of\ Solvent \dots equation\ 2.2$$

$$Wt\% = \frac{mass\ of\ Solute}{(mass\ of\ Solute + mass\ of\ Solvent)} \times 100 \dots\dots\dots equation\ 2.3$$

$$Mass\ of\ Solvent = density \times given\ Volume \dots\dots\dots\dots\dots. equation\ 2.4$$

Therefore, by making the mass of solute the subject of the formula:

$$Mass\ of\ Solute = \frac{Wt\% \times mass\ of\ Solvent}{100 - Wt\%} \dots\dots\dots\dots\dots\dots\dots equation\ 2.5$$

The resultant mass of the polymer given by the calculation is weighed and transferred into the solvent and stirred until it completely forms a homogenous solution. At times, heat can be applied before some polymers can completely dissolve e.g. polyacrylonitrile. Figure 2.9 is the schematic diagram of electrospinning set-ups.
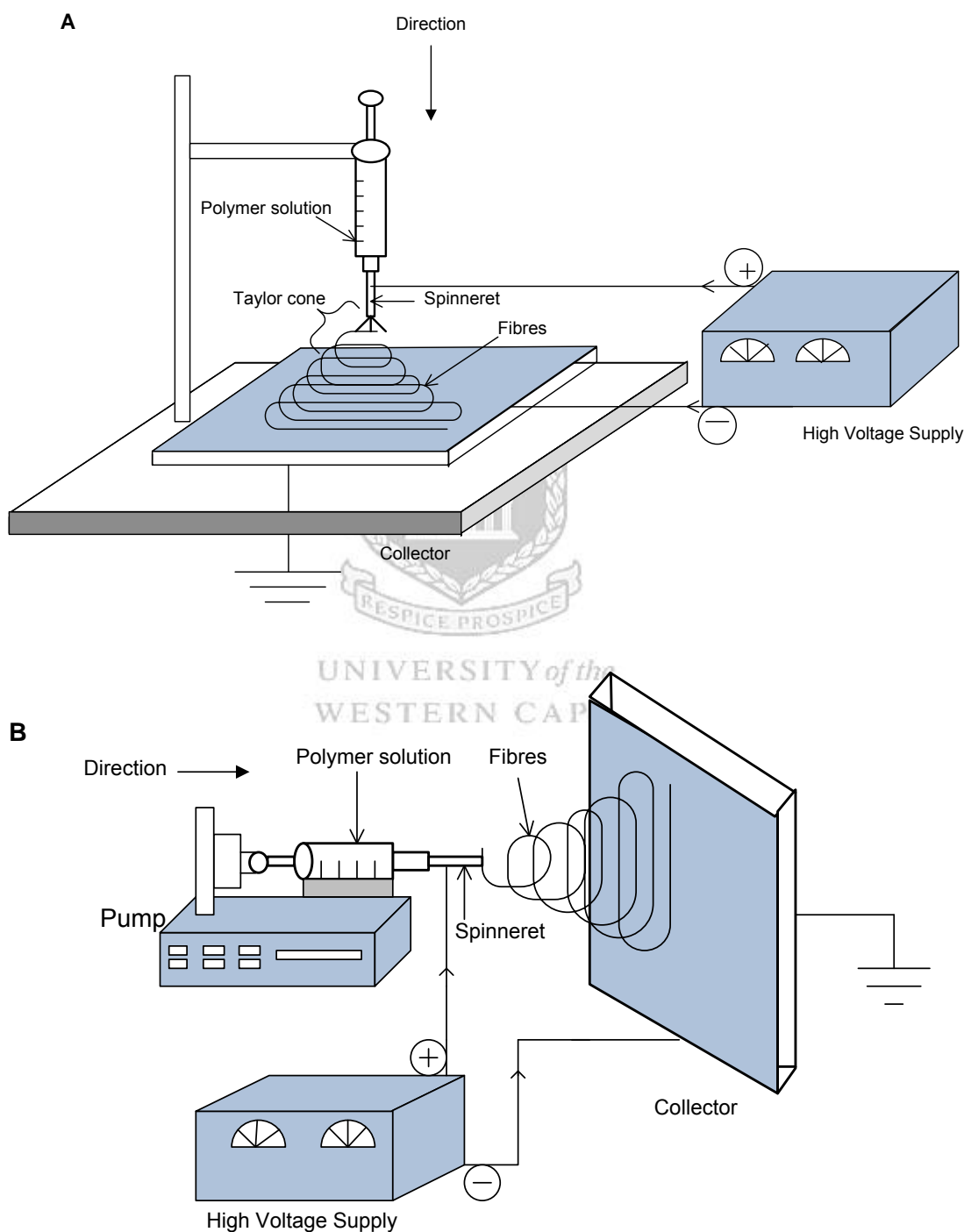
Figure 2.9: Vertical (A) and Horizontal (B) electrospinning set-ups.

Most electrospinning setups are either vertical (Figure 2.9 A) or horizontal (Figure 2.9 B) in alignment; however, due to the fact that researchers do have different interests in terms of the properties of fibres to be produced, other types of alignment/orientation can also be used in the laboratory (Stankus et al., 2006; Kidoaki et al., 2005). Basically, an electrospinning setup comprises three major components: a high voltage power supply, a spinneret (e.g., a pipette tip, needle) and a collector (usually a metal screen, aluminium covered-material, or rotating drum) (Fallahi et al., 2008; Saeed et al., 2008; Sill and Recum, 2008; Subbiah et al., 2005). During electrospinning, a polymer solution is introduced into a syringe. A metering syringe pump can be used to control the flow rate of the polymer solution. The voltage needed (usually from 8 kV -100 kV) is supplied by high voltage direct current (HVDC). The positive end of the HVDC is attached to the metallic needle of the syringe (which serves as electrode) to electrically charge the polymer solution. Consequently, the negative end of the HVDC is attached to the conductive collector screen (which serves as the counter-electrode) (Frenot and Chronakis, 2003). Basically, a polymer solution flowing through a capillary where a voltage is applied would form a stable "Taylor cone" because of a balance between surface tension and electrical forces within the liquid. The polymer solution jet is then emitted from the cone, which, as long as the polymer solution is sufficiently viscous would result in the formation of polymer nanofibres on the collector screen (Yun et al., 2007; Yu et al., 2006).

2.7.2 Factors that affect electrospinning of polymer solution

The parameters that affect electrospinning of the polymer solution are broadly grouped into three namely; the solution parameters (molecular weight of the polymer, concentration, viscosity, conductivity and surface tension), the process parameters (applied voltage, feed rate, types of collectors, motion of the target screen, distance between the spinneret tip and the collector and needle tip) and the ambient parameters (temperature, humidity and air velocity in the chamber) (Bhardwaj and Kundu, 2010; Huang et al., 2003). The interest of researchers when electrospinning the polymer solution is to have a setup that can electrospin fibres of (a) consistent and controllable diameters (b) defect-free (free of beads) and (c) collectable as continuous single fibres. However, research so far has shown that these

three targets are by no means easily achievable; this is due the aforementioned parameters. For instance, the polymer solution must have a concentration high enough to cause polymer entanglements yet not so high that the viscosity prevents polymer motion induced by the electric field. The solution must also have a surface tension low enough and a viscosity high enough to prevent the jet from collapsing into droplets before the solvent has evaporated. Again, changing the solution concentration directly affects other solution properties, such as the viscosity, conductivity and surface tension. So also, the morphology of the fibres can be affected upon increasing or decreasing the distance between the syringe needle and the collector. Increasing the distance or decreasing the electrical field strength decreases the bead density, regardless of the concentration of the polymer in the solution. Many of these parameters as a matter of fact are interwoven and a little deviation can affect the whole process. Therefore, optimisation of the process starting from the dissolution of polymer to solution parameters, process parameters and ambient parameters are essential. Typically, a trial-and-error approach has been employed in which solution properties and process parameters are varied until uniform, defect-free fibres are obtained (Chronakis, 2005; Li and Xia, 2004). The following subheadings describe the effects that these parameters have on spinability of the polymer solution and the resultant nanofibres.

2.7.3 Solution parameters

2.7.3.1   Concentration

Concentration is one of the major factors that can influence the ability of a polymer solution to produce nanofibres during the electrospinning process. For nanofibre formation to occur, a minimum solution concentration is required for sufficient chain overlap, otherwise uniform nanofibres will not be obtained (Shenoy et al., 2005). Once this minimum concentration is obtained, other process parameters can then be varied (Pham et al., 2006). At a low solution concentration, a mixture of beads and fibres are obtained and at high concentration the formation of continuous fibres are prohibited because of the inability to maintain the flow of the solution at the tip of the needle resulting in the formation of larger fibres (Sukigara et al., 2003). However, as optimum solution concentration is approached, nanofibres of spherical

shape, free of beads with uniform diameter are formed (Haghi and Akbari, 2007; McKee et al., 2004; Ryu et al., 2003; Liu and Hsieh, 2002; Deitzel et al., 2001). The diameter of the nanofibres produced by electrospinning has been found to increase with an increase in solution concentration when the same voltage is applied (Jun et al., 2003; Fong et al., 1999).

2.7.3.2 Viscosity

Solution viscosity (controlled by changing the polymer concentration) plays an important role in determining the range of concentrations from which continuous fibres can be obtained in electrospinning (Deitzel et al., 2001). For solutions that are too concentrated (and therefore too viscous), the droplet dries out at the tip before jets can be initiated, preventing electrospinning (Duan et al., 2004; Demir et al., 2002; Fong et al., 1999), thus there is a requirement of optimal viscosity for electrospinning either in solution or in melt (Sukigara et al., 2003; Deitzel et al., 2002; Buchko et al., 1999; Doshi and Reneker, 1995). The nature of elongational flow of the polymer jet, which is controlled by viscosity, determines the degree of stretching of the fibres (Raeesi et al., 2009; Shenoy et al., 2005). At a certain viscosity, a secondary jet may erupt from the main jet or Taylor cone, which is able to yield fibres of a narrower diameter; hence, different nanofibre diameter distribution may be produced (Ramakrishna et al., 2005; Demir et al., 2002).

2.7.3.3 Molecular weight

Molecular weight of the polymer reflects the number of entanglements of polymer chains in a solution. High molecular weight polymer solutions are good for electrospinning as they provide the desired viscosity for fibre formation (Bhardwaj and Kundu, 2010; Huang et al., 2003). A high molecular weight solution gives fibres with larger average diameters. It has been observed that too low molecular weight solutions are difficult to electrospin as enough entanglements of the polymer chain could not be achieved (Huang et al., 2003), however, even at a low polymer concentration, where sufficient number of entanglements of the polymer chains can be achieved, polymer nanofibres can be formed (Tan et al., 2005a; Deitzel et al., 2001).

2.7.3.4   Surface tension

The composition of the solution plays an important role in determining the surface tension of the polymer solution to be electrospun. Therefore the solvent(s) to be used and the mass of polymer must give the suitable minimum surface tension for the proper electrospinning of the polymer solution. Generally, the high surface tension of a solution can prevent easy electrospinning of the polymer solution, however at low surface tension, polymer solutions are easily electrospun with production of bead-free nanofibres even at lower electric field (Bhardwaj and Kundu, 2010; Hohman et al., 2001; Doshi and Reneker, 1995). During optimisation of surface tension for electrospinning of polymer solutions, a certain range suitable for electrospinning does occur (upper and lower boundaries of the electrospinning window) provided that all other variables are kept constant (Pham et al., 2006; Fong et al., 1999).

2.7.3.5   Conductivity/Surface charge density

Polymer solution conductivity is mainly determined by the polymer type, solvent used, and the availability of ionisable salts. It has been found that increasing the solution conductivity or charge density can be used to produce more uniform nanofibres with a decrease in the diameter. Low conductivity of the solution results in insufficient elongation of a jet by the electrical force to produce nanofibres, and beads may be observed (Kim et al., 2005a). If the solution is absolutely insulating, or the applied voltage is not high enough so that electrostatic force cannot overcome the surface tension, no fibre can be produced by electrospinning. One approach to increasing solution conductivity has been through the addition of salt to the polymer solution. Ionic salts such as KH_2PO_4, NaH_2PO_4, $LiCl$ and $NaCl$ were demonstrated to help in the production of uniform, reduced diameter and beadless nanofibres (Zong et al., 2002). It was hypothesised that some volatile salt additive would not remain in the fibres and therefore would not affect the properties of electrospun fibres (Jun et al., 2003). Conductivity has also been increased by the addition of alcohol to the solvent, resulting in smoother fibres with fewer beads present (Kim et al., 2005b).

2.7.4 Process parameters

2.7.4.1 Applied voltage/Field strength

In the electrospinning process, the surface tension of the solution determines the initiating voltage for electrospinning. The voltage must be high enough to overcome the surface tension of the polymer solution. A highly viscous or high concentration solution requires a high application of voltage to overcome its surface tension to initiate electrospinning (Buchko et al., 1999; Doshi and Reneker, 1995). At the optimum voltage applied, a stable solution jet is ejected from the surface of the droplet leading to the migration of the nanofibres toward the collector (Teo and Ramakrishna, 2006). Researchers have suggested that when higher voltages are applied, there is more polymer ejection and this facilitates the formation of a larger diameter fibre (Zhang et al., 2005b; Demir et al., 2002). Other researchers have also observed that a higher voltage causes greater stretching of the solution due to the greater columbic forces in the jet as well as a stronger electric field and these effects lead to reduction in the fibre diameter and also rapid evaporation of solvent from the fibres results (Heikkila and Harlin, 2008; Buchko, et al., 1999). At low voltages or field strengths, a drop is typically suspended at the needle tip, and a jet will originate from the Taylor cone producing bead-free spinning (assuming that the force of the electric field is sufficient to overcome the surface tension) (Deitzel et al., 2001). As the voltage is increased, the volume of the drop at the tip decreases, causing the Taylor cone to recede. The jet eventually moves around the edge of the tip, with no visible Taylor cone. The jet originates from the liquid surface within the tip, and beads are seen (Pham et al., 2006; Zhang et al., 2005b; Ding et al., 2002; Deitzel et al., 2001).

2.7.4.2 Feed rate/Flow rate

The flow rate of the polymer solution from the syringe is an important process parameter as it influences the jet velocity and the material transfer rate. There should always be a minimum flow rate of the spinning solution. Few studies have systematically investigated the relationship between solution feed or flow rate on fibre morphology and size (Megelski et al., 2002; Zong et al., 2002). In general, it was found that lower flow rates yielded nanofibres with smaller diameters as the solvent

will have enough time for evaporation (Zong et al., 2002). However, flow rates that were too high resulted in beading since nanofibres did not have a chance to dry prior to reaching the collector (Pham et al., 2006; Kim et al., 2005a; Zhang et al., 2005b; Zuo et al., 2005; Wannatong et al., 2004).

2.7.4.3   Types of collectors

The collector serves as a substrate where the nanofibres are collected. A collector can be a good conductive material such as aluminium foil, conductive paper, conductive cloth, wire mesh, rotating rod, rotating wheel, and water (Ko, 2006; Sundaray et al., 2004; Li et al., 2004; Xu et al., 2004). They can also be poor conducting materials such as a liquid e.g a methanol coagulation bath and even the human hand (Hohman et al., 2001). Collectors can also be designed to be static or placed on a rotatory drum so as to influence the isotropic or anisotropic alignment of the fibres in the mats (Lu et al., 2008; Xu et al., 2004). The use of metal as conductive collectors helps to dissipate the charges and also reduce the repulsion between the fibres. Therefore, the nanofibres collected are smooth and densely packed. Conversely, the fibres collected on poor conductive material as collectors do not dissipate the charges which repel each other; hence, the nanofibres are less densely packed (Ko, 2006). When nanofibres are collected on a static collector screen, anisotropy (i.e the property of being directionally dependent) in the in-plane tensile behaviour seems to not have been reported, in other words, they are isotropic (identical properties in all directions). However, when the membranes were obtained from a rotating drum, electrospun nanofibres have different properties in different directions i.e they are anisotropic (Lee et al., 2002). Frame collectors were shown to yield aligned fibres with a conductive frame producing better alignment than a poor conductive one (Zarkoob et al., 2004). Fibres that are collected on pure wire screens are easily transferred to other substrates compared to other collectors such as aluminium foil. Fibres that are collected using a rotating cylindrical drum collector are better aligned when compared to a stationary target (Dror et al., 2003; Zong et al., 2002). The use of high speed rotational collectors leads to a "fanning" effect and the evaporation of the solvent is much quicker compared to the stationary collectors (Baji et al., 2010; Yee et al., 2008). However, the speed must be monitored to avoid the breaking of the fibre jet. Meanwhile, the reason why a perfect alignment is difficult to achieve can be

attributed to the fact that the chaotic motions of polymer jets are not likely to be consistent and are less controllable (Yee et al., 2008; Zussman et al., 2006; Liu and Hsieh 2002; Kim et al., 2005a).

2.7.4.4 Distance between the collector and the nozzle

It has been found that a minimum distance is required to give the fibres sufficient time to dry before reaching the collector (Geng et al., 2005; Ki et al., 2005; Lee et al., 2004). The collection distance determines the jet flight time and the electric field strength needed (Demir et al., 2002). Reduction in the collection distance decreases the jet flight time and solvent evaporation time whereas when the electric field strength increases it causes instability of the Taylor cone and jet initiation (Ding et al, 2002; Fong et al., 1999). Increasing the collection distance resulted in reduced electric field strength which stabilised the Taylor cone to produce a single jet (Jarusuwannapoom et al., 2005).

The fibre diameter may decrease with increasing collection distance due to sufficient time for solvent evaporation as more time is given for solvent evaporation which further thins and splits the jet producing finer fibres (Yördem et al., 2008; Li et al., 2006). Conversely, studies have shown that increasing the collection distance can lead to increased fibre diameter. Lee et al. (2004) and Zhao et al. (2004) suggested that the electric field strength is weaker due to the longer distance, thus reducing its stretching which resulted in nanofibres with larger diameters. It has been reported that flatter fibres can be produced at closer distances but with an increase in distance rounder fibres have been observed (Pham et al., 2006; Huang et al., 2003). This is because of solvent remaining in the fibres; fibres tend to merge together when they come into contact and consequently are fused together. Deitzel et al. (2002) and Megelski et al. (2002) found that decreasing the collection distance induced the formation of beaded fibres while Demir et al. (2002) found that increasing the collection distance decreased the bead density.

2.7.4.5   Number of nozzle tip and placement

Some electrospinning set-ups could have more than one nozzle depending on the capacity of pumping machine and area of the target collector. This can be done to increase the rate of production of fibres or to produce blends of polymers (Theron et al., 2005). The use of multiple nozzle tips have also been used to prepare blends of PVA and cellulose acetate (Ding et al., 2004). Using four tips and varying the number containing PVA and cellulose acetate allowed for fibres with various weight ratios of PVA and cellulose acetate to be produced. Li et al. (2004) developed a coaxial, two-capillary spinneret. Using feeds consisting of two immiscible liquids, they were able to produce hollow nanofibres (Li et al., 2004).

2.7.5 Ambient parameters

Few studies have been conducted to examine the effects of ambient parameters (i.e., temperature and humidity) on the electrospinning process. Studies showed that they are also important parameters that affect the electrospinning process if not controlled. Generally, room temperature (25°C) is suitable for electrospinning but in some cases where the temperature is low, there might be a need to raise the temperature with the aid of an electric heater or other heating device. Investigations conducted by Mit-Uppatham et al. (2004) showed that the temperature range of 25°C-60°C was good for electrospinning of polyamide 6 fibres and they found that increasing the temperature yielded fibres with a decreased fibre diameter. The decrease in diameter was attributed to the decrease in the viscosity of the polymer solutions at increased temperatures. At higher temperature the rate of solvent evaporation from the ejected jet increases significantly and a skin is formed on the surface of the jet, which results in the collection of dry, smaller diameter fibre, with smooth surfaces (Raeesi et al., 2009; Deitzel et al., 2001; Koombhongse et al., 2001).

It has also been shown that controlling the humidity can aid the electrospinning of the polymer solution (Pham et al., 2006; Li and Xia, 2004). The variation in humidity during electrospinning of polystyrene solutions was studied and showed that by increasing humidity there is an appearance of small circular pores on the surface of the fibres; further increasing the humidity leads to the pores coalescing (Casper et al.,

2004). At a very low humidity, a volatile solvent may dry rapidly as the evaporation of the solvent is faster. Sometimes the evaporation rate is fast compared to the removal of the solvent from the tip of the needle and this would create a problem with electrospinning. As a result, the electrospinning process may only be carried out for a few minutes before the needle tip is clogged.

2.7.6 Characterisation of electrospun nanofibres

In order to empirically understand electrospinning process, assessment of the entire process from polymer selection to the nanofibre should be accurately carried out. Generally electrospun polymer fibres are characterised for better understanding of their geometry, physical and structural, mechanical, chemical and crystallinity properties (Lyons and Ko, 2005).

2.7.6.1   Geometric characterisations

Geometric properties of polymer nanofibres such as fibre diameter, diameter distribution, fibre orientation and fibre morphology can be characterised using scanning electron microscopy (SEM), transmission electron microscopy (TEM) and atomic force microscopy (AFM) (Demir et al., 2002; Li et al., 2002; Megelski et al., 2002). SEM is the quickest method for observing the surface morphology and diameters of electrospun fibres. Transmission electron microscopy (TEM) is another alternative for obtaining fibre diameters for extremely small fibres (<300 nm). The use of TEM does not require the sample to be in a dry state as that of SEM, hence, nanofibres electrospun from a polymer solution can be directly observed under TEM. Meanwhile, both instrumental analyses need only a small amount of sample. AFM is another and actually the best instrument to observe any type of surface morphology and exact descriptions of the fibre surface. For a precise measurement, two fibres crossing each other on the surface are generally chosen. The upper horizontal tangent of the lower fibre is taken as a reference, and the vertical distance above this reference is considered to be the exact diameter of the upper nanofibres (Kim and Reneker, 1999; Jaeger et al., 1996; Srinivasan and Reneker, 1995). AFM can also be used to characterise the roughness of fibres. The roughness value is the

arithmetic average of the deviations of height from the central horizontal plane given in terms of millivolts of measured current (Demir et al., 2002).

2.7.6.2   Chemical characterisations

Chemical characterisations are carried out to know the molecular structure of nanofibres. Surface chemical properties of fibres can be determined by attenuated total reflectance Fourier transform infra-red (ATR-FTIR) and X-ray photoelectron spectroscopy (XPS) analyses. The quickest method is done by ATR-FTIR. The peaks from the results would show the molecular component of the fibres (Huang et al., 2000). This technique plays a major role in characterising modified nanofibres (either surface or blend). Not only can the structure of surface modified/blend be detected but also the intermolecular interaction can be determined by the use of this method (Huang et al., 2001). XPS is used to characterise the surface modified fibres for any new bonds formed (Kampalanonwat and Supaphol in 2011; Deng et al., 2003a). Surface chemical properties of nanofibres can also be evaluated by their hydrophilicity, which can be measured by the water contact angle analysis of the nanofibres' membrane surface (Huang et al., 2003; Deitzel et al., 2002).

2.7.6.3   Physical characterisations

Physical characterisation or rather the transport properties of fibres include; air and vapour transport, electrical transport, thermal properties and porosity (Norris et al., 2000; Buchko et al., 1999). Air, vapour and liquid transport properties of electrospun nanofibres have been measured using an instrument called dynamic moisture vapour permeation cell (DMPC) (Gibson et al., 1999; Gibson et al., 1995). The instrument is designed to measure air permeability and moisture vapour transports of fabrics (Huang et al., 2003). Fibres that are cross-linked do have a significantly reduction in air and vapour transports (Schreuder-Gibson and Gibson, 2002). Wang et al. (2002) measured the conductivities of polyacrylonitrile (PAN) nanofibres by using a digital electrometer with two neighbouring contacts of 4 mm distance. The PAN nanofibres exhibited a resistance which was beyond the upper limit of the electrometer (Wang et al., 2002). The thermal properties of poly (ethylene terephthalate) (PET) and poly (ethylene naphthalate) (PEN) polymers were characterised using thermal gravimetric

analysis (TGA) (Kim and Lee, 2000). It was found that the electrospinning of these polymers resulted in a decrease of the glass transition temperature (Tg) and crystallization peak temperature (Tc) of PET and PEN respectively. Meanwhile, the crystalline melting peak temperatures (Tm) of PET and PEN were almost the same before and after electrospinning (Kim and Lee, 2000). The porosity and pore size of nanofibres are also characterised. The pore size measurement can be conducted by a capillary flow porometer or mercury porosimetry (Li et al., 2002; Schreuder-Gibson et al., 2002; Stillwell, 1996). *Brunauer, Emmett and Teller* (BET) is the most frequent method for determination of specific surface area of porous materials (Jing et al., 2016; Brunauer, et al., 1938). Jing et al. (2016) used BET to analyse PAN nanofibres before and after modification with diethylammonium dihydrogen phosphate (DEAP). The results showed a surface area 12.3 m^2/g and 9.4 m^2/g for modified PAN and pristine PAN, respectively. The increase in surface area after modification was attributed to an increase in roughness of the modified PAN nanofibres.

2.7.6.4   Mechanical characterisations

Mechanical characterisations of nanofibres such as Young's modulus, tensile strength, and the strain at break are performed by application of tensile test loads (Yee et al., 2008; Shields et al., 2004; Huang et al., 2004). A commercial nano-tensile testing system (Nano Bionix System, MTS, TN, USA) has been used to conduct the tensile test for the evaluation of mechanical properties of nanofibres (Naraghi et al., 2007; Yuya et al., 2007; Chew et al., 2006; Inai et al., 2005; Tan et al., 2005b). Mechanical characterisations of individual nanofibres may be difficult due to their very small dimensions (Baji et al., 2010; Fennessy and Farris, 2008; Wong et al., 2008; Li et al., 2002). This makes the established methods and standards for determining the mechanical behaviour of nanofibres inadequate. This is probably one of the main reasons why articles addressing the mechanical tests of single nanofibres are rare in the literature.

2.8   Electrospun polymers

To date, a large number of polymers have been successfully electrospun and substantial research has been carried out to gain in-depth understanding of the

electrospinning process for better control of fibre formation (Pereao et al., 2016; Bhardwaj and Kundu, 2010; Gopal et al., 2006; Subbiah et al., 2005; Wannatong et al., 2004; Huang et al., 2003). The choice of polymer to be electrospun could depend on the ease of dissolution in organic solvents, choice of fibres diameter and the proposed applications. This following subsection shall discuss the polymers that will be electrospun in this research.

2.8.1 Electrospinning of polyamide 6

Polyamide 6 (PA6) (Figure 2.10), also called nylon 6, is a polymer (made from caprolactam monomer) developed in order to reproduce the properties of nylon 6, 6. It is a semi-crystalline polymer, polymorphic and biodegradable because of the strong hydrogen bonds between molecular chains. Unlike other nylons, PA6 is formed via ring opening polymerisation and not condensation as in other polymers. It is generally white with a density of 1.14 g/cm^3. PA6 is tough with high tensile strength. It melts at 215°C. PA6 has found many applications in engineering plastics industries because of good mechanical properties. It has also found applications such as surgical suture, musical instruments, filaments, nets and gun frame.
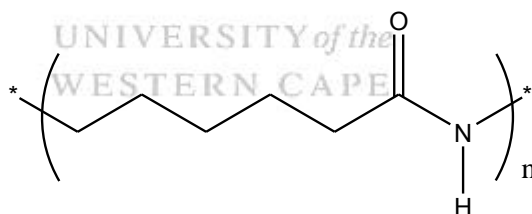
Figure 2.10: Structure of polyamide 6.

Polyamide 6 is known as the first commercially synthesised fibre. PA6 fibres are traditionally produced via, melt, dry and wet spinning, with diameters ranging from 10 to 500 micrometers (Zimmerman, et al., 1988; Gaylord and Piatzer, 1975). However with the growing interest in production of nano-materials, electrospinning has been used to produce PA6 nanofibres with diameters in the nanometer range. Electrospun PA6 has found application in filters, composite reinforcement, drug

carriers and tissue engineering scaffolds (Ryu et al., 2003; Dai et al., 2002; Deitzel et al., 2002).

Several studies have investigated the electrospinning parameters of PA6. Amongst these parameters are; concentration, voltage, flow rate, solvent and molecular weight (Nirmala et al., 2014; Heikkilä and Harlin, 2008). Moreover, parameters such as polarity of emitting electrode, strength of electric field, solution temperature, and addition of salt have also been studied (Supaphol et al., 2005; Mit-uppatham et al., 2004). PA6 nanofibres are usually prepared with a metallic salt to form a spider net morphology (Nirmala et al., 2010; Heikkilä and Harlin, 2008) (Figure 2.11). The morphology showed that it has high surface area to mass to volume ratio, small inter-fibrous pore size with high porosity. The concentration of 7 wt%, 8wt%, 10 wt%, 15 wt% and 22 wt% of PA6 have been electrospun in single or mixed solvents into nanofibres (Nirmala et al., 2014; Nirmala et al., 2010; Heikkilä and Harlin, 2008).
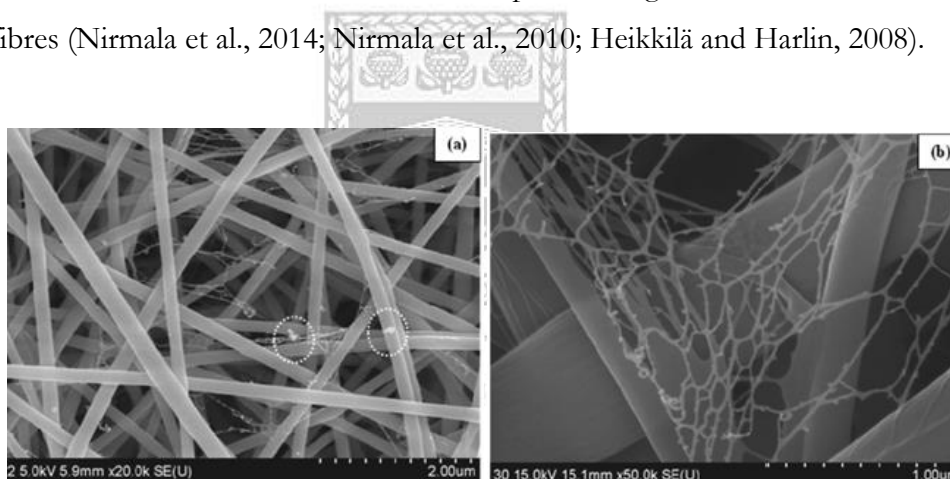
Figure 2.11: SEM images of PA6-nfs (a) ultrafine nanofibres and (b) spider net morphology (**Source**; Nirmala et al., 2010).

It has been noted that the solvent plays the most significant role when considering solution parameters. Generally, polymers with reactive functional groups may undergo chemical exchange with the solvents. For example, a polar protic solvent such as formic acid with high dielectric constant and low polarity can attack the lactam to produce a series of short chain oligomers ($CONH_2$) and formate (HCOO-) ions (Tsou et al., 2013; Nirmala et al., 2010). Table 2.4 shows that polyamide 6 has been electrospun into ultrafine nanofibres with fibre diameters as low as 8 nm in different solvents especially formic acid (Nirmala et al., 2014; Ding et al., 2006).

Table 2.4: Different solvents for electrospinning of PA6 (Nirmala et al., 2014).

Materials	Solvent	Key Factor	Ultrafine Nanofiber Diameter (nm)
Polyamide 6	Formic acid	Applied voltage	8-40
Polyamide 6	Formic acid + Dichloro Methane (3:2)	Solvent	13-34
Polyamide 6	Formic acid + acetic acid (3:2)	Solvent	8-38
Polyamide 6	Formic acid + acetic acid (4:1)	Solvent	8-32
Polyamide 6	Formic acid + Chlorophenol (1:1)	Solvent	8-30
Polyamide 6/Chitosan	Formic acid	Solvent	20-40
Polyamide 6/Lecithin	Formic acid	Solvent	10-30
PAN/nylon 6	Formic acid + acetic acid (4:1)	Monomer	20
PAA/Nylon 6	Formic acid	Monomer	19
Nylon 6	Formic acid + acetic acid (4:1)	Inorganic salt	10-30
PU	THF+DMF	Inorganic salt	10-30
PVA	Water	Inorganic salt	10-30
PAA	Water + ethanol	Humidity, applied voltage	10-20
Nylon 6	Formic acid	Humidity, applied voltage	10-20
PVA/ZnO	Water + zinc acetate solution	Metal oxide	25-50
Nylon 6/TiO$_2$	Formic acid + acetic acid (4:1)	Metal oxide	30-50

Note; PAN (poly acrylonitrile); PAA (polyacrylic acid); PU (polyurethane); PVA (poly vinyl alcohol); THF (tetrahydrofuran); DMF (N,N-dimethyl formamide); ZnO (zinc oxide).

Other solvents that have been used for electrospinning of PA6 include; dichloromethane, acetic acid, hexafluoroisopropanol, chlorophenol etc. Also mixtures of formic acid with solvents such as chloromethane, acetic and chlorophenol have also been used for electrospinning of polyamide 6 (Table 2.4). According to previous work, formic acid is considered to be the best solvent for electrospinning of PA6. This is because the conductivity of PA6 in formic acid is very high with the presence of free ions in solution (Tsou et al., 2013).

2.8.2 Electrospinning of polyacrylonitrile

Polyacrylonitrile (PAN) (Figure 2.12 (A)) is one of the most widely used synthetic polymers with an average annual production of 2.73 million tons (Fischer-Colbrie et al., 2007; Saurer Management, 2004).

Figure 2.12: Polyacrylonitrile (A) and copolymer of acrylonitrile and methylacrylate (B).

PAN and its copolymers are predominantly white powders and are stable up to a temperature of 250°C, after which they begin to turn brown due to degradation. Although PAN melts above 300°C, yet it is considered not useful for plastic materials because it degrades before melting. For several decades after the discovery of PAN in 1893, efforts made to convert PAN into fibres proved abortive because of the difficulty encountered during dissolution. The difficulty was recently explained to be as a result of electrostatic forces between the dipoles of adjacent nitrile ($C{\equiv}N$) groups (Figure 2.12 (A)) which invariably restrict the bond rotation, leading to a stiffer chain (Bai et al., 2006). This also explains why only strong polar solvents can dissolve PAN.

Electrospun PAN-nfs has attracted a great deal of attention due to varieties of outstanding characteristics such as good thermal stability, chemical resistance and good mechanical properties (Wang et al., 2007; Shoushtari et al., 2006; Deng and Bai, 2003). Also, PAN-nfs are resistant to most solvents, bacteria and photo irradiation (Saeed et al., 2008; Tahaei et al., 2008; Wan et al., 2006; Bilba et al., 2004; Shin et al., 2004). PAN has been cross-linked by radiation (Liu et al., 2012) or glutaraldehyde (Zhang et al., 2009). Cross-linking of PAN-nfs will impart some of its important physical properties, such as insolubility and resistance to swelling in common organic solvents (Zhang et al., 2009). PAN-nfs are hydrophobic with a low density (1.184 g/mL at 25°C) and this has prevented their use in some potential applications (Wang et al., 2007; Hochart et al., 2003), however, the surface modifications of PAN-nfs make them less hydrophobic (Neghlani et al., 2011).

Just like every other nanofibre, PAN-nfs and its surface modified analogues find many applications in the areas such as nanofiltration, composites, protective clothing,

nanosensors, gas separation technology, energy storage, pervaporation and biomedical applications (Nataraj et al., 2012; Neghlani et al., 2011; Zhang et al., 2010a; Frahn et al., 2004; Iwata et al., 2003). PAN-nfs have been widely used as precursor for carbon nanofibres (CNF) (Nataraj et al., 2012). This is because of its high carbon yield (approximately 56%). Also, a desired final structure of carbon in the nanofibres products with good stabilisation can be achieved when PAN-nfs are used. This is due to the formation of ladder structure via polymerisation of the nitrile groups (Nataraj et al., 2012; Yusof and Ismail, 2012; Liang et al., 2011; Xu et al., 2006). Apart from being used as precursor for CNF, PAN nanofibres have also been widely reported to serve as supports for enzymes and ligands (Mei et al., 2012; Zhang et al., 2010b; Jain et al., 2009; Jia and Yang, 2007; Jia and Du, 2006). The immobilisation of ligands on PAN-nfs is done to improve their adsorption capabilities and also to ensure their recovery and reusability; hence, the use PAN-nfs in adsorption studies are noteworthy. The complexation of transition metal catalysts on the surface of chemically modified PAN-nfs has also played a major role in catalysis most especially in Fenton's chemistry (Zhenbang et al., 2010; Ishtchenko et al., 2003; Vitkovskaya et al., 2003).

Though, solvents capable of dissolving PAN are now known, it is much easier to dissolve its co-polymer counterparts other than its homo-polymer analogue, especially when preparing them for electrospinning. This explains why most PAN nanofibres are co-polymers of acrylonitrile and most often methylacrylate (Figure 2.12 (B)) (Deng et al., 2003a). Polar solvents such as dimethylformamide (DMF), dimethylsulfoxide (DMSO), N-Methyl-2-pyrrolidone (NMP), dimethylacetamide (DMAC), dimethylsulfone and tetramethylsulfide, to mention a few, dissolve PAN. However, heating the mixture of PAN and any of the aforementioned solvents to a temperature of about 60^{0}C aids the faster and complete dissolution of PAN (Zhang et al., 2011; Ji et al., 2009).

According to available literature, DMF is the most used solvent for dissolution of PAN for electrospinning process (Table 2.5). Table 2.5 presents various parameters that have been used to electrospin PAN solutions and its inorganic blends. For quick optimisation, the concentration of the PAN solution is varied first while fixing other

parameters. The general trend for PAN is that; its fibre diameter increases with an increase in concentration and bead formation is often reported at higher concentrations, these observations were deduced from scanning electron microscopy (SEM) images (Horzum et al., 2012; Neghlani et al., 2011; Saeed et al., 2011; Zhang et al., 2010a; Saeed et al., 2008).

Table 2.5: Electrospinning of PAN solution and its composite with various parameters.

Authors	Materials	Solvents	Conc. (wt%)	Voltage applied (kV)	Distance (cm)	Flow rate (mL/hr)	Temp. (^{0}C)	Needle inner diameter (mm)	Fibre diameter (nm)
Chen et al., 2014	PAN/PMMA	DMF	8	15	12			0.8	432
Zhang et al., 2014	PAN	DMF		12	15	0.8	AB		320
Elzatahry, 2014	PAN/NiO	DMF		20	17	0.5			
Horzum et al., 2012	PAN	DMF	4	15	5	2	AB	0.2	122
Mei et al., 2012	PAN	DMF	10	17	15	4	20	0.6	539
Zhang et al., 2012	PAN/MnAc	DMF	9/17.5	15	15			1	200-350
Kampalanonwat and Supaphol., 2011	PAN	DMF	10	15	20		AB		192
Neghlani et al., 2011	PAN	DMF	10 & 12	20	15	0.2	AB	0.51	110/300
Saeed et al., 2011	PAN	DMF	15	20	15	1	50	0.5	300
Yu et al., 2010	PAN	DMF/H_2O	2,5,8	15	13	1.2	AB		
Zhang et al., 2010a	PAN	DMAC	12	15	15	1	25	0.3	200-400
Ji et al., 2009	PAN/ZnCl$_2$	DMF	7,15	14	15	0.5		0.3	290
Im et al., 2008	PAN/TiO$_2$	DMF	15	10		1.5		1.27	800
Saeed et al., 2008	PAN	DMF	10 & 15	20	15	1	50	0.5	100/300
Sutasinpromprae et al., 2006	PAN	DMF	9.5	30	15		30	0.47	

Note: DMF = Dimethylformamide, DMAC = Dimethylacetamide, MnAC = Manganese acetate, PMMA = Poly(methylmethacrylate) and AB = Ambient temperature.

Recently, the incorporation of inorganic salts or nanoparticles (fillers) into electrospun polymer nanofibres via blending before spinning is on the rise. Figures 2.13 (a) and (b) are SEM images of smooth PAN-nfs and PAN-nfs with fillers, respectively. Fillers such as the silver ion and copper nanoparticles (Zhang et al., 2011; Sang and Sung, 2003), ZnO, Al$_2$O$_3$ and MnO nanoparticles (Chu et al., 2005), manganese acetate (Zhang et al., 2012) and TiO$_2$ (Im et al., 2009) have been incorporated into PAN-nfs for various purposes.
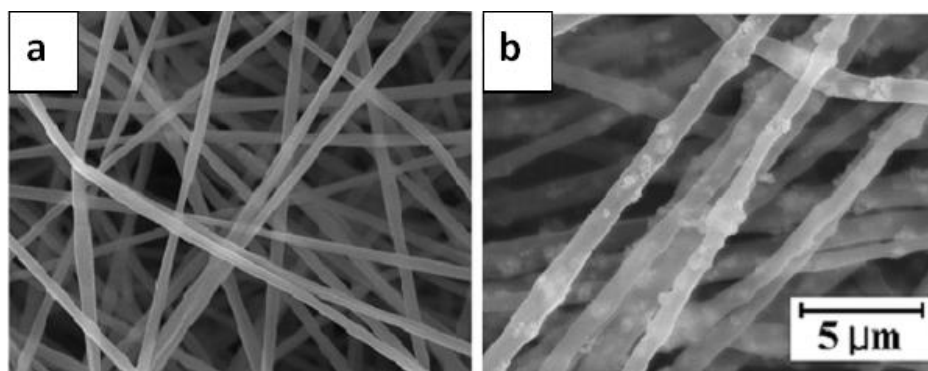
Figure 2.13: SEM images of (a) smooth PAN-nfs (Neghlani et al., 2011) and (b) PAN/TiO$_2$ composite nanofibres (Im et al., 2009).

PAN-nfs have also been used as a template to prepare nickel oxide nanostructure electrocatalysts (Elzatahry, 2014). Meanwhile, the major challenge in preparing these composite materials is the aggregation of clusters in the host matrix (not evenly dispersed) as shown for the case of TiO$_2$ in Figure 2.13 (b). This aggregation has been explained to be due to the repulsive forces between the positive charges of the fillers and that of the PAN (Im et al., 2009). Electrospun PAN-nfs can be difficult to handle due to the electrostatic forces on them. Meanwhile, commercially available anti-static guns can be used to remove these forces.

2.9   Surface modifications of polyacrylonitrile nanofibres

PAN-nfs surfaces are rarely active; however, chemical reactions can be carried out on its surface to make it active for any desire purpose. Chemical reactions such as amination, amidoximation and hydrolysis have been reported as methods for modifying the surfaces of PAN-nfs. Generally, the nitrile groups on PAN-nfs surfaces are the target of these chemical reactions (Zhang et al., 2014; Huang et al., 2013; Neghlani et al., 2011; Deng et al., 2003a). Other modification methods that have been reported include; plasma-induced and photo-induced graft co-polymerization (Chu et al., 2005; Zhao, et al., 2005; Zhao, et al., 2004; Choi et al., 2003; Ulbricht, et al., 1995). The presence of nitrile (CN) groups on PAN-nfs surfaces provides a good platform for chemical modifications. CN can undergo reactions with amines, hydroxylamine and alkaline. It can also undergo reduction using reducing agents such as LiAlH$_4$. All these reactions activate the surface of PAN

nanofibres for purposes such as enzyme and ligand immobilisation. Surface modification of PAN-nfs can damage the nanofibres; therefore, optimisation of reaction parameters such as time, initial concentration of reactant(s) and temperature are pertinent so as to maintain the integrity of the nanofibres (Ndayambaje et al., 2016).

For proper understanding and monitoring of chemical characteristics of chemically surface modified PAN-nfs, ATR-FTIR is the main and quickest technique to be explored as it gives all the newly introduced functional groups on the modified PAN-nfs. The FTIR spectrum of the PAN-nfs as shown in Figure 2.14 has the following characteristic peaks; the peak at 2930 cm^{-1} is assigned to C-H stretching vibration of CH$_2$ and the peak at 2241 cm^{-1} corresponds to the C≡N stretching vibration. The appearance of a peak at 1735 cm^{-1} which is assigned to the C=O stretching vibration showed that PAN-nfs is a copolymer of acrylonitrile and methylacrylate (Figure 2.12 (B) (Feng et al., 2011; Neghlani et al., 2011; Saeed et al., 2008; Deng et al., 2003a).
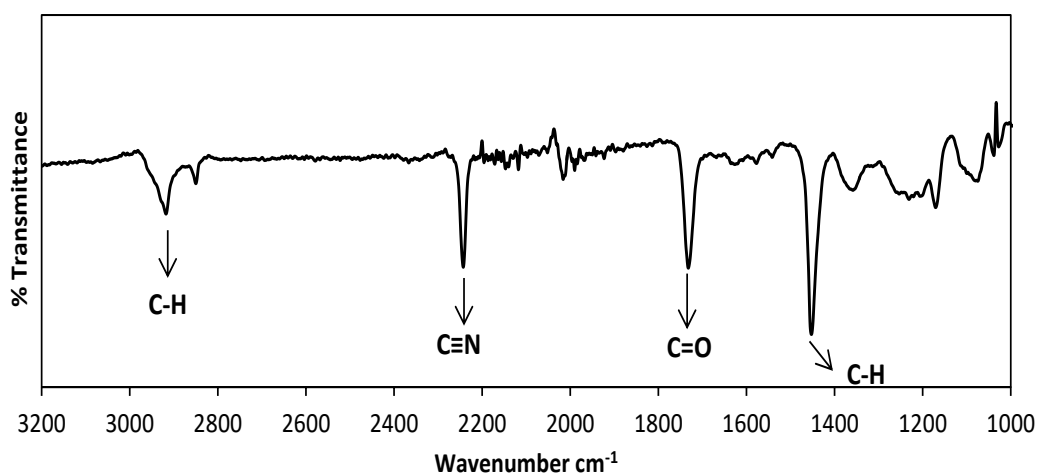
Figure 2.14: ATR-FTIR spectrum of PAN nanofibres.

The strong bands between 1350 cm^{-1} and 1465 cm^{-1} are of C H in-plane deformation vibration of CH$_2$ groups (Jain et al., 2009). After chemical surface modification, all these peaks mentioned can be shifted, reduced in intensity or may completely disappear, coupled with the appearance of new peaks.

2.9.1 Amination

Amination can be defined as the introduction of amines (most often primary amines) onto the surface of PAN nanofibres. This can be achieved in two ways; grafting and reduction. Grafting or immobilisation involves the reaction of amine groups, mostly the pendant amine compounds (Figure 2.15 (a), (b) and (c)) as well as hydrazine (Figure 2.15 (d)). Reduction on the other hand involves the reduction reaction of nitrile groups on PAN-nfs to primary amine groups. This often involves the complete change of the chemical structure of PAN-nfs, with no trace of nitrile group.
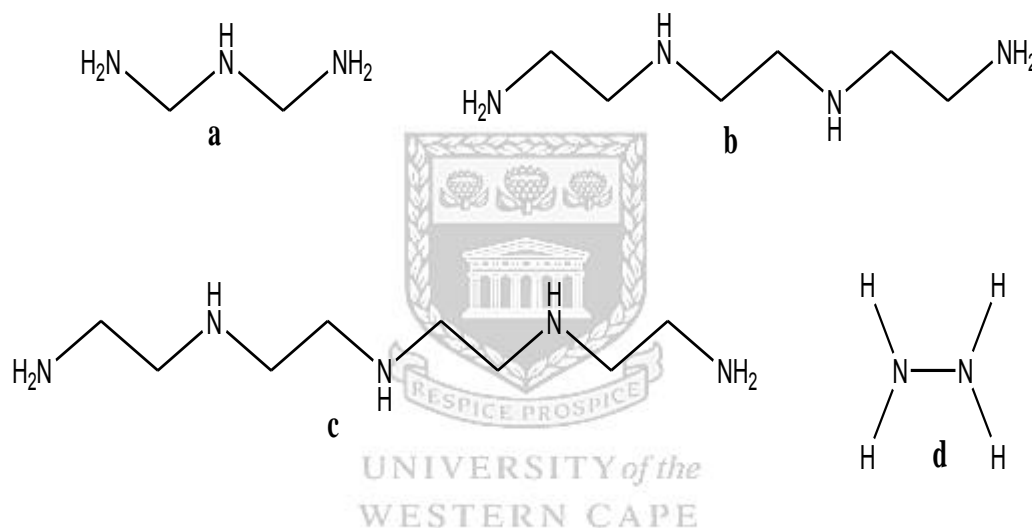
Figure 2.15: Structures of (a, b and c) pendant amines and (d) hydrazine.

2.9.1.1 Grafting of pendant amine groups

Pendant amine groups that have been grafted onto PAN nanofibres surfaces through this reaction include; diethylenetriamine (DETA) (Figure 2.15 (a)) (Neghlani et al., 2011; Kampalanonwat and Supaphol, 2010; Ko et al., 2004; Deng and Bai, 2003; Deng et al., 2003a), triethylenetetramine (TETA) (Figure 2.15 (b)) (Wang et al., 2011) and tetraethylenepentamine (TEPA) (Figure 2.15 (c)) (Chen et al., 2014). Generally, the experimental procedure involves the mixing and stirring of PAN-nfs and the amine group in a beaker at 95°C for about 24 to 30 hours (Deng et al., 2003a; Deng and Bai, 2003). After the reaction, the resultant aminated-PAN-nfs (APAN-nfs) is separated from the solution and rinsed with deionized water until pH 7, or washed in

distilled water and ethanol, then dried till constant weight and stored in a desiccator (Deng et al., 2003a). Other similar methods made use of sodium carbonate (Neghlani et al., 2011) or $AlCl_3.6H_2O$ (Kampalanonwat and Supaphol, 2010; Ko et al., 2004) as catalysts in the reaction medium mentioned above at 90°C for a maximum of 2 hours. Chen et al. (2014) in their reaction dissolved TETA in ethylene glycol (40 wt%) before adding PAN-nfs, the reaction took place at 70°C for 4 hours. Neghlani et al. (2011) reported an increase in the conversion of the nitrile group on PAN-nfs (from 8% to 60%) with increasing reaction time and temperature. An increase in temperature significantly accelerates the amination reaction of the PAN-nfs (Neghlani et al., 2011). Kampalanonwat and Supaphol, (2010) also reported a similar trend. Deng et al. (2003a) found that aminated PAN-nfs had zero point charge at about pH 8.1, in contrast with that of the PAN-nfs which is at pH 3.6.

From the SEM images, it was found that APAN-nfs exhibited similar morphology compared to the PAN-nfs, without any serious cracks or sign of degradation (Neghlani et al., 2011). The introduction of the amide or amine groups on the surface of the nanofibres can therefore be expected not to significantly change the surface morphology of PAN-nfs (Neghlani et al., 2011; Deng et al., 2003a).

Scheme 2.1 represents the acid catalysed amination reaction of PAN-nfs with diethylenetriamine. Deng et al. (2003a) compared the FTIR spectrum of PAN-nfs (Figure 2.16 (a)) to that of APAN-nfs (Figure 2.16 (b)).
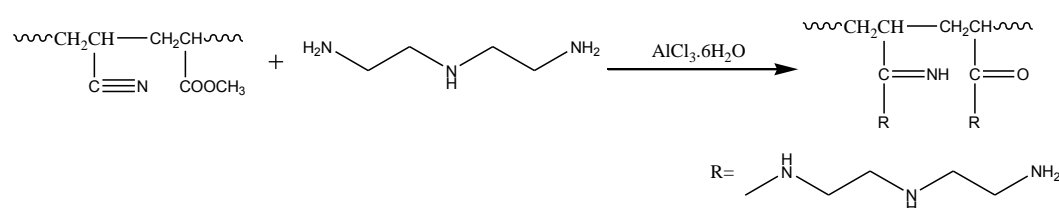
Scheme 2.1: Acid catalysed amination reaction of PAN-nfs with diethylenetriamine to form APAN (Kampalanonwat and Supaphol, 2010).
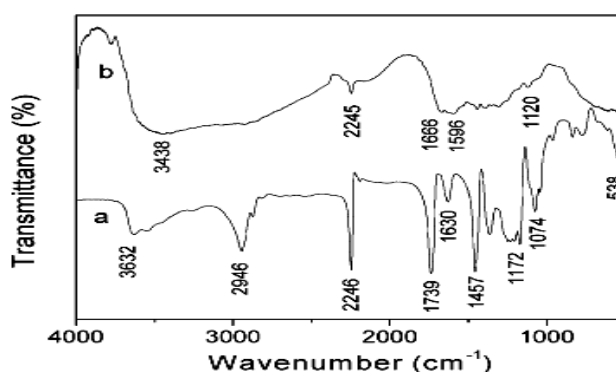
Figure 2.16: FT-IR spectra of (a) PAN-nfs and (b) APAN-nfs (Deng et al., 2003a).

The weak band at 3632 cm^{-1} on PAN-nfs spectrum was replaced by a strong broad band at 3438 cm^{-1} on APAN-nfs. Again, a strong broad band ranging from 3100 cm^{-1} to 3700 cm^{-1} also appeared on APAN-nfs spectrum. This band is usually assigned to the combination of the stretching vibration bands of both OH and NH groups (the overlapping of the vibrating bands of these two groups in the FTIR spectrum might made it impossible for individual identification). This led to their suggestion that many OH and NH groups were introduced onto the surface of the APAN-nfs. This could be surprising because OH was not expected; however, Deng et al. (2003a) explained that the OH group may be produced on the surface of the APAN-nfs by the hydrolysis of the ester group on the PAN-nfs (recall Figure 2.12 B). This was supported by the disappearance of the peaks at 2946 cm^{-1} (CH stretching), 1739 cm^{-1} (C=O stretching), and 538 cm^{-1} (C=O twisting), which indicates that the acetate ester group disappeared from the surface of the PAN-nfs after the hydrolysis. Meanwhile, the expected NH group may be introduced on the surface of the APAN-nfs by a reaction of diethylenetriamine with the nitrile group on the PAN-nfs. The nitrile group seemed to be hydrolysed into an amide group (–CO–NH$_2$) before it is further reacted with diethylenetriamine (Neghlani et al., 2011). The nitrile peak at 2246 cm^{-1} reduced significantly which corroborated the fact that the reaction had taken place on PAN-nfs. However this peak at 2246 cm^{-1} did not disappear completely, which suggests that not all nitrile groups on the surface of the PAN-nfs were converted during the reaction. Furthermore, the new bands at peaks of 1666 cm^{-1}, 1596 cm^{-1} and 1120 cm^{-1} on APAN-nfs spectrum can be assigned to the CO group in amide, the N-H group in amine, and the C-N group respectively. These bands are suggesting

61

that the amide and amine groups were introduced on the surface of the APAN-nfs at the carbons in the nitrile groups (Neghlani et al., 2011; Saeed et al., 2008; Deng et al., 2003a; Deng and Bai, 2003).

2.9.1.2   Grafting of hydrazine

Researchers have also reported the reaction between hydrazine ((Figure 2.15 (d)) and nitriles of PAN-nfs (Saeed et al., 2011). The reaction involves mixing hydrazine and PAN-nfs in a reaction vessel at 94°C over a range of time (Saeed et al., 2011). After the reaction, the hydrazine PAN-nfs (HZPAN-nfs) must be washed several times with distilled water to remove the unreacted hydrazine. Saeed et al. (2011) reported 5.2% increase in weight after the reaction proceeded for 2.5 hours at 94°C. From the SEM images, it was observed that hydrazine treatment did not seriously crack or degrade the PAN-nfs. Scheme 2.2 represents the reaction of PAN-nfs and hydrazine at 94°C for 2.5 hours as proposed by Saeed et al. (2011).
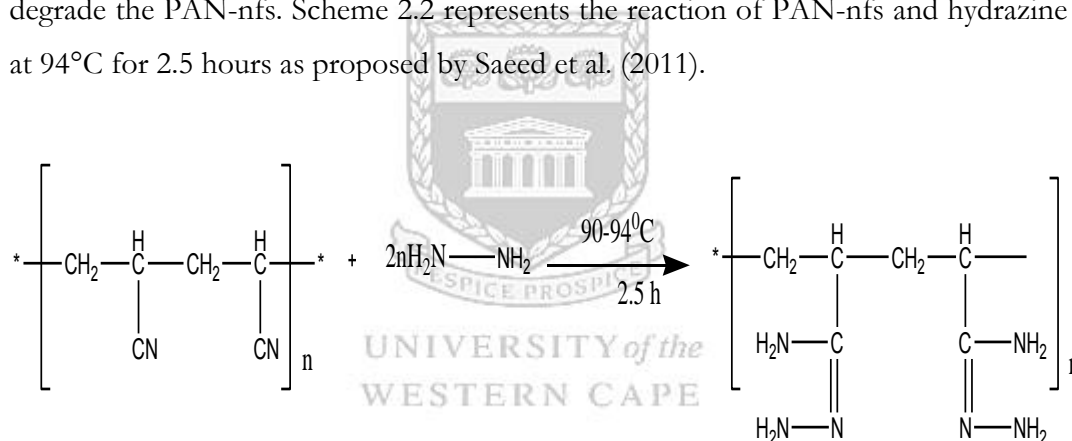
Scheme 2.2: Amination reaction of PAN-nf with hydrazine (Saeed et al., 2011).

Interestingly, hydrazine has been combined with other forms of surface modifications such as hydrolysis and amidoximation. Liu et al. (1999) prepared a chelating fibre with amino-carboxyl-tetrazine in three stages; (1) they reacted PAN-nfs and 800 mL of hydrazine in a reaction vessel for 2.5 h at 90 to 94°C. The resultant nanofibres were removed from the vessel and washed with water and oven dried. The hydrazine-modified PAN fibre (HZPAN-nfs) was then reacted with ethylenediamine at 95°C for 4 to 8 hours. The above dry product was finally reacted with 900 mL of 4% aqueous caustic soda solution for 5 hours at 80°C in a reaction vessel. The final nanofibres contained amino-carboxyl-tetrazine (Liu et al., 1999).

Chaudhary and Farrell, (2014) in their research investigated the modification of homo polymer polyacrylonitrile nanofibres. PAN-nfs were chemically modified and cross-linked using combinations of hydrazine hydrate and sodium hydroxide before being loaded with ferric hydroxide. The PAN reacted with hydrazine through a nucleophilic attack on the nitrile groups by the lone pair of electrons on the nitrogen atoms in hydrazine (Chaudhary and Farrell, 2014). During grafting of hydrazine, cross-linking may occur as a result of the bonding of hydrazine to adjacent polymer chains. In addition to cross-linking and amination of the fibres, treatment of PAN-nfs with hydrazine may also introduce carboxamide and carboxylate groups as a result of base catalysed hydrolysis reactions (Nesteronok and Soldatov, 2012). Other researchers have also functionalised the surface of PAN-nfs with both hydrazine and hydroxylamine (Zhenbang et al., 2010; Ishtchenko et al., 2003). According to Zhenbang et al. (2010) and Ishtchenko et al. (2003), they treated PAN-nfs with an aqueous solution containing 0.40 molL^{-1} hydrazine and 0.40 molL^{-1} hydroxylamine at pH 9.5 adjusted by sodium hydroxide for a given time range of 30 to 150 minutes at a temperature of 95°C. Scheme 2.3 is the reaction as presented by Zhenbang et al. (2010).
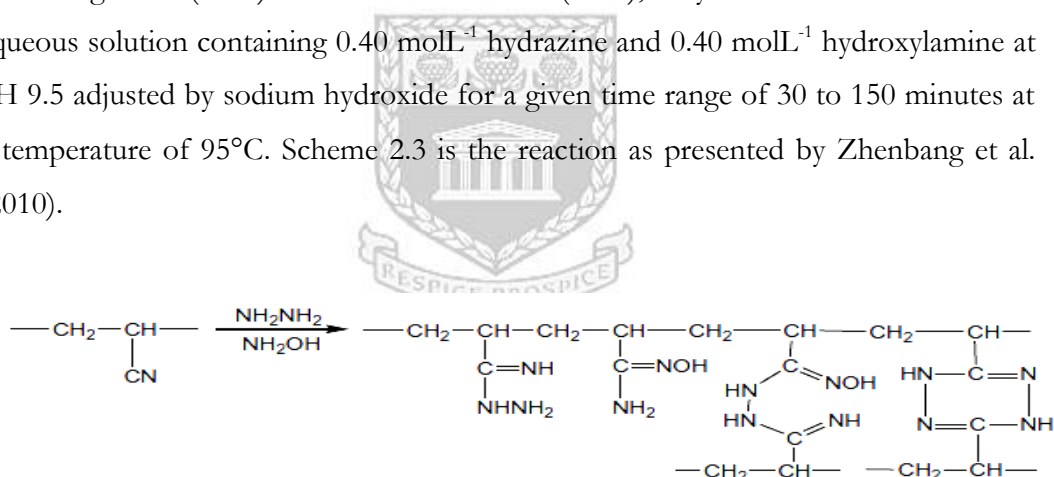
Scheme 2.3: Surface modification of PAN-nfs with hydrazine and hydroxylamine (Zhenbang et al., 2010).

The FTIR spectrum of HZPAN-nfs showed the presence of different functional groups than those of the pristine PAN-nfs. Saeed et al. (2011) compared the spectra of PAN-nfs (Figure 2.17 A (a)) to that of HZPAN-nfs (Figure 2.17 A (b)). On HZPAN-nfs spectrum, the band at 3414 cm^{-1} corresponded to the stretching vibration of amine (NH) and amino (NH$_2$) groups.
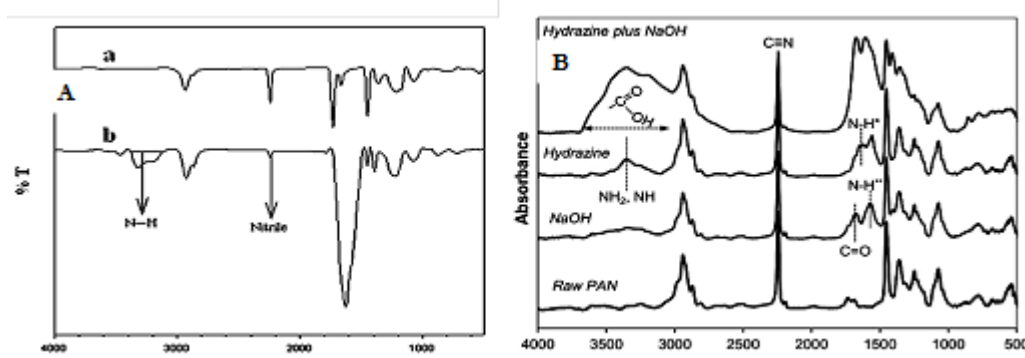
Figure 2.17: A (FTIR spectra of (a) PAN-nfs and (b) HZPAN-nfs) Saeed et al., 2011 and B (FTIR spectra of Hydrazine/NaOH-treated PAN-nfs) Chaudhary and Farrell, 2014.

The peaks at 1652 cm^{-1} and at 1561 cm^{-1} were assigned to the bending vibration of NH in amines and bending vibration for NH in amide respectively. As expected, the intensity of the nitrile peak 2241 cm^{-1} decreased significantly after treatment with hydrazine, this showed that the hydrazine was chemically attached to the PAN-nfs (Saeed et al., 2011; Saeed et al., 2008). Chaudhary and Farrell, (2014) reported additional functional group on the FTIR spectra of hydrazine/NaOH-treated PAN-nfs. The strong band ranging from 3000 cm^{-1} to 3630 cm^{-1} was assigned to the stretching vibration bands of amine groups, and also to the stretching vibration of hydroxyl groups (OH) in carboxylates (Figure 2.17 B: Hydrazine plus NaOH).

2.9.1.3   Reduction reactions

The nitrile group can be reduced by strong reducing agents such as lithium aluminumhydride (LiAlH$_4$). The reduction reaction brings about primary amine groups on the surface of PAN-nfs. The reaction is usually carried out in a 250 mL flask equipped with a water condenser. The equivalent quantities of LiAlH$_4$ and polyacrylonitrile PAN-nfs were reacted in an excess of pre-dried diethyl ether (120 mL) (Mei et al., 2012; Jain, et al., 2009; Leiriao et al., 2002). The reaction mixture was stirred continuously in a moisture free environment under a nitrogen blanket at room temperature for a range of times. The resultant yellowish PAN-nfs-NH$_2$ was thoroughly washed to remove the excess of LiAlH$_4$ and dried in vacuum (Mei et al., 2012; Jain et al., 2009). Reduced nanofibres obtained were stirred with 7.5 mL of 2 mM hydrochloric acid and 15 mL of distilled water for 1 hour. The excess of

hydrochloric acid was then titrated with 2 mM sodium hydroxide solution to determine the amount of hydrochloric acid consumed as the hydrochloride neutralized the amino groups of the reduced PAN-nfs (Jain et al., 2009; Leiriao et al., 2002). Jain et al. (2009) reported 108 μMg^{-1} while Leiriao et al. (2002) reported 8.3 μmol of amino group content after the reduction reaction. The SEM images revealed that the reduced PAN-nfs proceeded without considerable changes in the morphology of the PAN-nfs. The cross-sections of the nanofibres still remained round (Jain et al., 2009). Mei et al. (2012) reported an insignificant increase in fibre diameter after the reduction reaction. Scheme 2.4 is a reduction reaction as presented by Jain et al. (2009).

Scheme 2.4: Reduction of PAN-nfs with LiAlH4 (Jain et al., 2009).
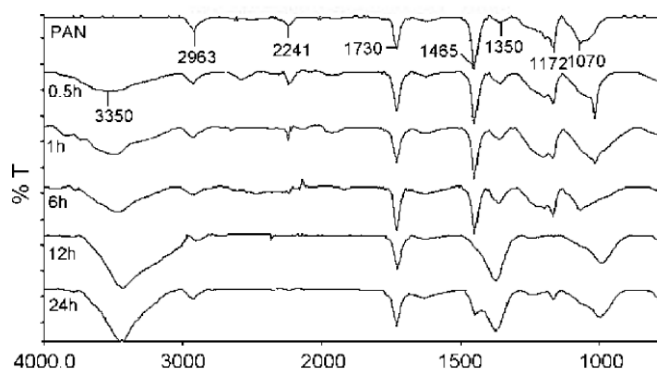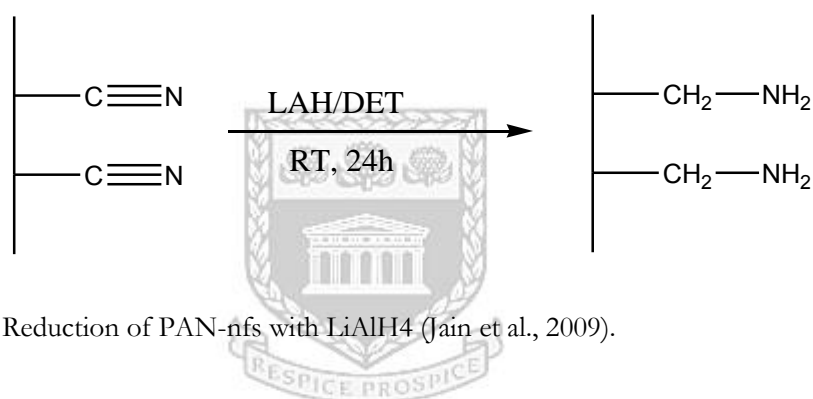
Figure 2.18: FTIR spectra of PAN-nfs and PAN-nf-NH$_2$ (Jain et al., 2009).

The introduction of primary amine groups on the PAN-nfs surfaces after reduction with LiAlH$_4$ was confirmed by the ATR-FTIR spectroscopy analyses by Jain et al. (2009) (Figure 2.18). A broad band that appeared from 3400 cm^{-1} to 3500cm^{-1} (Figure 2.18: 0.5 to 24 hours) was assigned to the N–H stretching vibration. This confirmed the formation of the primary amine groups. From Figure 2.18, it is obvious that as

the reduction time increased, the nitrile group peak at 2241 cm^{-1} decreased in intensity and completely disappeared in the spectra at 24 hours (Jain et al., 2009). This is as a result of complete reduction of nitrile group on PAN-nfs.

Thermal properties of unmodified and reduced PAN-nfs were studied under nitrogen atmosphere using differential scanning calorimetry (DSC) by Jain et al. (2009) (Figure 2.19). At the first cycle of heating, a transition at 96°C and a sharp peak at 150°C were observed on the DSC profile of unmodified PAN-nfs (Figure 2.19 (a)). The latter peak was attributed to the cyclisation of the pendant amine on the surface of PAN-nfs (Scheme 2.5). For the PAN-nfs reduced for 1 hour, the peak cyclisation temperature shifted to 166°C (Figure 2.19 (b)). However, PAN-nfs reduced for 6 h, did not show any cyclisation temperature (Figure 2.19 (c)). This was as a result of insignificant amount of nitrile groups on the surface of reduced PAN-nfs to initiate the cyclisation process upon heating (Jain et al., 2009).
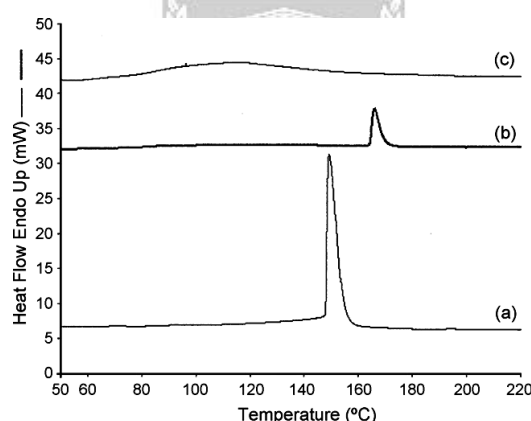
Figure 2.19: Cyclisation temperature of (a) unmodified PAN-nfs and (b) 1 hour reduced PAN-nfs and (c) 6 hour reduced PAN-nfs (Jain et al., 2009).
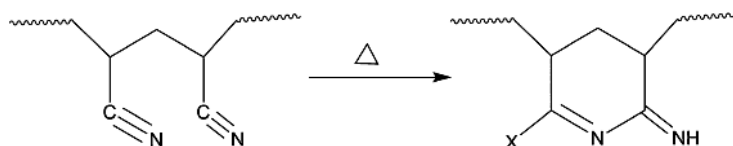
Scheme 2.5: Cyclisation of PAN-nfs (Jain et al., 2009).

2.9.2 Amidoximation

Another reaction that the nitrile group on PAN-nfs can undergo is amidoximation. The nitrile groups react with hydroxylamine to introduce amine and oxime group (-C=N-OH, a chemical group belonging to imines) onto the surface of PAN-nfs (Zhenbang et al., 2010). The hydroxylamine undergoes nucleophilic addition to the PAN-nfs surfaces and a subsequent arrangement follows to form carboximidamide. The experimental procedure involved weighing of hydroxylamine hydrochloride and sodium carbonate in a ratio of 1 to 1 (sodium carbonate was added to adjust the pH), dissolved in deionised water, and then added PAN-nfs. The mixture was agitated for 2 to 4 hours at 70°C (Zhang et al., 2014; Huang et al., 2013; Feng et al., 2011; Zhenbang et al., 2010; Saeed et al., 2008; Chu et al., 2005). Horzum et al. (2012) used sodium hydroxide instead of sodium carbonate and agitated the reaction for 2 days at room temperature. To avoid shrinkage of PAN-nfs during the reaction, Saeed et al. (2008) used a Teflon frame to hold the edges of the fibre mat. The resultant amidoximated PAN-nfs (AMPAN-nfs) were removed and washed with distilled water in order to remove the unreacted salts and then dried to constant weight. The AMPAN-nfs mat became brittle and the resulting nanofibres were soft and light yellow (Horzum et al., 2012; Saeed et al., 2008; Chu et al., 2005). The hydrophilic character of AMPAN-nfs was increased compared to pristine PAN-nfs (Horzum et al., 2012). SEM images revealed that the surface of AMPAN-nfs was rougher than that of the PAN-nfs (Figure 2.20). Meanwhile, there were no serious cracks or sign of degradation on the surface of the AMPAN-nfs after the chemical modification (Figure 2.20 (b)) (Huang et al., 2013; Horzum et al., 2012; Saeed et al., 2008).
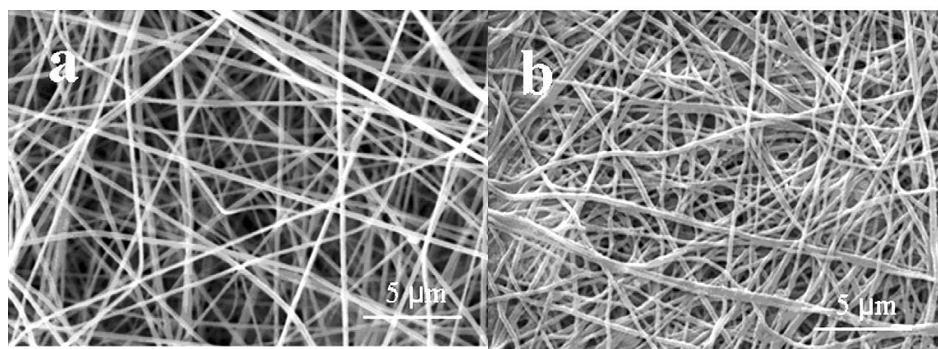
Figure 2.20: SEM images of (a) PAN-nfs and (b) AMPAN-nfs (Saeed et al., 2008).

The FTIR spectrum of the AMPAN-nfs (Figure 2.21) revealed a wide band ranging from 3670 cm⁻¹ to 3100 cm⁻¹ which corresponded to the N-H and O-H of the amidoxime groups stretching vibration (Chu et al., 2005). The characteristic stretching vibration C=N and N-O absorption bands at 1641 cm⁻¹ and 985 cm⁻¹ respectively also appeared on AMPAN-nfs spectrum. In addition, the decrease in the absorption band around 2241 cm⁻¹ indicated the conversion of the nitrile to the amidoxime group (Feng et al., 2011).
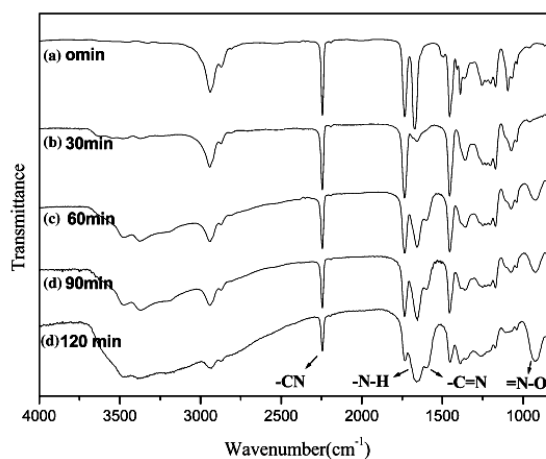
Figure 2.21: FTIR spectra of PAN-nfs and AMPAN-nfs with respect to time (Chu et al., 2005).

The peak of C=O in ester at 1730 cm⁻¹ was reduced due to the introduction of the hydroxamic acid groups, hence, the reaction also took place on the methylacrylate co-monomer (Saeed et al., 2008; Chu et al 2005). Scheme 2.6 represents the amidoximation reaction as proposed by Saeed et al. (2008).
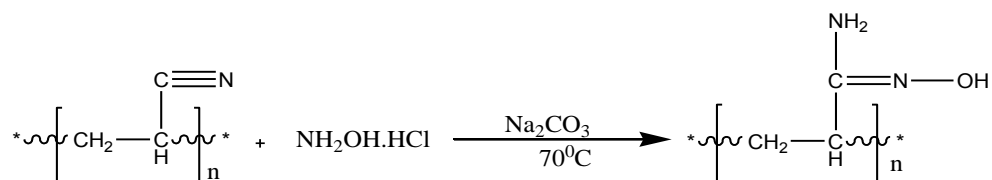
Scheme 2.6: Amidoximation of PAN-nfs (Saeed et al., 2008).

2.9.3 Hydrolysis

Among various methods of surface modification of PAN-nfs, alkaline hydrolysis is one of the most important and most frequently used, this is so because of its convenience and the platform it gives for further modifications. These are the reasons why hydrolysed PAN-nfs (HPAN-nfs) have been widely used as supports for the assembly of composite membranes. The hydrolysis with alkaline solution is based on the gradual conversion of nitrile groups on the PAN-nfs surface firstly into amide groups ($-CONH_2$), then into carboxyl $-COO^-$ groups (Wang et al., 2007; Wang et al., 2006; Ulbricht et al., 1995). In actual fact, alkaline hydrolysis of PAN-nfs can give different types of hydrolysed products. These products may include those with conjugated sequences of $-C=N-$, acrylamide, sodium acrylate, and amidine depending on the stage of the hydrolysis (Deng et al., 2003b). Bagheri et al., (2010) reported the conjugated sequences of $-C=N-$ on the HPAN-nfs with coherent $-NC-NH_2$ groups. At first, the alkali modifies the surface and then penetrates inside the nanofibres structure, before deterioration begins. Therefore, it is necessary to optimise reaction conditions such as the concentration of the alkaline, time and temperature so as to achieve the required characteristics of the PAN-nfs. PAN-nfs undergo colour changes during the reaction (Deng et al., 2003b). Once hydrolysis begins, the fibres become more hydrophilic. This enhances the aqueous alkali diffusion/imbibition into the nanofibres which subsequently enhances the hydrolysis. This explains why fibre weight loss is expected in hydrolysis treatment of nanofibres (Gupta et al., 2004).

During alkaline hydrolysis of PAN-nfs, the nitrile group decreases gradually, while the formation of amide and carboxyl groups follows smoothly. It was observed that some crosslinking took place during the hydrolysis reaction (Lohokare et al., 2006). This deactivated the hydrophilic groups (carboxylate) and their content stopped increasing (Zhang et al., 2010b; Lohokare et al., 2006; Gupta et al., 2004). It has been reported that the hydrolysis of PAN-nfs would lead to the reduction in initial pore size and mechanical strength (Zhang et al., 2010b; Zhu et al., 2007). Lohokare et al. (2008) reported that the hydrolysis of PAN-nfs surface by NaOH led to the formation of carboxylate groups and reduction in initial pore size and mechanical properties. Therefore, to ensure a suitable mechanical strength for the surface

modification of PAN-nfs, excess hydrolysis is not advised. Scheme 2.7 is the hydrolysis of PAN-nfs as proposed by Kampalanonwat and Supaphol, (2011).
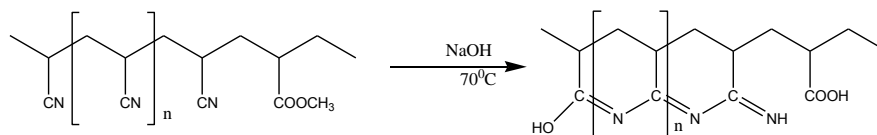
Scheme 2.7: Hydrolysis of PAN-nfs (Kampalanonwat and Supaphol, 2011).

Most alkaline hydrolysis reactions are carried out by reaction of the PAN-nfs with NaOH/KOH/LiOH in ethanol/water solution in a sealed chamber at temperatures between 60°C and 75°C. The hydrolysis of PAN-nfs is easily noticed by a change in colour from whitish to light yellowish (Kampalanonwat and Supaphol, 2011; Deng et al., 2003b). The resultant fibres are rinsed with de-ionized water until pH 7, and then dried in an oven at 40°C to constant weight. Zhang et al. (2010a) and Lohokare et al. (2006) did a post-treatment on hydrolysed PAN-nfs (HPAN-nfs) by putting it in 1 M HCl or 0.1 M HCl at room temperature for 120 minutes. The yellowish colour of HPAN-nfs turned white. The explanation given was that the nanofibres exhibited swelling by NaOH treatment followed by deswelling through HCl post-treatment. This is similar to pH responsive membranes.

The SEM images as shown in (Figure 2.22), the surface of HPAN-nfs with 3 wt% NaOH (Figure 2.22 (b)) was relatively smooth and uniform compared to PAN-nfs (Figure 2.22 (a)). Figure 2.22 (c) showed that after PAN-nfs were treated with 4 wt%, the fibre surface was corroded and became rough, indicating excess hydrolysis (Kampalanonwat and Supaphol, 2011; Deng et al., 2003b).
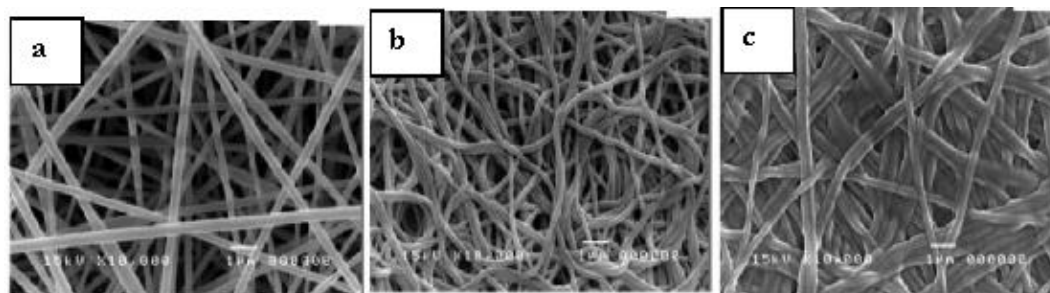
Figure 2.22: SEM images of (a) PAN-nfs (b) HPAN-nfs with 3 wt% NaOH (c) HPAN-nfs with 4 wt% NaOH (Kampalanonwat and Supaphol, 2011).

The FT-IR spectrum of HPAN-nfs was quite different from the pristine PAN-nfs (Deng et al., 2003b) (Figure 2.23). On the spectrum of HPAN-nfs (Figure 2.23 (b)), the broad adsorption band ranging from 3100 cm^{-1} to 3600 cm^{-1} corresponded to the stretching vibration of the OH group and this indicated the introduction of the OH groups onto the HPAN-nfs. Also, the new peaks at 1573 cm^{-1}, 1406 cm^{-1}, and 1224 cm^{-1} indicated the existence of imine (–C=N–) conjugated sequences in the hydrolysed PAN-nfs (Bagheri et al., 2010; Deng et al., 2003b). The intensity of the peak at 2946 cm^{-1} assigned to CH$_2$ was reduced significantly as a result of the hydrolysis of the ester group on the PAN-nfs.
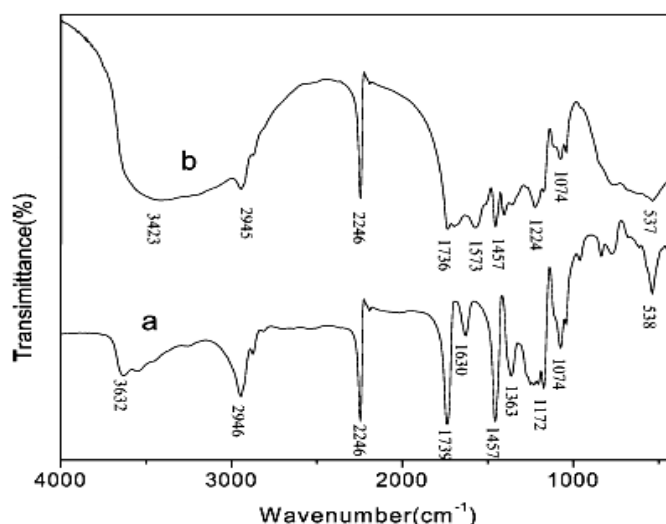
Figure 2.23: FTIR spectra of (a) PAN-nfs and (b) HPAN-nfs (Deng et al., 2003b).

The strong peaks at 1739 cm^{-1} and 538 cm^{-1} which were assigned to C=O on PAN-nfs became weak after the hydrolysis. This suggested that acetate ester was being removed from the PAN-nfs. There was no significant change on the nitrile peak at 2241 cm^{-1}, this meant that only a small part of the nitrile groups were converted to –C=N– groups (Figure 2.23 (b)). This served to corroborate the fact that excess hydrolysis is not advised otherwise the peaks would be reduced gradually and then completely disappear.

2.10   Surface modified PAN-nfs as supports

All surface modifications discussed earlier are often used to prepare (activate) PAN-nfs for immobilisation of materials such as organic ligands, enzymes, antibacterial agents and catalysts (Bode-Aluko et al., 2017b). This is done in most cases when the chemistry between the support and the material could not form a covalent bond or when there is a need to extend the application of the materials on the support. Tethering of enzymes or antibacterial agents to solid supports via functional groups can give characteristics such as specific absorption, greater stability and enhanced biological activities (Mei et al., 2012; Jain et al., 2009; Ishimura and Seijo, 1991). Modified PAN-nfs have extensively been used for the immobilisation of different enzymes for various industrial and biomedical applications such as biocatalysts, bioreactors and protein filtration (Iwata et al., 2003; Musale and Kulkarni, 1997). As mentioned earlier, PAN-nfs have a relatively hydrophobic surface; therefore, the driving force for protein adsorption is generally attributed to the hydrophobicity (Fischer-Colbrie, et al., 2007). PAN hollow fibres have also been used as dialyzers that enable low to middle molecule protein (urea, macroglobulin) removals and high flux dialysis therapy (Thomas et al., 2000; Valette et al., 1999). Examples of such fibres are produced by Hospal, a brand of Gambro in the USA, fabricated from an acrylonitrile/methallyl sulphonate copolymer. PAN-nfs and their composites have been widely used for adsorption and found to be efficient for removal of metal ions and organic pollutants from water (Chen et al., 2014; Neghlani et al., 2011; Kampalanonwat and Supaphol, 2010; Saeed et al., 2008; Deng and Bai, 2003; Deng et al., 2003a). Pendant amines immobilised on PAN-nfs have been used for removal and recovery of metal ions (Neghlani et al., 2011; Kampalanonwat and Supaphol, 2010; Saeed et al., 2008; Deng et al., 2003a). In the same vain, transition metal

catalysts have been immobilised upon various surface modified PAN-nfs for use especially in Fenton's chemistry (Zhenbang et al., 2010; Ishtchenko et al., 2003; Vitkovskaya et al., 2003). The next sub-section will discuss the chelating group to be immobilised on PAN-nfs in this research.

2.10.1 Amidoximes

Amidoximes are classified as oximes of amides (Figure 2.24) with a general structural formula of $RC(=NOH)(NRR^1)$, where R is an organic side chain and R^1 may be hydrogen.
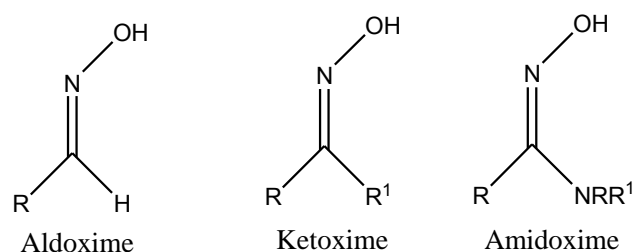
Figure 2.24: Structures of oximes.

Chelating functional groups of amidoximes are mainly the amide and hydroxide groups. The nitrogen and the oxygen act as the donor atoms of the functional groups respectively (Horzum et al., 2012; Nilchi et al., 2008a; Saeed et al., 2008; Tuzen et al., 2007). Amidoximes are easily synthesised through the conversions of the nitrile groups using hydroxylamine hydrochloride (Scheme 2.8) (Horzum et al., 2012; Saeed et al., 2008; Bernasek, 1957).
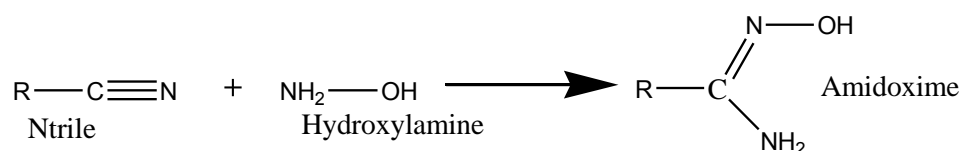
Scheme 2.8: Synthesis of amidoxime from nitrile group.

The nitrile groups of compounds such as 2-cyanopyridine, 4-cyanopyridine and cyanoguanidine (Figure 2.25) as well as polymers such as polyacrylonitrile (PAN) have been converted into amidoxime using hydroxylamine hydrochloride (Horzum et al., 2012; Wang et al., 2012b; Bernasek, 1957). Silica gel supported acrylonitrile functional groups have also been reacted with hydroxylamine under alkaline conditions to introduce amidoxime groups on them (Chen et al., 2012).
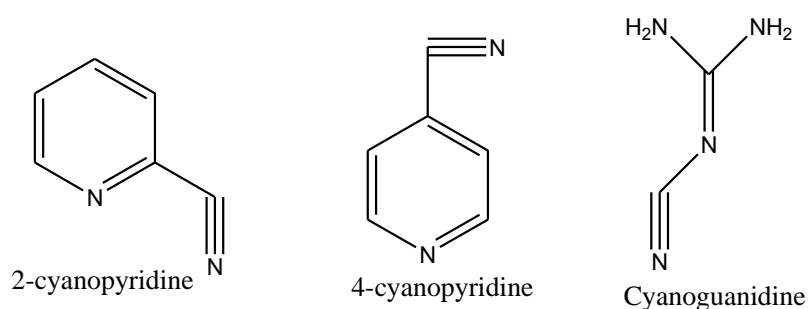
Figure 2.25: Structures of compounds that contain the nitrile groups.

Bernasek, (1957) prepared pyridine amidoximes by heating of the appropriate cyanopyridines (2-cyanopyridine or 4-cyanopyridine dissolved in ethanol) at 85°C with an aqueous solution of hydroxylamine hydrochloride (Scheme 2.9). The pH of the solution was maintained by the addition of sodium carbonate. A white crystalline solid (2-pyridine amidoxime or 4-pyridine amidoxime) was obtained (Bernasek, 1957).
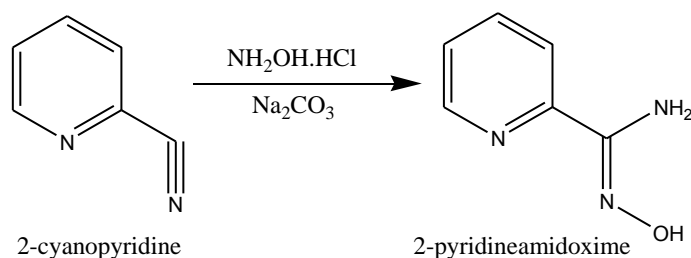
Scheme 2.9: Synthesis of 2-pyridine amidoxime with cyanopyridines.

Wang et al. (2012b) synthesised a novel chelating resin containing the amidoxime-guanidine functional group. They first functionalised chloromethylated polystyrene-divinylbenzene (CMPS) bead with dicyandiamide (DCDA) to give polystyrene-dicyandiamide resin (PS-DCDA). This was followed by the conversion of the nitrile end of PS-DCDA into amidoxime group (PSGA) by the reaction with hydroxylamine under alkaline condition (Scheme 2.10) (Wang et al., 2012b; Ma et al., 2011).
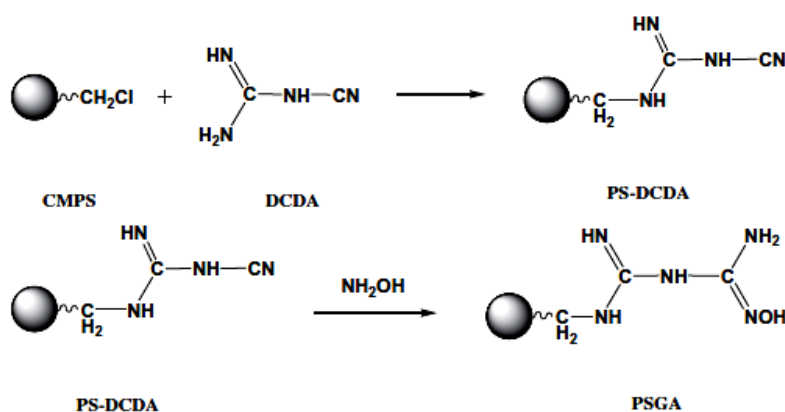
Scheme 2.10: Reaction pathways for synthesis of amidoxime-guanidine resin (Wang et al., 2012b).

Sanguineti et al. (2011) reported the synthesis of various amidoxime compounds from the conversion of nitroalkanes using metallating agents such as ethylmagnesium chloride and *n*-butyllithium (Sanguineti et al., 2011). Using 1-nitropropane as a model, Sanguineti et al. (2011) proposed the mechanism of the conversion of nitroalkane into amidoxime (Scheme 2.11). The mechanism involved the preparation of the corresponding thiohydroximate ester (Scheme 2.11 (6)) (R^1=CH_3, R=Ph) using thiophenol (RSH) under reflux with methanol.

Scheme 2.11 (6), being an oximino analogue of a thioester is expected to react with an amine group to give the corresponding amidoxime (Scheme 2.11 (7)) (R^1=CH_3, R^2=H, R^3=Ph). Figure 2.26 are some of the amidoximes synthesised by Sanguineti et al. (2011) from nitroalkanes.
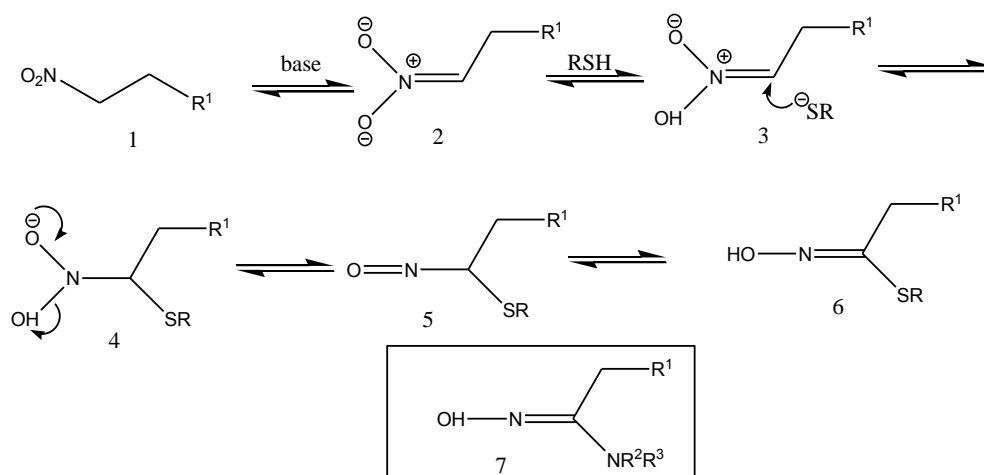
Scheme 2.11: Reaction mechanism for the synthesis of amidoxime from nitroalkanes (Sanguineti et al., 2011).
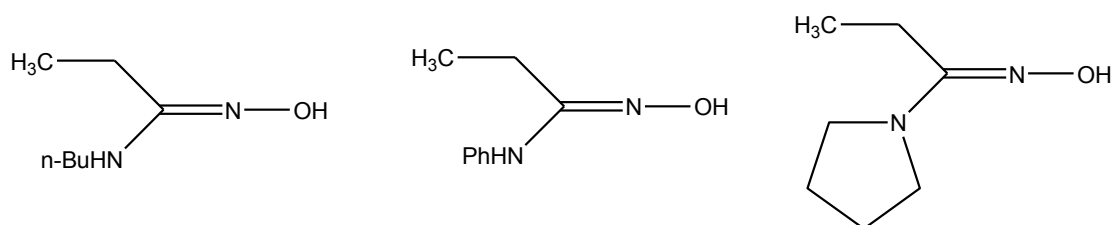
Figure 2.26: Structures of amidoximes synthesised from nitroalkanes (Sanguineti et al., 2011).

2.11 Adsorption of toxic metals using modified PAN-nfs

Chelation and ion-exchange have been considered as the critical adsorption mechanisms for toxic metal ions on various adsorbents (Chen et al., 2002; Jin and Bai, 2002). It has been reported that the presence of carboxyl, sulfonic and phosphonic groups on the surface of adsorbents favour metal ion adsorption via the ion-exchange mechanism, while the presence of nitrogen containing groups such as amino, hydrazine, thioamide and imidazoline, allowed metal ion adsorption through the chelation mechanism (Ndayambaje et al., 2016; Chen et al., 2002; Jin and Bai, 2002; Lacour et al., 2001; Coskun et al., 2000). In adsorption process, metal ions in the aqueous solutions are transported via diffusion or convection to the surfaces of the adsorbents and the metal ions get attached to the functional group(s) on the surface of the adsorbents. Table 2.6 presents the comprehensive details of previously adsorbed metal ions with the adsorption parameters ranging from the nature of adsorbents, the pH of adsorptions, the capacity of the adsorbents etc.

Table 2.6: Adsorption studies of toxic metals on various modified PAN-nfs (Bode-Aluko et al., 2017a).

Adsorbents	Techniques	Metals	Optimum pH	Quantity adsorbed	Authors
PAN-TETA	Batch	Cu(II), Cd(II)	6	Cu; 109, Cd; 99 mg/g	Soltanzadeh et al. 2013
PAN-TETA	Batch	Cr(VI)	5	133 mg/g	Wang et al. 2011
PAN-DETA	Batch	Pb(II), Cu(II)	4.5	Pb; 76, Cu, 31 mg/g	Deng et al. 2003a
PAN-TEPA	Batch	Cr(VI)	1	33.2 mg/g	Chen et al. 2014
PAN/PMMA TEPA	Batch	Cr(VI)	1	49.8 mg/g	Chen et al. 2014
PAN-DETA	Batch	Cu(II), Ag(I), Fe(II), Pb(II)		Cu;150, Ag; 155, Fe; 116, Pb; 60 mg/g	Kampalanonwat and Supaphol 2010
PAN-DEDA	Batch	CrO_4^{2-}, PO_4^{3-}	CrO_4^{2-}; 1.02; PO_4^{3-}; 2.89	CrO_4^{2-}; 5.7 PO_4^{3-}; 3.8 mmol/g	Ko et al. 2004
PAN-DEDA	Batch	Cu(II), Ni (II), Fe (II), Ag(I)		Cu(II); 4.49, Ni (II); 1.91 Fe (II); 3.76 Ag(I); 5.1	Ko et al. 2004
PAN-DEDA	Batch	Cu	6	11.6 mg/g	Neghlani et al. 2011
PAN+NHOH	Batch	Cu(II), Fe(III)		Cu; 215; Fe; 221 mg/g	Huang et al. 2013
PAN+NHOH	Batch	Cu(II), Pb(II)		Cu(II); 52.7, Pb (II); 263.45 mg/g	Saeed et al. 2008
PAN+NHOH	Batch	Cu(II), Cd(II)		Cu(II); 3.44, Cd(II); 4.55 mmol/g	Feng et al. 2011
PAN+NHOH	Column	U(VI)	4	85%	Horzum et al. 2012
PAN-OH	Batch	Cu(II)	4.5	27.95 mg/g	Deng et al. 2003b
PAN-OH	Batch	Cu(II)	5	31.3 mg/g	Kampalanonwat and Supaphol 2011
PAN-OH	Batch	Cu(II), Pb(II)		Cu(II); 114, Pb(II); 217 mg/g	Saeed et al. 2011
PAN-8Q	Column	Cu(II)	6	246 mol/g	Wen and Shan 2002
PAN-PPy	Batch	Cr(VI)	2	65.5 mg/g	Wang et al. 2014
PAN-DETA	Batch	Pb(II)	5.5	1520 mg/g	Hong et al. 2015
PAN-PIM	Batch	Ni(II)	5	0.7 mol/kg	Ndayambaje et al. 2016

Keys; PAN-TETA; triethylenetetramine, PAN-DETA; diethylenetriamine, PAN-TEPA; tetraethylenepentamine, PAN/PMMA-TEPA; poly(methyl methacrylate), PAN-DEDA; diethylenediamine, PAN+NHOH; amidoximated PAN, PAN-OH; hydrolyzed PAN, PAN-H; Hydrazine, PAN-8Q; 8-Hydroxyquinoline and PAN-PPy; polypyrrole PAN, PAN-PIM; PAN-2-(2-pyridyl)imidazole.

Toxic metals ions such as lead, cadmium, copper, mercury, uranium etc. have been adsorbed from their aqueous solutions with various modified PAN-nfs (Horzum et al., 2012; Neghlani et al., 2011; Saeed et al., 2008; Deng et al., 2003a). The adsorption studies were carried out by investigating parameters such as pH, initial concentration of metal ions, contact time, adsorbent dosage and temperature. So also, adsorption models such as isotherms, kinetics and thermodynamics parameters were used to determine the efficiency of the adsorption process.

2.11.1 Batch and column adsorption techniques

Functionalised PAN-nfs have been used in both batch and column adsorption techniques and are found to be effective (Horzum et al., 2012; Neghlani et al., 2011). In column techniques (flow continuous), the modified PAN-nfs were placed in a vertical column to form a bed and the aqueous solution containing the metal ions was run through the column (Horzum et al., 2012). However, in the batch technique, modified PAN-nfs were placed in a vessel containing the metal ions solution and shaken together over a period of time (Neghlani et al., 2011; Saeed et al., 2008; Deng et al., 2003a). After the adsorption process using either technique, the modified PAN-nfs can be regenerated and be reused in another cycle; however, regeneration and reuse are not often reported.

2.11.2 Effect of pH values

The most important factor highlighted in adsorption studies is the pH of the aqueous solution. The pH has effects on both the adsorbents and the metal ions in the solution. The chelating functional groups of the adsorbents can undergo dissociation at certain pH and also the surface charges can be affected. Therefore, stability tests are carried out on modified PAN-nfs in different pHs especially in acidic medium in order to make sure that the surface modified PAN-nfs retains it functionality throughout the adsorption process. It has been generally explained that; the pH of the solution affects the adsorptive process because of the protonation and deprotonation of the acidic and basic groups of the chelating ligands (Horzum et al., 2012; Neghlani et al., 2011; Deng et al., 2003a). At lower pH, the functional groups (active sites) of the adsorbent are less available for metal ions due to protonation of

the active sites at higher H^+ concentration. As the pH increases, the degree of protonation of the surface functional groups gradually reduces and approaches zero resulting in a gradual increase in the adsorption. Furthermore, pH affects the existent state of metal ions in solution to a certain extent. Metal ions are readily available for adsorption as pH increases. However, to prevent the metal ions from precipitation, a pH of greater than 7.0 is often not studied (Soltanzadeh et al., 2013). The pH of adsorption set-up especially when using modified PAN-nfs as adsorbents are often adjusted with 0.1 M HCl or 0.1 M NaOH (Ndayambaje et al., 2016).

Generally, higher adsorptions of metal ions are observed at higher solution pH values in the acidic region; meanwhile, chemical precipitation at higher pH must be avoided, so that removal could be related only to the adsorption process (Fu and Wang, 2011). Deng et al. (2003a) modified PAN-nfs with diethylenetriamine (PAN-DETA) for lead and copper ions. At pH below 2.3, almost no adsorption of lead and copper ions took place. A similar situation arose when Neghlani et al. (2011) used the same adsorbent for copper ions. This may be due to the protonation of the amine groups of PAN-DETA. As the pH increased from 2.3 to 3, the amount of copper ions adsorbed on the PAN-DETA increased and then appeared to approach a plateau, no further noticeable increase was observed for pH from 3 to 6 (Deng et al., 2003a). It was explained that, at higher pH, more amine groups are available to capture the metal ions (i.e., via the interaction of the metal ions with the lone-pair electrons of nitrogen). It may also be possible that when pH was below 2.3, the strong electrical repulsion prevented the metal ions from contacting the surfaces of the PAN-DETA, resulting in almost no adsorption of lead or copper ions on the PAN-DETA. With the increase of solution pH values, the electrical repulsion force became weaker and the metal ions may be transported to the surface of the PAN-DETA and become attached on the surface (Neghlani et al., 2011; Deng et al., 2003a). Kampalanonwat and Supaphol (2010) also used PAN-DETA for Cu(II), Ag(I), Fe(II), and Pb(II) adsorption. Increasing the initial pH of the testing solutions resulted in the amounts of the adsorbed metal ions reaching plateau values, and in most cases (except for the adsorption of Ag(I) ions), the amounts of the adsorbed metal ions decreased as the initial pH approached neutrality. This could be due to the competitive adsorption of the OH ions via the formation of the hydrogen bond,

resulting in the reduction of the adsorptive sites on the surface of the PAN-DETA nanofibres. Moreover, at higher pH levels, the concentration of OH ions is high enough to interact with the metal ions, reducing the availability of the metal ions in their free, hydrated form to interact with the amine groups of the DETA ligands. Soltanzadeh et al. (2013) modified PAN-nfs with triethylenetetramine (PAN-TETA) and used it as absorbent for copper and cadmium ions. Lower uptakes of both metals were observed at lower pH. This may be attributed to the partial protonation of the active groups and the competition of H^+ with metal ions for adsorption sites on the PAN-TETA. Adsorption efficiency increased with increased pH and achieved maximum sorption at pH 6. At this pH, the adsorbent is selective for Cu (Soltanzadeh et al. 2013). Deng et al. (2003b) hydrolysed PAN-nfs with NaOH for copper ions adsorption. At a pH less than 3, the amount of adsorption was very low (less than 2.8 mg/g), but the amount of adsorption increased sharply at a pH between 3.0 and 4.0 and reached up to 12.4 mg/g. However, no further increase of adsorption was observed for a pH increase between 4.0 and 6.0. Horzum et al. (2012) introduced amidoxime groups on surface of PAN-nfs for uranium ions adsorption. The per cent UO_2^{2+} uptake increased as pH levels increased from 3.0 to 4.0. The amidoximated PAN nanofibres seemed to demonstrate maximum sorption at pH 4.0. At this pH, the UO_2^{2+} ion is the main species (approximately 85%) among other chemical forms. At lower pH, uranium is still present in the form of free UO_2^{2+} ions; however, competitive sorption with protons occurs and ion-exchange interactions are favoured (Sylwester et al., 2000). Protonation can occur on the amino group of amidoxime (pKa 5.95) leading to a decrease in the chelating ability. Kampalanonwat and Supaphol (2011) also modified PAN-nfs in sodium hydroxide ethanolic/aqueous solution for adsorption of copper ions. A low adsorption was observed at low pH which was due to the competitive adsorption between the prevalently available H^+ and the Cu ions. The electrostatic repulsion between the protonated imine groups of the modified PAN-nfs and copper ions could be another reason for the very low adsorption values. The decrease in the amount of H^+, as the initial pH increased, resulted in less competitive adsorption on the available adsorptive sites as well as an increase in the number of the available adsorptive sites as the protonation of the imine groups on the hydrolysed PAN-nfs decreases. Away from this trend, Chen et al. (2014) used tetraethylenepentamine PAN-nfs (PAN-TETA) for chromium

adsorption. Good adsorption was observed at low pH. They proposed that H^+ was preferably adsorbed upon the surface of PAN-TETA causing the protonation of amine groups, which in turn favoured the sorption of anionic Cr(VI) species (such as $HCrO_4^-$ and CrO_4^{2-}) (Wang et al., 2011). At high pH values, the H^+ concentration significantly reduced and consequently decreased the adsorption of chromium. Similar pH patterns were reported for Cr(VI) sorption by aminated PAN-nfs (Deng and Bai, 2004), anion-exchange resins (Shi et al., 2009) and amine-modified celluloses (Anirudhan et al., 2009).

2.11.3 Point of zero charge

The point of zero charge (pzc) of a material is when the electrical charge density on a surface of the material is zero. In adsorption, the point of zero charge determines how easily a substrate is able to adsorb metal ions. Pzc is equivalent to the pH value only when H^+/OH^- are the potential determining ions. Deng et al. (2003b), in their adsorption experiments of copper ions using hydrolysed PAN-nfs (HPAN-nfs) observed that the point of zero potential of the nanofibres is at pH about 5.3. When the solution pH values were below 5.3, the pzc of the HPAN-nfs are positive and therefore the interaction between copper ions and the surface of the HPAN-nfs is electrostatically repulsive. Decreasing the solution pH increased the repulsive force between copper ions and the surface of the HPAN-nfs and thus inhibited the transport of copper ions from the bulk solution to the surface of the HPAN-nfs for adsorption to take place. Deng et al. (2003a) prepared aminated PAN-nfs with diethylenetriamine for adsorbing lead and copper ions from aqueous solutions. It was found that the pzc of the aminated PAN-nfs was at about pH 8.1, in contrast with that of the pristine PAN-nfs at pH 3.6, and the aminated PAN-nfs had significantly higher adsorption capacities for both lead and copper ions than the pristine PAN-nfs. The literature on the pzc studies of modified PAN are few and are rarely studied.

2.11.4 Effect of initial concentration

The initial concentration of a model toxic metal ion solution for adsorption is usually prepared in ppm (mg/L). For effective application of adsorbents towards environmental remediation, the initial metal concentration is usually prepared relative

to the World Health Organization (WHO) standards. In adsorption studies of modified PAN-nfs, it is generally noticed that the amount of metal ions adsorbed increase with an increase in the initial concentration of the metals ions. At a certain point, the concentration might attain a saturation plateau where there will be no space on the adsorbent to adsorb (Soltanzadeh et al., 2013; Horzum et al., 2012; Deng et al., 2003a). Soltanzadeh et al. (2013) and Deng et al. (2003a) showed that the amount of copper adsorbed on PAN-TETA increased with an increase in initial concentration. This was also reported by Deng et al. (2003b) when they used hydrolysed PAN for removal of Cu. Horzum et al. (2012) showed that amount of adsorbed uranyl ions on amidoximated PAN-nfs increased with the increase in the initial concentration of uranyl ions. Feng et al. (2011) also observed the same trend for Cu(II) and Cd(II) on amidoximated PAN-nfs (AMPAN-nfs). The initial increase in metal ion adsorption might be attributed to many available amidoxime groups in AMPAN-nfs. However, as more sites in the amidoxime groups were filled, it became difficult for more metal ions to find vacant sites. At the same time, the amount of metal ions adsorbed reached saturation sooner with an increase in the concentration of metal ions (Horzum et al., 2012; Feng et al., 2011).

2.11.5 Effect of contact time

It is a usual trend in adsorption studies that as the contact time increases, there is also an increase in amount of metal ions adsorbed. This is mainly due to a sufficiently large surface area and the availability of active sites of the adsorbent at the beginning of the adsorption process. The contact time could also be related to protonation time; as the time increases the protonation time also increases and the H^+ takes up the adsorption sites blocking other metal ions (Wang et al., 2014). Neghlani et al. (2011) observed that the amount of Cu(II) adsorbed onto the PAN-DETA increased rapidly in the first 20 minutes and then levelled off. Saeed et al. (2011) modified PAN-nfs with hydrazine for adsorption of Cu(II) and Pb(II) ions in aqueous solution. The amount of adsorption of both metal ions increased as the adsorption time increased. Kampalanonwat and Supaphol (2010) also observed that an increase in the contact time also resulted in a monotonous increase in the amounts of the metal ions adsorbed on PAN-DETA, which finally reached equilibrium at about 5 hours for Ag(I), Fe(II), Pb(II) and 10 hours for Cu(II). The removal rate of Cr(VI)

by PAN-TETA versus sorption time as plotted by Wang et al. (2011) showed that the sorption equilibrium was reached very fast and took only about 10 minutes. Fast kinetics was also reported by Ndayambaje et al. (2016) while using modified PAN-nfs for adsorption of Ni^{2+}. Kampalanonwat and Supaphol (2011) showed that for hydrolysed PAN-nfs (HPAN-nfs), the amounts of the Cu(II) ions adsorbed increased with an initial increase in contact time at the optimal pH of 5.0. The plateau values were reached after about 5 hours of immersion of HPAN-nfs.

2.11.6 Amount of adsorbents

The amount of modified PAN-nfs is rarely studied in adsorption. Meanwhile an increase in the amount of adsorbent would translate to an increase in the number of adsorption sites and thereby increase the adsorption of metal ions. Contrary to this, Soltanzadeh et al. (2013) reported that with the increase of adsorbent dosage (PAN-TETA) from 0.1 to 0.3 g, the copper ions sorption capacity decreased from 49.3 mg/g to 16.39 mg/g, while the cadmium ions sorption capacity decreased from 39.73 mg/g to 13.2 mg/g. It was attributed to the aggregation of adsorbent particles at high dosage, which reduced the total surface area of the adsorbent and resulted in an increase in the diffusion path length. In the case where the initial concentration of metal ion is kept constant, an increase in the amount of adsorbent would lead to a large number of sites available for a fixed concentration of metal ions (Soltanzadeh et al., 2013), meaning that saturation of the sites would not occur and the excess capacity of the adsorbent would be wasted.

2.11.7 Desorption and regeneration of adsorbents

Desorption of toxic metals from various modified PAN-nfs is carried out in order to recover the adsorbed metals and also to regenerate the adsorbents. Most desorption processes are carried out with acids or bases of different molar concentrations. This process must be carefully studied and optimised so as to avoid reduction in the active sites of the adsorbents by the regenerating agents. Kampalanonwat and Supaphol (2010) regenerated PAN-DETA with HCl of concentrations ranging from 2.0 M to 10.0 M after batch adsorptions of Cu(II), Ag(I), Fe(II) and Pb(II). Desorption of metal ions was carried out in 20 mL of each concentration of HCl. The results

obtained showed that desorption efficiency of over 90% was achieved for all the metals with 10 M HCl solution. Saeed et al. (2008) also carried out desorption test on amidoximated PAN-nfs after adsorption of Cu(II) and Pb(II) using 1 M HNO_3. Desorption percentages were 40 and 58 respectively within 2 minutes and after 1 hour, the amount of recovered metals were over 90%. As reported by Feng et al. (2011), Cu(II) and Cd(II) were desorbed from amidoximated PAN-nfs using 1 M HNO_3. The results showed 87% (Cu) and 92% (Cd) was desorbed after 60 minutes.

Desorption tests on uranyl ion-loaded amidoximated PAN-nfs as carried out by Horzum et al. (2012) showed that chelating agents can be good regenerating agents. $NaHCO_3$, EDTA, and ammonium citrate were used as chelating agents for the release of uranyl ions and the regeneration of the adsorbent. The desorption percentages of U(VI) were 80% for 0.5 M $NaHCO_3$, 45% for 0.5 M ammonium citrate and 34% for 0.1 M EDTA. Therefore, $NaHCO_3$ was adjudged as the desorbing eluent due to its relatively higher desorption yield. It was further explained that uranium forms negatively charged or neutral carbonate complexes and the adsorbed uranyl ions could be eluted from the sorbent using $NaHCO_3$ through the addition of carbonate ions to complex uranyl ions. After five cycles, the efficiency of sorption decreased from 86.0% to 59.5% while the recovery of U(VI) decreased from 80.0% to 55.0%.

Deng et al. (2003b) hydrolysed PAN-nfs with NaOH for removal of copper ions and subsequently desorbed the metal ions using 1.0 M HCl. In their work, up to 89% of the adsorbed copper ions were desorbed within 2 minutes, and the percentage of desorption reached 98% after 30 minutes. Kampalanonwat and Supaphol (2011) also hydrolysed PAN-nfs with NaOH in ethanolic/aqueous for removal of Cu ions. Desorption was likewise carried out in deionised water and 1.0 M HCl. The results were in agreement with the previous report by Deng et al. (2003b). Saeed et al. (2011) adsorbed Cu and Pb using hydrazine-PAN-nfs adsorbents. Desorption of the metal ions from metal-loaded hydrazine-PAN-nfs were carried out using 1.0 M HNO_3. Desorption percentage of Cu(II) and Pb(II) were 52% and 73% respectively in 15 minutes.

http://etd.uwc.ac.za/

It is worthy of note that in all these experiments reported above, the purpose of desorption was partially achieved because the authors only reported the recovery of the adsorbed metals, but the reusability of their adsorbents after regeneration was not checked. The reason is not clear, however, it is suggestive that chelating ability of their adsorbents after desorption using acids was jeopardized, hence no report on characterisation of their adsorbent after desorption using acids.

2.12   Chapter summary

This review has shown that although water covers the larger percentage of the earth, this does not imply that potable water is everywhere, and the water pollution nemesis is largely due to human and industrial activities. The wastewater coming out of industries and houses is largely polluted by inorganic and organic compounds. Water consuming industries such as textile and paint in-turn give out water largely polluted by dyes. Dyes, a colour compound group, seriously affect the properties of potable water, making water colour with odour. Several successes have been achieved in using the existing methods for the removal of dyes from water. Some of these methods would have to be combined to give better results. Among these methods are filtration and adsorption which are the easiest and most readily available methods. For these two methods, membranes and adsorbents with specific properties are essential.

Electrospinning has been recognised as a viable process that creates in nano-scale nanofibres. Presently, nanofibres have attracted the attention of researchers due to their remarkable micro and nano structural characteristics, high surface area and small pore size. The PA6 and PAN nanofibres are examples of nanofibres that have been produced through electrospinning. These polymers share excellent characteristics such as chemical resistance, good thermal stability and superior mechanical properties.

Track-etched membrane are basically produce in two steps; first by irradiation of polymer film by energetic heavy ions creating linear damage tracks, then by chemical etching of these tracks to create pores.

PAN-nfs can be chemically modified. This is done by targeting the nitrile group on it. As a result of this property, chelating groups such as amidoxime can be immobilised on it. The introduction of a preferred chelating group can be a good avenue in selecting the metals to be removed from solution even though pH of the solution may play a significant role on the oxidation state of the metals and the adsorbents. This brings to notice that for selectivity to be achieved, the adsorbents cannot be treated in isolation; thus parameters such as pH should be taking into considerations as well.

This research will critically look into two major methods for water purification; filtration and adsorption processes. Electrospun nanofibres and track-etched membrane will be used as membranes for removal of dyes. These two materials will also be combined for the same purpose. The research will further look into the functionalisation of PAN-nfs using 2-pyridine amidoxime ligand. The functionalised materials will be used for removal of toxic metal from water.

3   Introduction

This chapter will focus on the experimental aspect of this research. The first section presents the sources of materials and chemicals used for all the experiments. The second section includes all the experimental procedures for the synthesis, the fabrication of materials and their application experiments. The last section gives the basic backgrounds of all the analytical techniques used to characterise materials and samples that were used in this research.

3.1   Materials and chemicals

3.1.1   Sample handling and storage

All the chemicals used for this study were purchased (except 2-pyridine amidoxime which was synthesised and stored in a desiccator) and were kept in cool and dark places (separately according to their flammability and toxicity). The TiO_2-coated PET track-etched membrane was supplied by Joint Institute for Nuclear Research (JINR), Dubna, Russia, in a sealed plastic bag and was kept away from heat and UV light to avoid alteration in specification. All the electrospun nanofibres and the composite nanofibres/TiO_2-coated PET track-etched membranes were kept in a wax wrap prior to use to prevent mechanical damage. The surface modified PAN-nfs mats were stored in a desiccator.

3.1.2 List of chemicals

The sources and percentage purity of all the chemicals used in this study are presented in Table 3.1. For all the experiments and the solutions prepared, deionised water of conductivity 1.12 μS/cm was used.

Table 3.1: List of chemicals used in the study.

Reagents	Specification/ % Purity	Source
Polyacrylonitrile Powder (PAN)	Ave. Mol.W (150000)	Aldrich
Polyamide 6 pellet (PA6)	Density: 1.084 g/mL	Aldrich
Dimethyl formamide (DMF)	99.5	Merck
Formic acid	95	Sigma
2-pyrindine carbonitrile	99	Sigma
Hydroxylamine hydrochloride	99	Sigma
Sodium carbonate monohydrate	99.5	Sigma
Potassium hydroxide	99	Kimix
Aluminium chloride hexahydrate	99	Sigma
Nitric acid	90	Sigma
Ethanol	96	Sigma
Methanol	99.9	Merck
Deuterated dimethyl sulfoxide	99.9	Aldrich
Deuterated water	99.9	Aldrich
Rhodamine 6G	95	Sigma
Lead nitrate	99	Sigma
Ethylenediaminetetraacetic acid (EDTA)	95.9	Kimix

3.1.3 List of equipment

The Table 3.2 presents the list of equipment and their uses in this study.

Table 3.2: List of equipment.

Equipment	Applications
pH meter (Mettler Toledo, SCS200-K)	To determine pH of solutions
Conductivity meter (Thermo scientific, orion 5 star)	To measure the conductivity of deionise water
Fourier transform infrared spectroscopy (Thermo Scientific, Nicolet iS10)	To determine the functional groups of the nanofibres, the ligand and the functionalised PAN-nfs
Ultra violet visible spectroscopy (Thermo Electron Corporation, Nicolet Evolution 100)	To determine the absorbance of the dye solutions
High resolution scanning electron microscopy (HRSEM) (Field Emission High Resolution, Zeiss Gemini Auriga, Germany)	To determine the surface morphology of the track-etched membrane and the nanofibre mats
Electron dispersive X-ray Spectroscopy (EDS) (Field Emission High Resolution, Zeiss Gemini Auriga, Germany)	To indicate the presence of Ti on the PET track-etched membrane
Quorum Q150T ES Sputter Coater	For coating nanofibres with Au
Transmission electron microscopy (TEM) (FEI Tecnai G2 20 field-emission gun (FEG))	To check the surface and the internal structure of nanofibres
Thermal gravimetry analysis (PerkinElmer Frontier, TGA 4000)	To determine the thermal stability of nanofibres
Inductively coupled plasma-optical emission spectroscopy (Varian Radial, Varian 710-ES)	To determine the metal content in the water samples after adsorption/desorption experiments
Surface area and porosity analyser (Micrometrics, tristar)	To determine the BET surface area and the pore size distribution of the nanofibres
Nuclear magnetic resonance (Bruker Avance III HD 400 MHz)	To characterise 2-pyridine amidoxime ligand
Philips X-pert pro MPD X-ray diffractometer	To check the amorphous nature of pristine PAN-nfs and functionalised PAN-nfs
Metering pump (Pump 33, Harvard apparatus)	To give a steady flow rate during electrospinning and adsorption-filtration of dyes
High voltage direct current potential	To supply high voltage during electrospinning process
20 mL plastic syringe	To hold polymer solution during electrospinning and dye solution during adsorption
Teflon filter holder	To hold the membrane during adsorption-filtration of dye

3.2   Experimental methods of the study

The experimental method for this research comprises four main procedures namely: the electrospinning, the synthesis of ligand, the ligand immobilisation and the adsorption studies.

3.2.1 Electrospinning process

Figure 3.1 is the annotated schematic diagram of the electrospinning process that was used for the production of the nanofibres and the composite nanofibres track-etched membranes as presented in the following subsections.
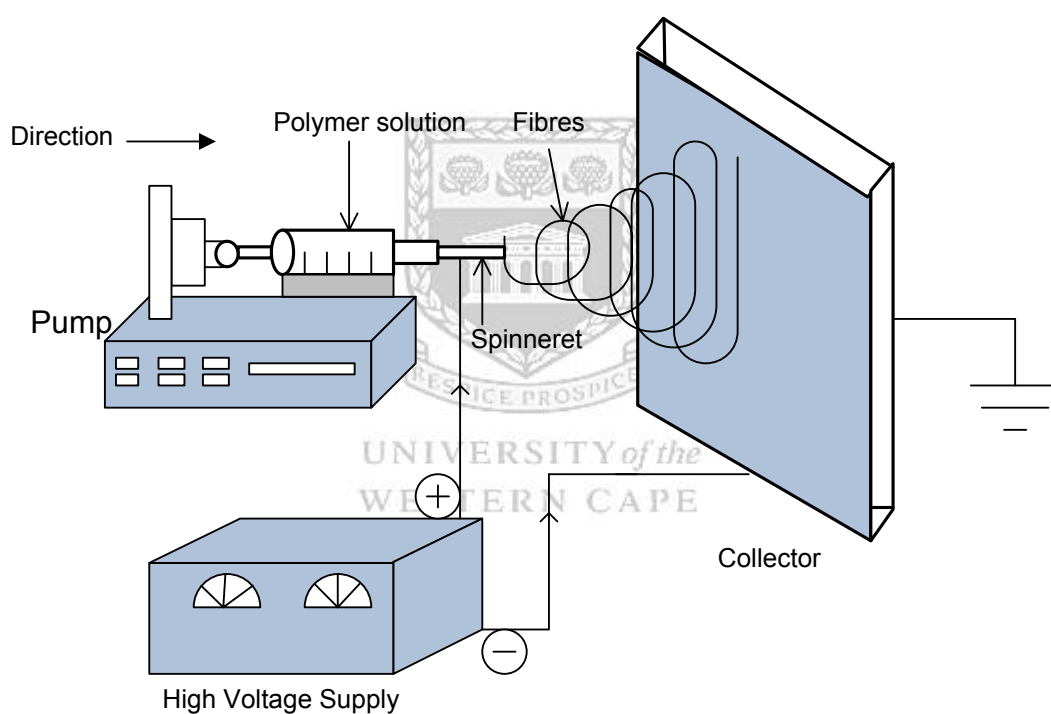
Figure 3.1: Electrospinning set-up.

3.2.1.1 Electrospinning of PA6 solution

The electrospinning procedure was adapted from previously conducted studies with minor modification (salt was not added and 0.2 mm inner diameter iron needle was used) (Heikkilä and Harlin, 2008). This experiment was carried out to optimise the electrospinning concentration for PA6. The following five PA6 concentrations in

brackets were calculated (according to equation 2.1) and prepared in formic acid (6 wt%, 8 wt%, 10 wt%, 12 wt% and 14 wt%). Each concentration was electrospun by introducing the polymer solution into a 20 mL syringe with 0.2 mm inner diameter iron needle. The syringe was fitted into a metering syringe pump (Figure 3.1). A stationary collector covered with A4 size Al foil was used. For the process parameters: the flow rate was set at 0.4 mL/hr, voltage of 25 kV was applied across the collection distance of 10 cm at room temperature of 28°C. All these parameters were kept constant for all the concentrations during electrospinning process that lasted for 4 hours. The nanofibres from the respective five concentrations were mechanically collected from the Al foil and transferred into wax wraps labelled with code names; 6 wt%, 8 wt%, 10 wt%, 12 wt% and 14 wt% respectively and stored in a cupboard. Each nanofibre was characterised using HRSEM technique. The average fibre diameter of nanofibres from respective concentration was measured from the HRSEM image using image J software. The optimal nanofibre (14 wt%) was further characterised using TEM, ATR-FTIR, TGA and BET techniques.

3.2.1.2 Electrospinning of PAN solution

The electrospinning procedure was adapted from the previously conducted studies with minor modification in the process parameters (Horzum et al., 2012; Neghlani et al., 2011). This experiment was carried out to optimise the electrospinning concentration for PAN. The following five PAN concentrations in bracket were calculated (according to equation 2.1) and prepared in DMF (4 wt%, 6 wt%, 8 wt%, 10 wt% and 12 wt%). Each concentration was electrospun by introducing the polymer solution into a 20 mL syringe with 0.2 mm inner diameter iron needle. The syringe was fitted into a metering syringe pump (Figure 3.1). A stationary collector covered with A4 size Al foil was used. For the process parameters: the flow rate was set at 0.4 mL/hr, voltage of 25 kV was applied across the collection distance of 15 cm at room temperature of 28°C. All these parameters were kept constant for all the concentrations during electrospinning process that lasted for 4 hours. The nanofibres from the respective 6 concentrations were mechanically collected from the Al foil and transferred into wax wraps labelled with code names; 4 wt%, 6 wt%, 8 wt%, 10 wt% and 12 wt% respectively and stored in a cupboard. Each nanofibre was characterised using HRSEM. The average fibre diameter of nanofibres from

respective concentration was measured from the HRSEM image using image J software. The optimal nanofibre (8 wt%) was further characterised using TEM, ATR-FTIR, TGA and BET techniques.

3.2.1.3 PET track-etched membrane (PET-TM)

PET track-etched membrane (PET-TM) was produced at Joint Institute for Nuclear Research (JINR), Dubna, Russia. The process involved the irradiation of PET membrane by swift heavy ions from cyclotron to create latent ion tracks in the polymer film. The PET latent tracks membrane then underwent chemical etching in an alkaline solution, which then convert the latent ion tracks into pores. Thereafter, PET-TM was coated with a thin film of TiO_2 using magnetron reactive sputtering method in order to make the membrane conductive (Rossouw et al., 2015). The PET-TM as received was characterised using HRSEM, ATR-FTIR, SEM-EDS and TGA techniques.

3.2.1.4 Electrospinning of PA6 on PET-TM

The optimised concentration from section 3.2.1.1 was prepared in formic acid and electrospun using the following parameters; the flow rate was set at 0.4 mL/hr, voltage of 25 kV was applied across the collection distance of 10 cm at room temperature of 28°C. A stationary collector covered with A4 size PET-TM instead of Al foil was used. The resultant composite nanofibres track-etched membrane was collected into a wax wrap labelled PET-TMPA6 and kept in a cupboard. The resultant composite membrane was characterised using HRSEM technique.

3.2.1.5 Electrospinning of PAN on PET-TM

The optimised concentration from section 3.2.1.2 was prepared in DMF and electrospun using the following parameters; the flow rate was set at 0.4 mL/hr, voltage of 25 kV was applied across the collection distance of 15 cm at room temperature of 28°C. A stationary collector covered with A4 size PET-TM instead of Al foil was used. The resultant composite nanofibres track-etched membrane was collected into a wax wrap labelled PET-TMPAN and kept in a cupboard. The resultant composite membrane was characterised using HRSEM technique.

3.2.2 Synthesis of 2-pyridine amidoxime (PyAMI)

The synthesis of 2-pyridine amidoxime was adapted from Bernasek, (1957) with little modifications. A solution containing 2.1 g (0.030 moles) of hydroxylamine hydrochloride and 1.845 g (0.0152 moles) of sodium carbonate monohydrate in 10 mL of deionised water in a 100 mL round bottom flask (RBF); was shaken for 30 seconds to speed up effervescence and then allowed to settle. Thereafter, the RBF was corked and the solution was heated to 60°C. 3.0 g (0.029 moles) of 2-pyridine carbonitrile was added in one portion to the solution above, followed by the addition of sufficient ethanol (approximately 10 mL) to dissolve the 2-pyridine carbonitrile. The temperature of the resultant mixture was raised to 90°C and maintained for 3 hours under reflux. The resultant product was cooled to zero degrees. The crystalline solid was filtered, washed twice with ice-cold water, transferred into a schott bottle, dried in a vacuum desiccator over calcium chloride. The dried PyAMI weighed 3.79 g (percentage yield; 96.1%). NMR, ATR-FTIR and TGA techniques were used to characterise PyAMI.

3.2.3 Base-catalysed immobilisation of PyAMI on PAN-nfs

0.0513 moles (6.874 g) of PyAMI and 0.0513 moles (2.805 g) of KOH were mixed and stirred together in a 200 mL glass beaker containing 50 mL deionised water for 15 minutes at 60°C before adding 0.5205 g of PAN-nfs. The reaction was carried out for different times (20, 40, 60 and 90 minutes) at 60°C. The resultant nanofibres were removed and washed with deionised water, and then air dried before drying in an oven over night at 40°C to constant weight. The same procedure was used for the mole ratio (PyAMI/KOH) 1:2. The resultant nanofibres were characterised using ATR-FTIR and HRSEM techniques.

3.2.3.1   Effect of KOH on PAN-nfs

2.8 g (0.052 moles) of KOH was dissolved in 50 mL deionised water in a 200 mL glass beaker. 0.512 g of PAN-nfs was transfered into the solution and stirred. The reaction was carried out for different times (20, 40, 60 and 90 minutes) at 60°C in a 200 mL glass beaker. The resultant nanofibres were removed and washed with deionised water, and then air dried before drying in an oven over night at 40°C to

constant weight. The resultant nanofibres were characterised using ATR-FTIR, HRSEM, TEM and TGA techniques.

3.2.4 Acid-catalysed immobilisation of PyAMI on PAN-nfs

6.8 g (0.051 moles) of 2-pyridine amidoxime and 4.8 g (0.022 moles) of $AlCl_3.6H_2O$ (Kampalanonwat and Supaphol, 2014), were transfered into 50 mL deionised water in a 200 mL glass beaker and stirred for 15 minutes at 60°C until PyAMI completely dissolved. Afterwards, 0.545 g of PAN-nfs was transferred into the solution. The reaction was carried out at different times (20, 40, 60 and 90 minutes) at 60°C. Upon the completion of the reaction time, the resultant nanofibres were washed with deionised water to remove the unreacted PyAMI, and then air dried before drying in an oven over night at 40°C to constant weight. The resultant nanofibres were characterised using ATR-FTIR, HRSEM, TEM, XRD, TGA and BET techniques.

3.2.4.1 Effect of water on PAN-nfs

0.5045 g of PAN-nfs was transferred to 50 mL of deonised water in a 200 mL glass beaker. The reaction was heated to 60°C. The experiment was carried out at different reaction times (20, 40 and 60 minutes). The resultant nanofibres were air dried before drying in an oven over night at 40°C to constant weight. The resultant nanofibres were then characterised using ATR-FTIR, HRSEM and TGA analysis.

3.2.5 Stability of PAN-PyAMI in different pH solutions

This experiment was carried out in order to determine the stability of PAN-PyAMI synthesised in section 3.2.4 in different pH solutions. 10 mL deionised water of different pH ranging from 2.0-6.0 were prepared in plastic vials using 0.1 M HNO_3 and 0.1 M NaOH. 0.1 g of PAN-PyAMI was inserted into each respective vial and shaken for 1 hour at 25°C. The resultant nanofibres were removed and air dried before drying in an oven over night at 40°C to constant weight. The resultant nanofibres were then characterised using ATR-FTIR analysis.

3.2.6 Stability of PAN-PyAMI in EDTA & HNO$_3$ solutions

This experiment was carried out in order to determine the stability of PAN-PyAMI synthesised in section 3.2.4 in the metal sequestering medium. This investigation is important in order to study the regeneration of PAN-PyAMI. The experiments were carried out by shaking 0.1 g of PAN-PyAMI in 10 mL of 0.01 or 0.1 or 1 M EDTA and 0.01 or 0.1 or 1 M HNO$_3$ at 25°C for 1 hour. The nanofibre samples were then washed with deionised water, air dried and then dried in an oven at 40°C for 1 hour. The resultant nanofibres were characterised using ATR-FTIR analysis.

3.2.7 Adsorption studies

The adsorption experiments were the last sets of experiments in this study. The experiments were carried out to investigate the performance of all the synthesised samples on the adsorption of organic and inorganic pollutants. The summary of the samples and their respective target pollutants are presented in Table 3.3.

Table 3.3: Summary of samples and their target pollutants.

Samples	Target pollutants
PA6-nfs PAN-nfs PET-TM PET-TMPA6 PET-TMPAN	Rhodamine 6G (RD)
PAN-nfs and PAN-PyAMI	Pb^{2+}

3.2.7.1   Theory and calculations

All the adsorption experiments were carried out at 25°C and the amount of pollutants adsorbed (mg/g) was calculated based on a mass balance equation as given in equation 3.1.

$$q_e = \frac{(C_o - C_e)}{M} V \ldots \ldots \ldots \ldots \ldots \ldots \ldots \ldots \ldots equation\ 3.1$$

where q_e is the equilibrium adsorption capacity per gram dry weight of the adsorbent (mg/g); C_0 is the initial concentration of the adsorbate in the solution (mg/L); C_e is the final or equilibrium concentration of adsorbate in the solution (mg/L); V is the volume of the solution (L); and *M* is the dry weight of the adsorbent (g).

The removal/adsorption (R) is defined as equation 3.2;

$$R = 1 - \frac{C_e}{C_0} \ldots \ldots \ldots \ldots \ldots \ldots \ldots \ldots \ldots \ldots \ldots equation\ 3.2$$

The percentage removal/adsorbed is defined as equation 3.3;

$$R = \left(1 - \frac{C_e}{C_0}\right) X\ 100 \ldots \ldots \ldots \ldots \ldots \ldots \ldots \ldots equation\ 3.3$$
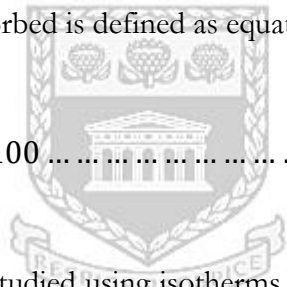
Adsorption experiments are studied using isotherms and kinetics modelings to know the details about the performance, the mechanisms, practical design and the operations of the adsorption systems. The following are the mathematical modelings that were used to study the adsorption behaviour of the adsorbates on the materials.

3.2.7.1.1   Adsorption isotherms

Adsorption isotherms describe how adsorbates (in liquid phase) interact with adsorbents. From the isotherms, the maximum sorption capacity can be obtained. Sorption equilibrium provides fundamental physiochemical information on the capacity of adsorbent to remove a unit mass of pollutant. This study only covers Langmuir and Freundlich isotherms.

Langmuir Isotherm: Langmuir isotherm is used to explain the adsorption of materials from liquid solutions with an assumption that monolayer adsorption onto a homogeneous surface with finite number of identical sites takes place. The Langmuir

isotherm is expressed as equation 3.4 and the linearised form of the model as equation 3.5.

$$q_e = \frac{q_m b C_e}{1 + b C_e} \dots \dots \dots \dots \dots \dots \dots \dots \dots \dots . equation \; 3.4$$

$$\frac{1}{q_e} = \frac{1}{q_m} + \frac{1}{b q_m} \frac{1}{C_e} \dots \dots \dots \dots \dots \dots \dots \dots . equation \; 3.5$$

where q_e (mg/g) is the adsorption capacity at equilibrium, C_e (mg/L) is the equilibrium concentration of the pollutant in the solution, q_m (mg/g) is the maximum monolayer adsorption capacity and b (L/mg) is the Langmuir constant related to the free energy of adsorption. The values of b and q_m can be obtained from the slope and the intercept of the straight line plotted from the linearised form of the Langmuir isotherm, respectively (Yang et al., 2011).

$$R_L = \frac{1}{1 + b C_0} \dots \dots \dots \dots \dots \dots \dots \dots \dots equation \; 3.6$$

From the Langmuir isotherms, the R_L factor can be calculated according to equation 3.6. This is a factor that determines the tendency between adsorbents and the adsorbate. The R_L value is classified into categories including $R_L > 1$, $0 < R_L < 1$, $R_L = 1$, and $R_L = 0$, suggesting that adsorption is unfavourable, favourable, linear and irreversible, respectively (Neghlani et al., 2011; Senturk et al., 2010).

Freundlich Isotherm: Freundlich isotherm is used to explain the empirical relationship that exists between the concentration of the adsorbates and the surface of the adsorbents in contact with it. The isotherm is applicable with an assumption that the adsorbate adsorbs onto the heterogeneous surface of an adsorbent. The Freundlich isotherm is expressed as equation 3.7 while the linearised form of the model can be expressed as equation 3.8.

$$q_e = K_F C_e^{1/n} \dots \dots \dots \dots \dots \dots \dots \dots \dots \dots \dots . equation \; 3.7$$

97

$$\ell\text{n}\,q_e = \ell\text{n}\,K_F + \frac{1}{n}\ell\text{n}\,C_e \dots\dots\dots\dots\dots\dots\dots\dots. \text{equation } 3.8$$

where q_e is the adsorption density at equilibrium and C_e is the equilibrium concentration of the pollutant in solution. n and K_F {mg/g $(\text{L/mg})^{1/n}$} are adsorption intensity of the adsorbent and Freundlich constants related to adsorption capacity, respectively. The value of n falling in the range of 1–10 indicates the favourable sorption. The values of n and K_F can be obtained from the slope and the intercept of the straight line plotted from the linearised form of the Freundlich isotherm, respectively (Uddin et al., 2009).

3.2.7.1.2   Adsorption kinetics

The kinetic performance of a given adsorbent is significant for the application. The kinetic analysis determines the rate of solute uptake which invariably gives the residence time required for completion of adsorption process. Kinetic models are used to examine the rate of the adsorption process and potential rate-controlling step. In this study, the kinetic data obtained from the batch adsorption experiments were analysed by using pseudo-first order and pseudo-second order models.

Pseudo first-order: The pseudo first-order equation also known as the Lagergren rate equation may be expressed as equation 3.9.

$$\frac{dq_t}{d_t} = k_1(q_e - q_t) \dots\dots\dots\dots\dots\dots\dots\dots\dots.. \text{equation } 3.9$$

where q_e and q_t are the amount of solute adsorbed (mg/g) at equilibrium and at time t (min), respectively, and k_1 is the rate constant of pseudo first-order sorption (min^{-1}).

$$\ell\,\text{n}(q_e - q_t) = \ell n q_e - k_1 t \dots\dots\dots\dots\dots\dots\dots\dots \text{equation } 3.10$$

Upon integrating the equation 3.9 with the boundary conditions $t = 0$ to $t = t$ and $q = 0$ to $q = q_t$, equation 3.10 is derived. The model can be validated by plotting $\ell\text{n}(q_e\text{-}q_t)$

versus *t* which should give a linear relationship having the slope as K_1 and ℓn q_e as the intercept (Dogan et al., 2009).

Pseudo second-order: The pseudo second-order equation is generally expressed as equation 3.11

$$\frac{dq_t}{d_t} = k_2(q_e - q_t)^2 \dots\dots\dots\dots\dots\dots\dots\dots equation\ 3.11$$

where k_2 is the rate constant of pseudo-second order sorption (g/mg/min). The integrated form of equation 3.11 using the boundary conditions *t* = 0 to *t* = *t* and *q* = 0 to *q* = *qt* becomes equation 3.12.

$$\frac{t}{q_t} = \frac{1}{k_2 q_e{}^2} + \frac{t}{q_e} \dots\dots\dots\dots\dots\dots\dots\dots\dots equation\ 3.12$$

The initial adsorption rate, *h* (mg/g/min) is expressed as equation 3.13;

$$h = k_2 q_e^2 \dots\dots\dots\dots\dots\dots\dots\dots\dots\dots\dots.\ equation\ 3.13$$

The second order kinetic equation can be validated by plotting *t*/*qt* against *t* of equation 3.12, which should give a linear relationship. The q_e and *h* can be determined from the slope and the intercept of the plot, respectively, hence, k_2 from equation 3.13.

3.2.7.2 Adsorption studies of dye

3.2.7.2.1 Calibration curves

The calibration curve experiment was performed by following the below protocol. Seven concentrations (1, 2, 3, 5, 7, 9 and 10 mg/L) of RD were prepared in deionised water and analysed using UV-vis spectrometry to monitor the absorbance of each concentration at wavelength of maximum absorbance of 527 nm. The calibration curve was obtained by plotting the absorbance against concentration.

3.2.7.2.2   Adsorption experiments

Unless stated specifically, the following absorption experiments were performed following the same protocol for every sample per given parameter. A certain concentration of RD was prepared by dissolving certain grams of RD in 100 mL ultrapure water in 100 mL volumetric flask. The continuous experiments were carried out in order to show that the nanofibres and the composite nanofibres track-etched membranes can remove dyes in a continuous process. A Teflon filter holder containing certain gram of the membrane (Table 3.3) of 12 mm diameter was fitted to the mouth of a 20 mL syringe containing 2 mL of RD. The syringe-filter holder system was then fitted to a metering syringe pump to push all solution through the filter at a certain flow rate. Figure 3.2 is the schematic diagram of the continuous flow set-up. The sample effluent was collected in a 20 mL plastic vial and the decrease in concentration was monitored using UV-vis spectrometry. All experiments were performed at room temperature (25°C).
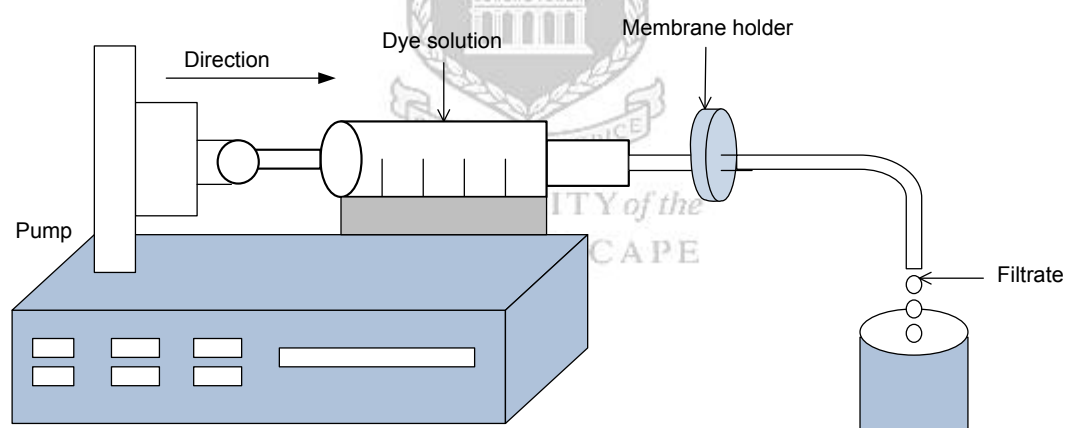
Figure 3.2: Schematic diagram of RD adsorption-filtration.

a. **The effect of initial concentration:** The effect of initial concentration was studied by preparing 2, 5, 10, 15 and 20 mg/L of RD solution (natural pH; 5.6) and was treated as described in 3.2.7.2.2 above at flow rate 1 mL/min. The quantity adsorbed (q_e) and the removal efficiency (R) were calculated according to equations 3.1 and 3.3, respectively. The adsorption isotherms were calculated according to equations 3.4 and 3.7.

b. **The effect of solution pH:** The effect of solution pH was studied by preparing 10 mL pH solutions of 1, 2, 4, 6, 8 and 10 of (optimum concentration; 10 mg/L from section (a) above) of RD using 0.1 M HNO_3 or 0.1 NaOH. The solutions were treated as described in 3.2.7.2.2. The quantity adsorbed (q_e) and the removal efficiency (R) were calculated according to equations 3.1 and 3.3, respectively.

c. **The effect of flow rate**: The effect of flow rate was also studied by varying the flow rate (using the metering syringe pump) (0.5, 1, 2 and 3 mL/min) of 10 mL of RD (at optimum concentration; 10 mg/L and pH; 10 from section (b) above) in the 20 mL syringe. The experiment was carried out as given in 3.2.7.2.2. The quantity adsorbed (q_e) and the removal efficiency (R) were calculated according to equations 3.1 and 3.3, respectively.

d. **Batch adsorption experiment:** This experiment was carried out in order to know the number of cycles of filtration each membrane can take. The optimum concentration; 10 mg/L and pH; 10 of RD was prepared and the solution was treated as described in section 3.2.7.2.2 with flow rate 1 mL/min. For each membrane (Table 3.3), the experiment was carried out in cycles by repeatedly introduced another 2 mL of RD until the equilibrium is obtained and the membrane in the filter holder could no longer adsorb solute. The quantity adsorbed (q_e) and the removal efficiency (R) for each batch were calculated according to equations 3.1 and 3.3, respectively.

3.2.7.2.3   Desorption and reusability experiments

The desorption study was adapted from previous work reported by Uddin et al. (2009) with little modification. Desorption experiment was studied as a function of pH in order to recover the adsorbent and the adsorbate. Desorption was carried out by putting the membrane previously used for adsorption of RD at optimum concentration; 10 mg/L, pH; 10 and flow rate; 1 mL/min. 2 mL of pH 1.8 solution of deionised water was pumped through the membrane. The resultant solution was collected and the concentration was measured using UV-vis spectrometry. The

percentage desorbed was calculated according to equation 3.3. The same membrane was reused to adsorb RD after desorption and the quantity adsorbed was calculated according to equation 3.1 (Yang et al., 2011; Uddin et al., 2009).

3.2.7.3 Adsorption studies of metal ions

3.2.7.3.1 Preparation of stock solution

A 1000 ppm stock solution of Pb^{2+} was prepared by weighing certain grams of $Pb(NO_3)_2$ salt and transferred into 1000 mL volumetric flask containing 500 mL deionised water. The solution was shaken to dissolve the salt and then deionised water was added to fill the volumetric flask to the 1000 mL mark. The stock solutions were stored in a fridge at a temperature of 10°C.

3.2.7.3.2 Adsorption experiments

The adsorption experiments were carried out in batch and in triplicate according to Ndayambaje et al. (2016) and Neghlani et al. (2011) with little modification. The adsorption experiments were carried out by investigating the effect of pH, the initial concentration and the effect of contact time using PAN-PyAMI synthesised in section 3.2.4 as adsorbent.

a. **Effect of solution pH:** The effect of solution pH was investigated to determine the adsorption capacity of PAN-PyAMI at different solution pH. 10 mL pH solutions 2.2, 3.1, 4.2, 4.9 and 6.1 of 200 mg/L of Pb^{2+} were prepared in a 20 mL plastic vial using 0.1 M HNO_3 and 0.1 M NaOH. 0.1 g of PAN-nfs or PAN-PyAMI was weighed and transferred into the respective solution (followed by pH re-adjustment) and shaken for 1 hour at 25°C with stirrer speed of 120 rpm. The resultant solution was filtered and analysed using ICP-OES and the adsorption capacity (q_e) and the percentage adsorption were calculated according to equations 3.1 and 3.3, respectively.

b. **The effect of initial concentration:** The effect of initial concentration was investigated in order to determine the adsorption isotherm of Pb^{2+} on PAN-

PyAMI. 10mL of 50, 100, 150, 200 and 250 mg/L of Pb^{2+} were prepared in 20 mL plastic vials at optimum pH; 4.9 (from section (a) above). 0.1 g of PAN-PyAMI was weighed and transferred into the solution and shaken for 1 hour at 25°C at a stirrer speed of 120 rpm. The resultant solution was filtered and analysed using ICP-OES and adsorption capacity (q_e) and the percentage adsorption were calculated according to equations 3.1 and 3.3, respectively. The experiment was modelled with Langmuir and Freundlich isotherms as described in section 3.2.7.1.1.

c. **The effect of contact time:** In order to study the adsorption kinetics, the effect of contact time was investigated. Seven samples containing 10 mL of 200 mg/L of Pb^{2+} at optimum pH; 4.9 (from section (a) above) were prepared in 20 mL plastic vials. 0.1 g PAN-PyAMI was weighed and transferred into each solution and shaken for 10, 20, 40, 60, 80, 100 and 120 minutes respectively at 120 rpm at 25°C. The resultant solutions were filtered and analysed using ICP-OES. The adsorption capacity (q_e) and the percentage adsorption were calculated according to equations 3.1 and 3.3, respectively. The adsorption kinetics was investigated using pseudo first-order and pseudo second-order kinetics models as described in section 3.2.7.1.2.

3.2.7.3.3   Desorption and reusability experiments

Desorption experiment was carried out in order to regenerate PAN-PyAMI. 0.1 g PAN-PyAMI was transferred into 10 mL of 200 mg/L Pb^{2+} adjusted to an optimum pH; 4.9 (from section 3.2.7.3.2 (a)), and shaken for 1 hour at 25°C after which the solution was filtered and the amount of metal ions adsorbed was determined by ICP-OES. The PAN-PyAMI after adsorption was washed with deionised water to remove un-adsorbed metal ions and then air dried before drying in an oven over night at 40°C. The dried metal loaded PAN-PyAMI mat was then transferred into 10 mL 0.01 or 0.1 or 1 M EDTA and shaken for 1 hour at 25°C for desorption of the metal ions. The resultant solutions from desorption were analysed using ICP-OES. The

regenerated PAN-PyAMI was reused for a number of cycles following the same procedure and conditions to determine the number of reusability cycles.

3.3 Characterisation techniques used in this study

Characterisation techniques are important to every study as they provide the basic information of every material, raw or synthesised, used for the research. The information ranges from the physical, mechanical and the chemical properties. The following sub-sections discuss the basic principles of the instrumental techniques and their applications in this study.

3.3.1 pH measurement

In this study, the pH measurement of all solutions used were done using a pH meter (mettle Toledo, SCS 220-K) at 25°C. Buffer solutions of pH 4.0 and 7.0 were used to calibrate the pH meter. After every measurement, the pH meter probe was rinsed with deionised water.

3.3.2 Ultraviolet-visible spectroscopy (UV-vis)

UV-vis is an absorption spectroscopy or reflectance spectroscopy that uses the light in the near UV and visible region. According to Beer's law (equation 3.14); absorbance of a solution, A, is directly proportional to the concentration, c, and the path length, l, of the absorbing species.

$$A\,(\lambda) = \varepsilon_\lambda lc \dots \dots \dots \dots \dots \dots \dots \dots \dots \dots \dots \dots \dots equation\ 3.14$$

where ε is the extinction coefficient (in $cm^{-1}.mol^{-1}.L$).

In this study, the absorbance of dyes solutions were analysed using UV-vis (Thermo Electron Corporation, Nicolet Evolution 100). About 2 mL of the sample mixture was poured into a UV-vis spectrometer quartz cuvette and then was analysed in the range of 300 nm to 700 nm.

3.3.3 High resolution scanning electron microscopy (HRSEM)

HRSEM is an instrumental analysis basically used for observing surface morphology of materials at a very small scale such as nanometer and micrometer. The machine produces a bean of electrons that hits the specimen resulting in the emission of X-rays. The electron recorder then picks up the rebounding electrons. The information from the electron recorder is translated onto a screen as three-dimensional images. Metal samples can be studied directly while a non-conducting material must undergo a pre-preparation. Sputter coating allows thin layer of conductive substance (usually gold or carbon) to be deposited on specimen with the use of an electric field and argon gas. Apart from images, HRSEM can also use energy-dispersive X-ray spectroscopy (EDS) to determine the elemental composition and elemental mapping. In this study, HRSEM (Zeiss Gemini Auriga) was used to analyse the surface morphology of all the nanofibres, the PET-TM, the composite membranes and the functionalised PAN-nfs. All the samples were coated with gold (except PET-TM) using Quorum Q150T ES Sputter Coater machine. The sample images from HRSEM were taken at different magnification levels.

3.3.4 Transmission electron microscopy (TEM)

TEM is an instrument that operates similarly to other electron microscopy techniques except that for TEM, the electron beams penetrate and interact with atoms of the materials, thereby leading to scattering of electrons. For this study, TEM was used to study the internal structure of the nanofibres. Each sample was prepared by drop-coating one drop of specimen solution onto a carbon coated copper grid. This was then dried under a xenon lamp for about 10 minutes, where after, the sample coated grids were analysed under the microscope. Transmission electron micrographs were collected using an FEI Tecnai G2 20 field-emission gun (FEG) TEM, operated in bright field mode at an accelerating voltage of 200 kV.

3.3.5 Thermal gravimetry analysis (TGA)

Thermal gravimetry analysis is a technique used to determine the changes in physical and chemical composition of a material by measuring the weight loss associated to an increase in temperature. The weight loss can be as a result of decomposition,

oxidation, or loss in moisture content. TGA can also be used to determine the organic and inorganic content. Generally, a small mass less than 5.0 mg of sample is required and the result is plotted on the screen as the sample loses weight with an increase in temperature. The thermal properties of PET-TM, PA6-nfs and PAN-nfs (before and after modification) were performed using TGA 4000 PerkinElmer thermal analyser. Approximately 4.0 mg of each sample of nanofibres was weighed using a sample holder and then placed in the machine. The TGA analysis was conducted under nitrogen and the heating rate of the sample was set at 20°C/min up to 800°C and then held for 1 minute at 800°C.

3.3.6 Fourier transform infrared spectroscopy (FTIR)

Fourier transform infrared spectroscopy is a technique used to determine the functional groups of a molecule. The technique measures an infrared spectrum of absorption or transmittance of a solid, liquid or gas. FTIR samples are usually prepared using potassium bromide (KBr) pellet method. However, for this study, the attenuated total reflectance (ATR) accessory was used. This is because the surface studies of the materials were only required. For the analysis, each sample was placed on the diamond crystal and the ATR holder was screwed in to make the sample have a good contact with the crystal. The FTIR was set to scan 64 times at a resolution of 2.0 cm^{-1} over the wavelength range of 4000 cm^{-1} to 650 cm^{-1} against the transmittance. After every scan, the baseline was corrected using the background spectrum previously obtained from the blank scan.

3.3.7 Surface area and porosity analyser

Surface area and porosity analyser is the instrument used to determine the *Brunauer, Emmett and Teller* (BET) surface area and pore size of porous materials. BET measurement is based on nitrogen adsorption–desorption measurement of gas on the material surface. The quantity of the gas adsorbed can then be determined by the Langmuir isotherm with an assumption that a monolayer of the gas molecules was adsorbed on homogenous surface of the material. From the results, the pore size of the material can be determined and classified as microporous (up to 2 nm) or mesoporous (2 nm to 50 nm). For this study, surface area and porosity analyser

(Micrometrics, tristar) was used to determine the BET surface area and pore size distribution of nanofibres.

3.3.8 X-ray diffraction (XRD)

X-ray diffraction (XRD) is a technique generally used in identification of crystalline materials, which could be minerals or inorganic compounds. However, for this research, the analysis was carried out to check the amorphous nature of PAN-nfs before and after functionalisation. XRD is based on the principle of bombarding material with accelerated electrons which invariably leads to the dislodgement of inner shell electron of the material, thereby generating X-ray. The results are recorded as a function of intensity of diffracted X-rays in relation to the rotating angle of the sample and the detector. For this research, XRD was carried out using Philips X-pert pro MPD X-ray diffractometer with Cu-K radiation, operated at 40 kV and 40 mA. The sample was scanned over a range range of 5° to 70° 2θ with the count step size set at 0.5 seconds per step/0.05 step size.

3.3.9 Nuclear magnetic resonance (NMR)

The nuclear magnetic resonance spectroscopy is a technique used for the elucidation of chemical structures of compounds. The NMR techniques read into the magnetic properties of atomic nuclei. If an atom in a molecule is surrounded by an intra-molecular magnetic field, the resonance frequency of the atom changes, thus giving insight to the electronic structure of the molecule. Samples for NMR can be solid (for solid state NMR) or liquid (for solution NMR). For this study, only solution NMR technique was used to study the amidoxime chelating groups. For solution NMR, 20 mg of PyAMI was dissolved in 500 μL DMSO-d$_6$ solvent in an NMR tube. For the sample, full scan of ^{1}H NMR, ^{13}C NMR and ^{13}C NMR DEPT techniques were used. The spectra were resolved and calibrated at 2.5 ppm and 39.5 ppm for DMSO peak of ^{1}H NMR and ^{13}C NMR, respectively.

3.3.10 Inductively coupled plasma-optical emission spectroscopy

The inductively coupled plasma-optical emission spectroscopy (ICP-OES) is a technique used in atomic spectroscopy. The principle behind the technique is

excitation-emission of elements in a sample. During the analysis, the sample is decomposed under enormous heat into hot gas thereby making the ions in the element free. At this high temperature, the ions went into excited and ionization state. When the excited atoms return to low energy position, emission rays are released which correspond to the photon wavelength. During ICP-OES analysis, the intensity of the light emitted at specific wavelength is measured and used to determine the concentration of the element(s) of interest. For this research, Varian Radial ICP-OES (High Matrix Introduction (HMI) accessory, Collision gas; Ar) was used to determine the quantity of metal ions (Pb^{2+}) during adsorption and desorption experiments. Table 3.4 presents the ICP-OES operating parameters.

Table 3.4: Inductively coupled plasma-optical emission spectroscopy operating parameters.

Instrument parameters	Instrument settings for the analysis
Sampling depth	8.5 mm
Sample flow rate (peristaltic pump)	50 rpm
Argon gas flow rate	5 L/min
Auxiliary gas flow rate	0.5 L/min
Applied radio frequency power (RF)	1150 W
Nebulizer argon gas	1.5 L/min
Sample flash time	300 s
Total integration time	30 s/metal analyte
Time scan acquisition	50 ms/point
Optics temperature	36°C
Generator temperature	24°C
Cooled spraying chamber temperature	4°C
Sample replication	Triplicates

4 Introduction

For scientific understanding of this study, it is imperative to characterise all the materials prepared. The characterisations of these materials were done in order to study the various properties such as surface morphology, physical properties, chemical properties and thermal properties. This chapter presents the characterisation results of both starting materials and the synthesised samples mentioned in chapter three.

4.1 Characterisation of nanofibres and membranes

4.1.1 Polyamide 6 nanofibres (PA6-nfs)

From the electrospinning experiments of PA6 in formic acid (section 3.2.1.1), PA6-nfs of different average fibre diameters (AFD) were obtained by varying the concentration (6, 8, 10, 12 and 14 wt%) of PA6 solution in formic acid and fixing other electrospinning process parameters at: applied voltage of 25 kV, flow rate of 0.4 mL/hr and collection distance of 10 cm at room temperature 28°C. The resultant PA6-nfs are characterised using HRSEM, TEM, ATR-FTIR, TGA and BET techniques. The results are presented in the following sub-sections.

4.1.1.1 HRSEM of PA6-nfs

To understand the effect of concentration on the fibre formation and the fibre diameter, HRSEM was used to observe the surface morphology of 6, 8, 10, 12 and 14 wt% PA6-nfs electrospun nanofibres in section 3.2.1.1. The HRSEM analysis was carried out as described in section 3.3.3. Each sample of PA6-nfs was coated with Au and was observed at different magnifications under HRSEM. Figure 4.1 is the HRSEM images of PA6-nfs at different polymer concentrations in formic acid. At 6 wt%, only a few strands of fibres were noticeable, the rest were beads.
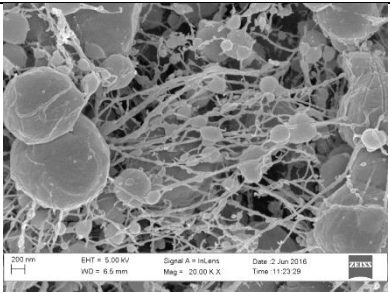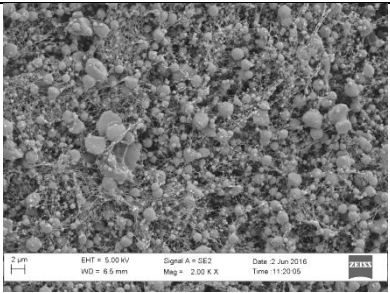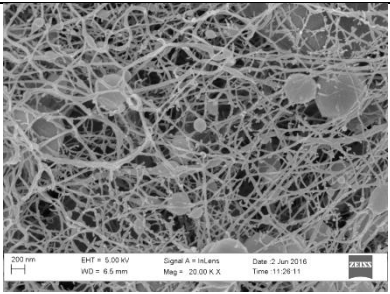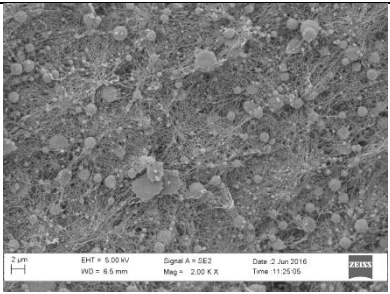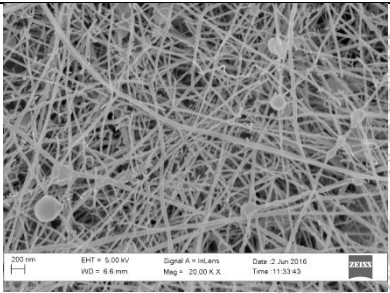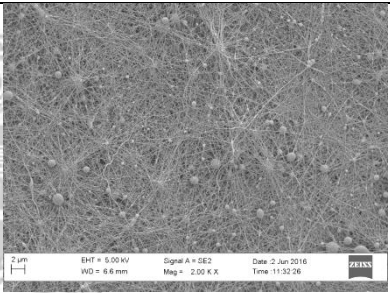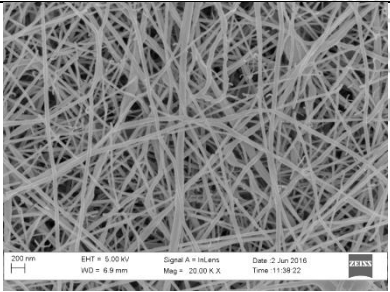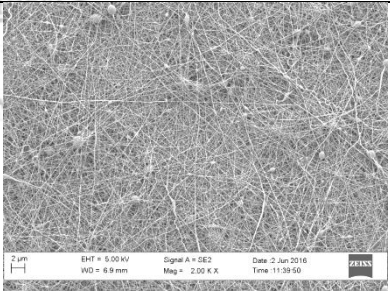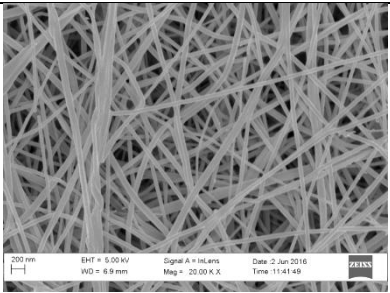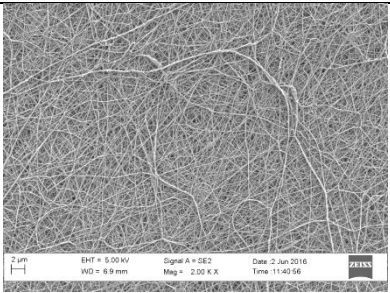
Conc.	SEM images at 20k magnification	SEM images at 2k magnification	AFD
6 wt%			30±7.1 nm
8 wt%			41±8.5 nm
10 wt%			43±8.9 nm
12 wt%			47±8.6 nm
14 wt%			52±9.8 nm

Figure 4.1: HRSEM images of PA6-nfs at different concentrations in formic acid.

110

The same structure was observed for 8 wt%, but with fewer beads. However, at 10 wt%, the HRSEM image shows that a good number of nanofibres were formed with very few beads. At 12 wt%, the beads had almost disappeared and finally, at 14 wt%, the image shows smooth nanofibres with no beads. The beading observed at lower concentration could be as a result of low viscosity of the solution at low concentration of PA6 in formic acid, which caused electrospraying instead of electrospinning simply because the solution could not remain long enough in the spinneret to be charged. This trend has also been reported for PA6 by Nirmala et al. (2014). It is therefore clear that as the concentration of PA6 in formic acid increased, the beads disappeared and more nanofibres were formed, with an optimum concentration of 14 wt% at electrospinning process parameters of; applied voltage of 25 kV, flow rate of 0.4 mL/hr, collection distance of 10 cm and the room temperature of 28°C. Further concentration above 14 wt% was not studied since the research is focusing on nanofibres without beads with minimal fibre diameter. The above optimal conditions were used to electrospin 14 wt% PA6 until ≈0.5 mm thickness of PA6-nfs was formed on the collector. The time to reach this thickness was 6 hours 45 minutes.

The average fibre diameter (AFD) (Figure 4.1) was determined using image J software by measuring the nanofibre diameter of at least 20 nanofibre strands on the HRSEM images. Figure 4.2 shows that the nanofibre diameter of PA6-nfs is directly proportional to polymer concentration (Bhardwaj and Kundu, 2010). Figure 4.3 shows the nanofibre diameter distributions at different concentrations.
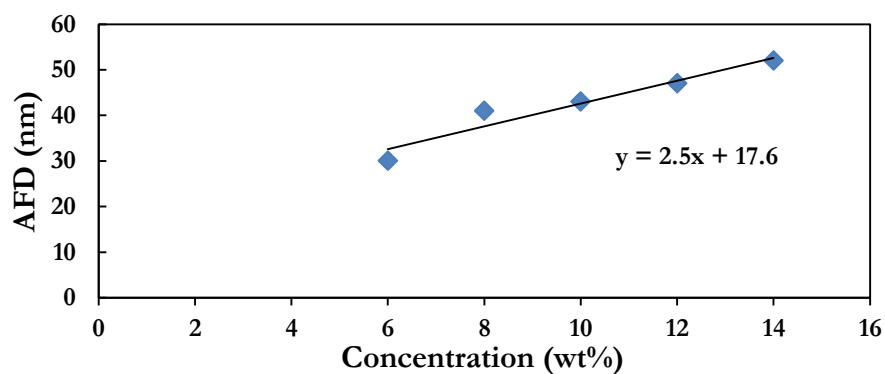
Figure 4.2: Graph showing the relationship between the average fibre diameters of PA6-nfs and the polymer concentrations.
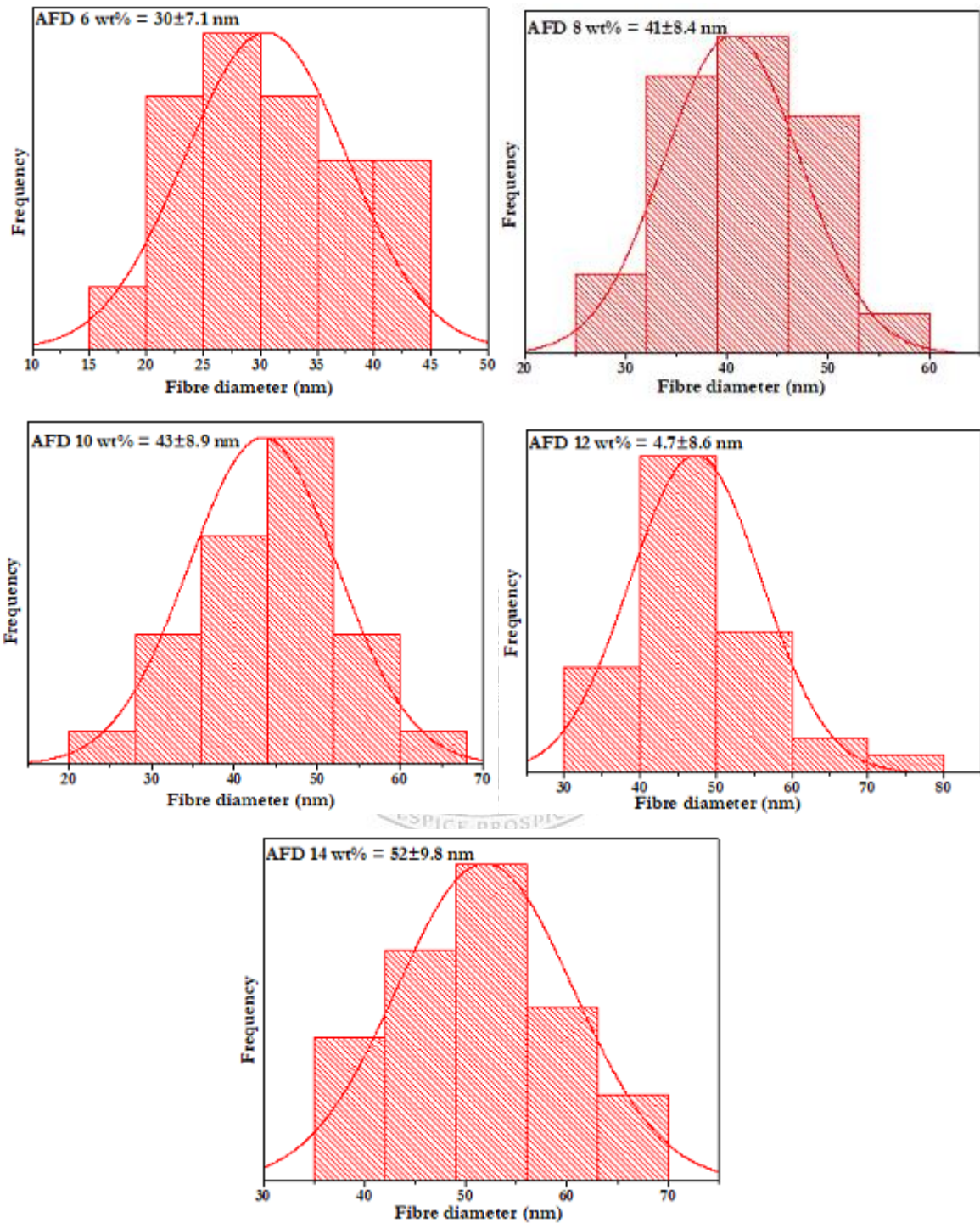
Figure 4.3: Fibre diameter distributions of PA6-nfs at different concentrations in formic acid.

The average fibre diameters of 30, 41, 43, 47 and 52 nm were determined for 6, 8, 10, 12 and 14 wt%, respectively. Even though, smaller diameters were obtained at lower concentrations, the dominant presence of beads is a defect and unwelcomed development (Bhardwaj and Kundu, 2010; Huang et al., 2003). The above findings shows that PA6 could be electrospun into nanofibres and beadless nanofibres could be achieved by increasing the concentration in formic acid. This is important to this research in order to know the parameters suitable for electrospinning of PA6-nfs composite membrane. For further characterisation, TEM technique was used to check the internal structure of 14 wt% PA6-nfs.

4.1.1.2 TEM of PA6-nfs

Having understood the surface morphology of 14 wt% PA6-nfs through HRSEM images, TEM technique was used to study the internal structure of 14 wt% PA6-nfs electrospun in section 3.2.1.1. The analysis was carried out as described in section 3.3.4. Figure 4.4 shows the TEM bright field images of 14 wt% PA6-nfs at scale values 0.2 μm (a) and 50 nm (b). The internal image shows that there were no dark zones/areas (Figure 4.4 (b), indicating that PA6-nfs was not a composite but rather a pure polymer nanofibre.
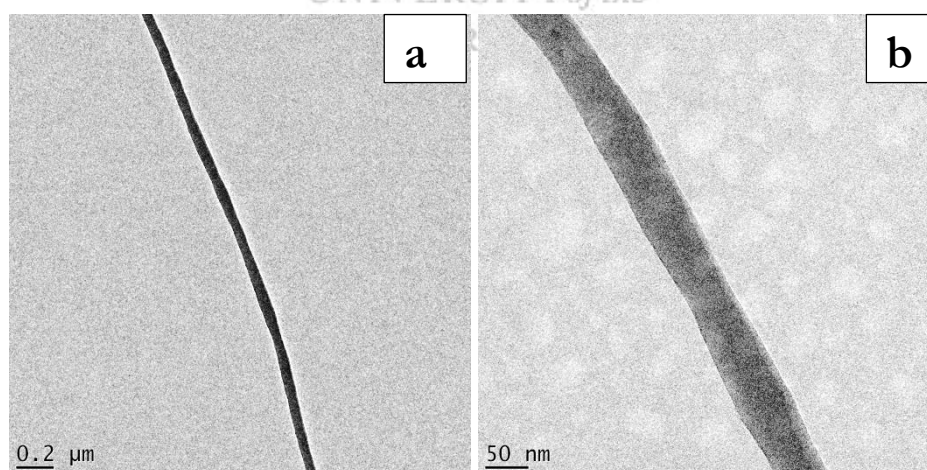
Figure 4.4: TEM bright field image of 14 wt% PA6-nfs at (a) 0.2 μm and (b) at 50 nm scale values.

The fibre diameter was also measured using image J software and found to be 51.6 nm which is in agreement with the HRSEM result for 14 wt% PA6-nfs (section

4.1.1.1). For further characterisation, ATR-FTIR was used to determine the chemical composition of PA6 nanofibres.

4.1.1.3   ATR-FTIR of PA6-nfs

The ATR-FTIR technique was used to understand and compare the chemical composition of PA6 polymer pellet and PA6-nfs. The ATR-FTIR analysis was performed as described in section 3.3.6 over the wavelength range of 650 to 4000 cm^{-1}. Figure 4.5 presents the ATR-FTIR spectra of 14 wt% PA6-nfs electrospun in formic acid from section 3.2.1.1 and the PA6 pellet that was dissolved in formic acid. For PA6 polymer pellet, the spectrum shows the main characteristic vibrations for NH, CH$_2$ and C=O.
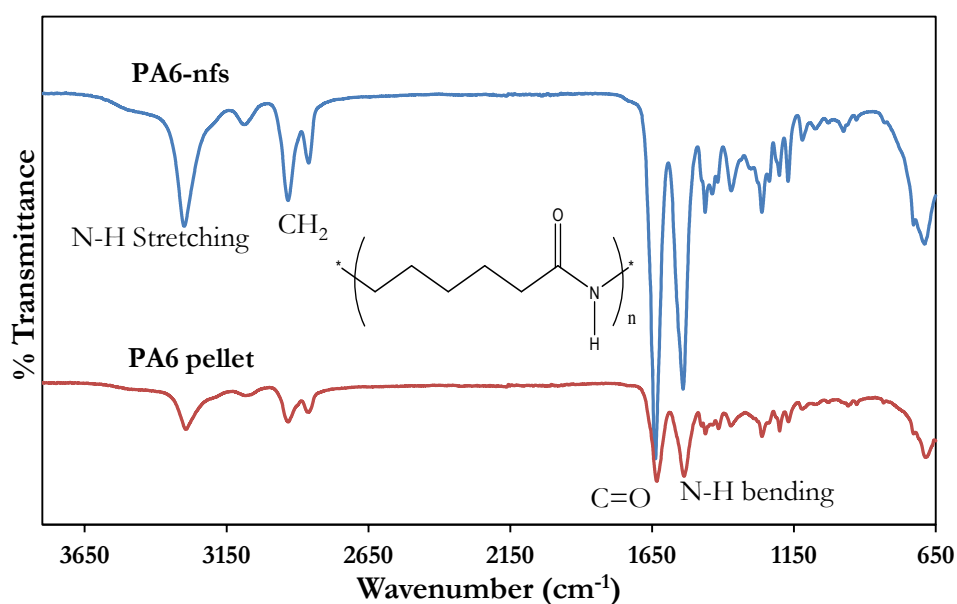
Figure 4.5: ATR-FTIR spectra of 14 wt% PA6-nfs and PA6 polymer pellet.

The peaks at 3284 cm^{-1} and 3062 cm^{-1} are assigned to N-H stretching, while the peaks at 2925 cm^{-1} and 2854 cm^{-1} are assigned to CH$_2$. The sharp C=O peak appeared at 1617 cm^{-1} while the peak at 1537 cm^{-1} is assigned to N-H bending (Guerrini et al., 2009). Other peaks that appeared at 1458 cm^{-1}, 1361 cm^{-1}, 1258 cm^{-1} and 680 cm^{-1} are assigned to C-H bend, C-N stretch, HN-C=O and N-H bending, respectively. Similarly, the spectrum of PA6-nfs shows the same peaks. This implies that no chemical alteration/reaction occurred during dissolution and electrospinning

of PA6 solution. For further characterisation, TGA analysis was used to determine the thermal properties of PA6-nfs.

4.1.1.4   TGA profile of PA6-nfs

The TGA analysis was carried out on 14 wt% PA6-nfs electrospun in formic acid from section 3.2.1.1 to investigate the thermal stability of PA6-nfs. The analysis was carried out as described in section 3.3.5. Figure 4.6 represents the TGA and thermal gravimetry derivative (DTG) profiles for PA6-nfs. The profiles show that PA6-nfs started losing its stability at about 350°C, and only underwent single stage decomposition afterwards given off volatile gases. The degradation trend was fast and complete, leaving no residue behind.
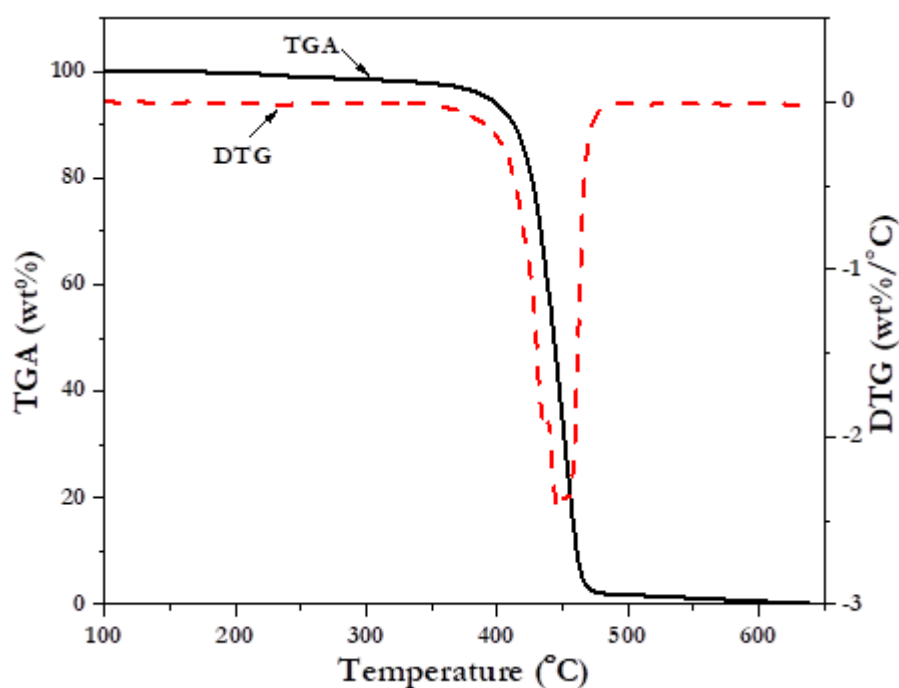
Figure 4.6: TGA and DTG profiles of 14 wt% PA6-nfs under nitrogen.

This pattern was also reported for PA6 by Pramoda et al. (2003). The above findings indicate that PA6-nfs are thermally stable up to 350°C and could be used for experiments at room temperature. For further characterisation, BET analysis was used to determine the surface area and pore size distribution of 14 wt% PA6-nfs.

4.1.1.5   Surface area and pore size analyses of PA6-nfs

Surface area and pore size analysis were conducted on 14 wt% PA6-nfs in order to determine the BET surface area and the pore size distribution. The analysis was carried out as described in section 3.3.7. BET surface area and pore size distribution were investigated by nitrogen adsorption–desorption measurement. Figure 4.7 is the nitrogen adsorption–desorption isotherms (inset; pore size distribution) showing the hysteresis loops, indicating the presence of mesopores.
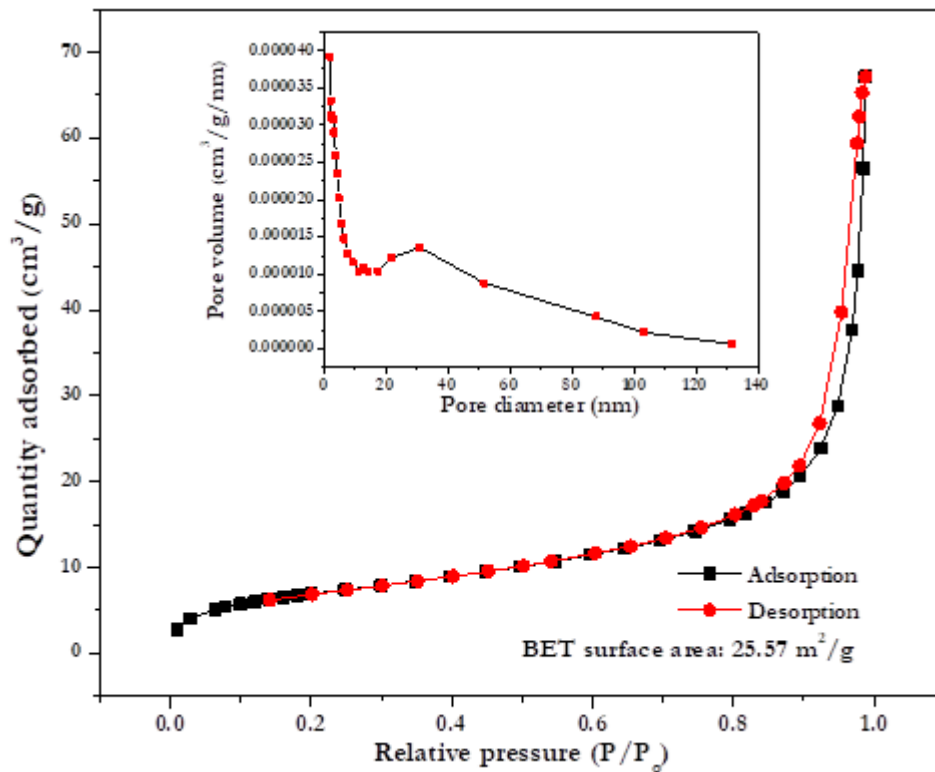
Figure 4.7: Nitrogen adsorption–desorption isotherms of 14 wt% PA6-nfs (inset; pore size distribution).

Based on BET analysis, the surface area of 14 wt% PA6-nfs was calculated to be 25.57 m^2/g. The surface area could be attributed to the fact that the materials are in nanometer range. The pore size distribution shows (Figure 4.7 inset) that 14 wt% PA6-nfs have mesopores between adjacent fibres with pore diameters in the range of 10 nm to 20 nm.

4.1.2 Polyacrylonitrile nanofibres (PAN-nfs)

From the electrospinning experiments of PAN in dimethyl formamide (section 3.2.1.2), PAN-nfs of different average fibre diameters (AFD) were obtained by varying the concentration (4, 6, 8, 10 and 12 wt%) of PAN in dimethyl formamide and fixing other electrospinning process parameters at; applied voltage of 25 kV, flow rate of 0.4 mL/hr and collection distance of 15 cm at room temperature 28°C. The resultant PAN-nfs are characterised using HRSEM, TEM, ATR-FTIR, TGA and BET techniques. The results are presented in the following sub-sections.

4.1.2.1 HRSEM of PAN-nfs

To understand the surface morphology of PAN-nfs electrospun as described in section 3.2.1.2, HRSEM was used to observe the surface morphology of various concentrations (4, 6, 8, 10 and 12 wt%) of electrospun PAN-nfs under high magnifications. The HRSEM analysis was carried out as described in section 3.3.3. Each sample of PAN-nfs was coated with Au and was observed at different magnifications under HRSEM. Figure 4.8 is the HRSEM images of PAN-nfs at different polymer concentrations in dimethyl formamide with their average fibre diameter (AFD). The images for 4 wt%, 6 wt% and 8 wt% show smooth nanofibre surfaces without beads. However, at a concentration 10 wt% and 12 wt%, there are the appearances of beads, which are conspicuous at 1000 magnification. The appearance of beads can be attributed to the higher concentration, resulting in higher surface tension, which invariably caused the polymer to clog at the end of the tip (preventing the easy ejection of the polymer fluid from the needle) thereby preventing the formation of a Taylor cone (Bhardwaj and Kundu, 2010). Therefore, instead of spinning, there was forceful ejection of polymer to the collector.
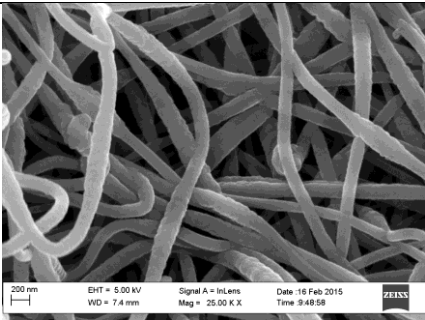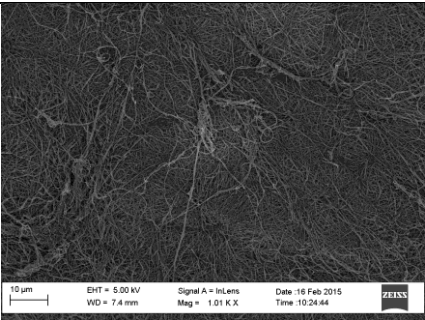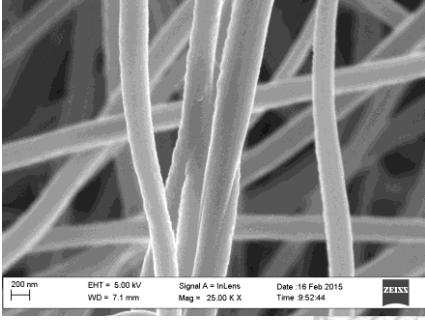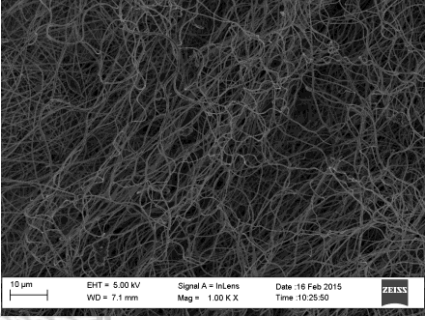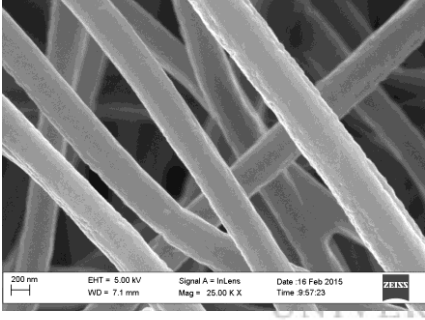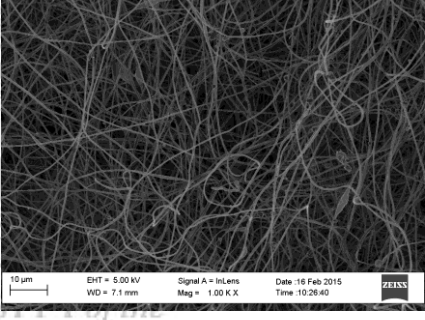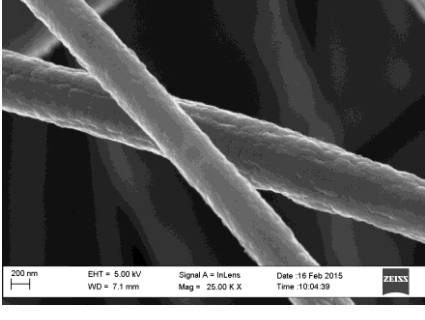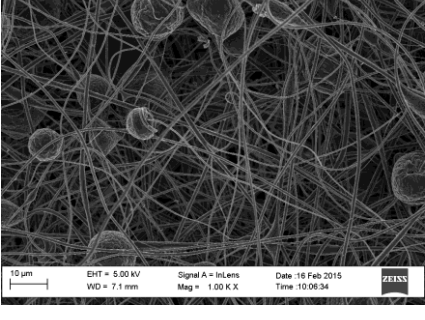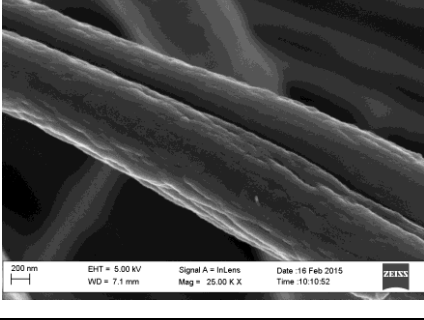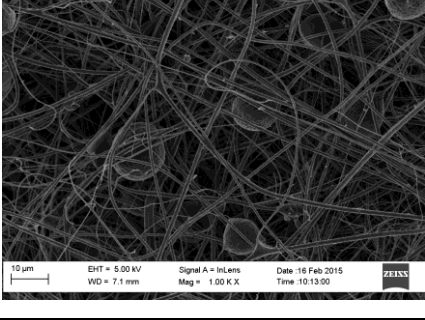
Conc	SEM images at 25k magnification	SEM images at 1k magnification	AFD
4 wt%			136±12 nm
6 wt%			247±30 nm
8 wt%			354±40 nm
10 wt%			457±66 nm
12 wt%			893±88 nm

Figure 4.8: HRSEM images of PAN-nfs at different concentrations in dimethyl formamide.

Furthermore, to determine the average fibre diameter, image J software was used to measure the nanofibre diameter of at least 20 nanofibre strands from the HRSEM images. Figure 4.9 shows that the fibre diameter of PAN-nfs is directly proportional to polymer concentration (Bhardwaj and Kundu, 2010). Figure 4.10 shows the fibre diameter distributions of different concentrations. The average fibre diameters of 136, 247, 357, 457 and 893 nm were determined for 4, 6, 8, 10 and 12 wt% respectively, thus, confirming that the polymer concentration is directly proportional to the nanofibre diameter. This trend has also been reported for PAN in DMF by Horzum et al. (2012) and Neghlani et al. (2011).
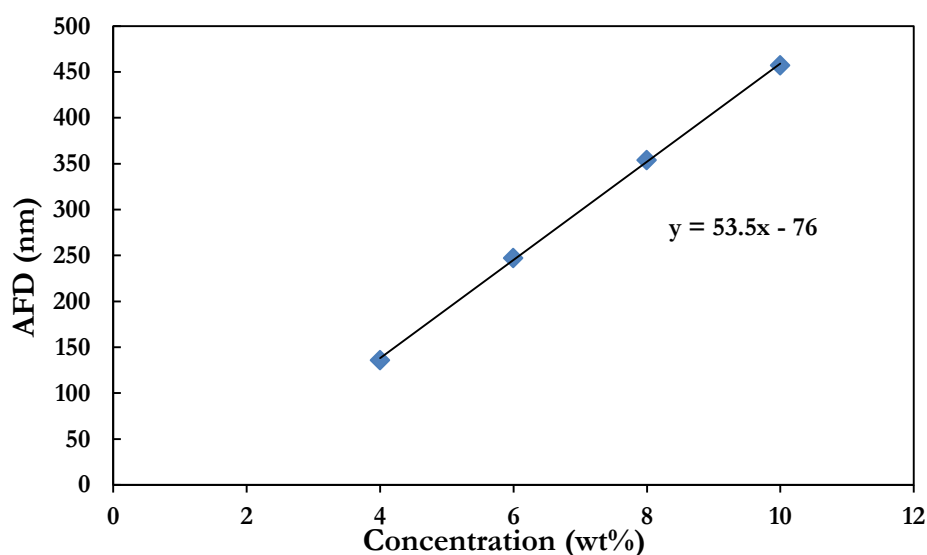
Figure 4.9: Graph showing the relationship between the average fibre diameters of PAN-nfs and the polymer concentration.

For this study, 8 wt% was therefore chosen as the optimum concentration at electrospinning process parameters of; applied voltage of 25 kV, flow rate of 0.4 mL/hr, collection distance of 15 cm and the room temperature of 28°C as 4 wt% and 6 wt% nanofibres were fragile and mechanically not strong enough because the number of entanglements of polymer chains in the polymer solution was not enough (Bhardwaj and Kundu, 2010). The above optimal conditions were used to electrospin 8 wt% PAN until ≈0.5 mm thickness of PAN-nfs was formed on the collector. The time to reach this thickness was 8 hours 22 minutes.
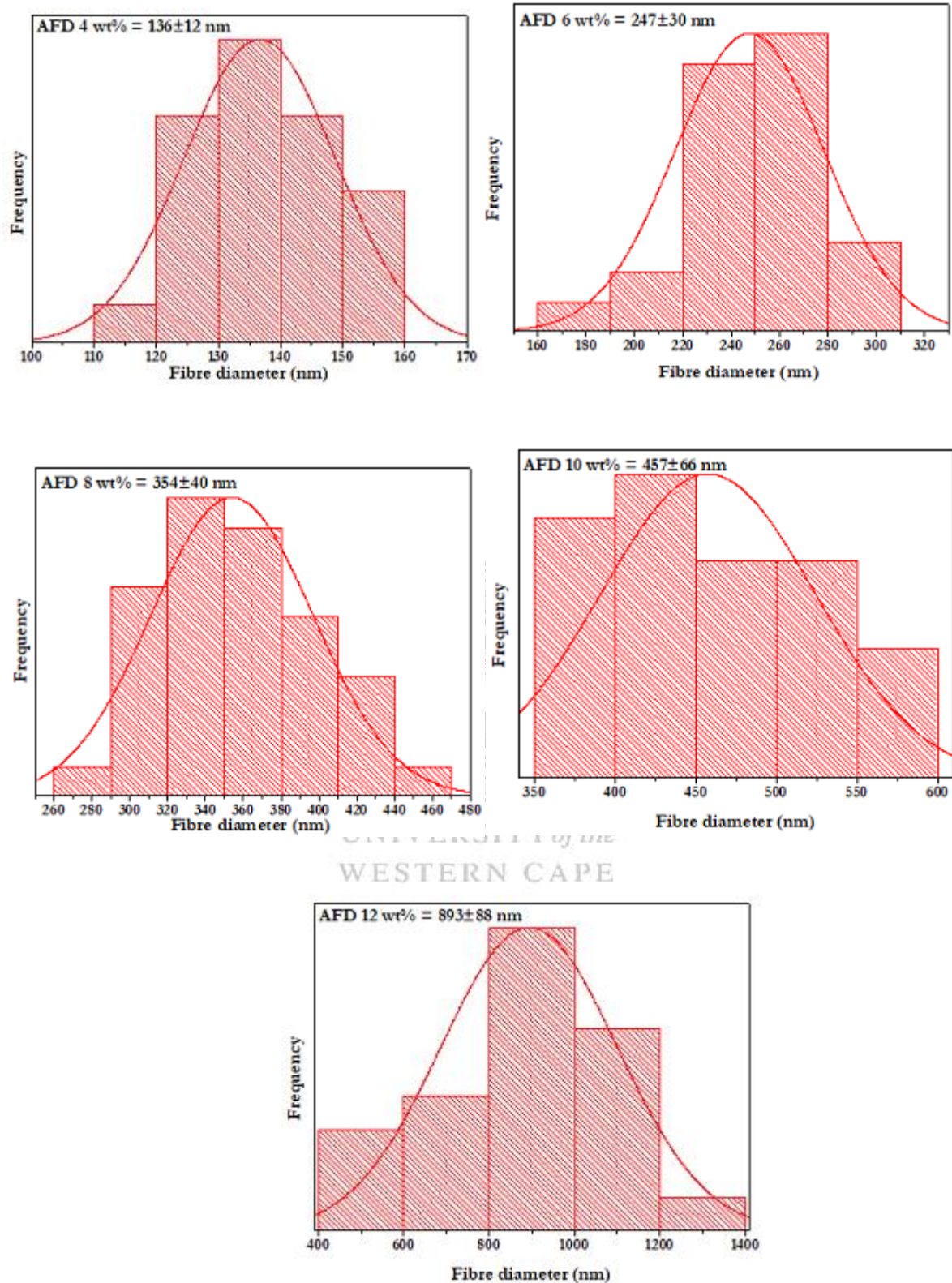
Figure 4.10: Fibre diameter distributions of PAN-nfs at different concentrations in dimethyl formamide.

The above findings show that PAN could be electrospun into nanofibres and beadless nanofibres could be achieved at lower concentration in dimethyl formamide. This is important to this research in order to know the parameters suitable for PAN-nfs composite membrane for the adsorption of dyes. For further characterisation, TEM was used to check the internal structure of 8 wt% PAN-nfs.

4.1.2.2   TEM of PAN-nfs

Having understood the surface morphology of 8 wt% PAN-nfs through HRSEM images, TEM technique was used to study the internal structure of 8 wt% PAN-nfs electrospun in section 3.2.1.2. The analysis was carried out as described in section 3.3.4. Figure 4.11 shows the TEM bright field images of 8 wt% PAN-nfs at scale values 0.2 μm (a) and 200 nm (b). The internal image shows that there were no dark zones/areas (Figure 4.11 (a), indicating that PAN-nfs was not a composite but rather a pure polymer nanofibre.
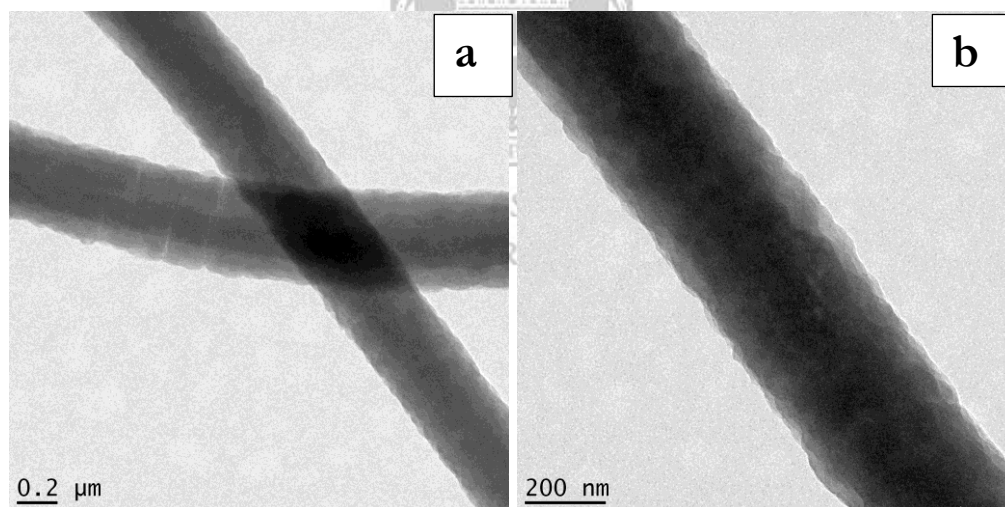
Figure 4.11: TEM bright field image of 8 wt% PAN-nfs at (a) 0.2 μm and (b) at 200 nm scale values.

The fibre diameter was also measured using image J software and found to be 370 nm which is in agreement with the HRSEM result for 8 wt% PAN-nfs (section 4.1.2.1). For further characterisation, ATR-FTIR was used to determine the chemical composition of PAN-nfs.

4.1.2.3 ATR-FTIR of PAN-nfs

The ATR-FTIR analysis was carried out to investigate the functional groups on PAN-nfs. This is important to this research as PAN-nfs would be used as support for ligands via chemical reaction. ATR-FTIR was also used to understand and compare the chemical composition of 8 wt% PAN-nfs and PAN powder so as to check if PAN chemical composition was affected during electrospinning. Figure 4.12 presents the ATR-FTIR spectra of 8 wt% PAN-nfs electrospun in DMF from section 3.2.1.2 and PAN powder that was used to prepared PAN solution in DMF.
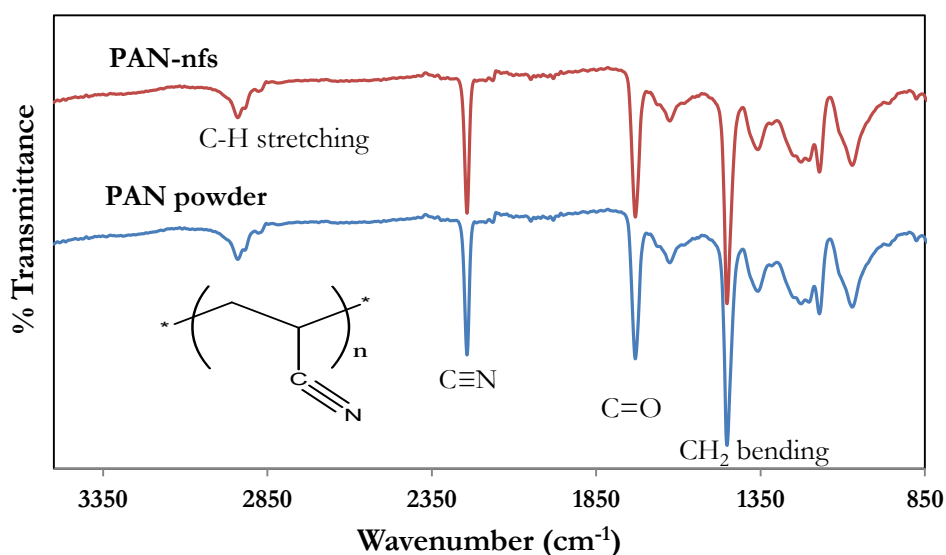
Figure 4.12: ATR-FTIR spectra of 8 wt% PAN-nfs and PAN powder.

The ATR-FTIR analysis was performed as described in section 3.3.6 over the wavelength range of 650 cm^{-1} to 4000 cm^{-1}. The ATR-FTIR spectrum of the PAN powder had the following characteristic peaks that are unique to PAN; the peak at 2924 cm^{-1} is assigned to C-H stretching vibration of CH_2 and the peak at 2241 cm^{-1} corresponded to the C≡N stretching vibration. The strong bands at 1450 cm^{-1}, 1345 cm^{-1} and 1220 cm^{-1} are assigned to the aliphatic CH group vibrations of CH_2 groups. The appearance of a peak at 1728 cm^{-1} on PAN-nfs which corresponds to the C=O stretching vibration is assumed to have come from the C=O of methylacrylate. This means that PAN is a copolymer of acrylonitrile and methylacrylate (Korobeinyk et al., 2012; Feng et al., 2011; Neghlani et al., 2011; Saeed et al., 2008; Deng et al., 2003a). Similarly, the spectrum of PAN-nfs shows the same peaks. The above

findings show that the chemical composition of PAN was not affected by electrospinning process. The main reactive site of PAN (nitrile) is present and could be ready for different chemical reaction such as amination, reduction etc. For further characterisation, TGA analysis was used to determine the thermal properties of PAN-nfs.

4.1.2.4   TGA profile of PAN-nfs

The TGA analysis was carried out on 8 wt% PAN-nfs (electrospun in DMF from section 3.2.1.2) to investigate the thermal stability of PAN-nfs. The analysis was carried out as described in section 3.3.5. Figure 4.13 presents the TGA and DTG profiles of PAN-nfs. The profiles show that PAN-nfs have three main weight loss stages.
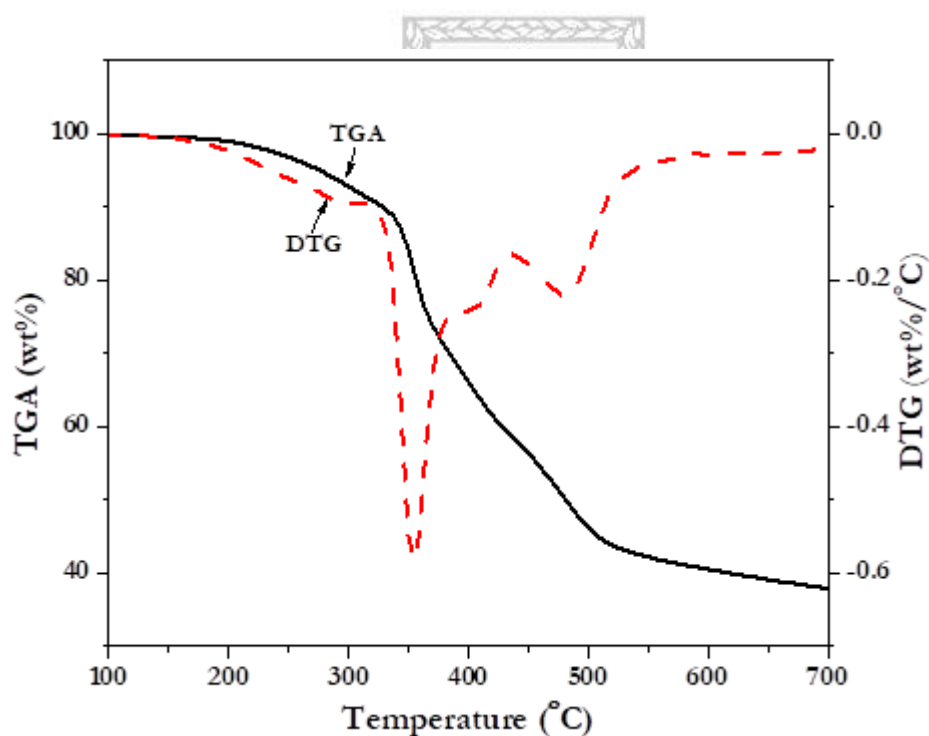
Figure 4.13: TGA and DTG profiles of 8 wt% PAN-nfs under nitrogen.

The PAN-nfs started losing their thermal stability at temperature around 190°C to 320°C with about 9% weight loss which is attributed to nitrile oligomerisation with production of volatile products (Korobeinyk et al., 2012). The second weight loss occurred rapidly between 320°C and 430°C with about 34% weight loss which is

attributed to the thermal degradation reaction of PAN-nfs (Chen et al., 2013; Korobeinyk et al., 2012). The third weight loss of about 18% occurred between 430°C and 580°C which is attributed to the decomposition of the carbon-carbon main chain (Chen et al., 2013). Thereafter, about 39% carbon residues were left behind. This is why PAN has been widely used as precursor for carbon nanofibres (CNF) (Nataraj et al., 2012). The above findings indicate that PAN-nfs are thermally stable up to 190°C and could be used for experiments at room temperature.

4.1.2.5   Surface area and pore size analyses of PAN-nfs

Surface area and pore size analysis were conducted on 8 wt% PAN-nfs in order to determine the BET surface area and the pore size distribution. The analysis was carried out as described in section 3.3.7. BET surface area and pore size distribution were investigated by nitrogen adsorption–desorption measurement. Figure 4.14 is the nitrogen adsorption–desorption isotherms (inset; pore size distribution) showing the hysteresis loops, indicating the presence of mesopores.
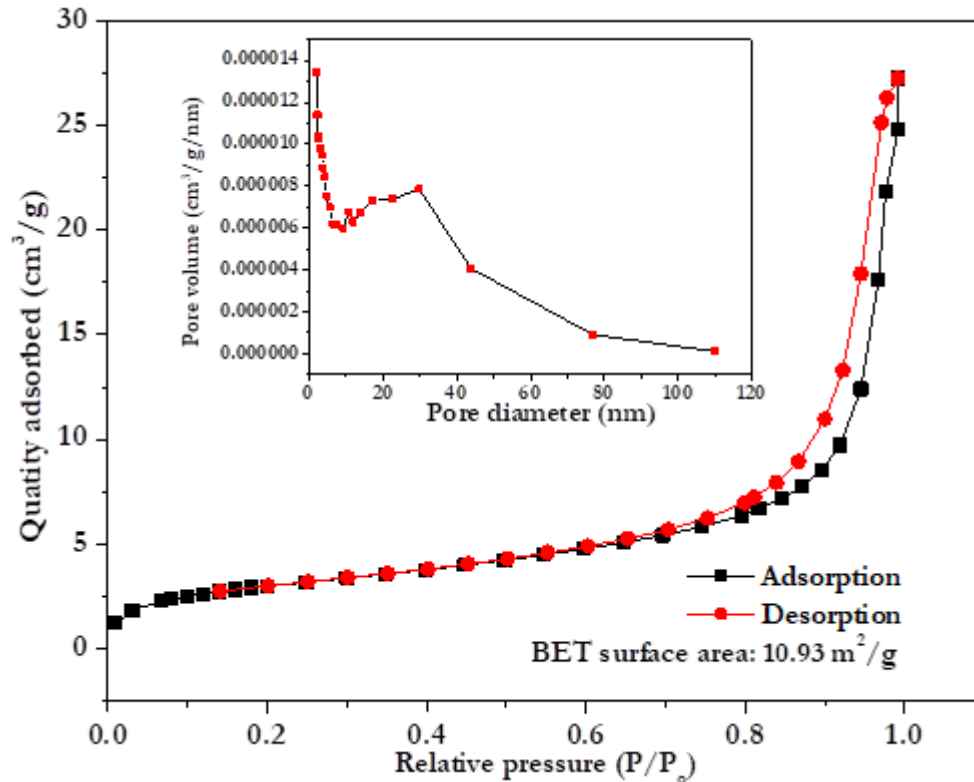
Figure 4.14: Nitrogen adsorption–desorption isotherms of 8 wt% PAN-nfs (inset; pore size distribution).

Based on BET analysis the surface area of 8 wt% PAN-nfs was calculated to be 10.93 m^2/g. The surface area could be attributed the fact that the materials are in nanometer range. The pore size distribution shows (Figure 4.14 inset) that there are mesopores between the adjacent 8 wt% PAN-nfs fibres with pore diameters in the range of 2 nm to 15 nm.

4.1.3 PET track-etched membrane (PET-TM)

The PET-TM is a porous membrane prepared by heavy ion irradiation and chemical etching and then coated with TiO_2 via magnetron sputtering method. The process has been previously described in sections 2.5.2 and 3.2.1.3. PET-TM, as provided by JINR was characterised using HRSEM, SEM-EDS, ATR-FTIR and TGA techniques. The results of each technique are presented in the following sub-sections.

4.1.3.1   HRSEM of PET-TM

The HRSEM analysis was carried out as described in section 3.3.3. PET-TM was not coated with Au as the membrane is conductive, and was observed at different magnifications under HRSEM. HRSEM technique was used to investigate the surface and the pores of PET-TM.

Figure 4.15 (a) shows that PET-TM has rough surfaces. Other scales, Figure 4.15 (b, c and d) show that PET-TM is actually a porous membrane. Figure 4.15 (d) specifically shows that the pores are uniformely distributed. Figure 4.16 shows the pore diameter distribution of PET-TM. The average pore diameter (APD) was measured to be 3.5±0.36 μm using image J software.
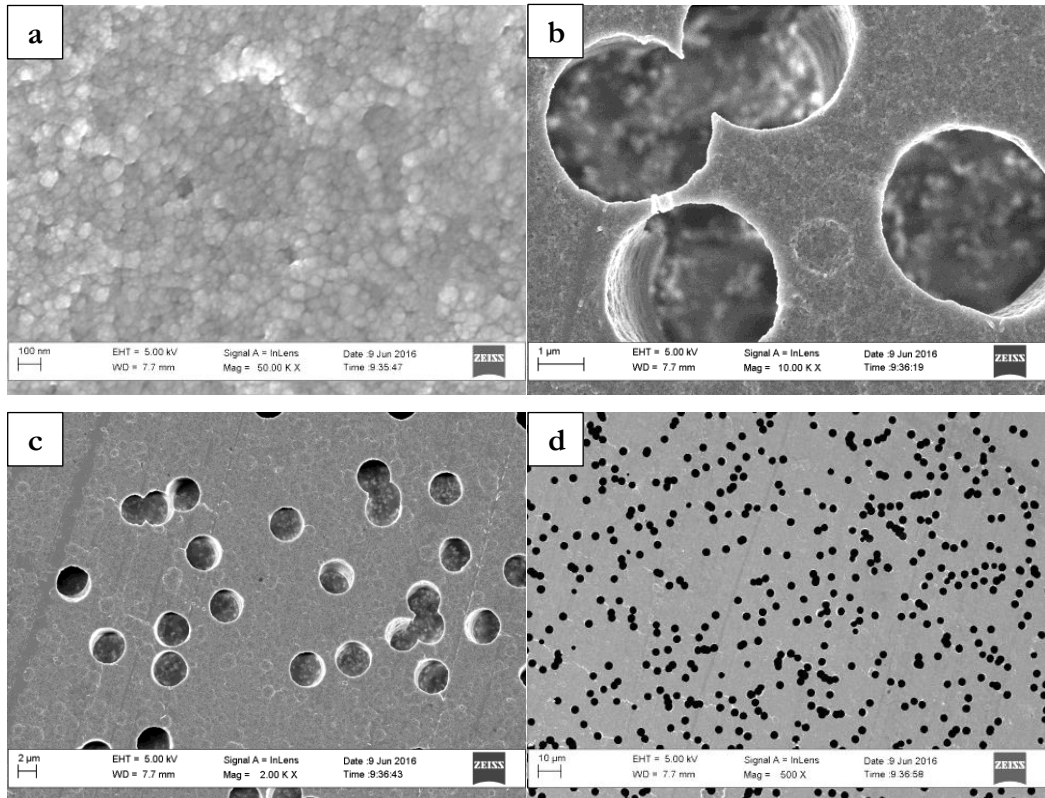
Figure 4.15: HRSEM images of PET-TM at (a) 100 nm (b) 1 μm (c) 2 μm and (d) 10 μm scale values.
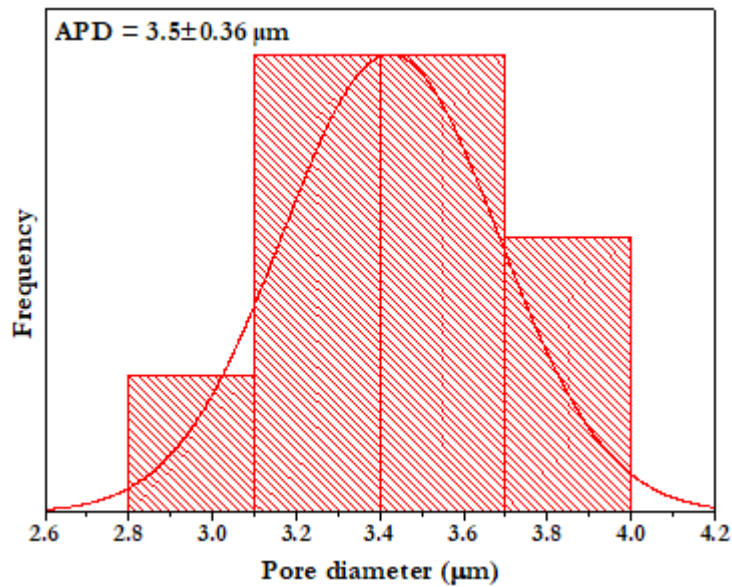
Figure 4.16: Pore diameter distributions of PET-TM.

Figure 4.17 is the cross sectional view of the PET-TM. It shows that the pores completely went through the membrane. The pore length is measured to be 17 μm,

126

which is equivalent to the thickness of the PET-TM. The large pores is important to this research as less pressure will be required for the liquid to pass through the membrane and the composite membrane during the adsorption of dyes.
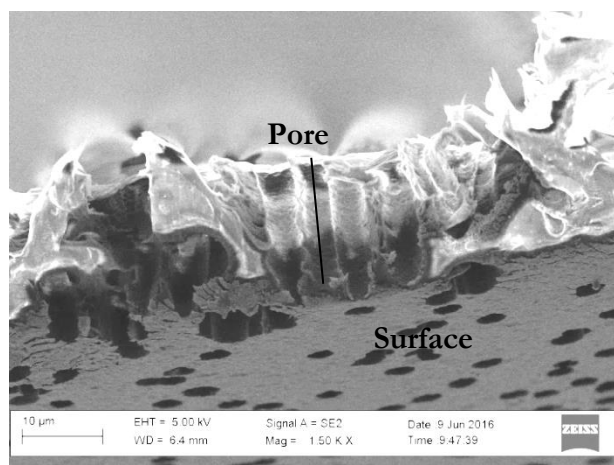
Figure 4.17: HRSEM image of cross-sectional view of PET-TM.

For further characterisation, EDS was used to indicate the presence of TiO_2 on PET-TM.

4.1.3.2   Energy disperse X-ray spectroscopy of PET-TM

For the energy-dispersive X-ray spectroscopy (EDS), the analysis was carried out as described in section 3.3.3. The PET-TM was not coated with Au as the membrane is conductive after been coated with TiO_2 via magnetron sputtering method at JINR as described in sections 2.5.2 and 3.2.1.3. The EDS analysis was used to indicate the elemental composition on the surface PET-TM.

Figure 4.18 is the EDS of PET-TM. The result shows the peak signals of Ti appearing at 0.6, 4.7 and 5.0 KeV respectively, with total atomic percentage of 1.87 (check inset table on Figure 4.18), thus indicating that PET-TM was coated with TiO_2. The choice of TiO_2 was based on the fact that it can make the membrane conductive. Also TiO_2 break down organic pollutants such as dyes, pesticides and herbicides under UV light irradiation (Zhang et al., 2003a).

Element	Atomic %
C	73.51
O	24.62
Ti	1.87
Total	100
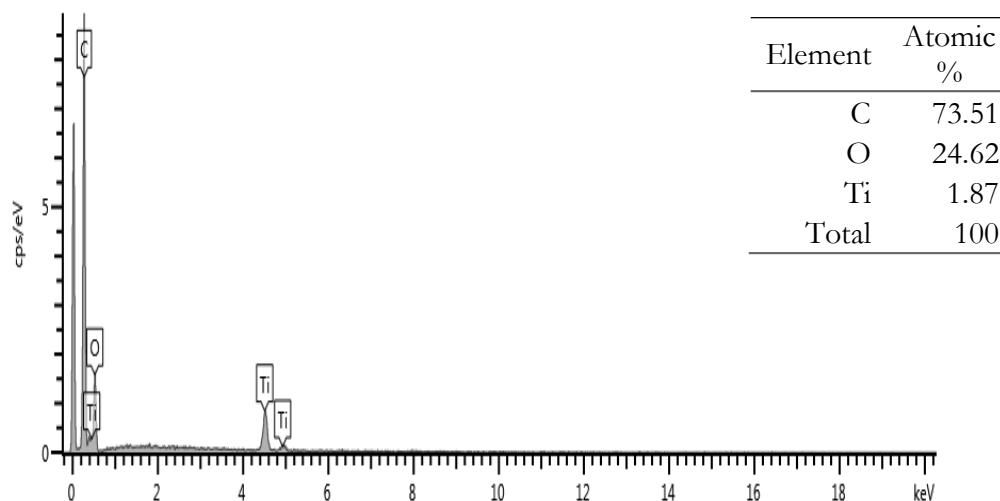
Figure 4.18: SEM-EDS of PET-TM showing the presence of Ti.

4.1.3.3   ATR-FTIR of PET-TM

ATR-FTIR was also used to understand and compare the chemical composition of PET-TM and PET pellet in order to check if the chemical composition of PET-TM was affected during irradiation, etching and coating. The ATR-FTIR analysis was performed as described in section 3.3.6 over the wavelength range of 650 to 4000 cm^{-1}. Figure 4.19 is the ATR-FTIR of TiO$_2$ coated PET-TM made from section 3.2.1.3 at JINR and that of PET pellet.
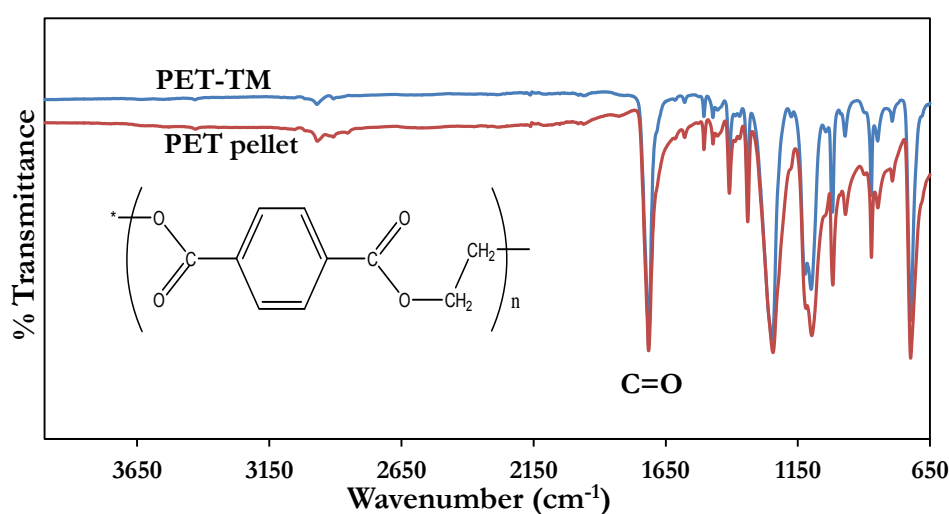
Figure 4.19: ATR-FTIR spectra of PET-TM and PET polymer pellet.

The spectrum of PET-TM as shown in Figure 4.19 shows the prominent peaks that are identical to a PET pellet. The absorption bands between 3050 cm⁻¹ and 2885 cm⁻¹ have been attributed to aromatic and aliphatic C–H bond stretching. The sharp peak at 1710 cm⁻¹ is assigned to the ester carbonyl bond stretching. The peaks between 1467 cm⁻¹ and 1338 cm⁻¹ are attributed to the bending and wagging vibrational modes of the ethylene glycol moiety, while the peak at 1235 cm⁻¹ is assigned to the ester group stretching. Other peaks such as at 1091 cm⁻¹ is assigned to the methylene group and the ones at 1016 cm⁻¹ and 735 cm⁻¹ to the aromatic bands (Chen et al., 2012). For further characterisation, TGA analysis was used to determine the thermal properties of PET-TM.

4.1.3.4   TGA profile of PET-TM

The TGA analysis was carried out as described in section 3.3.5 to determine the thermal stability of PET-TM. Figure 4.20 presents the TGA and DTG profiles of PET-TM with one single stage of decomposition. The PET-TM started losing its stability at a decomposition temperature of about 250ºC till 430°C with about 5% weight loss which might be as a result of volatile gases.
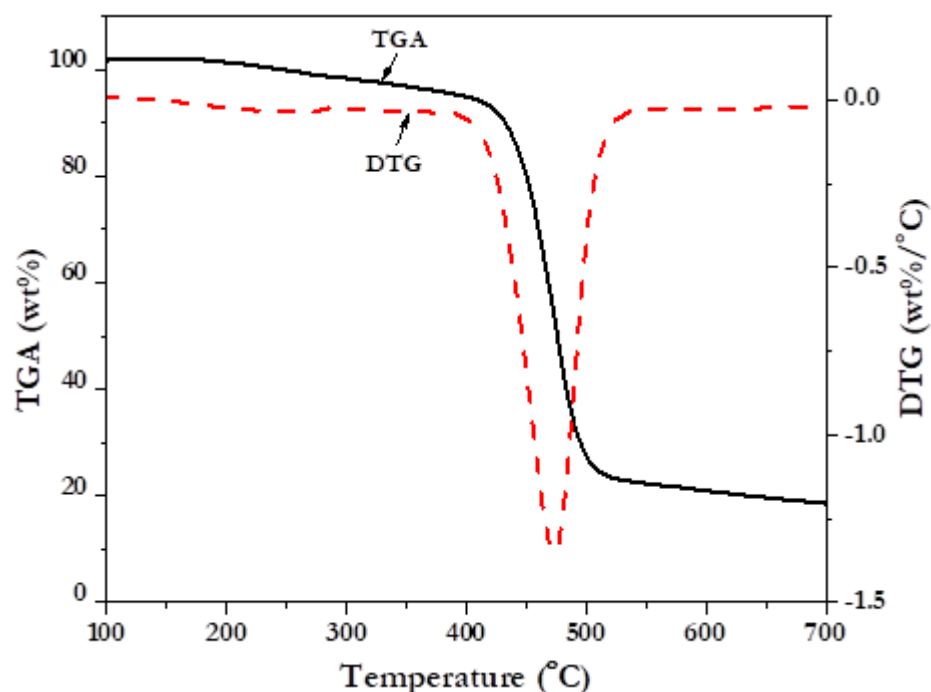
Figure 4.20: TGA and DTG of PET-TM under nitrogen.

PET-TM finally underwent single stage decomposition between 430°C and 530°C with a weight loss of 71% which is attributed to the degradation of the carboxylic acid and the naphthalene ring (Papageorgiou et al., 2014), leaving 20% (suggested to be carbon and the inorganic (Ti)) residue behind. Similar trend was also observed for PET by Gashti et al. (2012), though no TGA literature was found for TiO_2 coated PET-TM.

4.1.4 PET-TMPA6

To prepare composite membrane, PA6-nfs and PET-TM was combined together through electrospinning process as described in section 3.2.1.4. The optimised concentration 14 wt% PA6-nfs from section 3.2.1.1 was prepared in formic acid and electrospun using the following parameters; applied voltage of 25 kV, flow rate of 0.4 mL/hr, collection distance of 10 cm and room temperature of 28°C onto a stationary collector covered with A4 size PET-TM which was used instead of Al foil. The electrospinning time of 6 hours 45 minutes was used to achieve ≈0.5 mm thickness of PA6-nfs on PET-TM. PET-TMPA6 produced (being a composite of PET-TM and PA6-nfs), was only characterised using HRSEM technique. This is because the two components (PA6-nfs and PET-TM) have been previously characterised and the ATR-FTIR and the TGA results of PET-TMPA6 will not give sensible results since there was no chemical interaction between the two components.

4.1.4.1   HRSEM of PET-TMPA6

The HRSEM analysis was carried out as described in section 3.3.3. PET-TMPA6 was coated with Au so as to make the PA6-nfs conductive. HRSEM technique was used to investigate the surface and the pores of PET-TMPA6 at different magnifications.

Figure 4.21 is the HRSEM images of PET-TMPA6. The images show that the PA6-nfs can be seen through the pores of PET-TMPA6 (Figure 4.21), confirming that the pores of PET-TM was through and that the membrane has been successfully covered by PA6-nfs through the electrospinning process. This is being reported for the first time to the best of my knowledge that electrospinning was used to synergise

nanofibres and track-etched membranes to form composite nanofibres track-etched membrane.
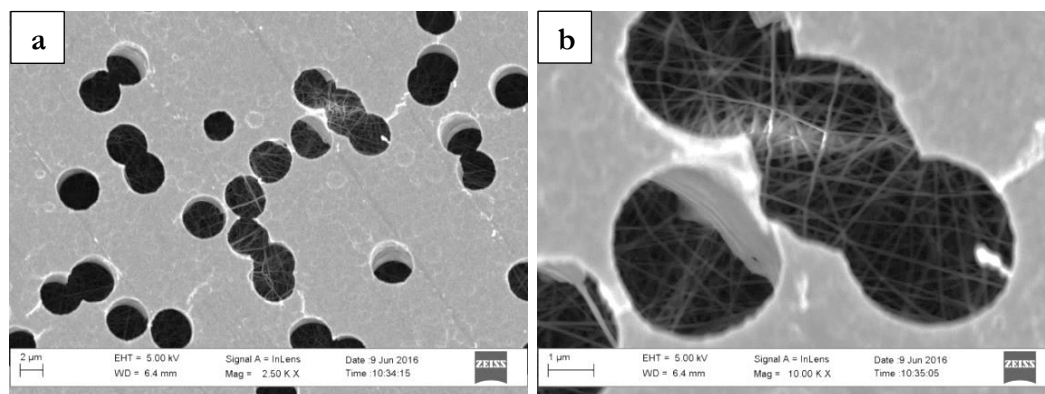
Figure 4.21: HRSEM images of PET-TMPA6 at (a) 2 μm and (b) 1 μm scale values.

The PET-TMPA6 was made in order to combine the use of nanomaterials and porous membrane for adsorption-filtration purposes. Both materials, nanofibres and track-etched membrane have been previously reported for adsorption and filtration processes respectively, hence their combination are proposed as better adsorbent.

4.1.5 PET-TMPAN

To prepare another composite membrane, PAN-nfs and PET-TM was combined together through electrospinning process as described in section 3.2.1.5. The optimised concentration 8 wt% PAN-nfs from section 3.2.1.2 was prepared in DMF and electrospun using the following parameters; applied voltage of 25 kV, flow rate of 0.4 mL/hr, collection distance of 15 cm, room temperature of 28°C and a stationary collector covered with A4 size PET-TM was used instead of Al foil. The electrospinning time of 8 hours 22 minutes was used to achieve ≈0.5 mm thickness of PAN-nfs on PET-TM. PET-TMPAN (being a composite of PET-TM and PAN-nfs), was only characterised using HRSEM technique. This is because the two components (PAN-nfs and PET-TM) have been previously characterised and the ATR-FTIR and the TGA results of PET-TMPAN will not give sensible results since there was no chemical interaction between the two components making the composite.

4.1.5.1   HRSEM of PET-TMPAN

The HRSEM analysis was carried out as described in section 3.3.3. PET-TMPAN was coated with Au so as to make the PAN-nfs conductive. HRSEM technique was used to investigate the surface and the pores of PET-TMPAN at different magnifications. Figure 4.22 is the HRSEM images of PET-TMPAN.
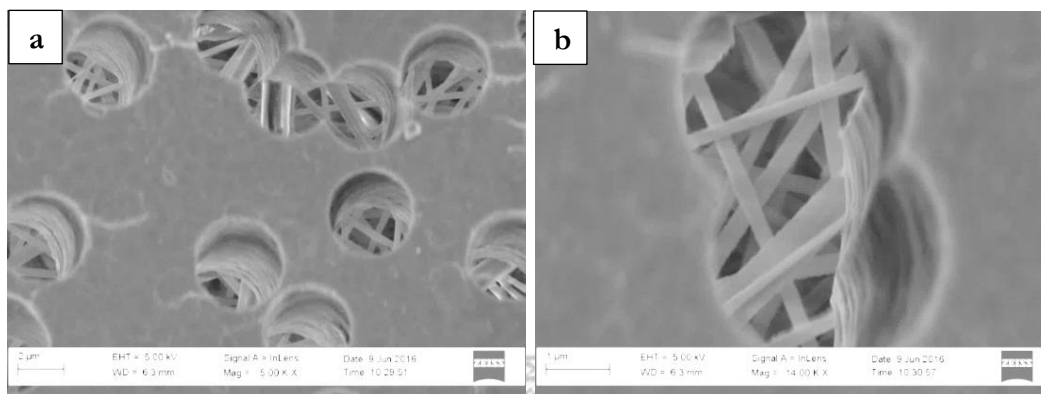
Figure 4.22: HRSEM images of PET-TMPAN at (a) 2 μm and (b) 1 μm scale values.

The images show that the PAN-nfs can be seen through the pores of PET-TMPAN (Figure 4.22), confirming that the pores of PET-TM was through and that the membrane has been successfully covered by PAN-nfs through the electrospinning process.

4.1.6   Summary of characterisations of nanofibres and membranes

For this subsection, PA6 in formic acid and PAN in DMF were electrospun into PA6-nfs and PAN-nfs, respectively. The concentration of each polymer was optimised to produce smooth nanofibres free of beads. Further experiments were carried out to combine the nanofibres (PA6-nfs and PAN-nfs) and PET-TM (provided by JINR) via electrospinning process. The use of track-etched membrane as collector is being reported for the first time from this research. PET-TMPA6 and PET-TMPAN were made in order to combine the use of nanomaterials and porous membrane for adsorption-filtration purposes. One application aspect of this research would be based on the use of PA6-nfs, PAN-nfs, PET-TM, PET-TMPA6 and PET-TMPAN as membranes for the filtration of dye from solution in chapter five.

4.2   Characterisation of PyAMI and PAN-PyAMI

This subsection gives insight into the immobilisation experiments of PyAMI on PAN-nfs. It starts with the characterisation of 2-pyridine amidoxime (PyAMI) synthesised in section 3.2.2. 8 wt% PAN-nfs previously electrospun and characterised under sections 3.2.1.2 and 4.1.2 respectively was chosen as the support for PyAMI. After the immobilisation reaction, PAN-PyAMI is produced and subsequently characterised.

4.2.1   Synthesis of PyAMI

The synthesis of 2-pyridine amidoxime (PyAMI) as adapted from Bernasek, (1957) was carried out as described in section 3.2.2 by reacting hydroxylamine hydrochloride with 2-pyridine carbonitrile at 90°C. Sodium carbonate monohydrate was added to maintain the pH at 6.5. The resultant PyAMI was characterised using NMR, ATR-FTIR and TGA techniques. The results from these techniques are presented in the following sub-sections.

4.2.1.1   NMR analysis of PyAMI

The resultant PyAMI from section 3.2.2 was characterised using NMR analysis as described in section 3.3.9, to investigate the functional groups on PyAMI and to confirm the structure of the ligand. ^{1}H, ^{13}C and distortionless enhancement of polarisation transfer (DEPT) NMR techniques were used to analyse PyAMI in deuterated DMSO.

Figure 4.23 is the ^{1}H NMR spectrum of PyAMI. The spectrum shows the proton of the hydroxyl (δ 9.8, H-9), the presence of protons of pyridine (δ 7.4-8.6, H-1, H-2, H-3 and H-4) and protons of the primary amine (δ 5.7, H-10). This confirmed the presence of OH, NH_2 and pyridine ring of PyAMI in deuterated DMSO. Furthermore, the total number of protons from ^{1}H NMR; 7, conformed to the number of protons on PyAMI. The NMR assignments of PyAMI ligand are shown in Table 4.1.
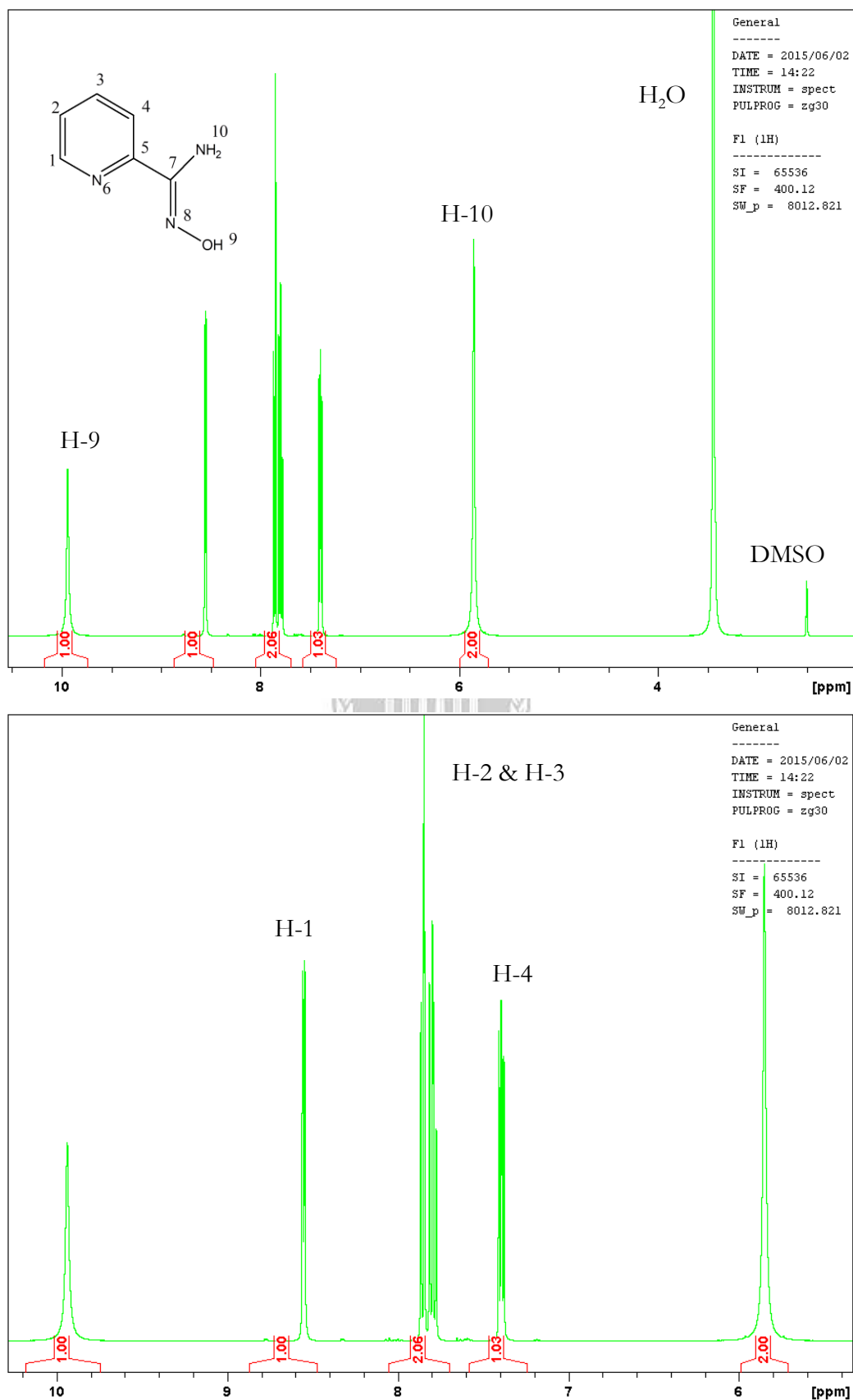
Figure 4.23: ^{1}H NMR of PyAMI in deuterated DMSO.

Table 4.1: Assignment of NMR spectra of PyAMI.

¹³C NMR		¹H NMR		
Carbon No.	Chemical shift ppm	Chemical shift ppm	Proton No.	Multiplicity
C-7	150.0	-	-	-
C-5	149.6	-	-	-
C-1	148.3	8.55	H-1	d, 1H
C-2	124.2	7.79	H-2	m, 1H
C-3	136.7	7.86	H-3	m, 1H
C-4	119.5	7.39	H-4	d, 1H
-	-	9.94	H-9	br, 1H
-	-	5.85	H-10	br, 2H

Note: d = doublet, m = multiplet, br = broad

To further confirm the presence of OH and NH_2, the deuterated water (D_2O) test was carried out on PyAMI. The test is based on the fact that D_2O has the tendency of exchanging with the protons of OH and amine. Therefore the disappearance of the protons will confirm their presence. D_2O was mixed with PyAMI and analysed using ^1H NMR. The spectrum (Figure 4.24) shows the disappearance of OH and NH_2 peaks. This implies that D_2O did exchange with the protons of OH and NH_2, thereby confirming the presence of OH and NH_2 on PyAMI.
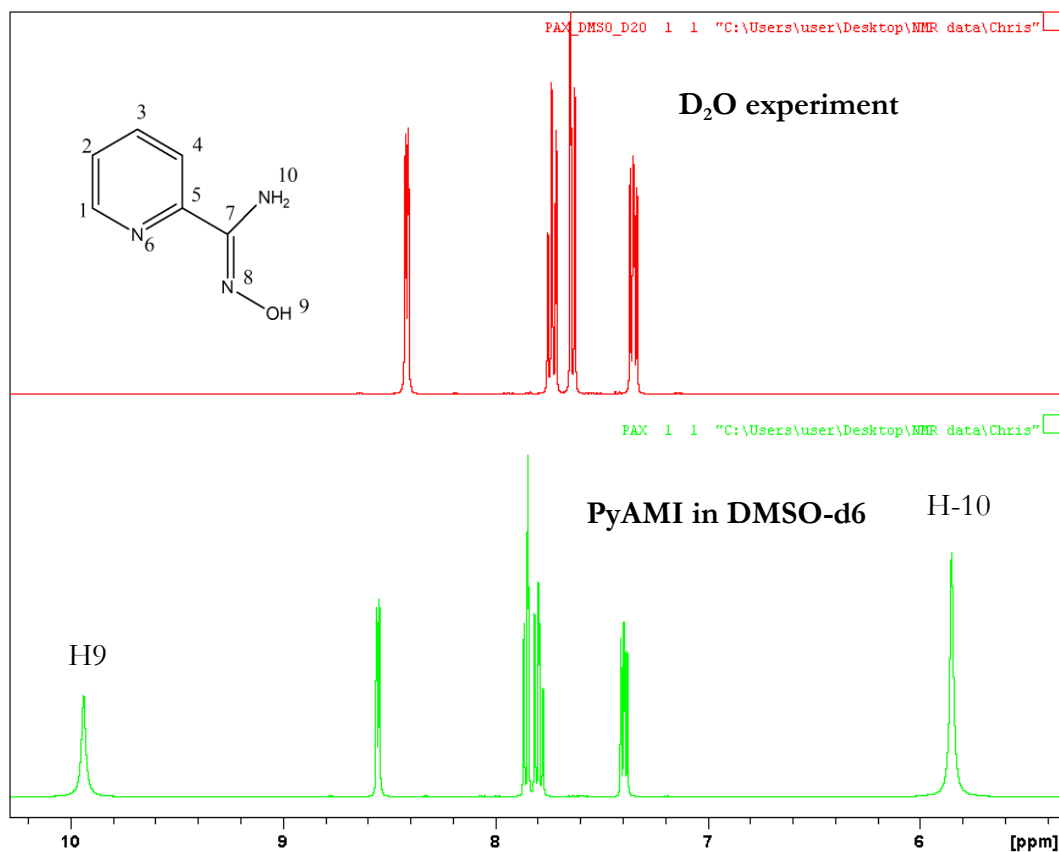
Figure 4.24: ^{1}H NMR results of PyAMI in deuterated DMSO and PyAMI in D_2O.

Further NMR analysis was done to confirm the chemical structure of PyAMI. Figure 4.25 is the ^{13}C NMR spectrum of PyAMI. The spectrum confirmed that PyAMI contains 6 carbon atoms. The two peaks at 151-149 ppm are assigned to the quaternary carbon of PyAMI (C-7 and C-5) as they do not carry hydrogen atom. The other peaks at 148, 136, 124 and 119 ppm are assigned to C-1, C-3, C-2 and C-4, respectively.

Figure 4.26 is the distortionless enhancement by polarisation transfer (DEPT) of PyAMI. The experiment would determine the multiplicity of carbon atom substituted with hydrogen. The appearance of four peaks further confirmed the presence of C-1, C-2, C-3 and C-4 which are the only set of carbon atoms carrying hydrogen atoms in PyAMI. From the NMR results, ^{1}H NMR confirmed that PyAMI has the presence of OH and NH_2 and a total of 7 protons.
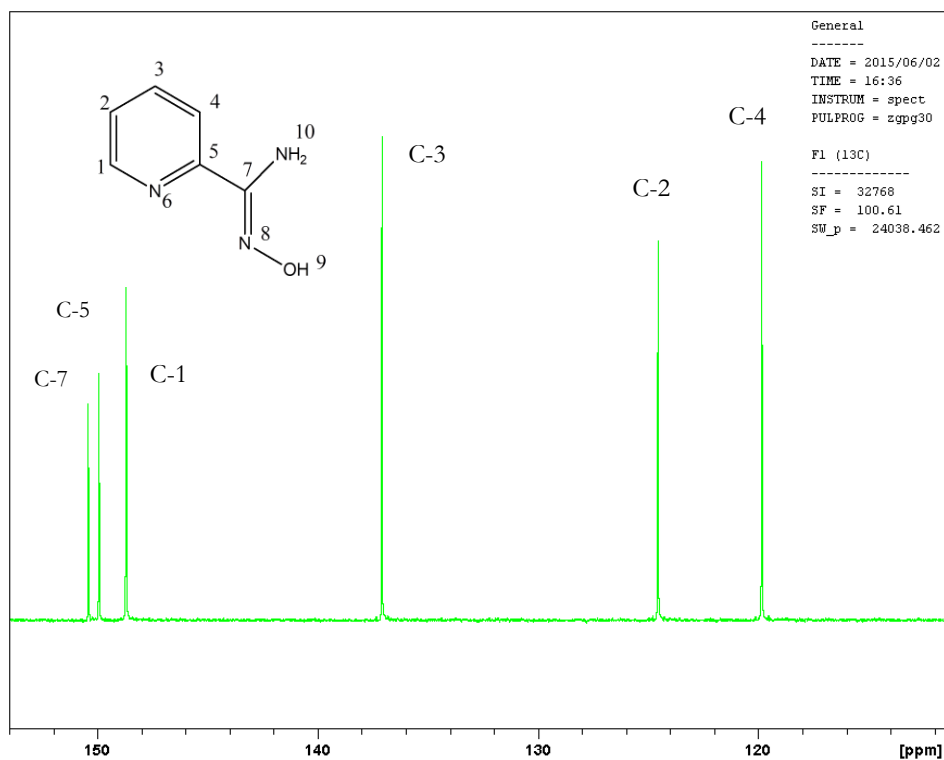
Figure 4.25: ^{13}C NMR of PyAMI in deuterated DMSO.
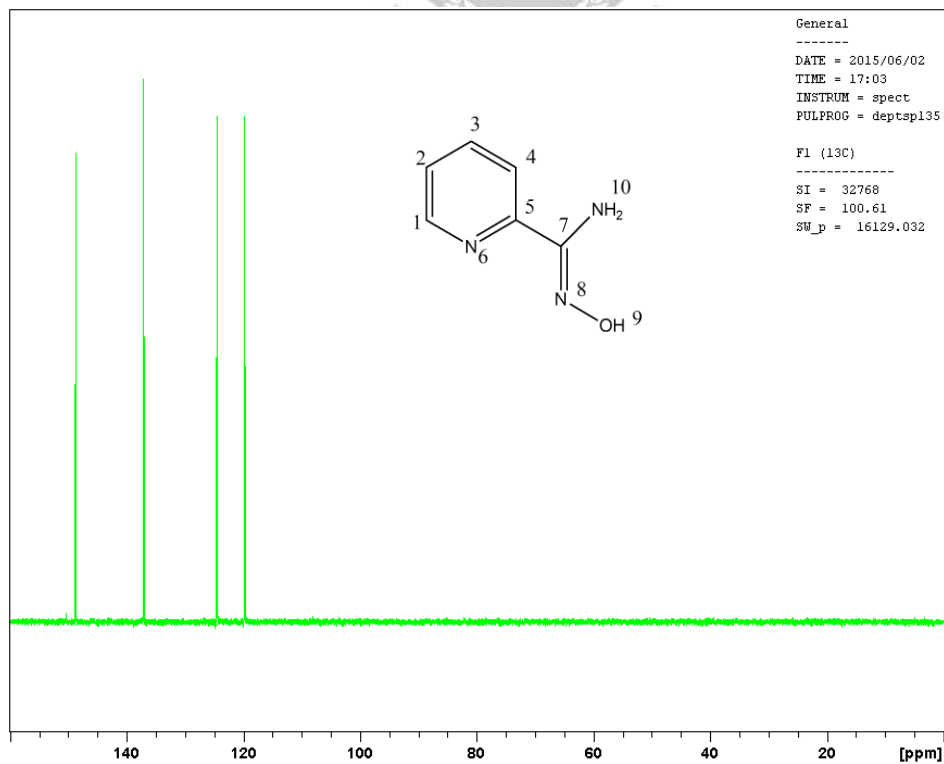
Figure 4.26: ^{13}C NMR DEPT of PyAMI in deuterated DMSO.

http://etd.uwc.ac.za/

The presence of reactive OH and NH_2 moieties on PyAMI is important for the immobilisation of the ligand on a support. The two moieties could undergo nucleophilic addition using either the electron pair on neutral nucleophile nitrogen or oxygen. Other experiments such as ^{13}C NMR and ^{13}C NMR DEPT also confirmed the structure of PyAMI in terms of carbon structure; hence PyAMI structure was confirmed and would be immobilised on PAN-nfs for Pb^{2+} adsorption.

4.2.1.2   ATR-FTIR spectrum of PyAMI

ATR-FTIR analysis was used to investigate the functional groups on PyAMI synthesised in section 3.2.2. The ATR-FTIR analysis was performed as described in section 3.3.6 over the wavelength range of 650 cm^{-1} to 4000 cm^{-1}. Figure 4.27 is the ATR-FTIR spectrum of PyAMI. The spectrum shows the main peaks that could be attributed to pyridine and amidoxime groups. The spectrum shows two sharp peaks at 3458 cm^{-1} and 3340 cm^{-1} which could be assigned to N-H and OH stretching bands.
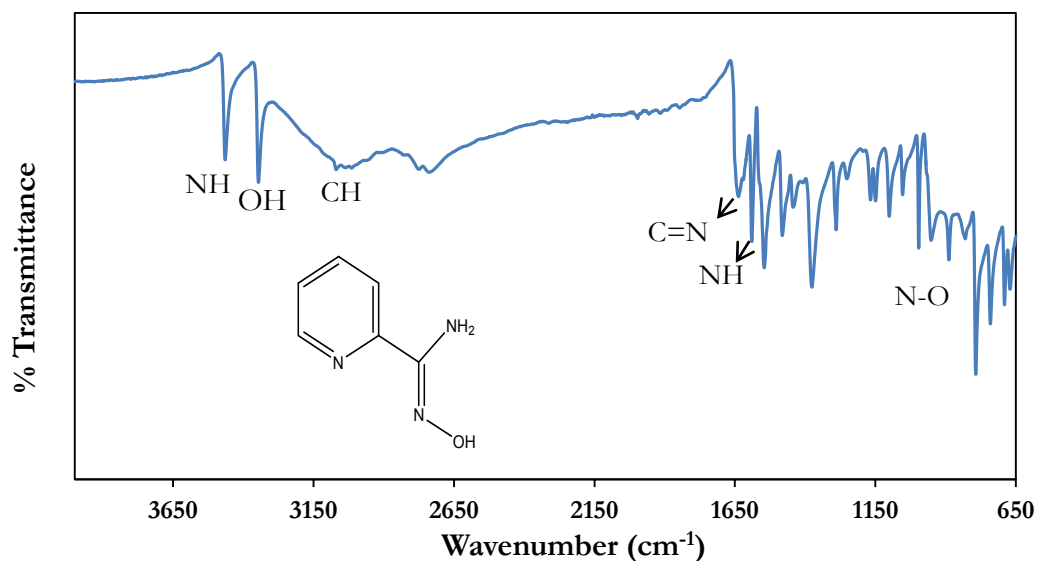
Figure 4.27: ATR-FTIR spectrum of synthesised PyAMI.

The peak at the range of 3100-3010 cm^{-1} is assigned to CH stretching of pyridine ring. The peak at 1620 cm^{-1} corresponds to C=N of oximes, while, the band at 1550 cm^{-1} corresponds to NH bending vibration. The aromatic C–H in-plane bending of

aromatics rings are observed in the region 1300 cm⁻¹–1000 cm⁻¹. The peaks between 996 cm⁻¹—939 cm⁻¹ is assigned to N-O stretching vibration of the amidoxime group. The ATR-FTIR spectrum of PyAMI also confirms the results from NMR analysis. It is important to study and note these peaks belonging to PyAMI as they will serve as indicators when proper immobilisation of the ligand has taken place on PAN-nfs under section 4.2.3.

4.2.1.3 TGA profile of PyAMI

The thermal gravimetry analysis was used to investigate the thermal profile of PyAMI as set out in section 3.3.4. Figure 4.28 presents the TGA and DTG profiles of PyAMI. The result shows that PyAMI underwent single stage decomposition given off volatile gases. PyAMI was fairly stable up to 200°C and thereafter underwent single decomposition between 200°C and 290°C, leaving about 4% carbon residue behind. This shows that PyAMI is a pure single organic compound.
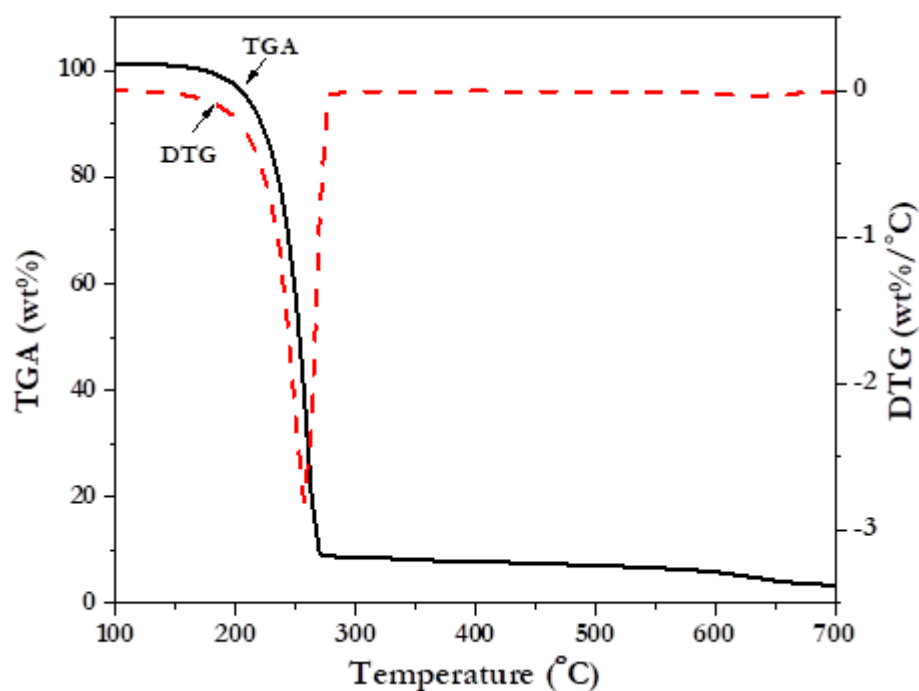
Figure 4.28: TGA and DTG profiles of PyAMI under nitrogen.

4.2.2 Immobilisation concept of 2-pyridine amidoxime on PAN-nfs

For effective immobilisation of a ligand on a support, it is imperative to investigate the proper reaction pathways that can bring the two together. For the case of 2-pyridine amidoxime (PyAMI) ligand and PAN-nfs (support), the first step is to identify the reactive functional groups on the two materials. The functional group on the PAN-nfs is a nitrile group which is fairly electrophilic while the functional groups on the PyAMI are hydroxide and primary amine which are nucleophilic. However, it might still be difficult to immobilise any ligands on PAN-nfs unless the nitrile group is made more electrophilic. This can be done via electrophilic assistance using a brønsted acid such as $AlCl_3.6H_2O$ (Scheme 4.1) (Kampalanonwat and Supaphol, 2014). A carbocation is thus generated on the carbon of the nitrile and this is susceptible to nucleophilic attack (Scheme 4.2).

$$Al(H_2O)_6{}^{3+}{}_{(aq)} \; + \; H_2O_{(l)} \quad \rightleftharpoons \quad Al(H_2O)_5(OH)^{2+}{}_{(aq)} \; + \; H_3O^+{}_{(aq)}$$

$$\left[Al(H_2O)_6\right]^{3+}{}_{(aq)} \quad \rightleftharpoons \quad \left[Al(H_2O)_5(OH)\right]^{2+}_{(aq)} \; + \; H^+{}_{(aq)}$$

Scheme 4.1: Brønsted acidity of $AlCl_3.6H_2O$.
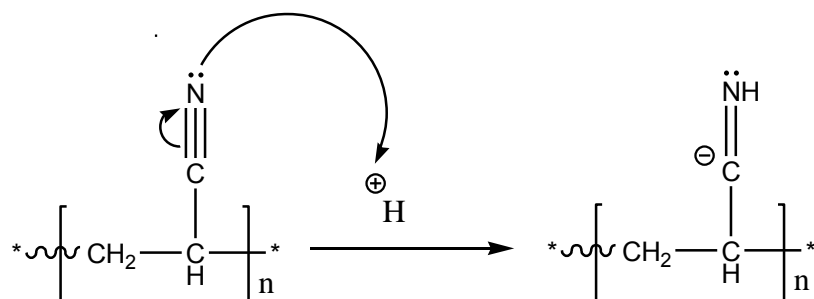
Scheme 4.2: Formation of carbocation on PAN-nfs in acidic medium.

The ligand PyAMI can be immobilised either by direct or in a deprotonated form. The former can perform a nucleophilic addition using either the electron pair on neutral nucleophile nitrogen or oxygen (Scheme 4.3 and Scheme 4.4).
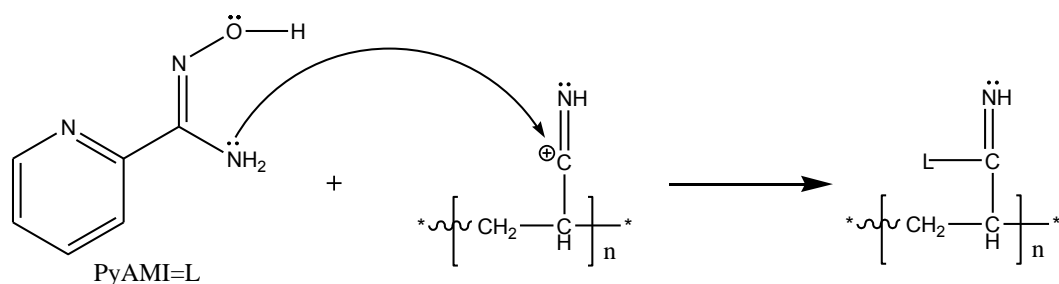
Scheme 4.3: Reaction of PyAMI using nitrogen with PAN-nfs from Scheme 4.2.
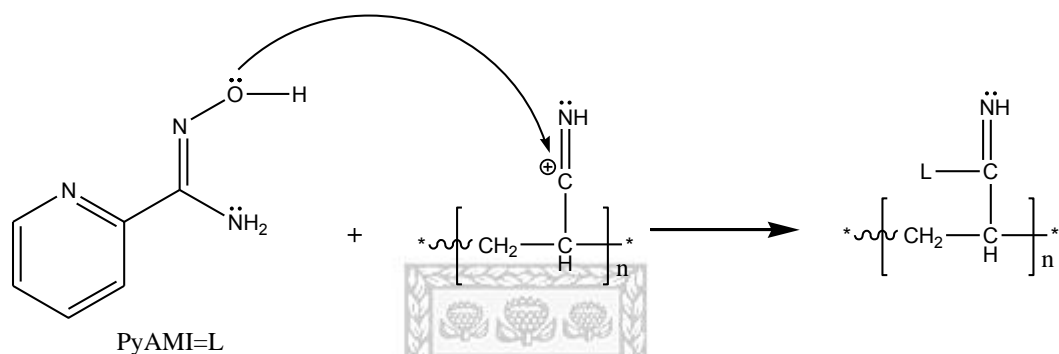
Scheme 4.4: Reaction of PyAMI using oxygen with PAN-nfs from Scheme 4.2.

The reaction mechanism of Scheme 4.3 in more feasible as nitrogen is more nucleophilic compare to oxygen. De-protonation can also occur on the hydrogen of OH from PyAMI in basic medium (Ndayambaje et al., 2016) (Scheme 4.5), thereby a suggesting reaction with PAN-nfs according to Scheme 4.6.
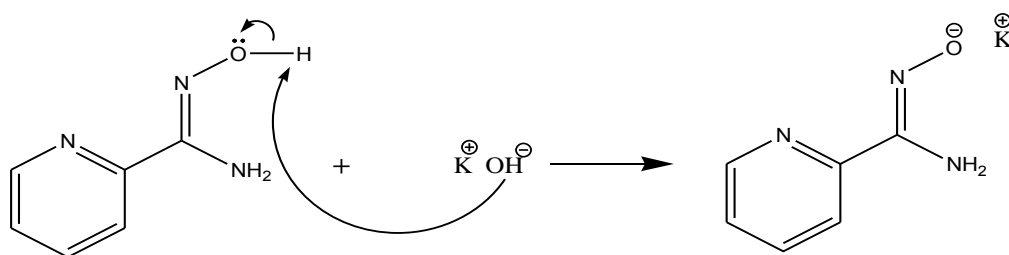
Scheme 4.5: De-protonation of PyAMI on the hydroxide.
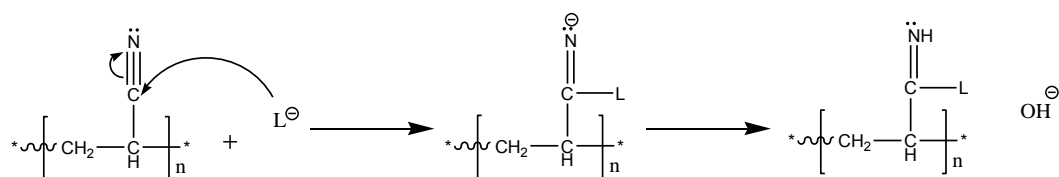
Scheme 4.6: Reaction of PyAMI from Scheme 4.5 with PAN-nfs.

http://etd.uwc.ac.za/

4.2.3 Preparation of PAN-PyAMI

The immobilisation of PyAMI on PAN-nfs was investigated by various experiments as described in sections 3.2.3 and 3.2.4. The resultant PAN-PyAMI nanofibres of each experiment was characterised using ATR-FTIR, HRSEM and TGA techniques.

4.2.3.1 Base-catalysed immobilisation of PyAMI on PAN-nfs

This experiment was carried out to immobilise PyAMI on 8 wt% PAN-nfs as described in section 3.2.3 in basic medium according to literature (Ndayambaje et al., 2016). The preparation of PAN-PyAMI with alkaline hydrolysis was carried out with respect to time and concentration of KOH. The experiment was first monitored using ATR-FTIR technique before other techniques. The ATR-FTIR spectra of the PAN-PyAMI from 1:1 of PyAMI/KOH experiment are presented in Figure 4.29.
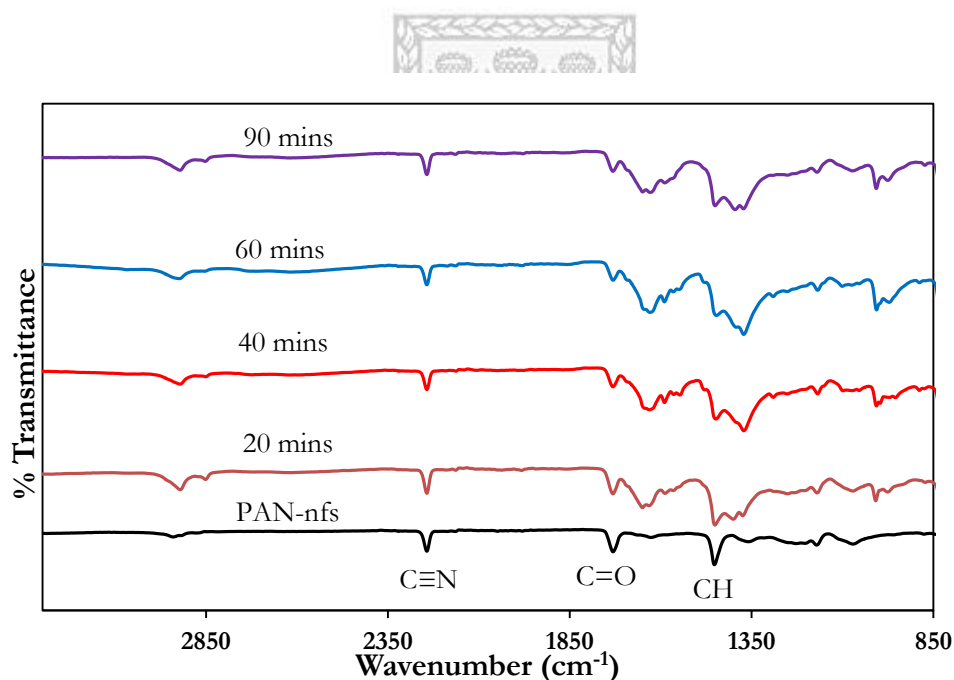
Figure 4.29: ATR-FTIR spectra of PyAMI/KOH 1:1 reacted with PAN-nfs as function of reaction time.

The ATR-FTIR analysis was performed as described in section 3.3.6 over the wavelength range of 850 cm^{-1} to 4000 cm^{-1}. The spectrum of PAN-nfs showed the main characteristic peak at 2241 cm^{-1} which is assigned to the nitrile group. The peak that appeared at 1718 cm^{-1} corresponds to C=O while the peak at 1444 cm^{-1} is assigned to CH$_2$. The spectrum at 20 minutes shows a peak at 1620 cm^{-1} started appearing. This peak became obvious at 60 minutes but reduced a little at 90

minutes. The peak could be either assigned to the C=N from the ligands (oximes) or the C=N from reduction of nitrile of PAN-nfs.

Also at 40 minutes two other shoulders appeared at 1560 cm^{-1} and 1360 cm^{-1} which could be assigned to —C=NH and C—N, respectively. These peaks are also observed at 60 and 90 minutes. All these new peaks that appeared over time could be as a result of immobilisation of PyAMI, however, their intensity proved otherwise. These results did not clearly show that PyAMI is immobilised on PAN-nfs as the peaks of PAN-nfs were still predominant and peaks characteristics of pyridine and amidoximes are still vague. Also new bonds were expected to be pronounced if proper immobilisation had taken place.
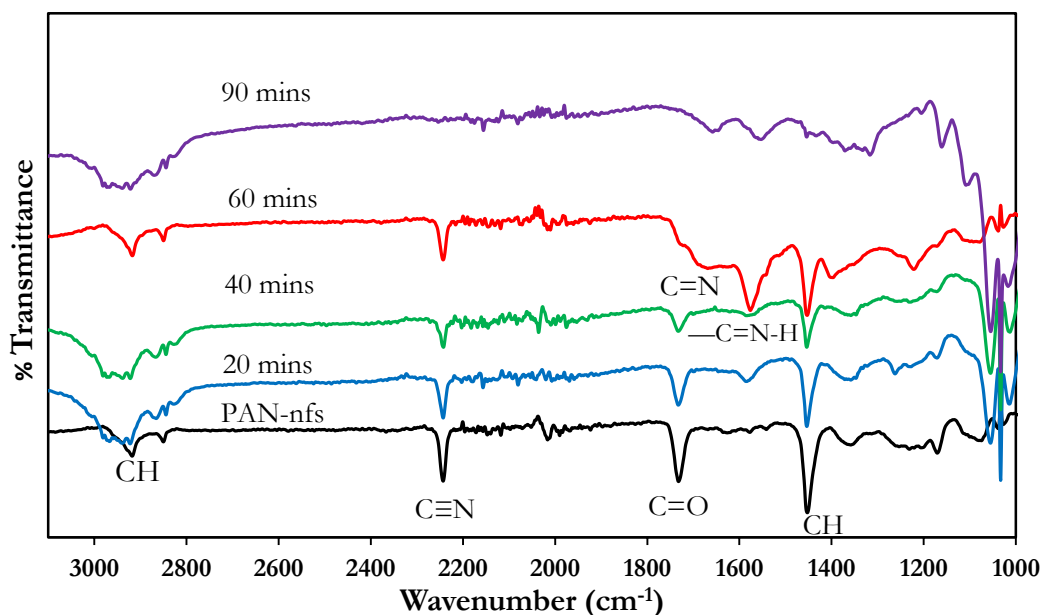
Figure 4.30: ATR-FTIR spectra of PyAMI/KOH 1:2 reacted with PAN-nfs as function of reaction time.

The second experiment (PyAMI/KOH mole ratio 1:2) (Figure 4.30) started showing —C=NH peak (1580 cm^{-1}) at 20 minutes of reaction time. The NH peaks became pronounced as the reaction time increased from 40 to 60 minutes, which might be indicating the presence of more active sites from PyAMI. Also included at 60 minutes is the peak at 1698 cm^{-1} which either corresponds to C=N from PyAMI or as a result of hydolysis of C≡N to C=N. At 90 minutes, the PAN-nfs are deformed

and the characteristic peak of PAN-nfs at 2241 cm⁻¹ (C≡N) is completely gone. This
was confirmed by SEM analysis.

The HRSEM analysis was carried out as described in section 3.3.3. PAN-PyAMI was
coated with Au and was observed at different magnifications under HRSEM. The
HRSEM images (Figure 4.31) of PAN-PyAMI shows that the immobilisation of
PyAMI on PAN-nfs in basic medium affected the surface morphology of PAN-nfs.

Figure 4.31: HRSEM images of (a) pristine PAN-nfs (b) PAN-PyAMI 20 mins (c) PAN-
PyAMI 60 mins and (d) PAN-PyAMI 90 mins.

As the immobilisation time increased, the PAN-PyAMI nanofibres were
progressively fused together (Figure 4.31 (b) and (c)) and later started to disintegrate
(Figure 4.31 (d)). The average fibre diameter also increased from 354 nm to 392 nm.
To understand this trend, the effect of hydrolysis on PAN-nfs was then studied.

4.2.3.2 Effect of hydrolysis on PAN-nfs

This experiment was carried out as set out in section 3.2.3.1 to show the effect of KOH on PAN-nfs and to differentiate the ATR-FTIR peaks that are associated to hydrolysis of PAN-nfs from immobilised PyAMI ligand. Figure 4.32 presents the ATR-FTIR spectra of the hydrolysis reaction.
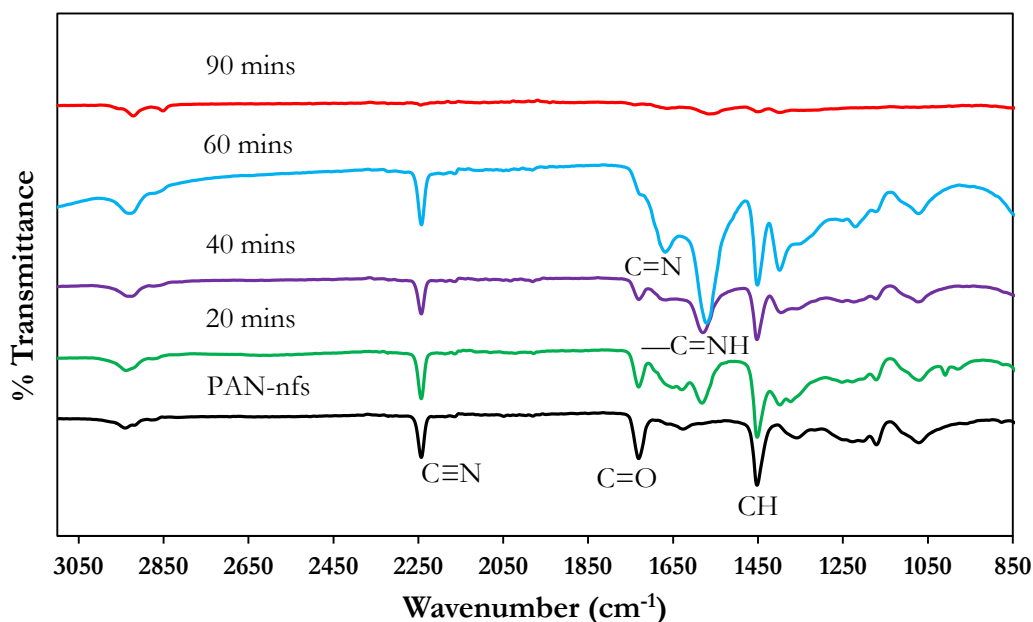
Figure 4.32: ATR-FTIR spectra of hydrolysis of PAN-nfs.

The ATR-FTIR spectra (Figure 4.32) of the hydrolysis of PAN-nfs using KOH shows peak such as 1559 cm^{-1} (—C=NH) at 20 minutes. This peak became prominent at 40 and 60 minutes. At 40 and 60 minutes, another peak at 1659 cm^{-1} appeared (as a results of further hydrolysis of —C≡N) which is assigned to —C=N. At 90 minutes, non of these peaks appeared (similar to what was obtained in section 4.2.3.1, at 90 minutes). Comparing the ATR-FTIR results of this experiment and that of section 4.2.3.1 (Figure 4.29 and Figure 4.30), it is obvious that the peaks assigned to —C=NH and C=N might not be as a result of immobilisation of PyAMI but from the hydrolysis of PAN-nfs. HRSEM was used to observe the surface mophology of the hydrolysed PAN-nfs.

The HRSEM images of hydrolysed PAN-nfs (Figure 4.33) were observed and compared to that of section 4.2.3.1 (Figure 4.31). The results shows that the hydrolysed PAN-nfs also fused together as the KOH hydrolysis time increased without the presence of PyAMI ligand. The fibre diameter also increased from 312 nm to 390 nm. These two observations correlate with surface morphology of PAN-nfs nanofibres obtained from section 4.2.3.1. Therefore, the surface roughness and fusion are ascribed to the KOH induced hydrolysis reaction and is not necessarily due to the cross-linking or immobilisation of PyAMI on PAN-nfs. This fusion of PAN-nfs has also been reported by Kampalanonwat et al. (2011) and Deng et al. (2003b) under similar conditions using NaOH at 60°C.
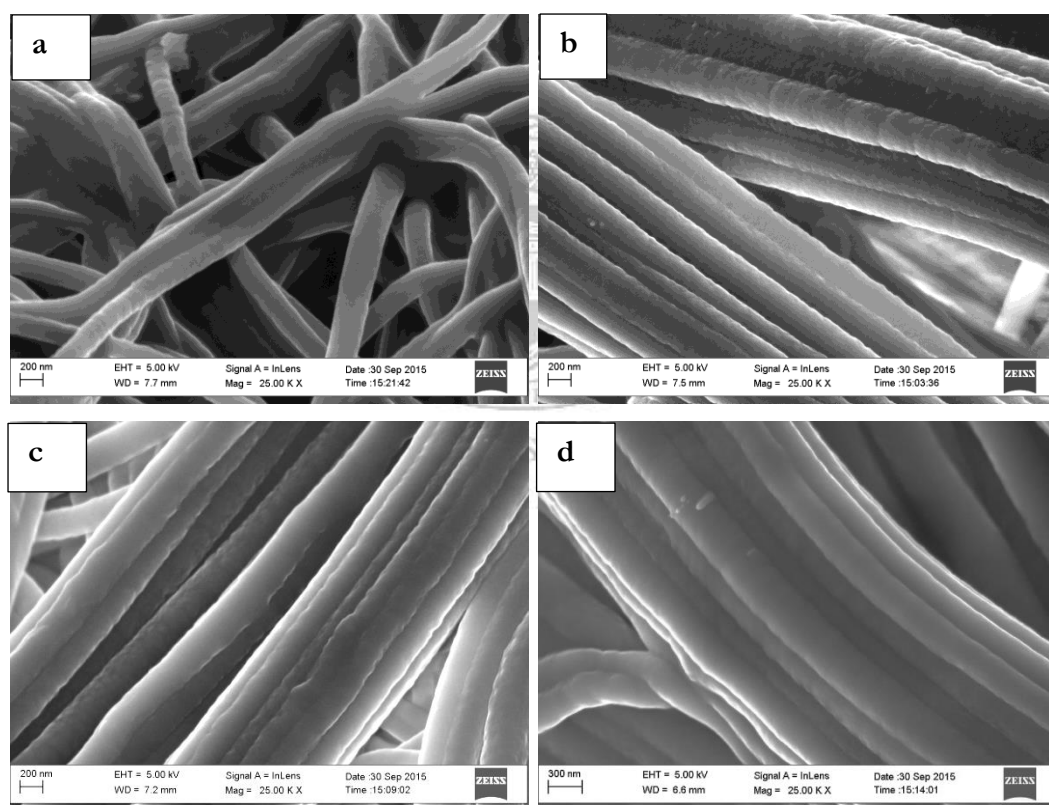
Figure 4.33: HRSEM images of hydrolysed PAN-nfs (a) 20 mins (b) 40 mins (c) 60 mins and (d) 90 mins.

TEM analysis was also used to observe the internal structure of hydrolysed PAN-nfs. The analysis was carried out as described in section 3.3.4. Figure 4.34 shows the TEM bright field image of hydrolysed PAN-nfs. The results show that the

nanofibres were flattened (Figure 4.34 (a) and (b)) after the hydrolysis reaction when compared to the pristine PAN-nfs (Figure 4.34 (c)).
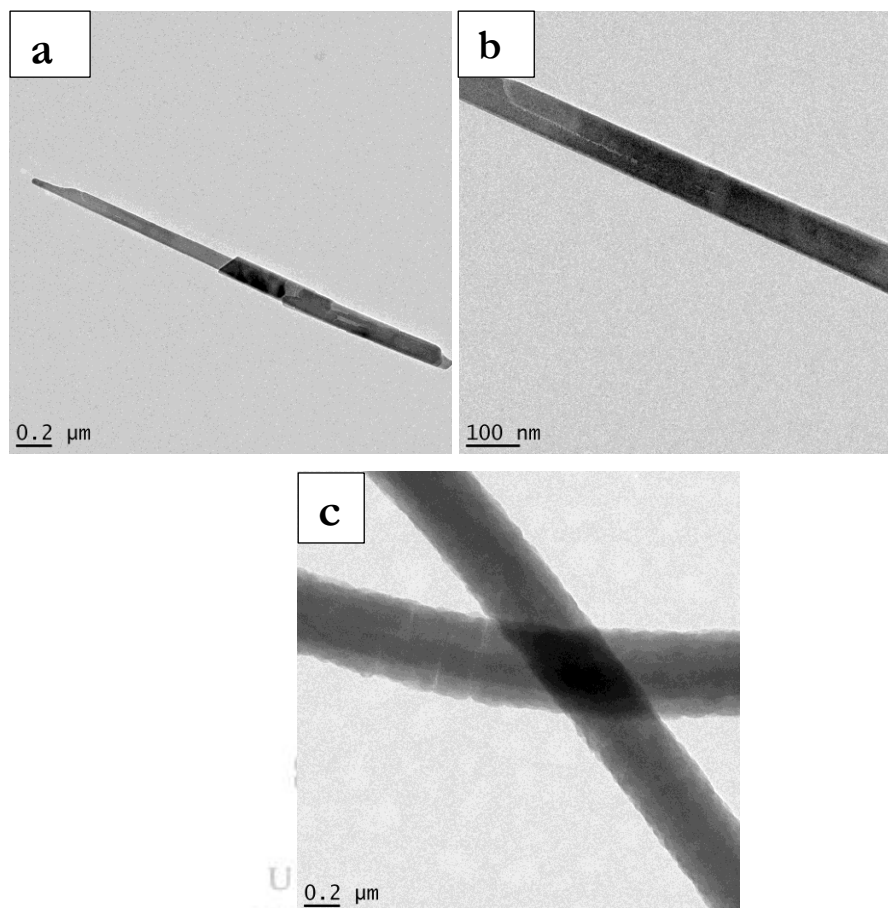
Figure 4.34: TEM bright field image of hydrolysed PAN-nfs at {(a) 0.2 μm and (b) at 100 nm scale values} and pristine PAN-nfs (c).

The TGA analysis was conducted under nitrogen and the heating rate of the sample was set as described in section 3.3.5. Figure 4.35 is the TGA analysis of pristine PAN-nfs and hydrolysed PAN-nfs. The TGA analysis was compared to that of PAN-nfs in terms of the fibre degradation at 60°C. The thermal profile shows that the pristine PAN nanofibres only start losing mass at a temperature of around 190°C not at 60°C as previously described in section 4.1.2.4.
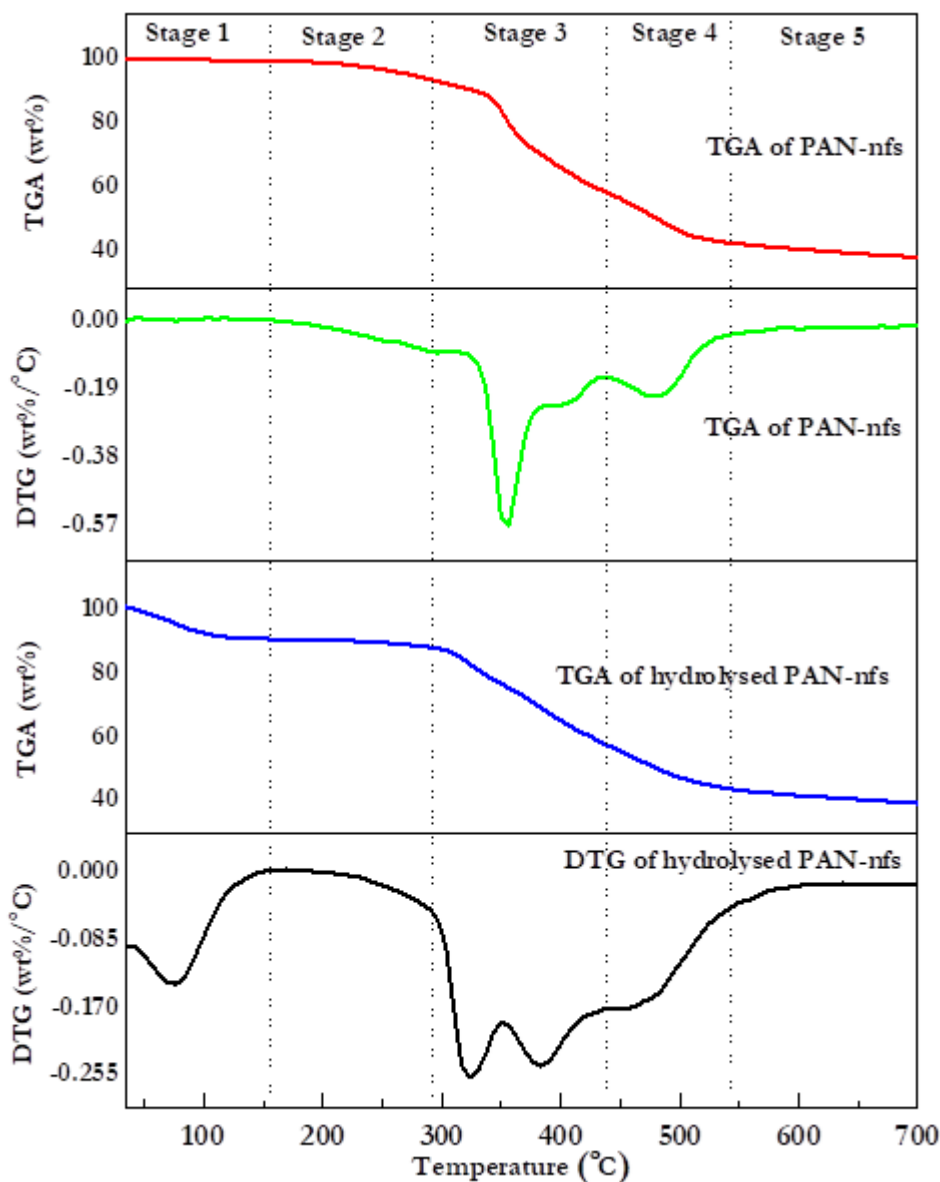
Figure 4.35: TGA and DTG of pristine PAN-nfs and hydrolysed PAN-nfs under nitrogen.

Meanwhile, PAN-nfs treated with KOH started to thermally degrade at 50°C until 130°C losing about 8% mass, and then stabilised (Stage 1; Figure 4.35). The loss in mass might be due to the weakened structure of PAN-nfs due to hydrolysis. Stages 2, 3 and 4 degredation of the pristine and hydrolysed PAN-nfs showed similar trend, however, at stage 3, for hydrolysed PAN-nfs, the thermal degradation reaction of PAN-nfs and the decomposition of the carbon-carbon main chain occurred between 310°C and 390°C (lower than pristine PAN-nfs). Stage 5 is the carbon residue of about 38% left behind. The results further confirmed that the roughness and disintegration of PAN-nfs was as a result of KOH induced hydrolysis and not due to

the temperature used or the immobilisation of PyAMI. No literature was found to compare the results with.

In summary, based-catalysed immobilisation reaction pathway was not suitable as the PAN-nfs was disintegtrating as a result of hydrolysis. Also, the nano-integrity of PAN-nfs was jeopardized as the nanofibre strands were fused together and could no longer be referred to as nanofibres. Therefore, another reaction pathway was employed for the immobilisation of PyAMI on PAN-nfs as described in section 3.2.4. The results of this pathway are discussed in the next section.

4.2.3.3   Acid-catalysed immobilisation of PyAMI on PAN-nfs

This experiment was carried out to immobilise PyAMI on PAN-nfs in acidic medium as described (Kampalanonwat and Supaphol, 2014) in section 3.2.4. The preparation of PAN-PyAMI with $AlCl_3.6H_2O$ catalyst was carried out with respect to time (20, 40, 60, and 90 minutes) at 60°C. The experiment was first monitored using ATR-FTIR technique before other techniques. The ATR-FTIR analysis was performed as described in section 3.3.6 over the wavelength range of 850 to 4000 cm^{-1}. Figure 4.36 presents the ATR-FTIR spectra of the acid-catalysed reaction.
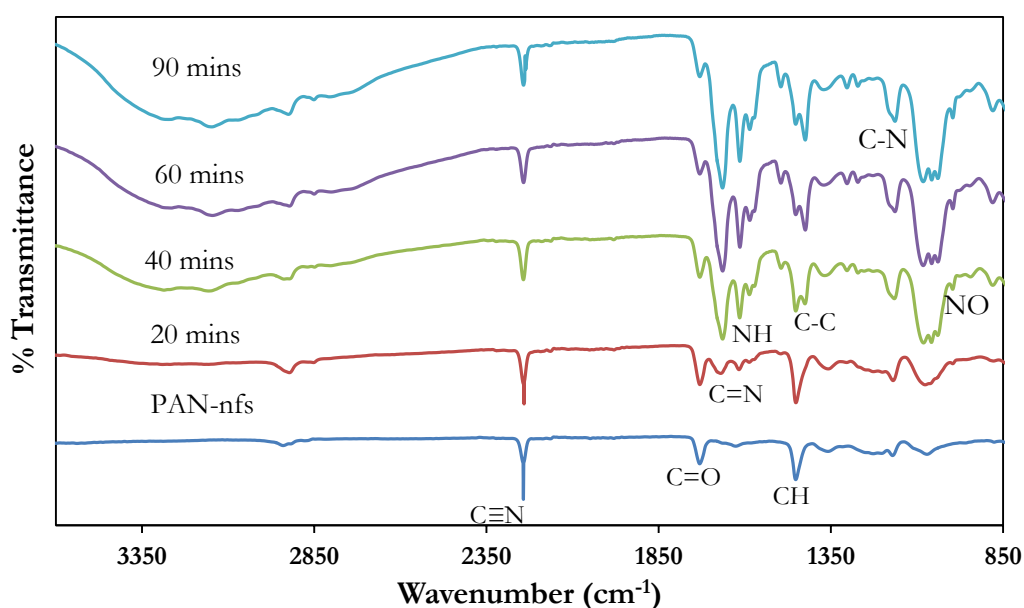
Figure 4.36: ATR-FTIR spectra of acid-catalysed immobilisation of PyAMI on PAN-nfs as function of reaction time.

The results from ATR-FTIR spectra of acid-catalysed immobilisation of PyAMI on PAN-nfs (Figure 4.36) shows some interesting peaks as the reaction time increased from 20 minutes to 90 minutes. At 20 minutes, 1654 cm^{-1} (C=N) started to appear as a result of PyAMI. However at 40 minutes, other peaks such as 1605 cm^{-1} (C—NH bending vibration), and 968 cm^{-1} (N-O) also appeared. Also a peak at 1145 cm^{-1} which is suspected to be the new bond formed is attributed to C-N (aliphatic amines) (recall Scheme 4.3). The peak at the range of 3181 cm^{-1}—3030 cm^{-1} is assigned to CH stretching of pyridine ring. The broad band range between 3437 cm^{-1} and 3030 cm^{-1} could be assigned to OH of PyAMI. These peaks are indicating the presence of PyAMI on PAN-nfs when compared to pristine PAN-nfs (Figure 4.36).

The intensity of these peaks increased as the reaction time increased. All the aforementioned peaks appeared at 60 mins with more intensity. However at 90 mins, the intensity of these peaks remained the same as 60 mins. There was also the reduction of the carbonyl ester peak (1715 cm^{-1}) as the reaction time increased, which also indicates the disappearance of the methylacrylate group as a result of hydrolysis. The peak associated with the nitrile group of the PAN-nfs at 2240 cm^{-1} also decreased in its intensity as the conversion time increased. The ATR-FTIR results of PAN-PyAMI shows that PyAMI was immobilised on PAN-nfs because of the presence of PyAMI FTIR peaks on PAN-nfs.

The integrity check of these peaks was investigated by control reaction of PAN-nfs with water as described in section 3.2.4.1. 0.5 g PAN-nfs was immersed in water at 60°C for 40 or 60 minutes for 1 hour. The resultant nanofibres were dried in an oven over night at 40°C to constant weight. The nanofibres were characterised using ATR-FTIR.

The ATR-FTIR spectra of PAN-nfs reaction with water (Figure 4.37) shows that water did not introduce any peak on the surface of PAN-nfs over time as there were no new peaks on the spectra of the time reaction when compared with the pristine PAN-nfs. Therefore, it is concluded that all new peaks appearing in Figure 4.36 were as a result of immobilisation of PyAMI on PAN-nfs.
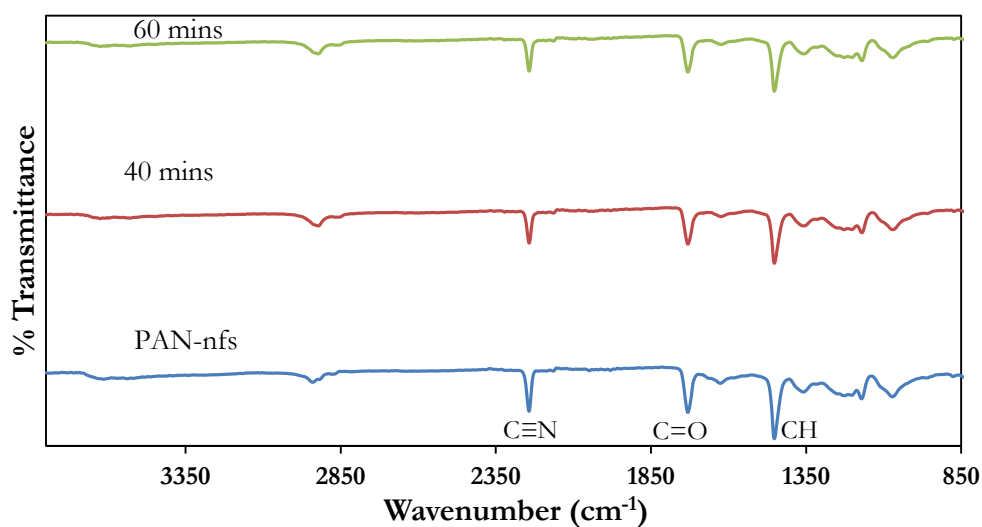
Figure 4.37: ATR-FTIR spectra of pristine PAN-nfs reacted with water.

HRSEM analysis was also used to check the surface morphology of PAN-PyAMI. Figure 4.38 presents the HRSEM of PAN-PyAMI. The HRSEM analysis was carried out as described in section 3.3.3.
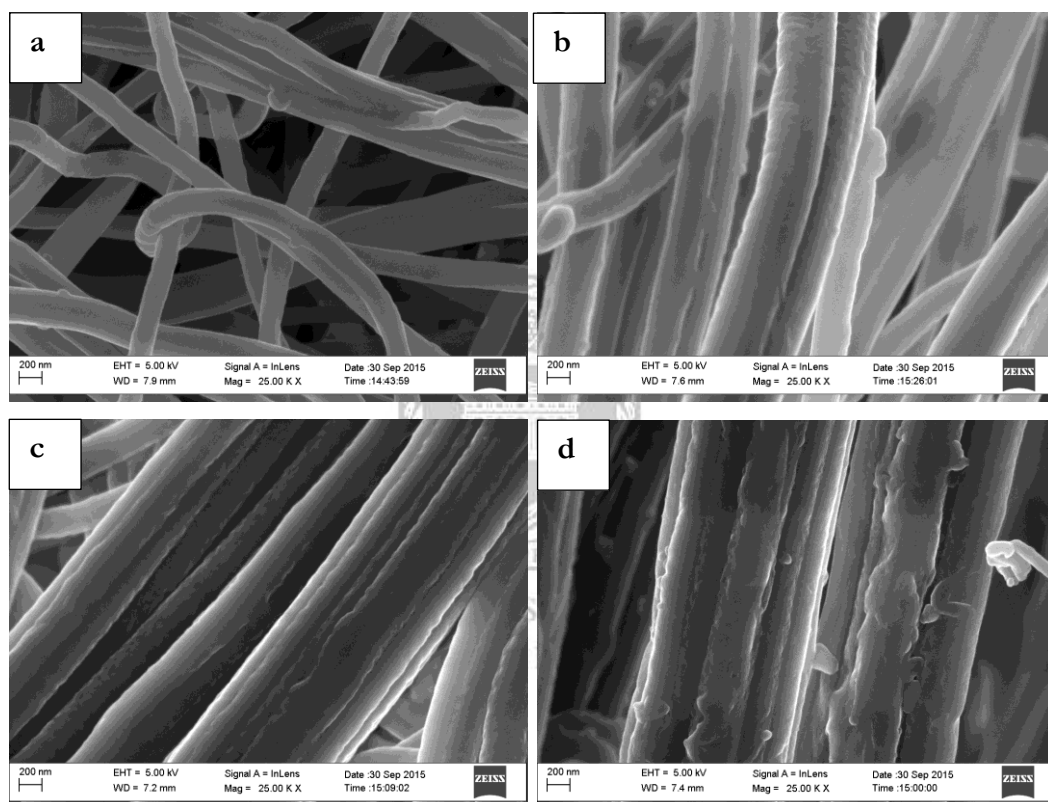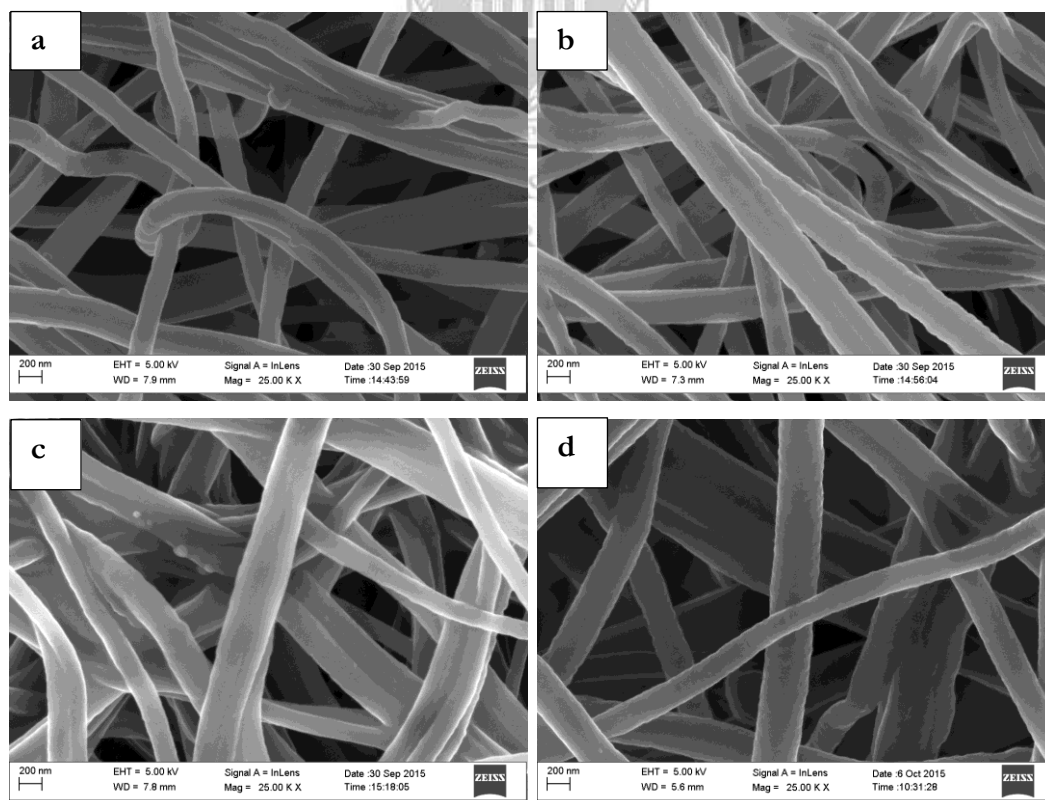

Figure 4.38: HRSEM images of (a) pristine PAN-nfs (b) PAN-PyAMI 20 mins (c) PAN-PyAMI 40 mins and (d) PAN-PyAMI 60 mins.

Each sample of PAN-nfs was coated with Au and was observed at different magnifications under HRSEM. The HRSEM images of PAN-PyAMI Figure 4.38 (b) 20 mins, Figure 4.38 (c) 40 mins and Figure 4.38 (d) 60 mins when compared with pristine PAN-nfs (Figure 4.38 (a)) shows that the immobilisation of PyAMI on PAN-nfs in acidic medium did not significantly affect the surface morphology of PAN-nfs with respect to time. The HRSEM images show that the surface morphology of the functionalised PAN-nfs showed no degradation as the reaction time increased as it was in contrast to the based-catalysed immobilisation reaction in section 4.2.3.1.

TEM analysis was used check the internal structure of PAN-PyAMI. The analysis was carried out as described in section 3.3.4. Figure 4.39 shows the TEM bright field image of PAN-PyAMI. The internal image of PAN-PyAMI became dark. This might be as a result of immobilisation of PyAMI on PAN-nfs.
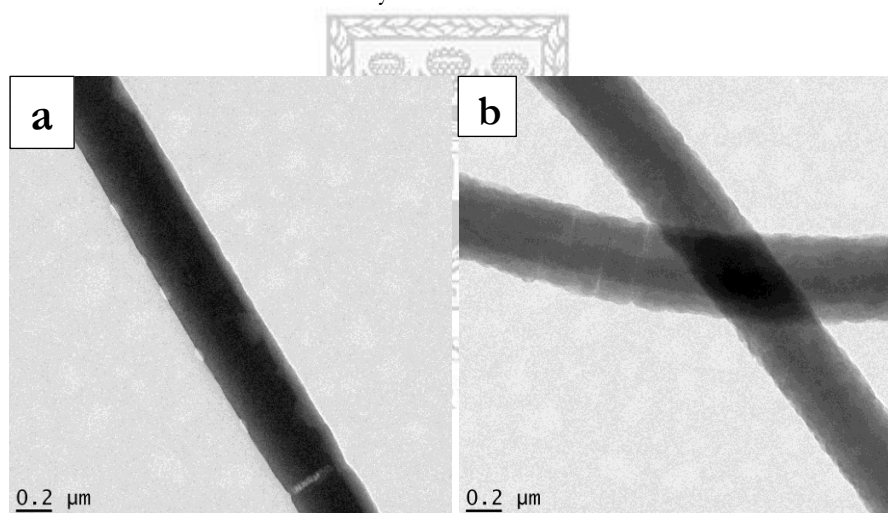
Figure 4.39: TEM bright field image of (a) PAN-PyAMI and (b) pristine PAN-nfs.

The X-ray diffraction (XRD) analysis was carried out as described in section 3.3.8 to check the change in the amorphous phase of PAN-nfs before and after immobilisation of ligand. Figure 4.40 presents the XRD patterns of PAN-nfs and PAN-PyAMI. For PAN-nfs, a strong diffraction peak centered at 17.3° corresponds to the hexagonal lattice and a weak diffusion peak centered at 27.2° was obsreved (He et al., 2015). The sharp diffraction peaks at 27.2° and 17.3° were also observed for PAN-PyAMI; however the intensities of the peaks decreased due to the immobilised ligands on PAN-nfs.
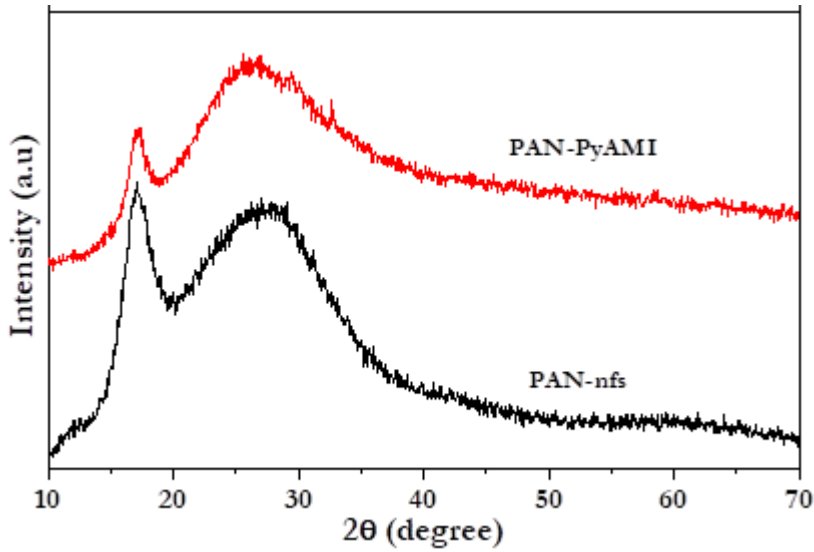
Figure 4.40: XRD patterns of PAN-nfs and PAN-PyAMI.

Surface area and pore size analysis were also conducted on PAN-PyAMI synthesised in this section in order to determine the BET surface area and the pore size distribution (Figure 4.41). The analysis was carried out as derscibed in section 3.3.7
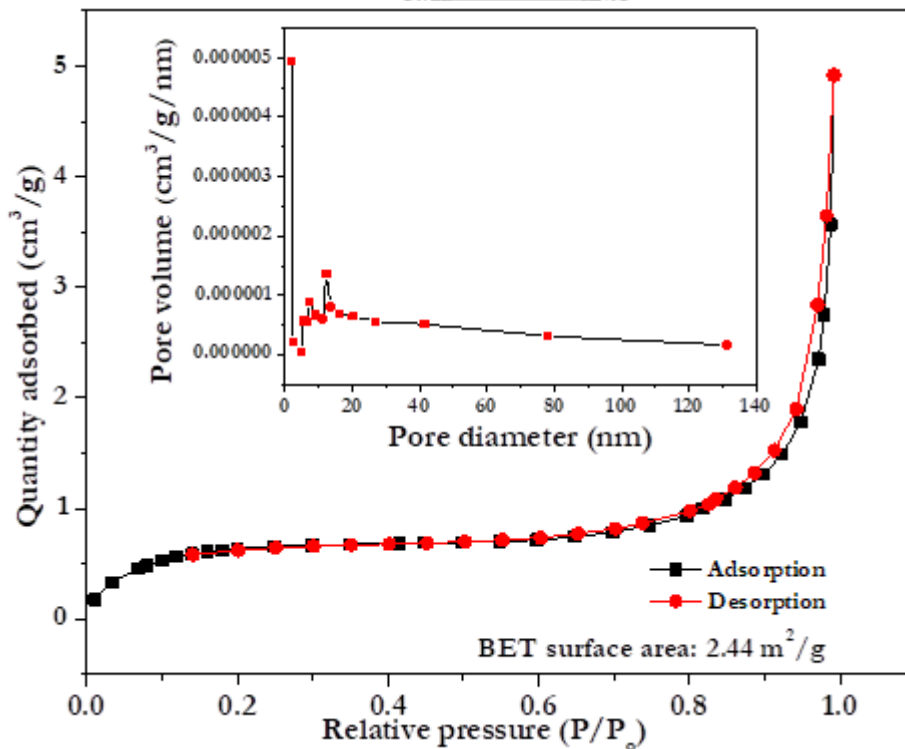
Figure 4.41: Nitrogen adsorption–desorption isotherms of PAN-PyAMI (inset; pore size distribution).

BET surface area and pore size distribution were investigated by nitrogen adsorption–desorption measurement. Figure 4.41 shows the nitrogen adsorption–desorption isotherms (inset; pore size distribution) with hysteresis loops, indicating the presence of mesopores between adjacent fibres in the range of 10 nm to 20 nm. Based on BET analysis the surface area of PAN-PyAMI showed a drastic reduction in BET surface area. The BET surface area was calculated to be 2.44 m^2/g compared to pristine PAN-nfs which was calculated to be 10.93 m^2/g in section 4.1.2.5. The reduction in surface area could be attributed to the immobilisation of the ligand on PAN-nfs which may have caused some crosslinking.

4.2.3.3.1   Estimation of ligand immobilised on PAN-nfs

For empirical purpose, it is scientifically important to determine in mass the amount ligand that was attached to the support in this study. However, due to experiment errors, only estimation could be done. For this research, a novel method was employed to estimate the amount of ligand (PyAMI) immobilised on support (PAN-nfs). The method involves a systematic study of TGA profile of PAN-nfs and PAN-PyAMI. The TGA analysis was conducted on PAN-nfs and PAN-PyAMI respectively of approximately the same weight (3.966 mg) under a nitrogen atmosphere and the heating rate of the sample was set at 20°C/min up to 800°C and then held for 1 minute at 800°C (section 3.3.5).

Figure 4.42 shows the thermogravimetric analysis profile and their respective derivatives during degradation of PAN-nfs and PAN-PyAMI under nitrogen atmosphere. Based on DTG of PAN-nfs, the thermal profile of PAN-nfs was divided into five stages (Figure 4.42). The TGA profiles of PAN-nfs and PAN-PyAMI was fairly stable at stage 1, meanwhile, at stage 2; PAN-nfs and PAN-PyAMI lost weight of approximately 10% and 20%, respectively. The 10% weight loss for PAN-nfs was attributed to the loss of volatiles at temperatures between 210°C and 325°C. For PAN-PyAMI, 10% could also be attributed to the loss of volatiles from PAN-nfs, however, the remaining 10% weight loss could have been as a result of the loss of ligand immobilised on PAN-nfs.
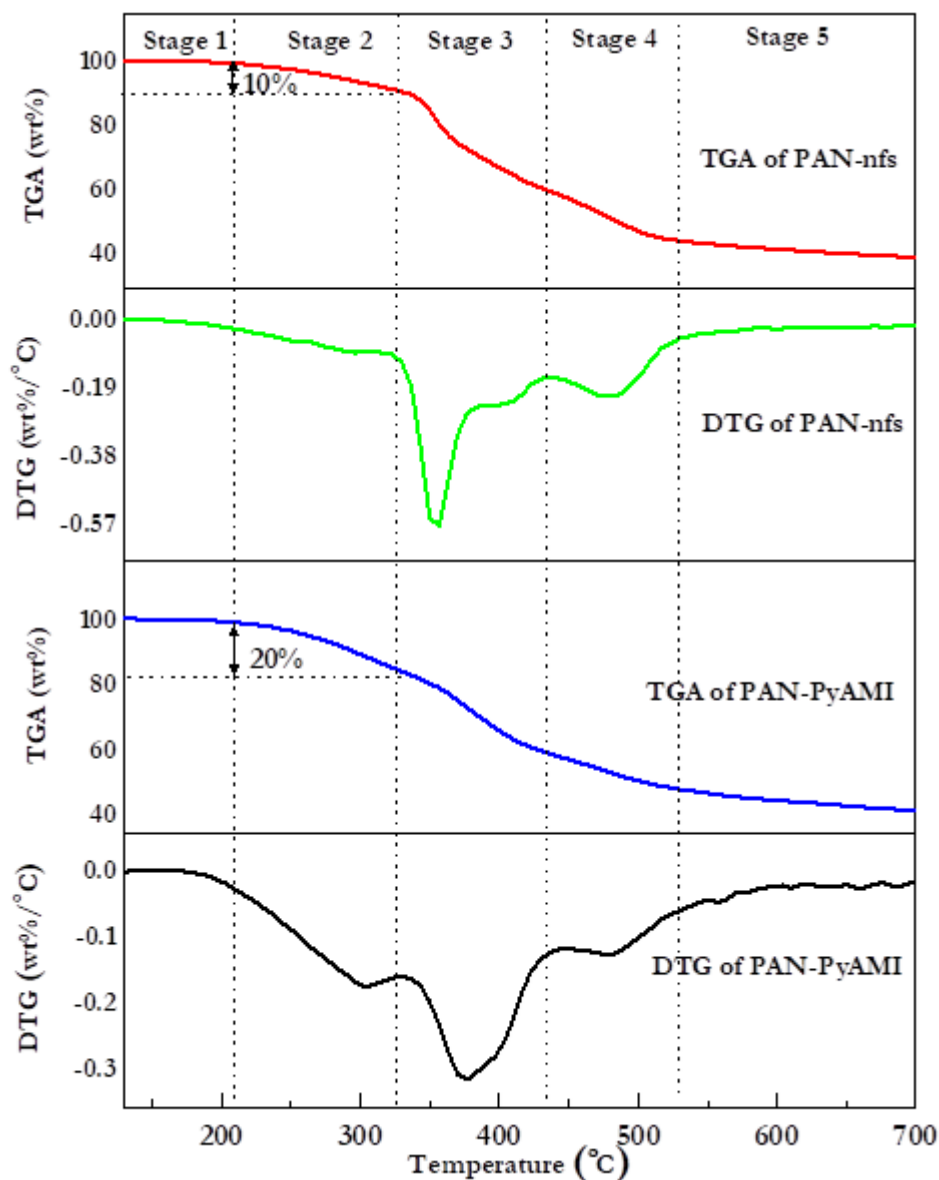
Figure 4.42: TGA and DTG of pristine PAN-nfs and PAN-PyAMI under nitrogen.

To estimate the mass of ligand immobilised per gram of PAN-nfs, the following estimation and explanation were made; mass of PAN-nfs or PAN-PyAMI = 0.003966 g (mass weighed for TGA analysis); percentage mass loss at stage 2 (PAN-nfs) = 10%; percentage mass loss at stage 2 (PAN-PyAMI) = 20%; difference in percentage = 10%; 10% of 0.003966 g given off at stage 2 = 0.0003966 g of PyAMI. The actual mass of PAN-nfs in PAN-PyAMI = 0.003966-0.0003966 = 0.0035694 g. Therefore, for every 1 g of PAN-nfs, 0.111 g of PyAMI was immobilised. From Figure 4.42, stages three, four and five followed a similar pattern. According to TGA profile PyAMI, the ligand was not expected to have remained at these stages.

Thermal gravimetry analysis results of PAN-nfs compared with PAN-nfs treated with H_2O at 60°C (Figure 4.43) followed a similar profile at the second stage indicating that PAN-nfs was stable in water at 60°C and that the extra 10% weight loss observed between 210°C and 325°C of PAN-PyAMI (Figure 4.42) could be due to the loss of ligands immobilised on PAN-nfs.
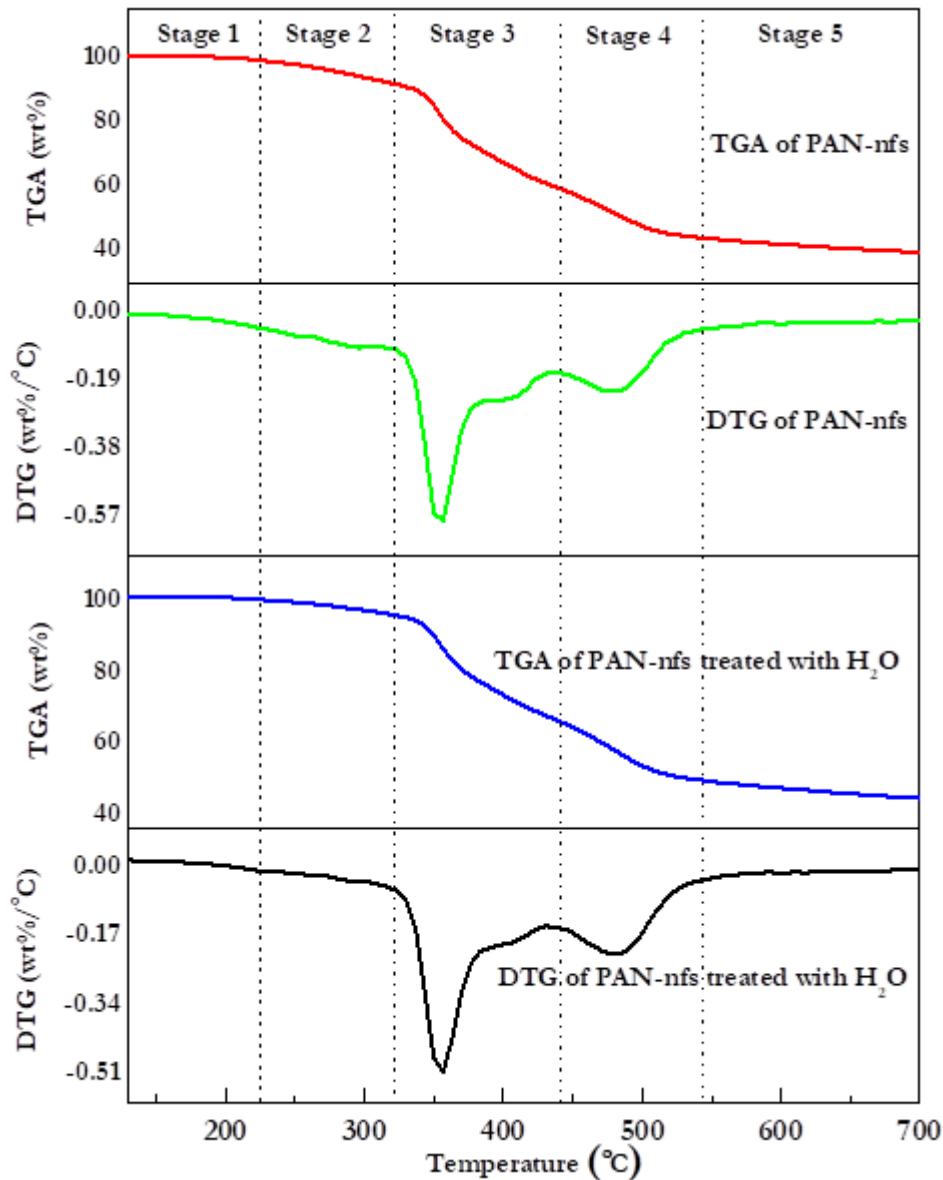
Figure 4.43: Thermal profile of pristine PAN-nfs and PAN-nfs treated with H_2O under nitrogen.

4.2.4 Stability and regeneration tests

PAN-PyAMI is primarily synthesised for adsorption studies, therefore, it is important to test its stability in different pH solutions. This will give an idea of which pH PAN-PyAMI will work best. So, also for the purpose of regeneration of PAN-PyAMI after adsorption, a preliminary test was carried out to understand the best solutions for stripping off adsorbed metals from PAN-PyAMI without losing the ligand for the sake of reusability. The following subsections are the results of experiments described in sections 3.2.5 and 3.2.6.

4.2.4.1 Stability of PAN-PyAMI in different pH solutions

The stability of PAN-PyAMI was done as described in section 3.2.5. The ATR-FTIR analysis was performed as described in section 3.3.6 over the wavelength range of 850 cm^{-1} to 4000 cm^{-1}. Figure 4.44 presents the ATR-FTIR spectra of stability test of PAN-PyAMI in different pH solutions prior to its use as an adsorbent.
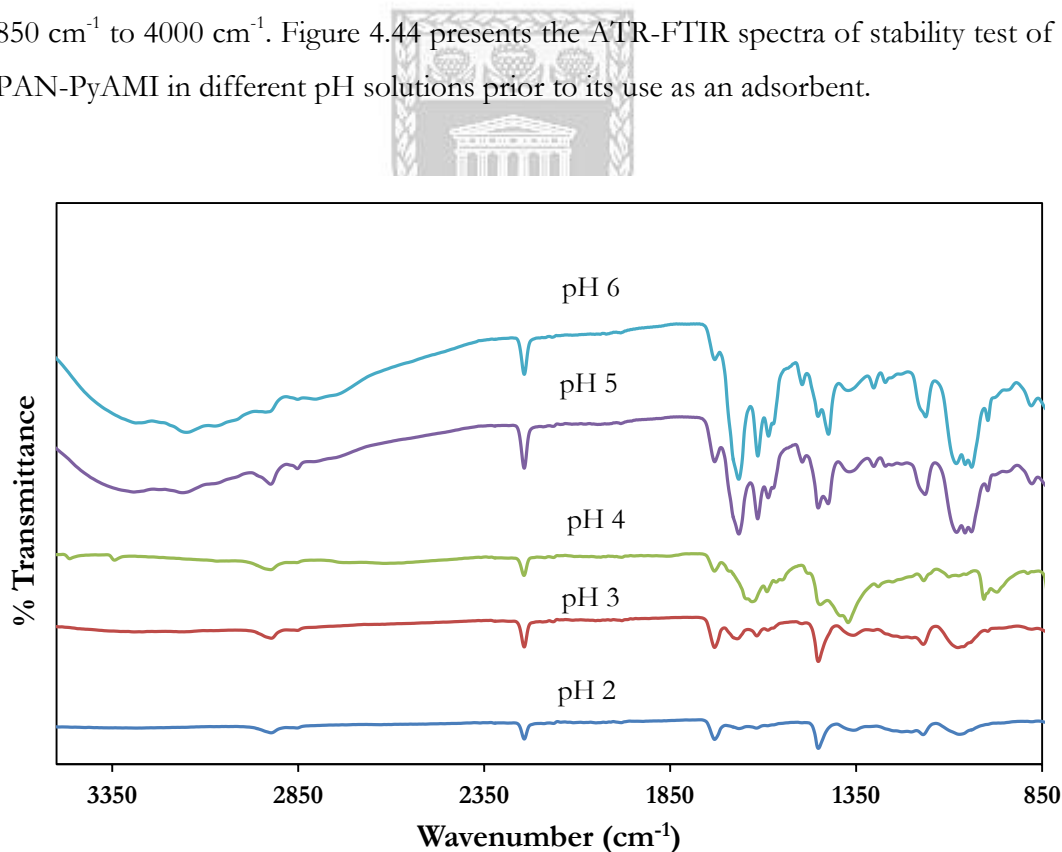
Figure 4.44: ATR-FTIR spectra of PAN-PyAMI at different pH solutions.

The results show that the PyAMI moiety was stable at pH 6 and pH 5. However, at pH 4, some of the peaks of PyAMI have started to disappear. At pH 3 and pH 2, the peaks attributed to PyAMI were all lost. The results imply that the PAN-PyAMI could only be used effectively in solutions of pH 5 and 6 as all the chelation sites from PyAMI are present. It could also function at pH range of 3.5 to 4.5; however, adsorption efficiency of PAN-PyAMI after subsequent regeneration might be declining due to low availability of chelating sites as some of the sites might be weakened.

4.2.4.2   Regeneration study of PAN-PyAMI

Most studies done on the regeneration of functionalised nanofibres are carried out in acidic medium. However, most of these studies never went ahead to reuse the nanofibres or even re-characterised the nanofibres after the acid regeneration. For this study, regeneration was carried on PAN-PyAMI using 0.1 M EDTA and 0.1 M HNO_3 at 25°C for 1 hour as described in section 3.2.6. The resultant PAN-PyAMI was characterised using ATR-FTIR (Figure 4.45).
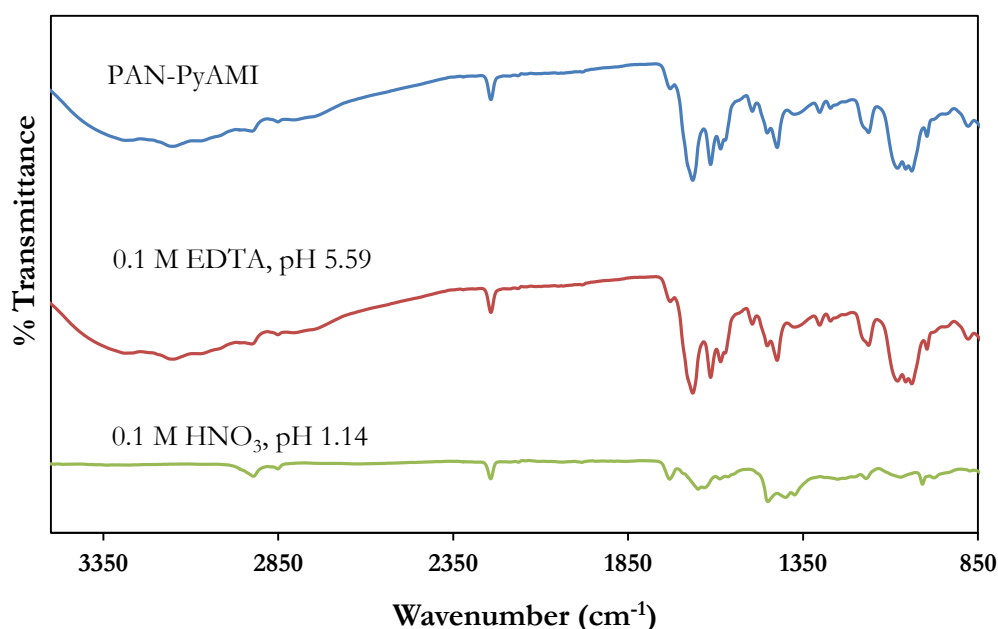
Figure 4.45: ATR-FTIR spectra of PAN-PyAMI showing regeneration studies in EDTA and HNO_3.

The ATR-FTIR analysis was performed as described in section 3.3.6 over the wavelength range of 650 cm^{-1} to 4000 cm^{-1}. From the ATR-FTIR spectra of the acid regeneration of PAN-PyAMI (Figure 4.45), the acid medium of 0.1 M HNO$_3$ (pH 1.14) removed all the immobilised PyAMI from PAN-nfs surfaces. This might be the challenge other authors have been facing without reporting. However, when weak acid such as EDTA (pH 5.59) was considered, the spectrum shows that PyAMI moieties were stable and not lost. Apart from the fact that the pH (5.59) was in the correct range for PAN-PyAMI application, EDTA is considered as one of the best metal chelate solution. Therefore, for this study, EDTA will be used for the regeneration of PAN-PyAMI.

4.2.5 Summary of characterisations of PyAMI and PAN-PyAMI

For this subsection, 2-pyridine amidoxime was synthesised and subsequently characterised using NMR analysis. To achieve one of the goals of this study, PyAMI was immobilised on PAN-nfs. From the literature, two reaction pathways were investigated. The hydrolysis reaction was considered not suitable as the PAN-nfs were fused together and later disintegrated. However, the acid catalysed reaction using AlCl$_3$.6H$_2$O was considered better as the nanofibres integrity were retained. The ATR-FTIR results showed the peak of the ligands on the PAN-nfs, thus confirming that PyAMI was immobilised on PAN-nfs. The stability of PAN-PyAMI was checked with different experiments. The stability of the material was checked in different pH solutions and acid. The material was not stable at lower pH as the ligands were washed away, hence PAN-PyAMI could only function at pH range above 4.5. Likewise, regeneration in acids such as HNO$_3$ led to washing away of the ligands, however, weak acid such as EDTA was suitable for the regeneration as the integrity of PAN-PyAMI was retained.

For further studies, PAN-PyAMI synthesised as described in section 3.2.4 in the acid-catalysed reaction pathway and characterised in this chapter was used as adsorbent for adsorption of Pb^{2+} in aqueous solution and the results are presented in chapter six.

5   Introduction

This chapter provides the results for the adsorption experiments of rhodamine 6G (RD) as described in section 3.2.7.2. The experiment was set-up in continuous flow mode according to Figure 3.2. The samples that were used as adsorbents (membranes) for these experiments are; polyamide 6 nanofibres (PA6-nfs), polyacrylonitrile nanofibres (PAN-nfs), polyethylene terephthalate (PET-TM), composite PET-TM PA6-nfs membrane (PET-TMPA6) and composite PET-TM PAN-nfs membrane (PET-TMPAN) which were produced and characterised as presented in chapters three and four, respectively. The aim of this experiment was to investigate the performance of all the aforementioned materials on the adsorption of organic pollutants such as dyes (RD). The initial and the final concentrations of RD from each experimental set-up were monitored using UV-vis spectrometry. The results for each set of experiments are discussed in the following sub-sections.

5.1   Calibration curve experiment of RD

The calibration curve experiment (or the absorption spectroscopy) of RD was set out as described in section 3.2.7.2.1. It was carried out to determine the calibration linear plot of concentration vs absorbance for rhodamine 6G so that subsequent concentrations from other experiments could easily be determined. For this experiment, seven concentrations (1, 2, 3, 5, 7, 9 and 10 mg/L) of RD were prepared (natural pH 5.67) and the absorbance of each concentration (in quartz cuvette) was measured using a UV-vis spectrometer in the wavelength range of 400–600 nm as described in section 3.3.2.

Figure 5.1 is the absorption spectra of RD at different concentrations in mg/L. The results show that the UV absorbance increased as the concentration of RD increased from 1 mg/L to 10 mg/L.
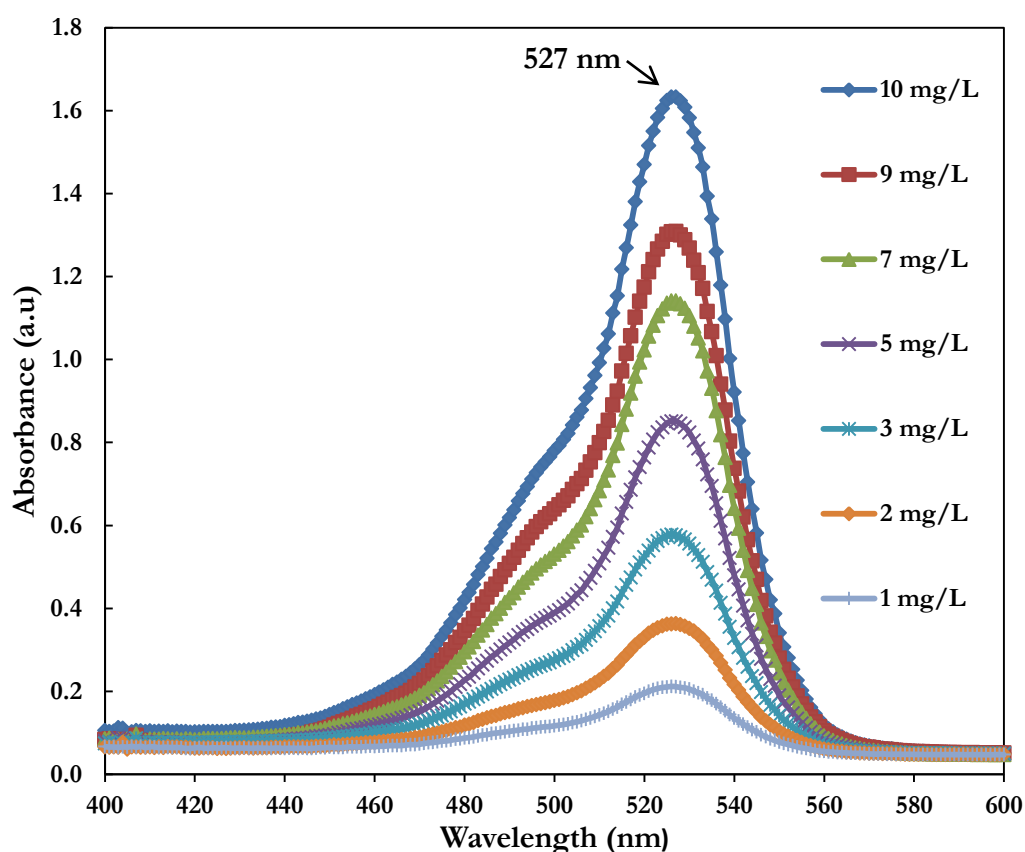
Figure 5.1: UV absorption spectra of freshly prepared aqueous solutions of RD (at different concentrations in mg/L, pH 5.6).

The increase in the absorbance is in correlation with Beer's law as described in section 3.3.2. The main absorbance peak that appeared at 527 nm in the visible region (400-600 nm) is attributed to the basic xanthene structure of RD (Figure 2.5 (a)) which is due to $\pi \rightarrow \pi^*$ transition. This band at 527 nm (which appeared in every concentration in Figure 5.1) confirmed the presence of RD in all the concentrations prepared. The observed shoulder around 498 nm indicates the presence of dimer species of RD. This shoulder was also reported by Saini et al. (2005) for RD.

To show the relationship between the concentration of RD and the absorbance peak at 527 nm, the correspondent absorbance at 527 nm wavelengths for each concentration of RD was plotted against the concentrations of RD (Figure 5.2). The results show that as the concentration of RD increased, the absorbance of RD also increased. This corroborated the earlier plot of absorbance against wavelength (Figure 5.1), thereby confirming the direct proportionality of absorbance and

concentration, however, according to linearity of the Beer's law, high concentrations (high absorbance) are excluded, hence the linear range was chosen between 0 and 7 mg/L. To find a linearised equation describing the relationship between absorbance and concentration, a best line fit was plotted according to Figure 5.3 for the linear region.
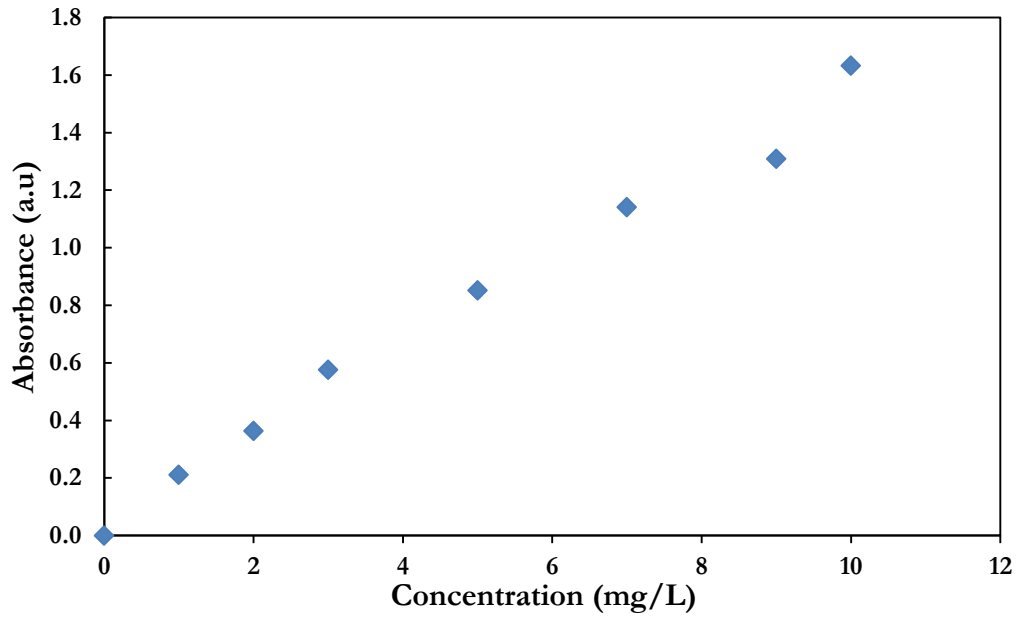
Figure 5.2: The calibration curve showing the relationship between absorbance and concentration of RD at UV absorbance of 527 nm.
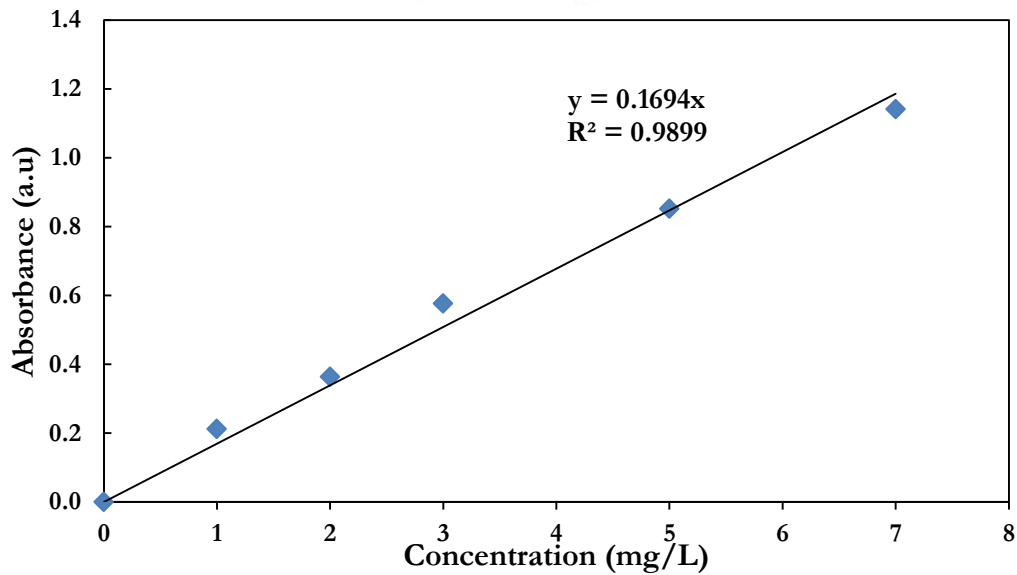
Figure 5.3: Linear calibration plot of RD.

The plot gave a linear relationship between concentration and UV absorbance with equation y = 0.1694x having a correlation coefficient R^2 of 0.9899. The equation y = 0.1694x; where y; absorbance; x; final concentration was then used in the subsequent adsorption experiments to determine the concentration of RD at every given absorbance.

5.2   Adsorption experiments of RD

All adsorption experiments of RD were performed as set out in section 3.2.7.2.2. The experiments were set-up in continuous flow mode according to Figure 3.2, in order to test the ability of the samples prepared (through electrospinning) and characterised in chapters three and four respectively for the removal of RD in a continuous method of filtration {nanofibres samples were; PA6-nfs and PAN-nfs, track-etched membrane; PET-TM and the composite nanofibres track-etched membrane; PET-TMPA6 and PET-TMPAN}. The experiments were performed by investigating the effect of initial concentration, initial pH and the effect of flow rate on the adsorption-filtration of RD from aqueous solution. UV-vis spectrometry was used to monitor the decrease in concentration of each RD aqueous sample after passing through each membrane. The quantity and the percentage of RD adsorbed were calculated according to equations 3.1 and 3.3, respectively. The results for all the adsorption experiments from section 3.2.7.2.2 are presented in the following sub-sections.

5.2.1 The effect of initial concentration

The effect of initial concentration was studied as described in section 3.2.7.2.2 (a) by preparing five concentrations (2, 5, 10, 15 and 20 mg/L) of RD solution (natural pH; 5.6) and 2 mL of each concentration was flowed through 0.0026 g of adsorbent according to section 3.2.7.2.2 at a flow rate 1 mL/min at 25°C. The experiment was carried out in order to determine the optimum concentration suitable for the subsequent set of experiments. The absorbance of each concentration (initial and final) was measured using UV-vis spectrometry in the wavelength range of 400–600 nm as described in section 3.3.2. The quantity adsorbed (q_e) by each membrane (PA6-nfs, PAN-nfs, PET-TM, PET-TMPA6 and PET-TMPAN) and the percentage

adsorbed efficiency (R) were calculated according to equations 3.1 and 3.3, respectively. The adsorption isotherms, Langmuir and Freundlich, were calculated according to equations 3.5 and 3.8 respectively in order to determine the best fit model for the adsorption experiments.

Figure 5.4 and Figure 5.5 present the effect of initial concentration on the quantity and the percentage of RD adsorbed, respectively, on composites and control membranes. The quantity adsorbed of RD (q_e) increased as the concentration increased from 2 mg/L to 10 mg/L for PET-TMPAN, PET-TMPA6, PAN-nfs and PA6-nfs.

	PET-TMPAN	PET-TMPA6	PAN-nfs	PA6-nfs	PET-TM
2	1.38	0.97	1.22	0.88	0.70
5	2.81	2.44	1.98	1.31	0.69
10	4.49	4.66	3.93	2.60	0.20
15	4.37	4.73	3.79	2.69	0.19
20	4.50	4.69	3.90	2.53	0.21
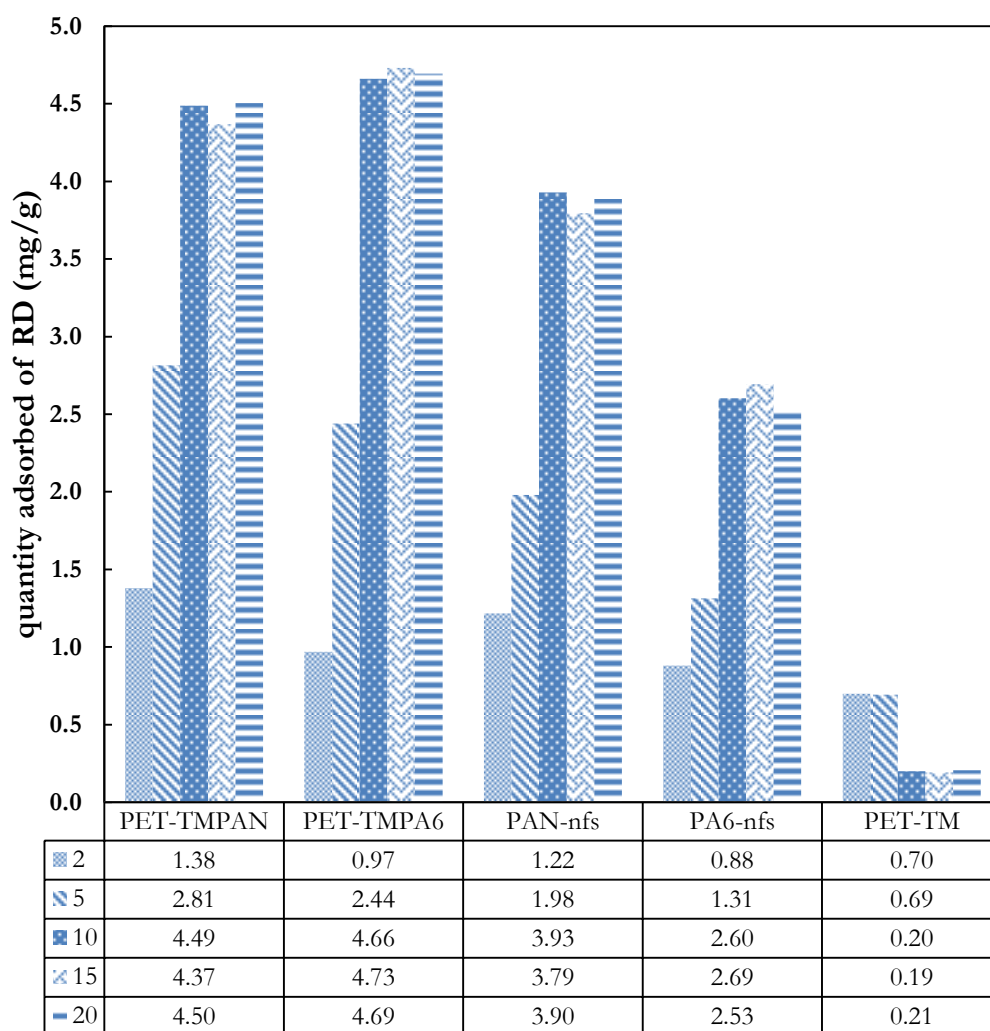
Figure 5.4: Effect of initial concentration on quantity adsorbed of RD on membranes at pH 5.6, weight of adsorbent; 0.0026 g, flow rate; 1 mL/min.

The increase in the quantity adsorbed could simply be due to the fact that all adsorption sites were not occupied by RD molecules at lower concentrations, and therefore more molecules could still find adsorption sites to occupy as the concentration increased. However, at a certain concentration, a saturation plateau was attained where there were no further adsorption sites available to adsorb RD.

	PET-TMPAN	PET-TMPA6	PAN-nfs	PA6-nfs	PET-TM
2	99.59	70.62	87.87	63.76	50.44
5	81.26	70.47	57.18	37.75	20.03
10	64.80	67.29	56.73	37.59	2.89
15	63.96	66.93	55.84	38.13	2.49
20	63.16	67.14	56.35	37.14	2.53
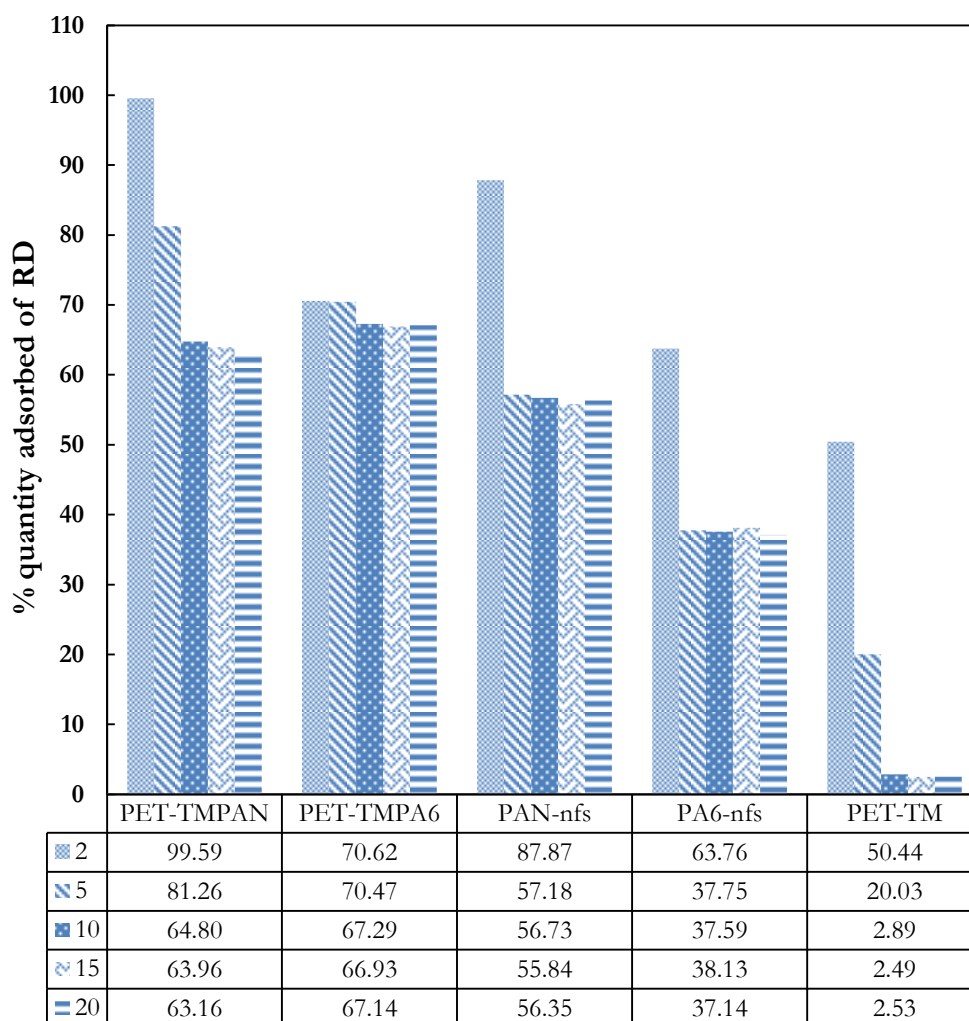
Figure 5.5: Percentage quantity adsorbed of RD at different concentrations by membranes at pH 5.6, weight of adsorbent; 0.0026 g, flow rate; 1 mL/min.

For PET-TMPAN, PET-TMPA6, PAN-nfs and PA6-nfs, saturation was reached at 10 mg/L while for PET-TM; saturation was reached at 5 mg/L (Figure 5.4). The saturation results at 10 mg/L show the capacities of the composite membranes (PET-TMPAN and PET-TMPA6) and that of the nanofibres (PAN-nfs and PA6-nfs). At 10 mg/L (Figure 5.4), the composite membranes, PET-TMPAN and PET-

TMPA6, have higher capacities when compared to the nanofibres, PAN-nfs and PA6-nfs, and the track-etched membrane, PET-TM. The capacity of PAN-nfs at 10 mg/L, 3.93 mg/g went up to 4.49 mg/g in the composite with PET-TM. Likewise for PA6-nfs, the capacity 2.60 mg/g went up to 4.66 mg/g in the case of the composite with PET-TM. The results show that nanofibres and track-etched membrane work better in composite form. However, the low adsorption capacity of PET-TM shows that RD went through the pores of the track-etched membrane.

From Figure 5.4 and Figure 5.5, the quantity adsorbed and percentage RD removal at 10 mg/L were; PET-TMPAN (4.49 mg/g, 64.80%), PET-TMPA6 (4.66 mg/g, 67.29%), PAN-nfs (3.93 mg/g, 56.73%) and PA6-nfs (2.60 mg/g, 37.59%). Further increase in RD concentration show little or no increase in the quantity adsorbed (q_e). At this point, the adsorption sites of the adsorbents have become saturated as the concentration of RD increased further. The optimum concentration was therefore attained at 10 mg/L. PET-TM however, being a porous membrane of pore size 3.5 μm attained its optimum concentration at 5 mg/L. Further increase in RD concentration shows a decrease in the quantity adsorbed of RD on PET-TM, from 0.69 mg/g (5 mg/L) to 0.20 mg/g (10 mg/L). This trend could be as a result of the large pore size of PET-TM which had low sorption properties between the RD in solution and the PET-TM surfaces.

When comparing the contribution of each component of the composite membranes (PET-TMPAN and PET-TMPA6) as presented from their individual performance (Figure 5.6) at 10 mg/L, it is obvious that the nanofibres are contributing more to the adsorption of RD at 10 mg/L than track-etched membrane, even though the percentage contribution of each component could not be ascertained in the composite form. Overall, the combination of the respective nanofibres and track-etched membrane gave the best RD adsorption, with close capacities, and PET-TMPA6 being slightly higher with 2.5% than PET-TMPAN (Figure 5.6).
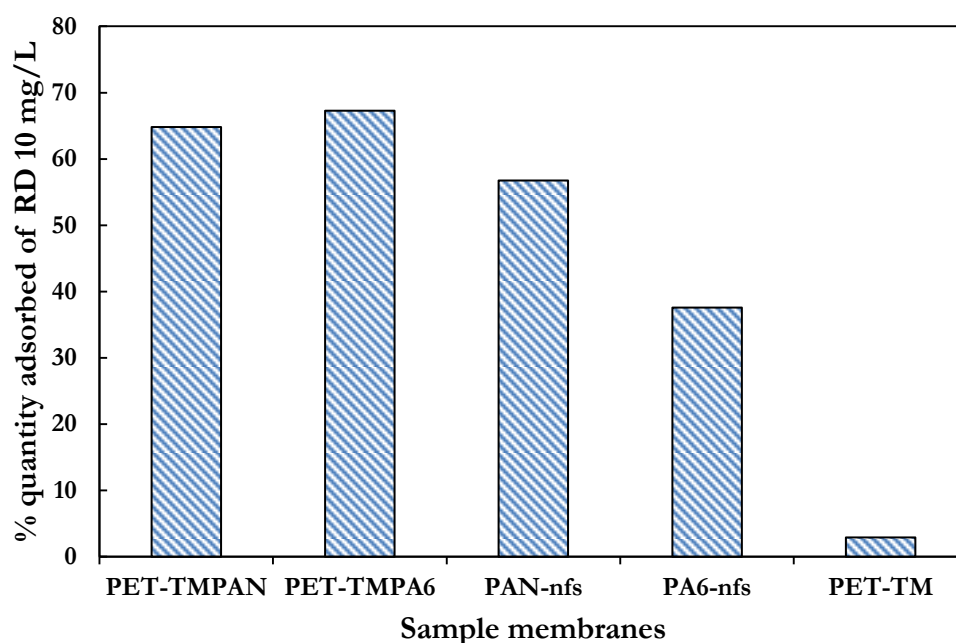
Figure 5.6: Percentage quantity adsorbed of RD at 10 mg/L by membranes at pH 5.6, weight of adsorbent; 0.0026 g, flow rate; 1 mL/min.

When considering the percentage performance of each membrane at other concentrations (Figure 5.5), the general trend is that the adsorption performance of each membrane decreased as the concentration increased from 2 mg/L to 10 mg/L. The adsorption sites were in excess and available to adsorb RD cations at lower concentration. Therefore, there is a tendency that almost all the RD molecules could be adsorbed at lower concentration. For this research, all the membranes used performed best at concentration 2 mg/L of RD. PET-TMPAN gave the best result of 99.59 percentage adsorption at 2 mg/L. The performance was reduced to 81.26% and 64.80% at 5 mg/L and 10 mg/L, respectively. A similar percentage trend was observed for PET-TMPA6 (70.62%, 70.47% and 67.29%), PAN-nfs (87.87%, 57.18% and 56.73%), PA6-nfs (63.76%, 37.75% and 37.59%) and PET-TM (50.44%, 20.03% and 2.89%).

It is worthy of note that no literature was found on the adsorption of dyes using nanofibres and composites nanofibre track-etched membrane for the sake of comparison. However, the next sub-sections will discuss the adsorption isotherms that were used to model the adsorption process of each membrane.

5.2.1.1   Adsorption isotherms

The adsorption of the composites and the control membranes were modeled with Langmuir and Freundlich isotherm models. For the Langmuir isotherm, it is assumed that monolayer adsorption occurs on a homogeneous surface. The linearised form of the model is expressed as equation 3.5 (recall from section 3.2.7.1.1). For the Freundlich isotherm, it is assumed that the adsorbate adsorbs onto the heterogeneous surface of an adsorbent. The linearised form of the model is expressed as equation 3.8 (recall from section 3.2.7.1.1).

The experimental equilibrium data of RD for PA6-nfs (Figure 5.7), PAN-nfs (Figure 5.8), PET-TM (Figure 5.9), PET-TMPA6 (Figure 5.10) and PET-TMPAN (Figure 5.11) were compared with their theoretical equilibrium data obtained from Langmuir and Freundlich isotherm models in order to determine the best fit model for the adsorption experiments. The adsorption data were analysed according to the linear form of Langmuir isotherm and Freundlich isotherm (equations 3.5 and 3.8), respectively. Table 5.1 presents the isotherm parameters for adsorption of RD.
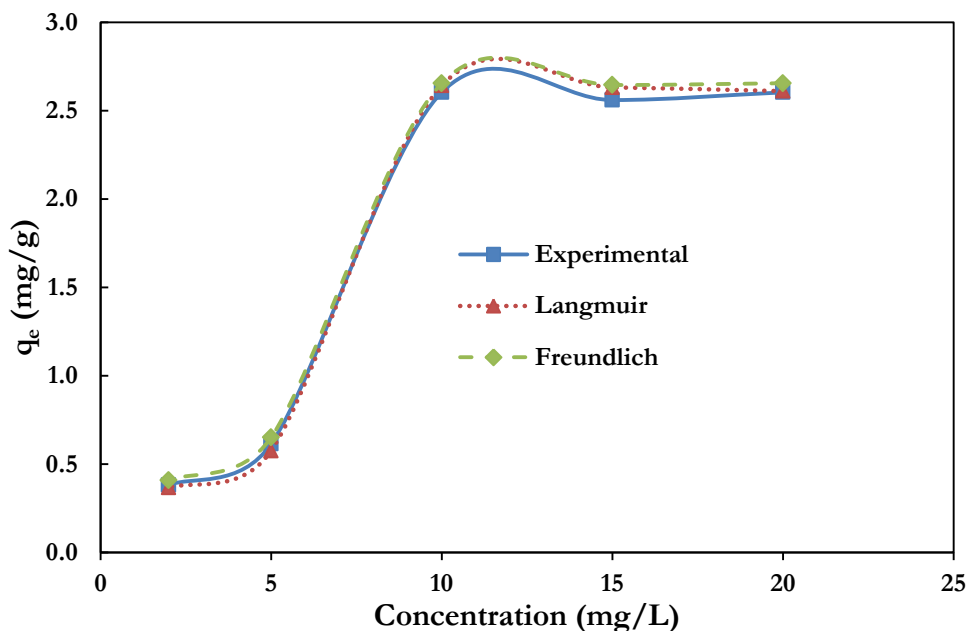
Figure 5.7: Equilibrium isotherms of RD adsorption on PA6-nfs.
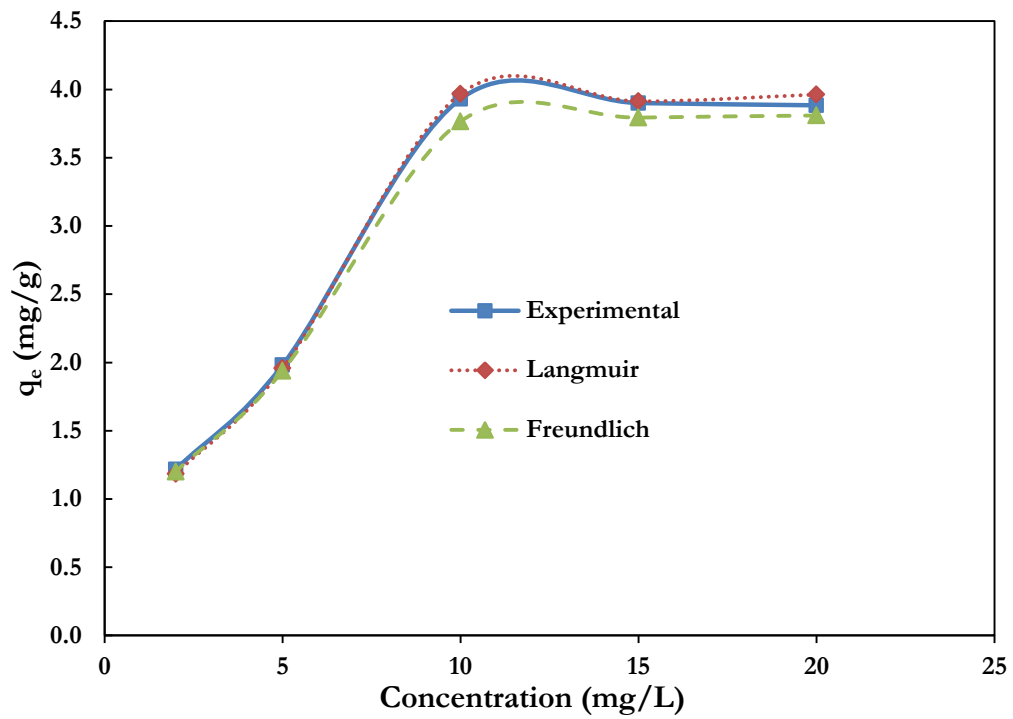
Figure 5.8: Equilibrium isotherms of RD adsorption on PAN-nfs.
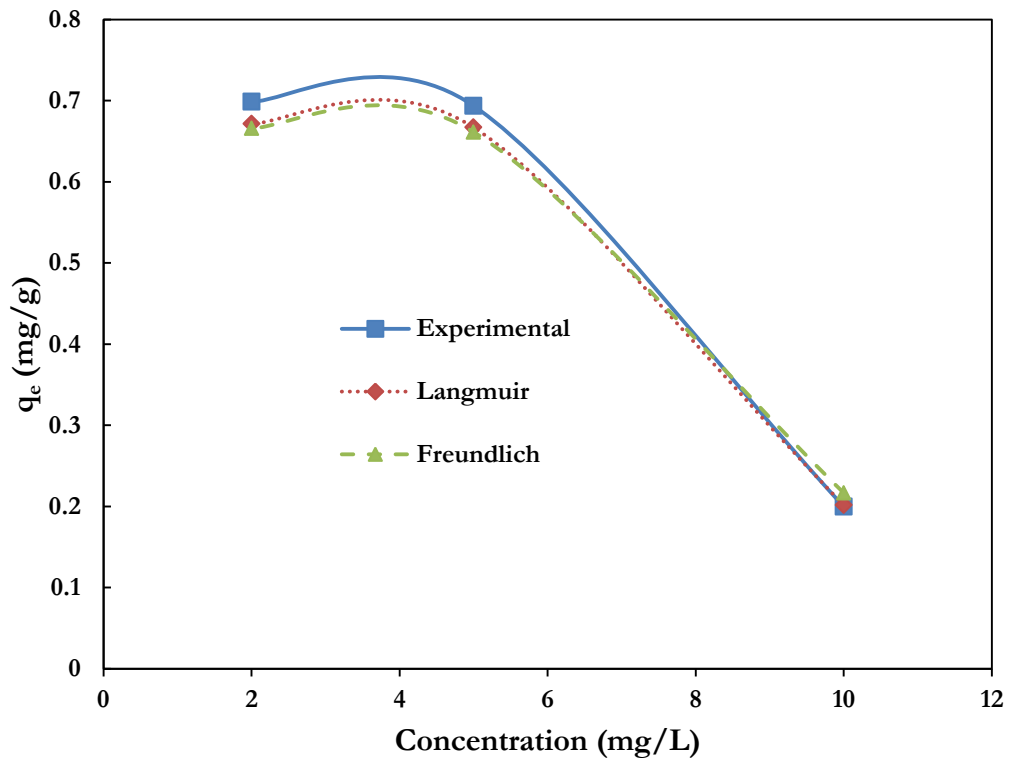
Figure 5.9: Equilibrium isotherms of RD adsorption on PET-TM.
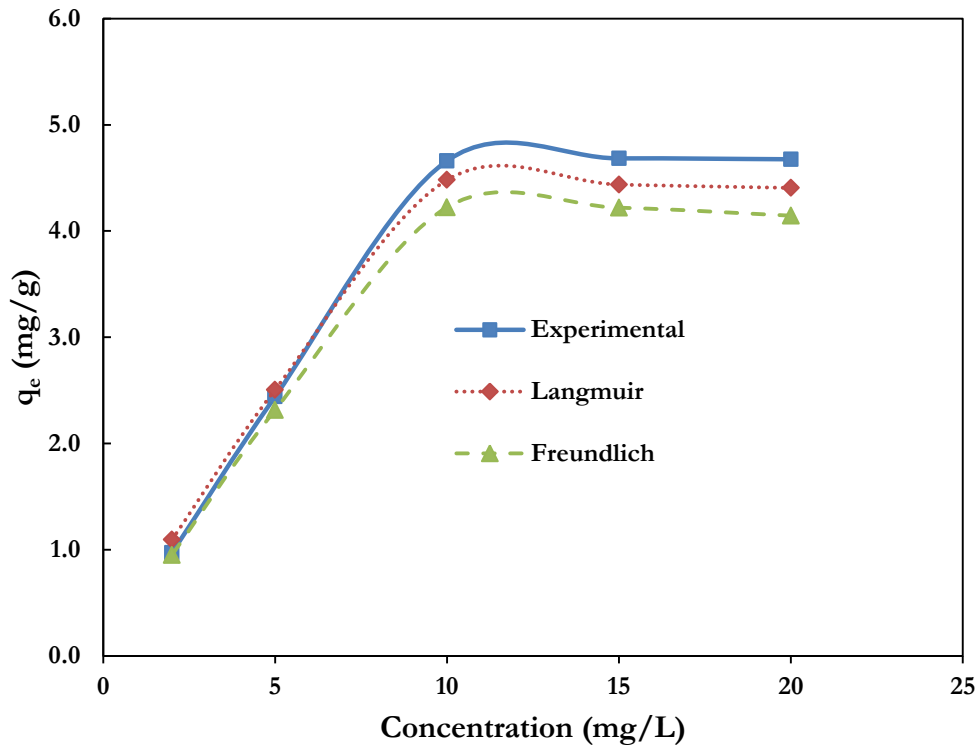
Figure 5.10: Equilibrium isotherms of RD adsorption on PET-TMPA6.
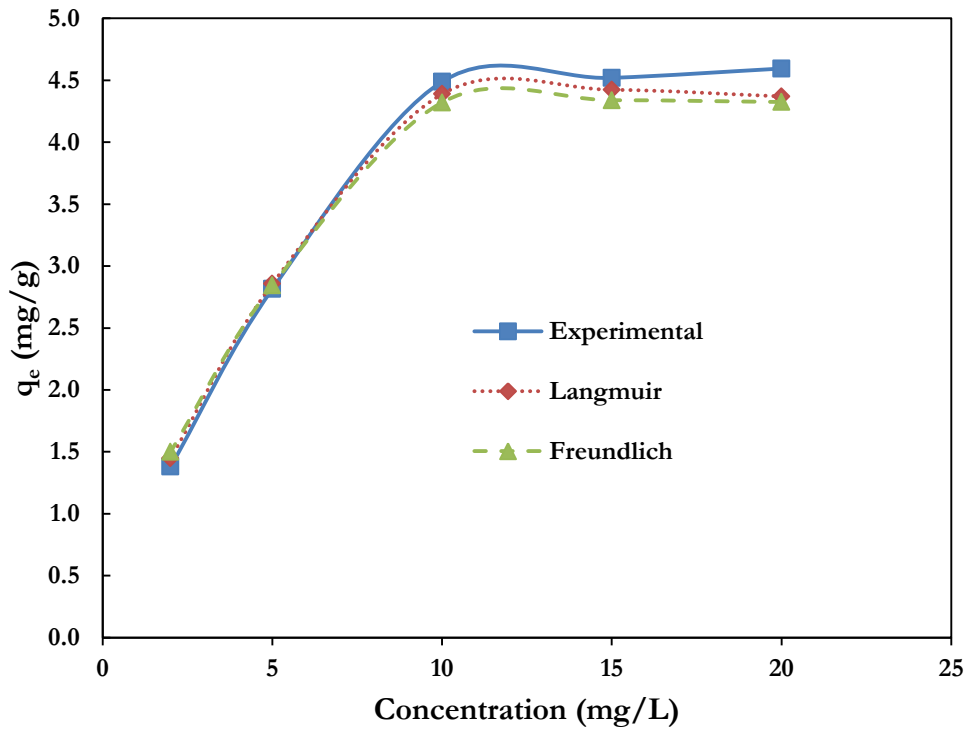
Figure 5.11: Equilibrium isotherms of RD adsorption on PET-TMPAN.

From all isotherms figures, both the control membranes and the composites membranes experimental data were well fitted to the Langmuir isotherms, indicating that the monolayer adsorption of RD occurred on homogenous surfaces of all the membranes. This implies that the surface of all the adsorbents offers a homogeneous adsorption process. Moreover, the correlation coefficient R^2 values (Table 5.1) for the Langmuir model were all greater than that of the Freundlich model, suggesting that the adsorption processes were in the form of a monolayer. Also, the values of R_L (Table 5.1) calculated according to equation 3.6 for Langmuir isotherm ranged from 0 to 1, suggesting that a favourable adsorption took place (Senturk et al., 2010). On the other hand, the values of *n* calculated from the Freundlich isotherm were either 1 or less than 1, indicating that the adsorption processes were not favourable under the studied conditions (Uddin et al., 2009).

Table 5.1: The isotherm parameters for adsorption of RD onto composites and control membranes at 10 mg/L (R^2 are from appendices A, B, C, D and E).

		PET-TMPAN	PET-TMPA6	PAN-nfs	PA6-nfs	PET-TM
Experimental	q_e	4.4888	4.6615	3.9298	2.6039	0.1999
Langmuir isotherms	q_e	4.3988	4.4811	3.9678	2.6419	0.2018
	R^2	0.9996	0.9999	0.9989	0.9990	0.9997
	q_m	111.11	149.25	71.43	20.00	20.00
	b	0.0063	0.0047	0.0123	0.0355	0.0351
	R_L	0.9405	0.9553	0.8902	0.7380	0.7401
Freundlich isotherms	q_e	4.3212	4.2242	3.7675	2.6556	0.2167
	R^2	0.9825	0.9987	0.9886	0.9938	0.9953
	K_F	0.8353	0.9674	0.7334	0.7047	0.7557
	n	1.1446	1.0337	0.9909	1.0196	1.1587

In summary, when comparing the performance of the initial materials (PA6-nfs, PAN-nfs and PET-TM) and the composite membranes (PET-TMPA6 and PET-TMPAN), it is obvious that the PAN-nfs gave the best performance among the initial materials with 56.73% removal of initial concentration of 10 mg/L (pH 5.6) at

a flow rate of 1 mL/min when compared to PA6-nfs and PET-TM which gave 37.59% and 2.89% percentage removal, respectively. In their composite form, PET-TMPA6 gave 67.29% while PET-TMPAN gave 64.80% which are better results than all the initial materials at the same applied conditions. Therefore, the aim of this research to combine nanofibres and track-etched membranes to achieve synergetic results for the adsorption of dyes was accomplished. Meanwhile, further experimental parameters were investigated in order to increase the uptake capacities of these samples. The next sub-section investigated the effect of pH upon the adsorption of RD.

5.2.2 The effect of solution pH

The effect of pH is one of the important variables to study in adsorption processes. This is because the chemistry of dye molecules and the surface of the adsorbent are strongly affected by the pH of the solution. In this study, the effect of solution pH was studied by preparing six solutions of pH 1, 2, 4, 6, 8 and 10 containing RD 10 mg/L concentration. The pH was adjusted using 0.1 M HNO_3 or 0.1 M NaOH and 2 mL of each solution was treated as described in section 3.2.7.2.2 using 0.0026 g of adsorbent at a flow rate 1 mL/min. The absorbance of each concentration (initial and final) was measured using the UV-vis spectrometer in the wavelength range of 400–600 nm as described in section 3.3.2. The quantity adsorbed (q_e) and the percentage adsorption (R) were calculated according to equations 3.1 and 3.3, respectively.

Figure 5.12 and Figure 5.13 present the effect of the initial pH on the quantity of RD adsorbed on membranes and their percentage removal, respectively. The RD quantity adsorbed increased as the pH increased from 1 to 10 for each sample; PET-TMPAN (3.99 mg/g (57.58%) to 6.32 mg/g (91.27%)), PET-TMPA6 (1.07 mg/g (15.51%) to 4.89 mg/g (70.66%)); PAN-nfs (1.99 mg/g (19.25%) to 4.56 mg/g (65.97%)), PA6-nfs (1.09 mg/g (15.75%) to 2.55 mg/g (36.80%)) and PET-TM (0.91 mg/g (12.35%) to 1.70 mg/g (24.53%)). At lower pH values, the number of negatively charged adsorbent sites decreased because of the prevalent presence of protons in the RD solution, thus, leading to the electrostatic repulsion between positively charged RD cations and membrane surfaces.

pH	PET-TMPAN	PET-TMPA6	PAN-nfs	PA6-nfs	PET-TM
1	3.99	1.07	1.99	1.09	0.91
2	4.12	1.30	2.14	1.29	1.01
4	4.62	1.98	2.17	1.39	1.01
6	5.26	2.09	3.93	1.64	1.18
8	6.00	3.45	4.44	2.52	1.23
10	6.32	4.89	4.56	2.55	1.70
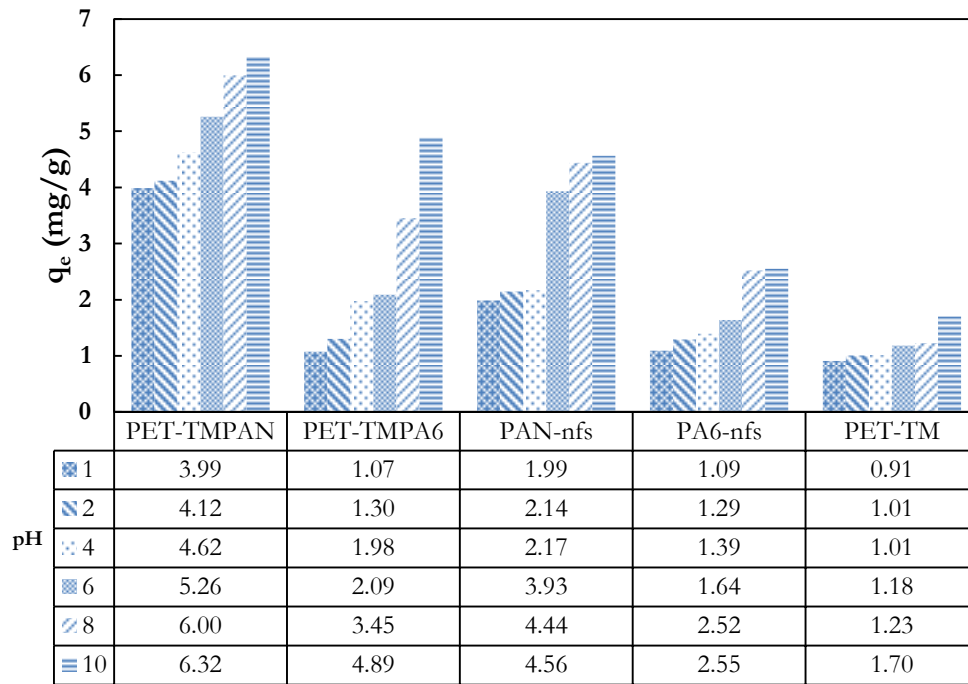
Figure 5.12: Effect of pH on RD quantity adsorbed (initial concentration; 10 mg/L, weight of membranes; 0.0026 g; flow rate; 1 mL/min).

	PET-TMPAN	PET-TMPA6	PAN-nfs	PA6-nfs	PET-TM
1	57.58	15.51	19.25	15.75	12.35
2	59.49	18.80	27.70	18.60	13.19
4	66.73	28.55	28.67	20.09	14.57
6	75.91	29.53	50.27	23.67	17.70
8	86.56	45.19	60.36	34.11	18.82
10	91.27	70.66	65.97	36.80	24.53

Figure 5.13: Percentage quantity adsorbed of RD at different pH solutions (initial concentration; 10 mg/L, weight of membranes; 0.0026 g; flow rate; 1 mL/min).

This led to an increase in competition effects between protons in the solution and the RD cations thereby decreasing the adsorption of RD. However, as the pH increased, the adsorbent surface sites were more negatively charged, hence, electrostatic interaction of RD cations with negatively charged adsorbent surfaces increased leading to an increase in RD cations adsorption. As a result, an initial pH 10 was selected for further adsorption experiments.

The quantity and percentage adsorbed at pH 10 (Figure 5.12 and Figure 13) were; PET-TMPAN (6.32 mg/g, 91.27% adsorption), PET-TMPA6 (4.89 mg/g, 70.66% adsorption), PAN-nfs (4.56 mg/g, 65.97% adsorption), PA6-nfs (2.55 mg/g, 36.80% adsorption) and PET-TM (1.70 mg/g; 24.53% adsorption). From Figure 5.14, PAN-nfs gave the best percentage removal of 65.97% RD removal among the initial control materials, while its composite with PET-TM (PET-TMPAN) gave 91.27% RD removal (the best results overall) for initial concentration (10 mg/L), weight of membranes (0.0026 g) and flow rate (1 mL/min) parameters.

Figure 5.14: Percentage quantity adsorbed RD at pH 10 (initial concentration; 10 mg/L, weight of membranes; 0.0026 g; flow rate; 1 mL/min).

The results show that pH had a greater effect pH on the adsorption of RD when compared with the previous results of adsorption obtained at pH 5.6 (section 5.2.1). The percentage adsorption of RD increased from 64.80% to 91.27% for PET-TMPAN and 67.29% to 70.66% for PET-TMPA6. Further experiments were performed to determine the effect of flow rate on RD adsorption.

5.2.3 The effect of flow rate

The optimisation of flow rate in the adsorption process is important in order to save time and energy. The effect of the flow rate was studied by varying the flow rate (0.5, 1, 2, and 3 mL/min) of the RD solution (initial concentration 10 mg/L; pH 10) in a syringe fitted into a metering syringe pump. The experiment was carried out as set out in section 3.2.7.2.2 using 2 mL of RD solution and 0.0026 g of adsorbent. The absorbance of each concentration (initial and final) was measured using UV-vis spectrometry in the wavelength range of 400–600 nm as described in section 3.3.2. The quantity adsorbed (q_e) and the percentage adsorption (R) were calculated according to equations 3.1 and 3.3, respectively.

Figure 5.15 and Figure 5.16 present the effect of flow rate on the quantity of RD adsorbed on control and composite membranes and their percentage adsorption, respectively. The RD (q_e) decreased as the flow rate increased from 0.5 to 3.0 mL/min for each sample; PET-TMPAN (6.78 mg/g (96.01%) to 3.82 mg/g (54.16%)), PET-TMPA6 (5.27 mg/g (74.68%) to 1.15 mg/g (16.29%)), PAN-nfs (4.48 mg/g (63.47%) to 1.88 mg/g (26.59%)), PA6-nfs (3.35 mg/g (47.47%) to 1.65 mg/g, (23.32%)) and PET-TM (1.80 mg/g (25.53%) to 0.30 mg/g (4.22%)).

The decrease in the adsorption as the flow rate increased could be due to the effect of contact time, the lower the flow rate, the more contact time the RD molecules in solution would have with the adsorbents allowing electrostatic attraction to occur, hence the more RD adsorption. The contact time could also be related to protonation time. We recall from pH optimisation (section 5.2.2) that the adsorbent surface sites should be more negatively charged so that the electrostatic interaction of RD cations with negatively charged adsorbent surfaces would increase, thereby increasing the RD adsorbed.

	PET-TMPAN	PET-TMPA6	PAN-nfs	PA6-nfs	PET-TM
0.5	6.78	5.27	4.48	3.35	1.80
1	6.32	4.89	4.29	2.55	1.70
2	4.47	2.44	3.41	2.40	0.33
3	3.82	1.15	1.88	1.65	0.30
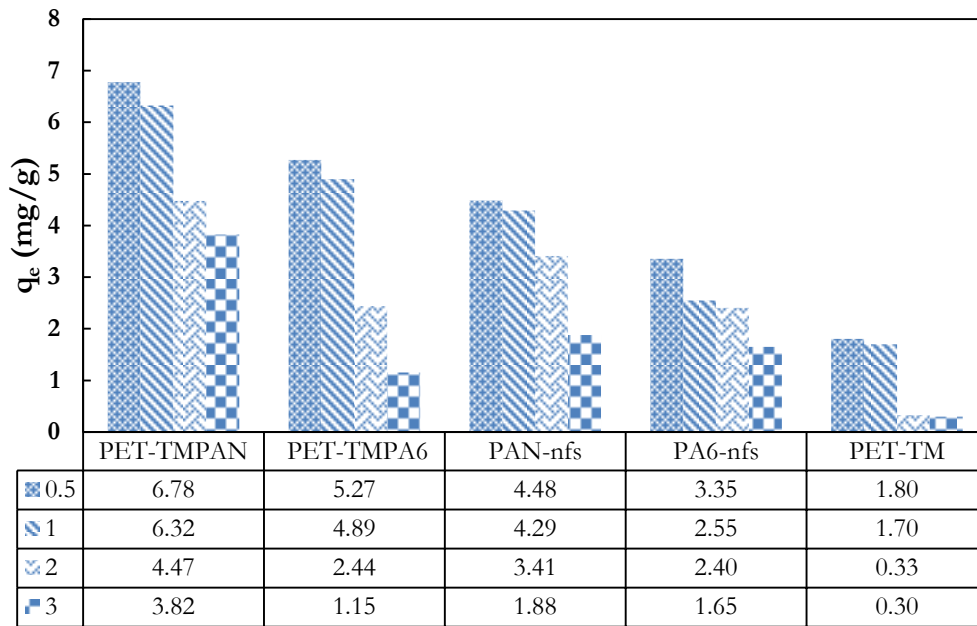
Figure 5.15: Effect of varied flow rate (0.5-3 mL/min) on quantity adsorbed of RD (initial concentration; 10 mg/L, pH; 10; weight of membranes; 0.0026 g).

	PET-TMPAN	PET-TMPA6	PAN-nfs	PA6-nfs	PET-TM
0.5	96.01	74.68	63.47	47.47	25.53
1	89.56	69.33	60.81	36.11	24.07
2	63.36	34.50	48.34	34.04	4.63
3	54.16	16.29	26.59	23.32	4.22
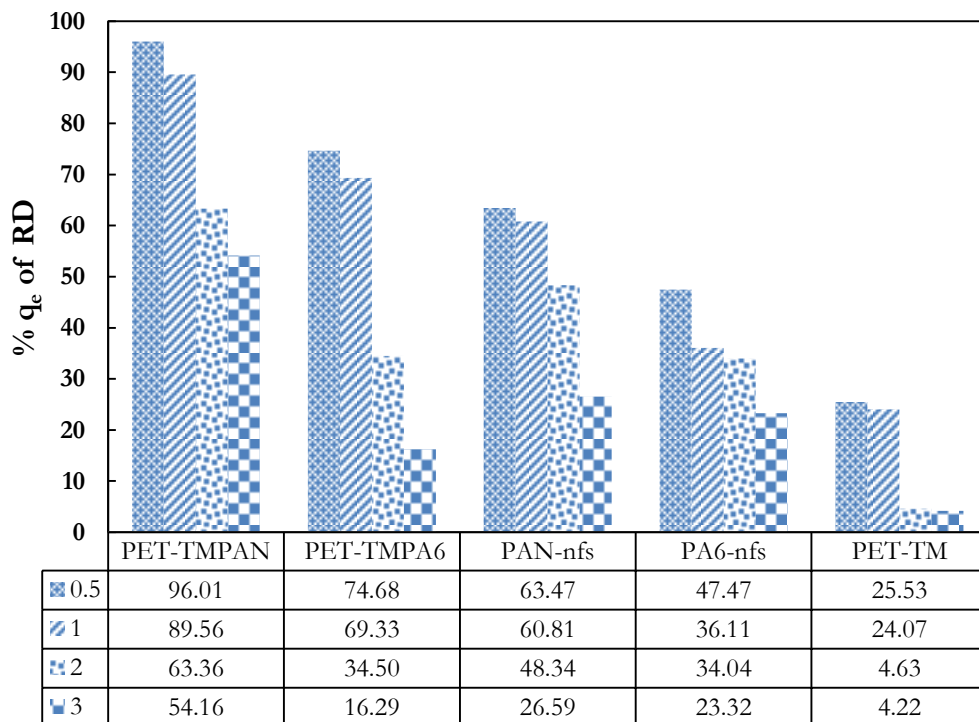
Figure 5.16: Effect of varied flow rate (0.5-3 mL/min) on percentage adsorption of RD (initial concentration; 10 mg/L, pH; 10; weight of membranes; 0.0026 g).

Therefore, at a lower flow rate, the RD in solution would have sufficient contact time to interact with the surface of the adsorbent compared to at high flow rate; the

RD in solution would have insufficient contact time to equilibrate. From the results, 0.5 mL/min gave the highest adsorption for all the membranes, however, when considering the time it would take to complete the set of experiments, 1 mL/min was considered for further experiments.

5.2.4 Batch adsorption experiment

The batch adsorption experiments were carried out in order to determine the saturation capacity of each membrane. RD solution of concentration 10 mg/L (pH 10) was prepared and was treated with 0.0026 g of adsorbent as set out in section 3.2.7.2.2 with a flow rate of 1 mL/min. For each membrane (Table 3.3), the experiment was carried out by repeatedly introducing 2 mL of RD (10 mg/L) into the adsorption system (Figure 3.2) until the equilibrium was reached and the membrane in the filter holder could no longer adsorb solute. The absorbance of each concentration (initial and final) was measured using UV-vis spectrometry in the wavelength range of 400–600 nm as described in section 3.3.2. The quantity adsorbed (q_e) and the percentage adsorption (R) were calculated according to equations 3.1 and 3.3, respectively.

Figure 5.17 and Figure 5.18 present the results for the batch adsorption of RD on different adsorbents. The RD adsorption was decreasing as the number of batches increased from 1 to 8. The quantity adsorbed steadily decreased from the 1st batch and till the 5th batch for PET-TMPAN (6.32 mg/g (91.04%) to 1.04 mg/g (15.03%)), PET-TMPA6 (4.89 mg/g (70.45%) to 1.22 mg/g (17.61%)), PAN-nfs (4.29 mg/g (61.78%) to 1.36 mg/g (19.61%)), PA6-nfs (3.45 mg/g (49.66%) to 1.28 mg/g, (18.55%)) and PET-TM (1.69 mg/g (24.46%) to 0.97 mg/g (14.08%)). This reduction in quantity adsorbed could be due the fact that after every adsorption, RD molecules occupied the adsorption sites thereby reducing the number of available sites for the subsequent adsorption batch. This would gradually continue until no site was available for adsorption.
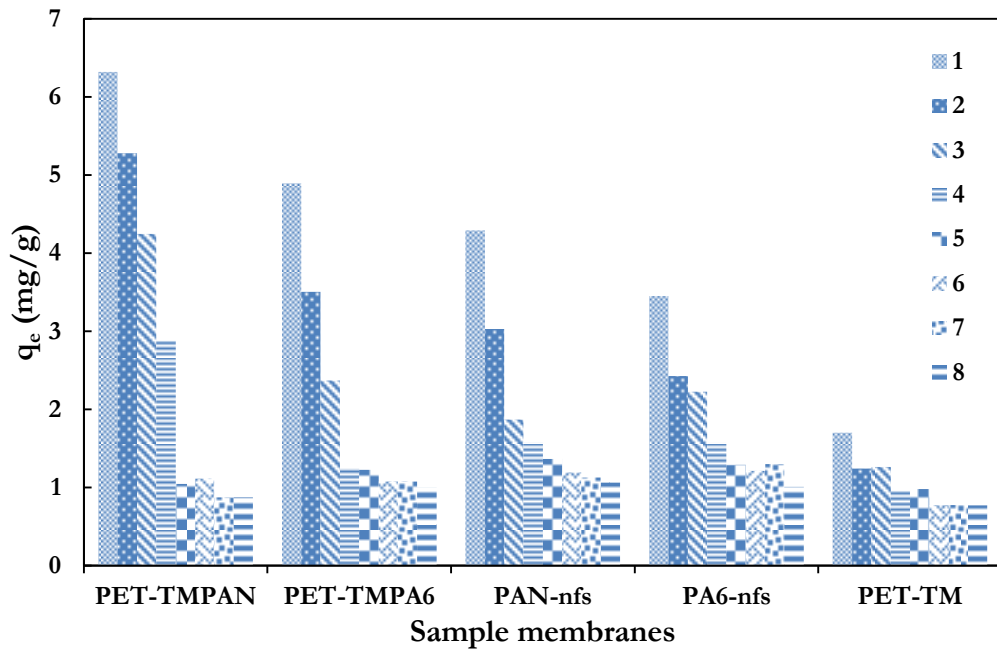
Figure 5.17: Batch adsorption (quantity adsorbed) of RD (initial concentration; 10 mg/L, pH; 10; weight of membranes; 0.0026 g; flow rate; 1 mL/min).
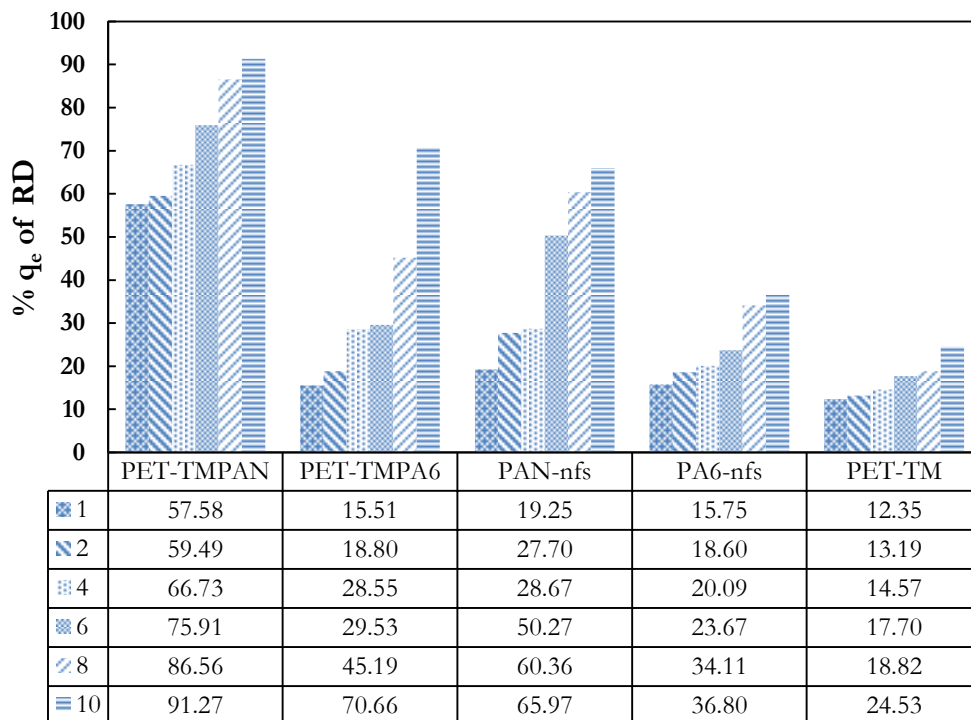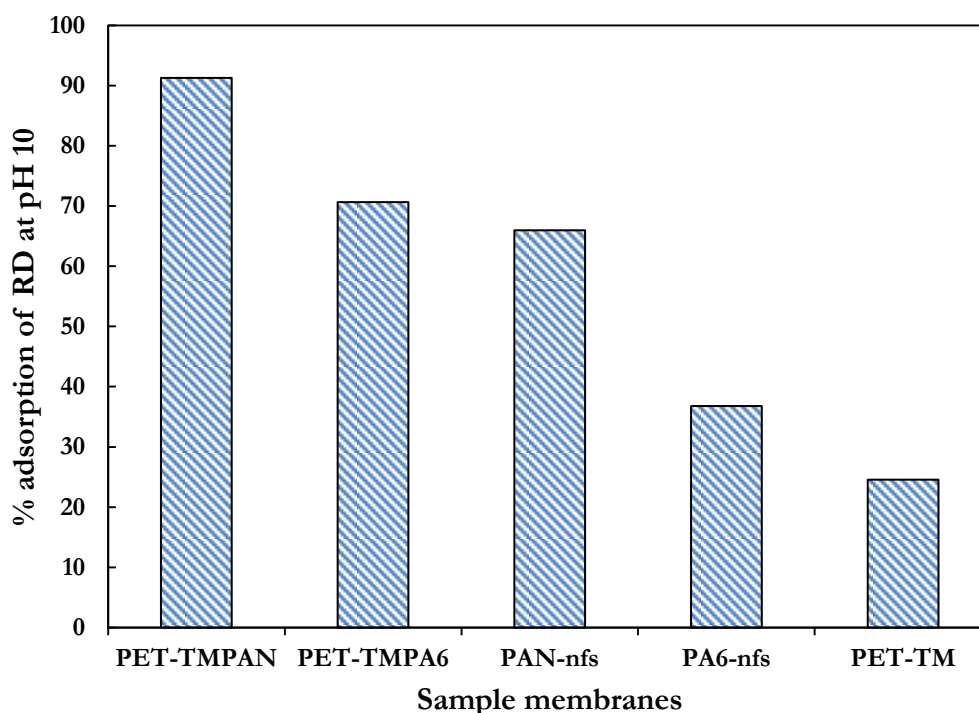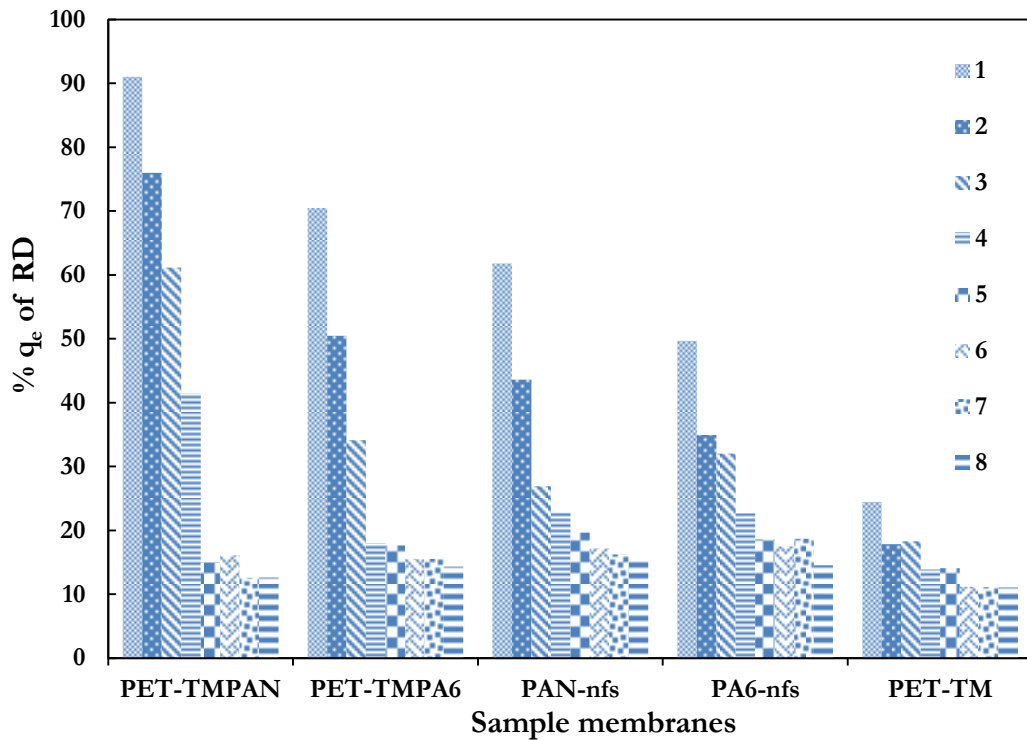

Figure 5.18: Percentage quantity adsorbed of RD (initial concentration; 10 mg/L, pH; 10; weight of membranes; 0.0026 g; flow rate; 1 mL/min).

From the 5th batch to the 8th batch, there was no significant difference in the quantity adsorbed meaning that the membranes have reached their saturation level at the 5th batch and there were no adsorption sites left. This could in other words be called fouling. Fouling is one of the drawbacks in membrane separation processes; however, the next sub-section of the research would discuss how the fouling effect could be reduced. Meanwhile, Table 5.2 shows that at the first batch, PET-TMPAN adsorbed the best (91%) compared to PET-PA6 (70.45%), PAN-nfs (61.17%), PA6-nfs (49.66%) and PET-TM (24.46%). At the 5th batch, all the membranes could adsorb an average of only 16% RD. In order to overcome the fouling effect, desorption experiments were performed on each of the membranes. The results are discussed in the next sub-section.

Table 5.2: Summary of batch percentage performance of each membrane.

Samples	Highest % adsorbed	Lowest % adsorbed	Batch of saturation
PET-TMPAN	91.01	15.03	5
PET-TMPA6	70.45	17.63	5
PAN-nfs	61.17	19.61	5
PA6-nfs	49.66	18.55	5
PET-TM	24.46	13.54	4

5.3 Desorption and reusability experiments

Desorption experiments were carried out in order to regenerate the adsorbents and remove fouling from the membrane. Desorption experiments were carried out as set out in section 3.2.7.2.3. It was carried out by putting the membrane previously used for adsorption of RD of concentration 10 mg/L, pH 10 at flow rate 1 mL/min into a filter holder. Thereafter, 2 mL of deionised water adjusted with 1M H_2SO_4 to pH 1.8 was pumped through the membrane at a flow rate 1 mL/min. The resultant solution was collected and the concentration was measured using UV-vis spectrometry. The percentage desorbed was calculated according to equation 3.3. For reusability experiments, the same membrane that was desorbed was reused to adsorb RD using the same parameters of the previous adsorption and the quantity adsorbed (q_e) and the percentage adsorbed were calculated according to equations 3.1 and 3.3,

respectively. Figure 5.19 and Figure 5.20 are the results for the total percentage desorbed and the quantity desorbed per batch from each membrane, respectively.
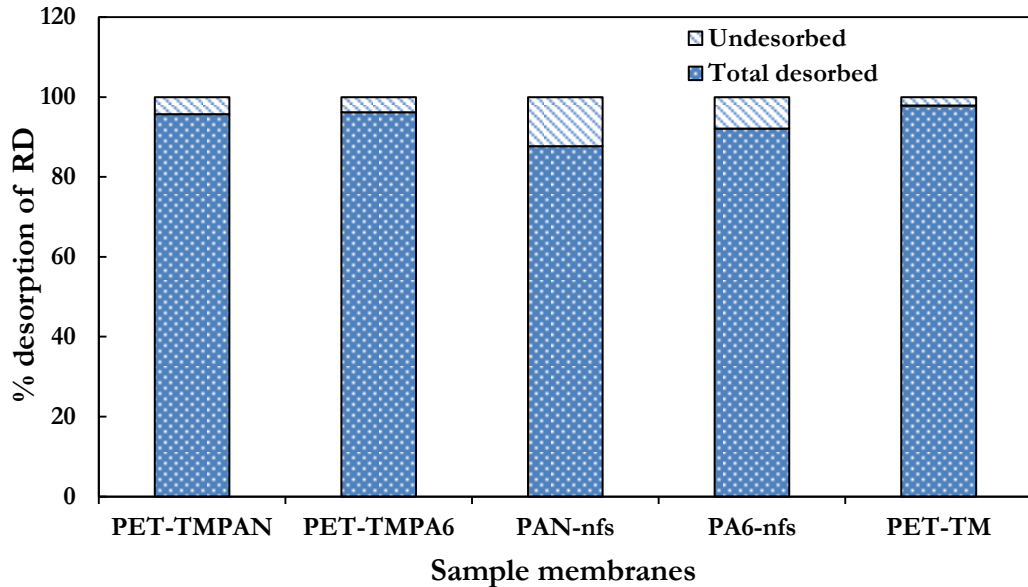
Figure 5.19: Percentage desorption of RD (initial concentration; 10 mg/L, pH; 10; weight of membranes; 0.0026 g; flow rate; 1mL/min after 3 cycles).

	PET-TMPAN	PET-TMPA6	PAN-nfs	PA6-nfs	PET-TM
Initial adsorbed	6.49	5.07	3.45	3.73	1.76
1st desorption	3.20	3.28	1.70	1.75	0.87
2nd desorption	2.21	1.39	1.20	1.17	0.76
3rd desorption	0.81	0.21	0.13	0.52	0.09
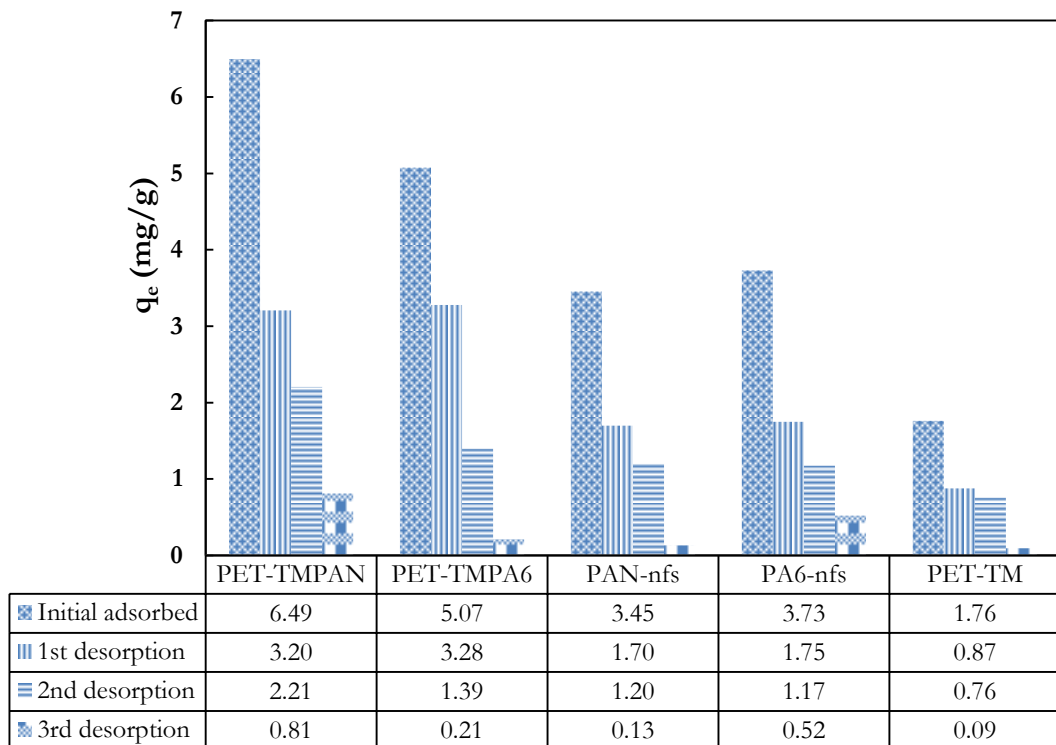
Figure 5.20: Desorption experiment of RD from membranes (initial concentration; 10 mg/L, pH; 10; weight of membranes; 0.0026 g; flow rate; 1mL/min).

The results showed that all the membranes could be regenerated for three or more batches of desorption using deionised water adjusted with 1 M H_2SO_4 to pH 1.8. The quantity desorbed was gradually decreasing as the number of desorption batches increased from 1 to 3. However, after the 3rd batch, the total percentage of desorption and the undesorbed RD (of the initial adsorbed RD) showed that 95% was desorbed from PET-TMPAN, remaining 4.2%, 96% was desorbed from PET-TMPA6, remaining 3%, 87% was desorbed from PAN-nfs, remaining 12%, 92% was desorbed from PA6-nfs, remaining 8% and 98% was desorbed from PET-TM, remaining 2% (Figure 5.19). Desorption was based on the fact that at lower pH (1.8), there is a prevalence protons which invariably displaces the RD cation and make the surface of the membranes positively charged, thereby triggering the electrostatic repulsion between the protonated surface of membrane and that of the cation of RD (Uddin et al., 2009). Further desorption of RD after the 3rd desorption batch on these membranes could no longer be detected by UV-vis spectroscopy. However, it is suggested that further desorption cycles could lead to 99% desorption of RD from all the membranes thereby allowing regeneration of all the membranes.

All the membranes regenerated above were reused in order to test if their efficiency could still remain the same as previously. Figure 5.21 presents the results of the reusability of all the membranes at the same condition (initial concentration; 10 mg/L, pH; 10; weight of membranes; 0.0026 g; flow rate; 1 mL/min). The results show that there was a reduction in the RD adsorption when compared to the initial adsorption capacities of fresh membranes in this trend; PET-TMPAN (6.49 mg/g to 5.37 mg/g), PET-TMPA6 (5.07 mg/g to 4.44 mg/g), PAN-nfs (3.45 mg/g to 2.95 mg/g), PA6-nfs (3.73 mg/g to 2.68 mg/g) and PET-TM (1.75 mg/g to 1.62 mg/g). This reduction could be as a result of the undesorbed RD in the first batch, thus suggesting that more than three batches of desorption should be made in order to achieve better regeneration of the materials.

Meanwhile the percentage reduction in efficiency of each membrane was plotted (Figure 5.22) and it was shown that PET-TMPAN has 17.26% reduction, so for PET-TMPA6 12.29%, PAN-nfs 14.62%, PA6-nfs 28.17% and PET-TM 8.042%.
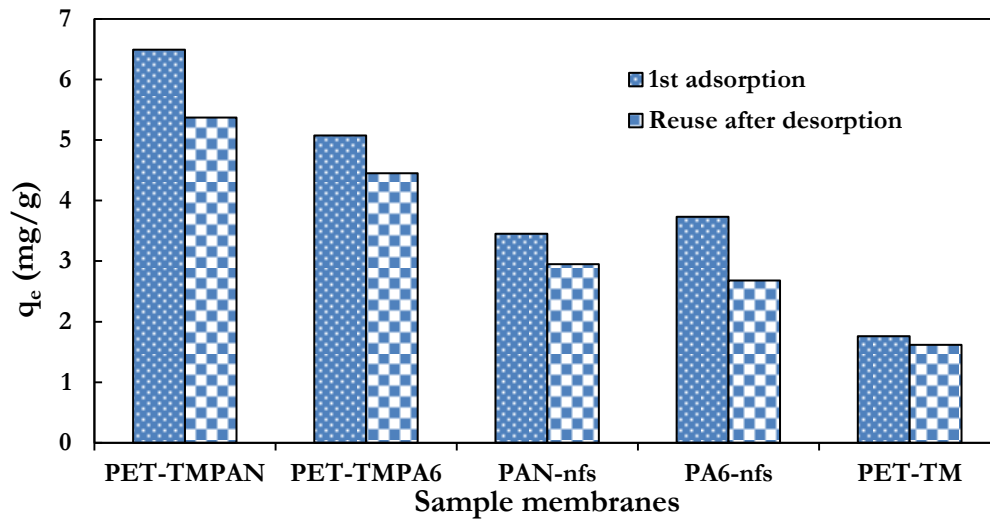
Figure 5.21: Quantity adsorbed of RD on regenerated membranes (initial concentration; 10 mg/L, pH; 10; weight of membranes; 0.0026 g; flow rate; 1 mL/min).
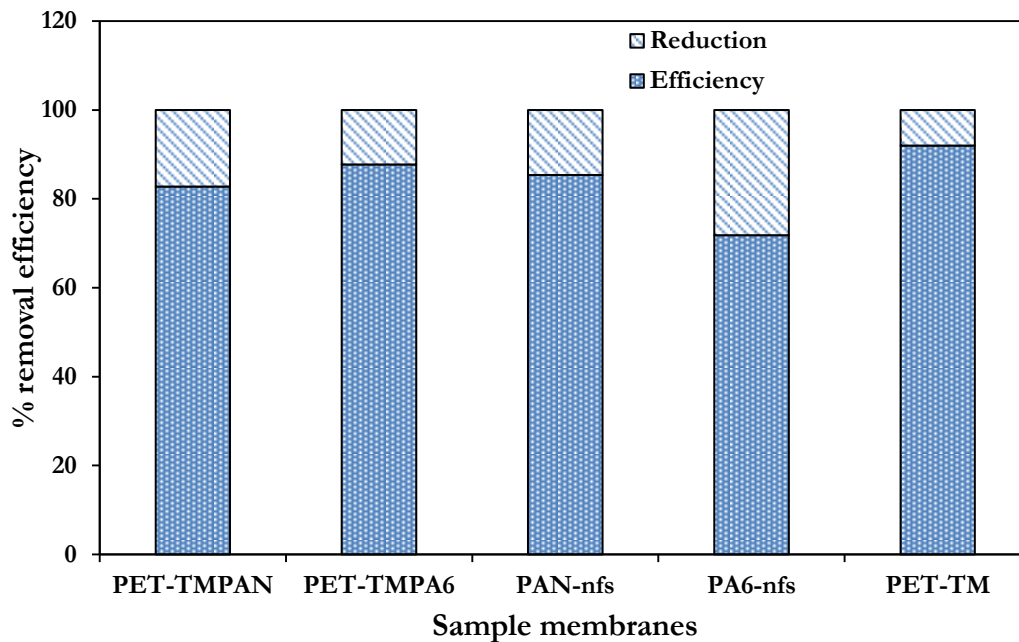
Figure 5.22: Percentage reduction in removal efficiency of membranes on RD (initial concentration; 10 mg/L, pH; 10; weight of membranes; 0.0026 g; flow rate; 1 mL/min).

The results show that all the materials could not maintain 100 per cent performance after being previously used. However, the reduction in performance could not be fixed at a certain value as it depended on the initial concentration of RD previously adsorbed.

5.4   Chapter summary

The purpose of this chapter was to address and compare the performance of the composite membranes fabricated and characterised in chapters three and four for the removal of organic pollutants such as RD dye. The results showed and prove that the following membranes; PET-TMPAN, PET-TMPA6, PAN-nfs, PA6-nfs and PET-TM could all adsorb RD from aqueous solution. The highlight of the results was that the composite membranes (PET-TMPAN and PET-TMPA6) gave much better adsorption results when compared with the control materials (PAN-nfs, PA6-nfs and PET-TM). After optimisation, the adsorption of RD from 2 mL solution by these membranes could be best achieved for 10 mg/L of RD when the initial pH was 10 and at a flow rate of 0.5 mL/min (though 1 mL/min was chosen for convenience) using 0.0026 g of each membrane. For these parameters, PET-TMPAN could take 91.27% of RD, PET-TMPA6, 70.66%, PAN-nfs, 65.97%, PA6-nfs, 36.80% and PET-TM 24.53%. The best result came from the combination of PAN-nfs and PET-TM (PET-TMPAN). This may be due to fact that PAN-nfs has a surface charge and at higher pH (with more of OH), there was attractive forces between the surface of PAN-nfs and cation of RD. This could be said for PAN-nfs, as it has the best RD adsorption among the control membranes. At lower concentration, these composite membranes (PET-TMPAN and PET-TMPA6) could remove approximately 100 per cent of RD. Furthermore, all the membrane could be regenerated (using water of lower pH).

CHAPTER SIX

6   Introduction

This section provides the results for all the experiments on the adsorption of toxic metal (Pb^{2+}) as set out in section 3.2.7.3. The adsorbents used for these experiments are PAN-nfs (electrospun in section 3.2.1.2 and characterised in section 4.1.2) and PAN-PyAMI (synthesised by immobilising PyAMI on PAN-nfs in section 3.2.4 and characterised in section 4.2.3.3). The experiments were set-up as batch adsorption processes. The aims of these experiments were to investigate the performance of PAN-nfs or PAN-PyAMI on the adsorption of inorganic pollutants such as Pb^{2+} and to test for the reusability of PAN-PyAMI. The initial and the final concentrations of Pb^{2+} from each experimental set-up were monitored using ICP-OES as described in section 3.3.10. The results for each set of experiment are discussed in the following sub-sections.

6.1   Adsorption experiments

The adsorption experiments were carried out in batch mode as set out in section 3.2.7.3. The adsorption experiments were carried out by investigating parameters such as the effect of pH, the initial adsorbate concentration and the effect of contact time on the adsorption of Pb^{2+} in aqueous solution. All the concentrations of Pb^{2+} for the adsorption process were prepared from the 1000 mg/L stock solution of Pb^{2+} prepared in section 3.2.7.3.1 and stored in a fridge at a temperature of 10°C. The results for each set of parameters are discussed in the following sub-sections.

6.1.1 Effect of solution pH

The effect of pH on the adsorption of Pb^{2+} was carried out in batch mode and in triplicate (as indicated in error bars) as set out in section 3.2.7.3.2 (a). The pH was investigated to determine the adsorption capacity of PAN-PyAMI or PAN-nfs at different pH solutions. 10 mL of aqueous solutions of pH 2.2, 3.1, 4.2, 4.9 or 6.1 containing 200 mg/L of Pb^{2+} were prepared and were shaken with 0.1 g of PAN-nfs or PAN-PyAMI at a stirrer speed of 120 rpm for 1 hour at 25°C. The resultant solution was filtered and analysed using ICP-OES as described in section 3.3.10 and the adsorption capacities (q_e) and the percentage adsorption (R) of PAN-nfs or PAN-PyAMI were calculated according to equations 3.1 and 3.3, respectively.

Figure 6.1 and Figure 6.2 present the quantity of Pb^{2+} adsorbed and the percentage Pb^{2+} adsorbed on PAN-nfs or PAN-PyAMI, respectively at different initial pH. The results showed that the adsorption capacity increased as the pH increased from 2.2 to 4.9, and decreased after 4.9. The results revealed that the adsorption capacity of PAN-nfs or PAN-PyAMI adsorbents vary significantly dependent upon the initial pH of the Pb^{2+} aqueous solution. At lower pH, the active sites of the adsorbent are less available for metal ions due to protonation of the active sites at higher H^+ concentration leading to electrostatic repulsive effects between the surface of the adsorbent and Pb^{2+} in the solution. However, as the pH increased, the number of H^+ decreased and the degree of protonation of the surface functional groups was gradually reduced, which increased the adsorption capacity of the adsorbent. The adsorption capacity of PAN-PyAMI gradually increased as the pH increased from 2.2 to 4.9 and the maximum adsorption capacity for Pb^{2+} (4.70 mg/g or 22.5%) was achieved at pH 4.9. The results for PAN-nfs showed that a maximum adsorption capacity of 1.54 mg/g or 8% was achieved at a pH of 3.1. The difference in adsorption capacity between PAN-nfs and PAN-PyAMI is obviously due to the presence of the chelating ligand (PyAMI) on PAN-PyAMI. This confirmed two facts; firstly, the surface of PAN-nfs is passive and needs to be functionalised for adsorption of metal ions, and secondly, that PyAMI ligand has been successfully immobilised on PAN-nfs, hence creating active adsorption sites on PAN-nfs.
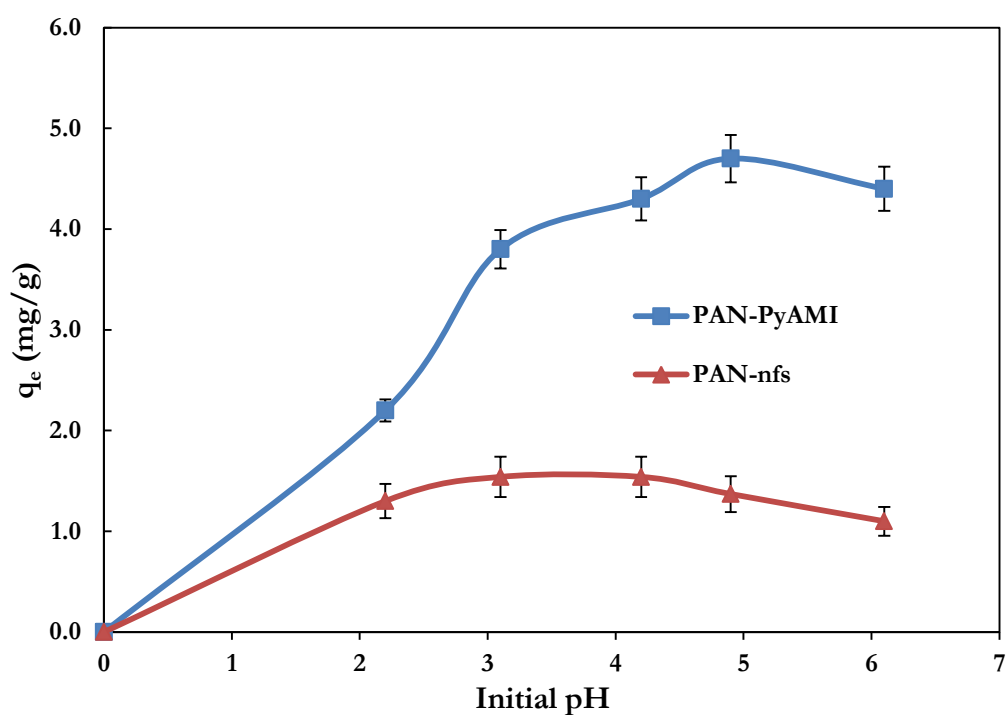
Figure 6.1: Effect of initial pH on quantity adsorbed of Pb^{2+} (initial concentration; 200 mg/L, weight of adsorbent; 0.1 g, contact time; 1 hour).

Figure 6.2: Effect of initial pH on the percentage adsorption of Pb^{2+} by PAN-PyAMI and PAN-nfs (initial concentration; 200 mg/L, weight of adsorbent; 0.1 g, contact time; 1 hour).

Meanwhile, the adsorption capacity of PAN-PyAMI decreased as the pH increased further from 4.9 to 6.1. This was due to the formation of hydrated lead(II) ions at a pH above 4.9 resulting in the decrease binding capability of Pb^{2+}. This is a common trend for adsorption of Pb metal as has been reported by several authors (Hong et al., 2015; Musyoka et al., 2011; Powell et al., 2009). Therefore, to prevent the metal ions from precipitation, a pH of greater than 7.0 was not studied. Thus, the initial solution pH of 4.9 was chosen for subsequent adsorption experiments on PAN-PyAMI and further adsorption experiments on PAN-nfs was discontinued due to its low adsorption capacity.

6.1.2 The effect of initial concentration

The effect of initial adsorbate concentration on the adsorption of Pb^{2+} was carried out as described in section 3.2.7.3.2 (b). It was investigated in order to determine the optimum Pb^{2+} concentration for 0.1 g of PAN-PyAMI and also to determine the adsorption isotherm of Pb^{2+} on PAN-PyAMI. 10 mL of 50, 100, 150, 200 and 250 mg/L of Pb^{2+} of pH 4.9 were prepared. 0.1 g of PAN-PyAMI was shaken with each solution for 1 hour at 25°C at a stirrer speed of 120 rpm. The resultant solution was filtered and analysed using ICP-OES as described in section 3.3.10 and the adsorption capacity (q_e) and the percentage adsorption (R) were calculated according to equations 3.1 and 3.3, respectively.

Figure 6.3 and Figure 6.4 present the quantity of Pb^{2+} adsorbed and the percentage adsorbed on PAN-PyAMI at different initial concentrations, respectively. The results show that the adsorption capacity increased as the initial concentration increased from 50 mg/L to 150 mg/L. At 150 mg/L, the equilibrium capacity of PAN-PyAMI of 3.17 mg/g (21%) was achieved and thereafter saturation was reached and the adsorption of Pb^{2+} was no longer increasing. This may be due to the fact that at lower concentration, more adsorption sites were available; hence Figure 6.4 shows that the percentage adsorption decreased as the initial concentration increased. The adsorbent could take up to 33% of 50 mg/L of Pb^{2+}. As the initial concentration increased, the adsorption sites were completely filled and could no longer adsorb Pb^{2+} from the solution. Adsorption isotherm models were applied in the next sub-section to model the adsorption process.
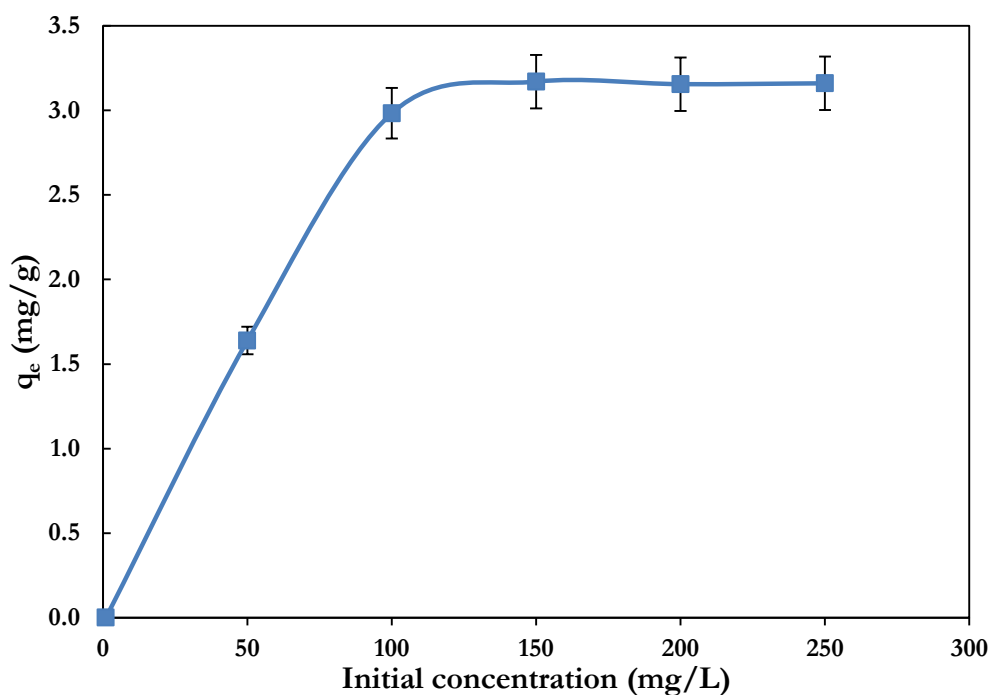
Figure 6.3: Effect of initial concentration on quantity adsorbed of Pb^{2+} on PAN-PyAMI at pH; 4.9, weight of adsorbent; 0.1 g, contact time; 1 hour.
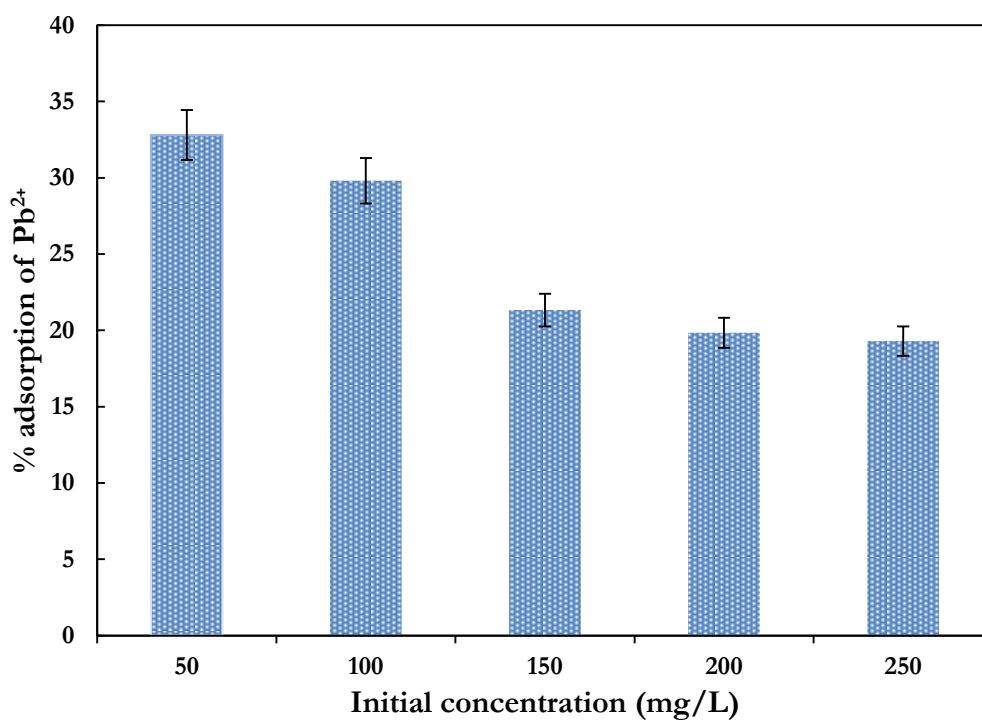
Figure 6.4: Effect of initial concentration on percentage adsorption of Pb^{2+} on PAN-PyAMI at pH; 4.9, weight of adsorbent; 0.1 g, contact time; 1 hour.

6.1.2.1　　Adsorption isotherms

The adsorption isotherms were determined using Langmuir and Freundlich isotherm models according to equations 3.5 and 3.8, respectively. Adsorption isotherms are used to draw relationships between the adsorbate concentration in the solution and the amount adsorbed onto the adsorbent. Langmuir and Freundlich isotherms are the most commonly used models for the solid–liquid phase. The Langmuir model suggests that adsorption takes on specific homogenous sites of the adsorbent surface, hence the assumption that once a metal ion occupies a site, no further adsorption takes place on the site. The linearised form of the model is expressed as equation 3.5 (recall from section 3.2.7.1.1). For the Freundlich isotherm, it is assumed that the adsorbate adsorbs onto the heterogeneous surface of an adsorbent. The linearised form of the model is expressed as equation 3.8 (recall from section 3.2.7.1.1).

Figure 6.5 presents the results for the equilibrium isotherms of Pb^{2+} on PAN-PyAMI. The experimental equilibrium data of Pb^{2+} for PAN-PyAMI was compared with theoretical equilibrium data obtained from the Langmuir and Freundlich isotherm models in order to determine the best fit model for the adsorption experiments. The adsorption data were analysed according to the linear form of the Langmuir isotherm and Freundlich isotherm equations 3.5 and 3.8, respectively. For this experiment, the adsorbate was the Pb^{2+} while the adsorbent was PAN-PyAMI.

From Figure 6.5, the experimental data were well fitted with the Langmuir isotherm, indicating that the monolayer adsorption of Pb^{2+} occurred on the homogenous surface of PAN-PyAMI. Moreover, the correlation coefficient R^2 values (Table 6.1) for the Langmuir model (0.9998) was closer to 1.000 than that of the Freundlich model (0.9963), suggesting that the adsorption process was due to monolayer formation. Also, the values of R_L (Figure 6.6) calculated according to equation 3.6 for the Langmuir isotherm ranged from 0 to 1, suggesting that favourable adsorption took place (Neghlani et al., 2011).
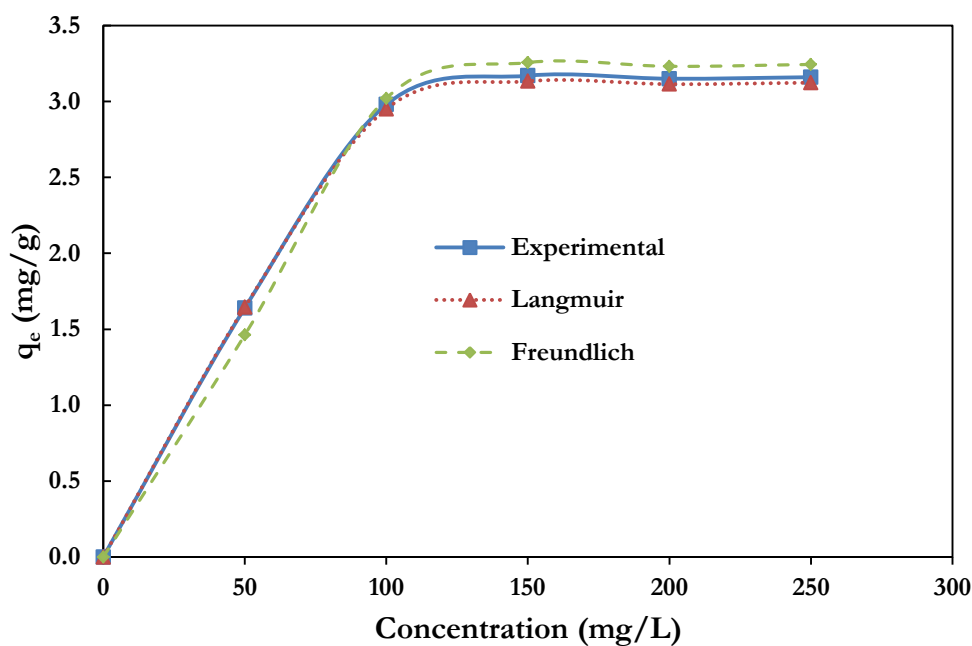
Figure 6.5: Equilibrium isotherms of Pb^{2+} adsorption on PAN-PyAMI.
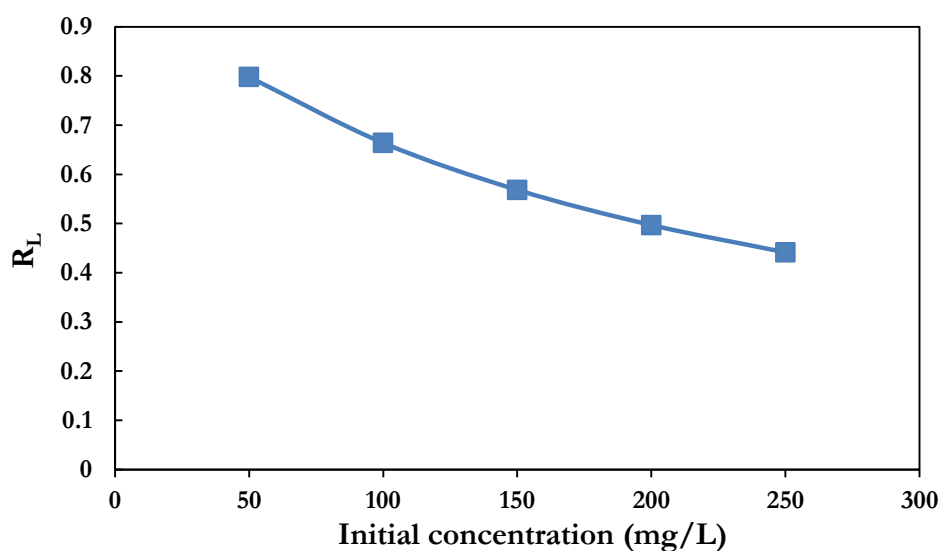
Figure 6.6: R$_L$ for the adsorption of Pb^{2+} on PAN-PyAMI.

Table 6.1: Langmuir and Freundlich constants for Pb^{2+} adsorption on PAN-PyAMI (R^2 from appendix F).

Isotherm models	Parameters	R^2
Langmuir	q$_m$ = 20, *b* = 0.00506	0.9998
Freundlich	K$_F$ = 0.1225, *n* = 1.0647	0.9963

6.1.3 The effect of contact time

Contact time is an important parameter in determining the performance of adsorbents. In order to study the adsorption kinetics, the effect of contact time on adsorption of Pb^{2+} on PAN-PyAMI was investigated. The effect of contact time on the adsorption of Pb^{2+} was carried out as set out in section 3.2.7.3.2 (c). Seven samples containing 10 mL of 200 mg/L of Pb^{2+} at pH 4.9 were shaken with 0.1 g PAN-PyAMI for 10, 20, 40, 60, 80, 100 or 120 minutes respectively at 120 rpm. The resultant solutions were filtered and analysed using ICP-OES as described in section 3.3.10. The adsorption capacity (q_e) and the percentage adsorption (R) were calculated according to equations 3.1 and 3.3, repectively. The adsorption kinetics was investigated using pseudo first-order and pseudo second-order kinetics models according to equations 3.10 and 3.12 (recall section 3.2.7.1.2), respectively.

Figure 6.7 and Figure 6.8 present the quantity and the percentage of Pb^{2+} adsorbed on PAN-PyAMI at different contact times respectively. It was found that the rate of adsorption of Pb^{2+} on PAN-PyAMI steadily increased from 10 to 60 minutes, and thereafter, the adsorption rate slowed down after 60 minutes, and increased no further after 80 minutes indicating that the adsorbent was saturated for Pb^{2+}.
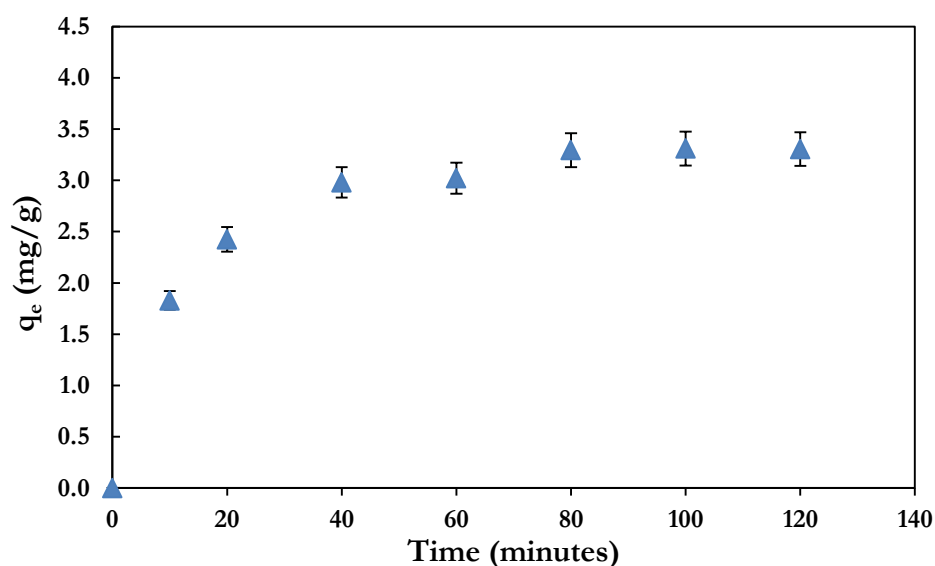
Figure 6.7: Effect of contact time on quantity of Pb^{2+} adsorbed using PAN-PyAMI (initial concentration; 200 mg/L, weight of adsorbent; 0.1 g, initial pH; 4.9).
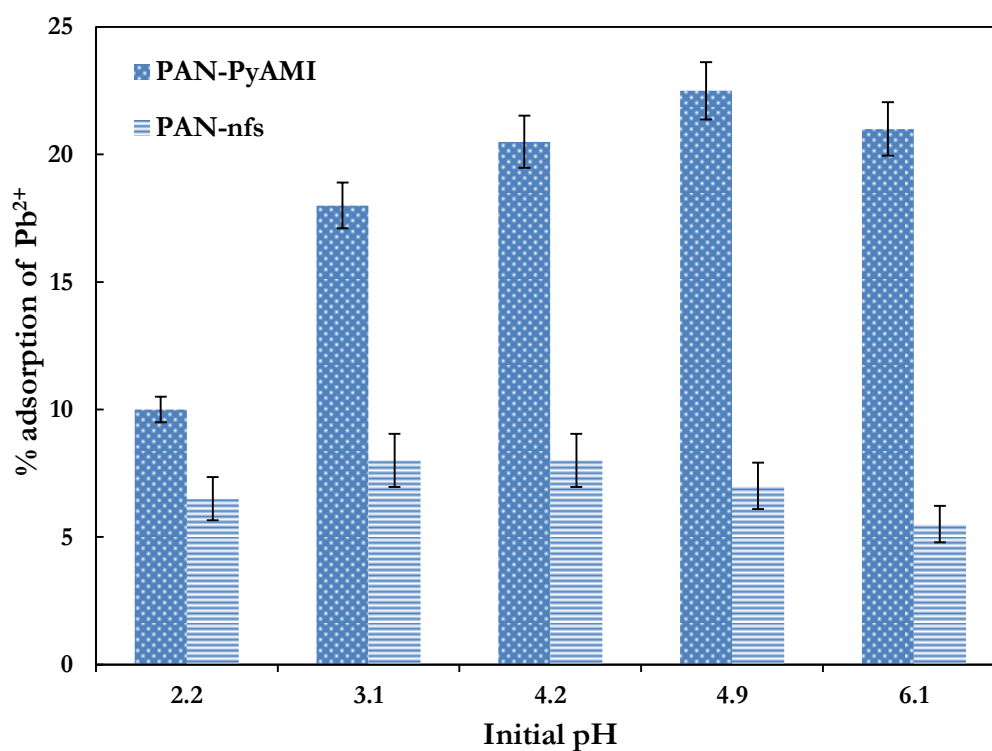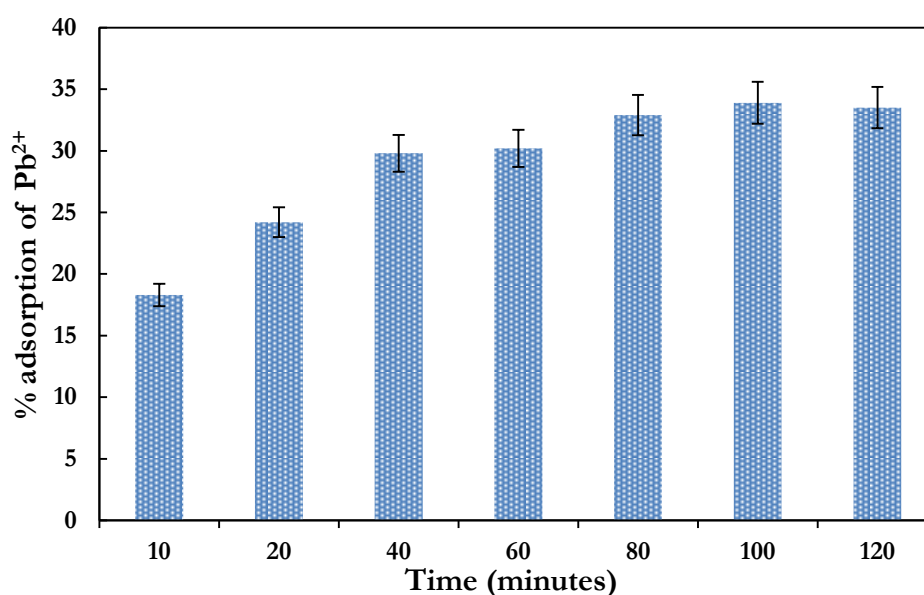
Figure 6.8: Effect of contact time on percentage adsorption of Pb^{2+} using PAN-PyAMI (initial concentration; 200 mg/L, weight of adsorbent; 0.1 g, initial pH; 4.9).

The steady increase in the adsorption rate in the first 60 minutes could be due to the availability of many adsorption sites on the surface of PAN-PyAMI and as the contact time increased further, the amount of Pb^{2+} adsorbed gradually reached a maximum when there was no more significant metal ion removal taking place because all the active sites on PAN-PyAMI had been occupied by metal ions. The adsorption capacity at equilibrium time (80 minutes) was calculated to be 3.29 mg/g (32.9%).

6.1.3.1   Adsorption kinetics

Adsorption kinetics models are used to examine the rate of the adsorption process and potential rate-controlling step. In this study, the kinetic data obtained from batch studies were analysed by using pseudo-first order and pseudo-second order equations 3.10 and 3.12, respectively (recall from section 3.2.7.1.2).

Figure 6.9 and Figure 6.10 show the pseudo first-order and pseudo second-order plot respectively, and Table 6.2 provides the evaluated parameters of the two kinetic models.
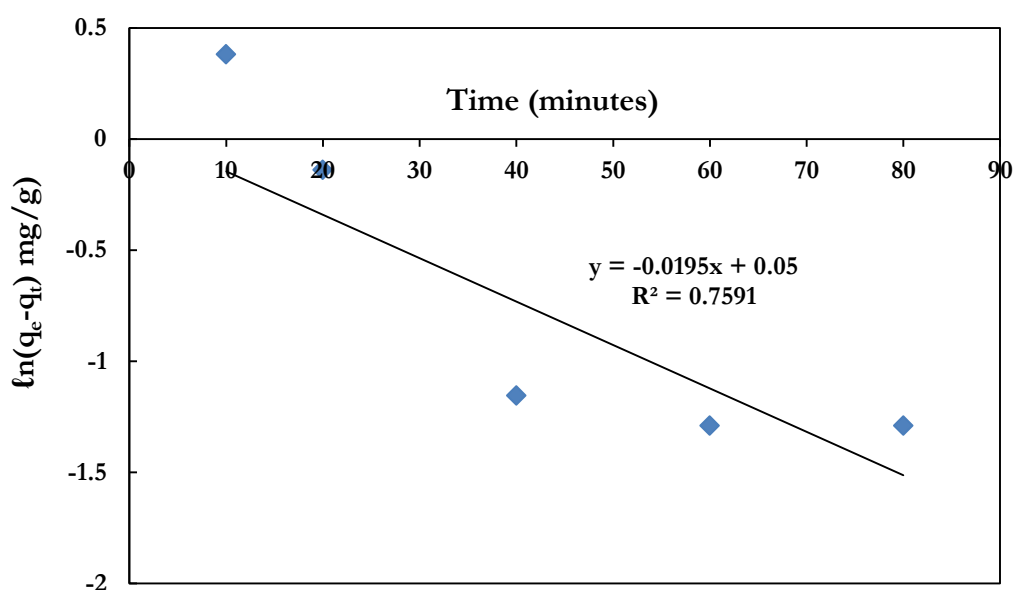
Figure 6.9: Pseudo first-order rate equation plot for Pb^{2+} adsorption onto PAN-PyAMI.
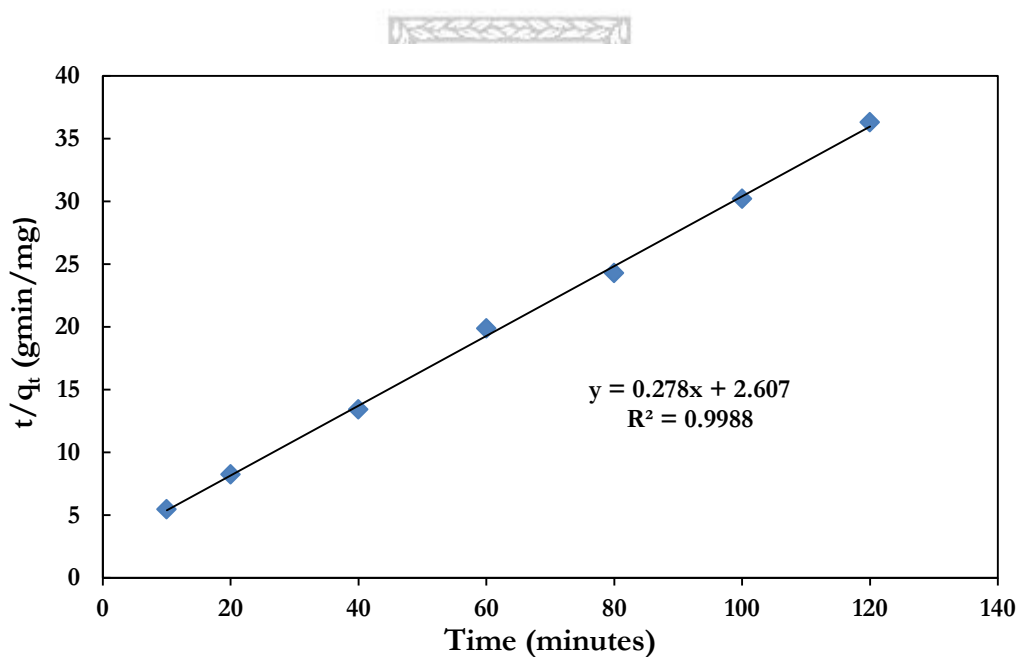
Figure 6.10: Pseudo second-order rate equation plot for Pb^{2+} adsorption onto PAN-PyAMI.

Table 6.2: Kinetic model parameters for Pb^{2+} adsorption onto PAN-PyAMI.

Pseudo first-order			Pseudo second-order		
q_e (mg/g)	K_1 (min^{-1})	R^2	q_e (mg/g)	K_2 (g/mg/min)	R^2
1.0513	0.0195	0.7591	3.5970	0.0296	0.9988

The R^2 value obtained for the pseudo second-order kinetics model from the plot of t/qt against time (Figure 6.10) was closer to 1.000 (0.9988) when compared with the R^2 value obtained from the plot of ℓn(q_e-q_t) against time (Figure 6.9) for pseudo first-order (0.7591). This shows that the pseudo second-order kinetic model is more applicable to describe the adsorption kinetic data of Pb^{2+} onto PAN-PyAMI. Also, the calculated values of q_e in the pseudo-second order (3.59 mg/g) (Table 6.2) was in proximity to the experimental value (3.29 mg/g, section 6.1.3).

6.2 Desorption and reusability experiments

Desorption and reusability experiments were carried out as set out in section 3.2.7.3.3. Desorption experiments were carried out in order to regenerate 0.1 g PAN-PyAMI previously used for adsorption of Pb^{2+} at variables; pH 4.9, initial concentration 200 mg/L at 1 hour contact time, at 25°C. The adsorbent PAN-PyAMI was regenerated by desorbing Pb^{2+} from the mat using 10 mL of 1 M, 0.1 M or 0.01 M EDTA (Note; for this study, acid was not used to regenerate PAN-PyAMI because of the functional ligands instability at solution pH of less than 4.5 (recall from section 4.2.4)). The resultant solution was filtered and analysed using ICP-OES as described in section 3.3.10 and the percentage desorbed was calculated according to equation 3.3. The regenerated PAN-PyAMI was reused to adsorb Pb^{2+} following the same procedure and variables pH 4.9, initial concentration 200 mg/L at 1 hour contact time, at 25°C.

Figure 6.11 presents the regeneration of PAN-PyAMI loaded with Pb^{2+} using 10 mL of 1 M, 0.1 M or 0.01 M EDTA. The results show that regeneration of PAN-PyAMI varies dependent on the concentration of EDTA. 1 M EDTA gave the highest desorption of 95% (4.92 mg/g) out of 5.16 mg/g previously adsorbed. 0.1 M EDTA desorbed 89% (4.85 mg/g) out of 5.44 mg/g while 0.01 M EDTA gave the lowest result, desorbing 25% (1.31 mg/g) out of 5.10 mg/g previously adsorbed on PAN-PyAMI. However, after desorption using 1 M EDTA at first cycle of regeneration, PAN-PyAMI became brittle and could no longer be re-used. Therefore, further study was carried out using 0.1 M EDTA to regenerate PAN-PyAMI.
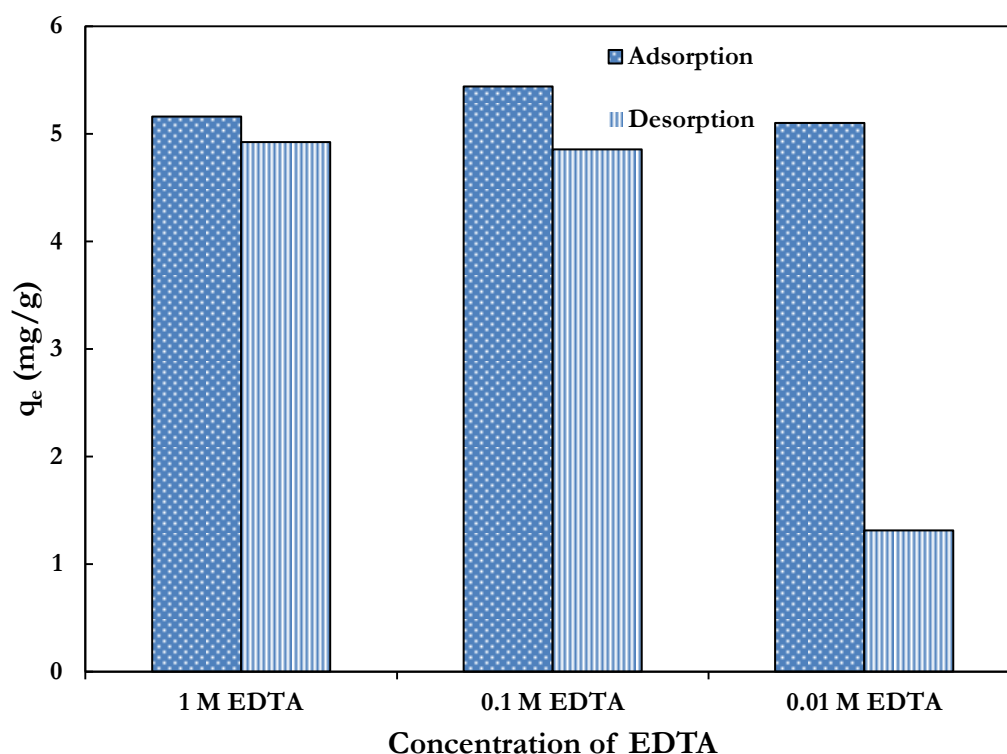
Figure 6.11: Regeneration of 0.1 g PAN-PyAMI loaded with Pb^{2+} using different concentrations of EDTA.

Figure 6.12 presents desorption and reusability of PAN-PyAMI after adsorption of Pb^{2+} at conditions; initial concentration; 200 mg/L, pH; 4.9; weight adsorbent; 0.1 g and contact time; 1 hour. The results show that PAN-PyAMI can be regenerated using 0.1 M EDTA after been previously used for adsorption of Pb^{2+} and can be subsequently reused for at least 4 cycles. For the first cycle, out of 5.65 mg/g previously adsorbed by PAN-PyAMI, 4.54 mg/g, 81% (Figure 6.13) was desorbed. Thereafter, for the Pb^{2+} adsorption cycle with PAN-PyAMI, 84% and 84% desorption was achieved for second and third desorption cycles, respectively (Figure 6.13). However as the reuse cycles increased from 2 to 4, the adsorption capacities of PAN-PyAMI decreased from 5.26 to 1.46 mg/g. The loss in capacity could be due to the gradual loss of PyAMI on PAN-nfs or due to Pb^{2+} that was irreversibly adsorbed.
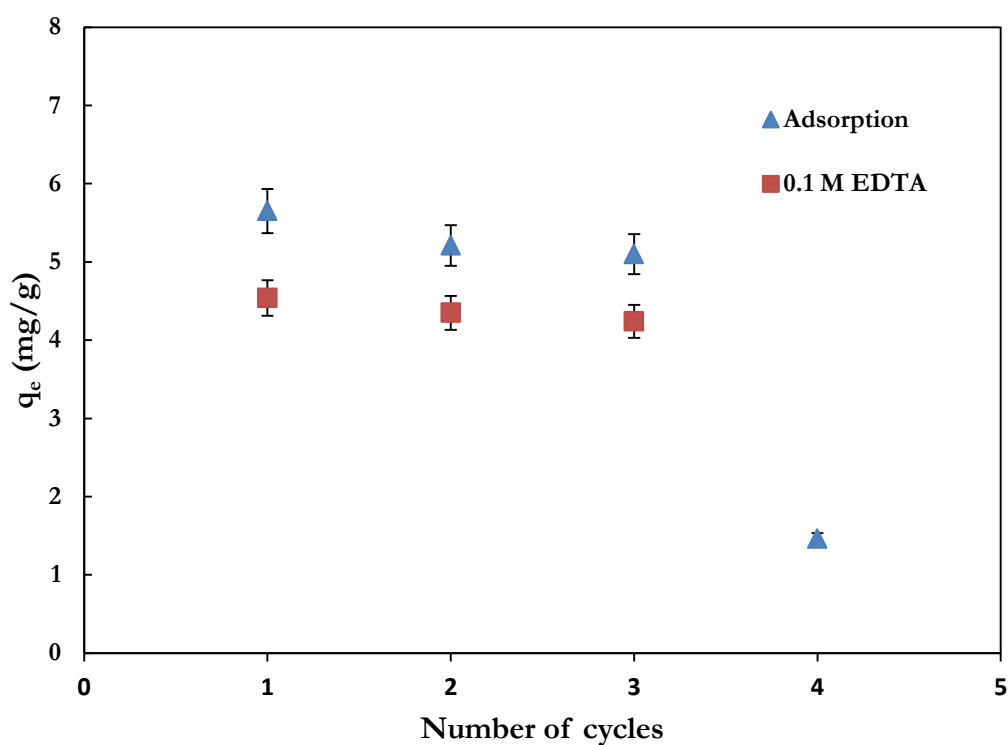
Figure 6.12: Desorption and reusability test of PAN-PyAMI on Pb^{2+} (initial concentration 200 mg/L, weight of adsorbent; 0.1 g, initial pH; 4.9, contact time; 1 hour, 0.1 M EDTA).
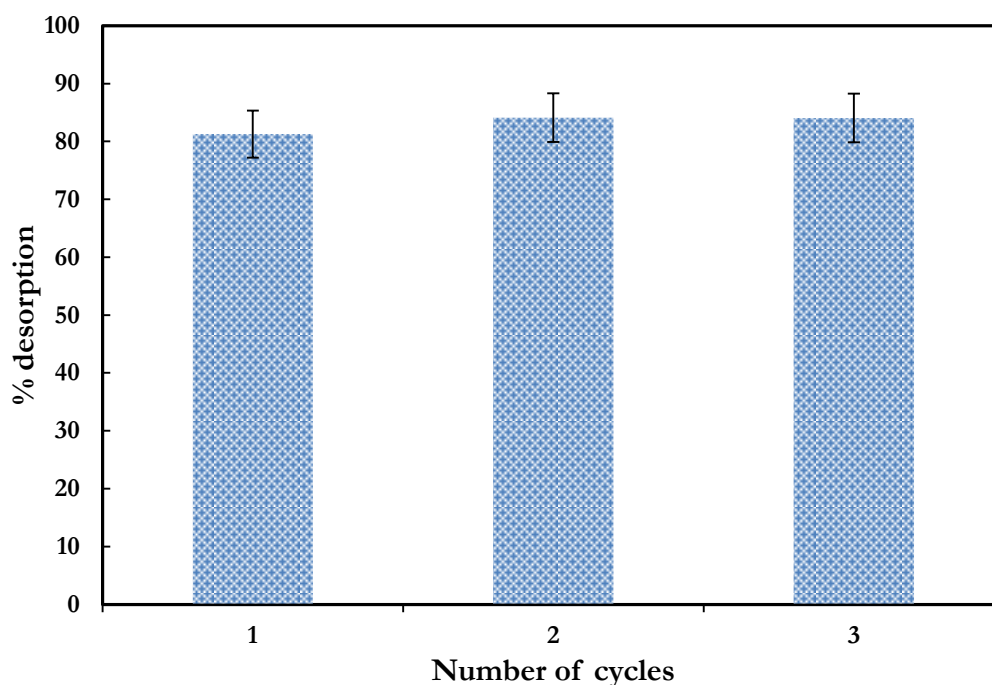
Figure 6.13: Percentage desorption of Pb^{2+} adsorbed onto PAN-PyAMI with respect to number of cycles using 0.1 M EDTA (initial concentration 200 mg/L, weight of adsorbent; 0.1 g, contact time; 1 hour).

To check which of the two possibilities (or both) mentioned earlier was responsible for the reduction in adsorption capacities of PAN-PyAMI, SEM-EDS, SEM-EDS mapping and ATR-FTIR techniques were employed. SEM-EDS and SEM-EDS mapping were used to indicate the availability of Pb^{2+} on PAN-PyAMI after the 1st and the 4th adsorption cycles (Figure 6.14). The results show that PAN-PyAMI adsorbed to its surface Pb^{2+} (Figure 6.14 (a)) after the first adsorption, however, the presence of Pb^{2+} was reduced significantly after the 4th adsorption (Figure 6.14 (b)). The reduction in adsorption capacity could be due to the reduction in active adsorption sites as a result of loss of ligands on PAN-PyAMI.
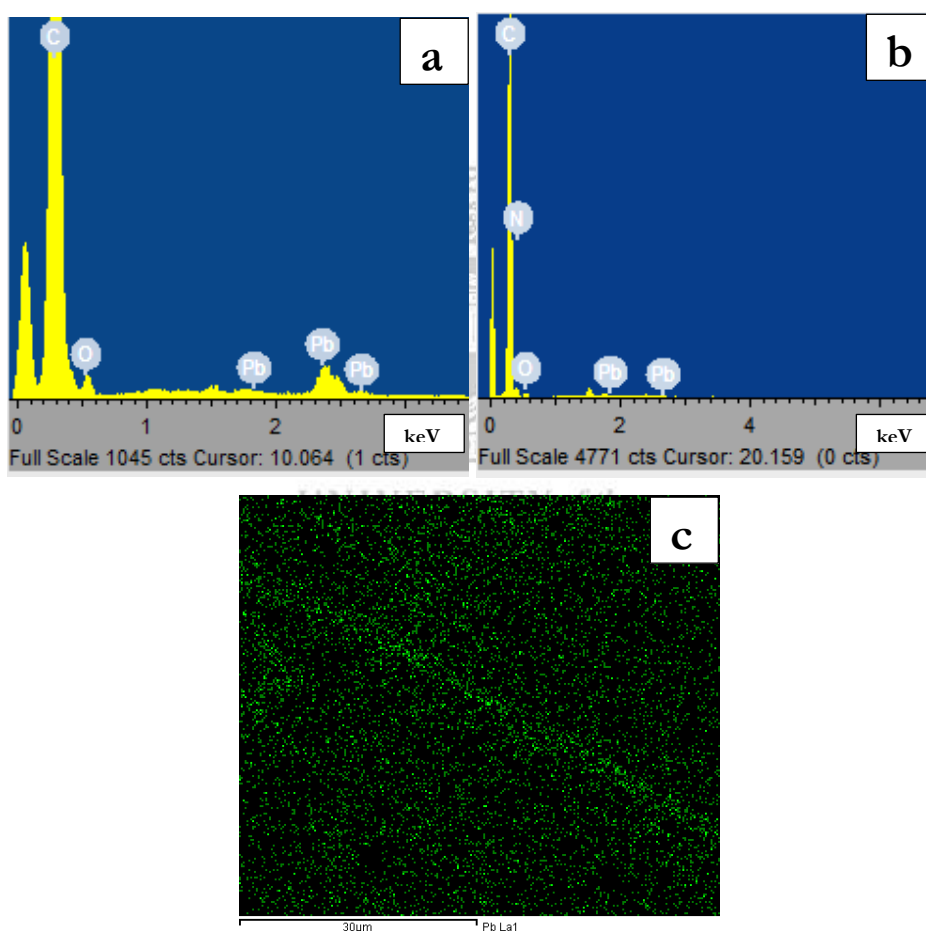
Figure 6.14: SEM-EDS {(a) PAN-PyAMI after 1st adsorption cycle of Pb^{2+} and (b) PAN-PyAMI after 4th adsorption cycle of Pb^{2+}} and (c) SEM-EDS mapping of PAN-PyAMI after 1st adsorption cycle of Pb^{2+}.

Meanwhile, SEM–EDS mapping shows (Figure 6.14 (c)) that the entire surface of the PAN-PyAMI was covered with Pb^{2+} (green spots) after the 1st adsorption, which

implies that the surface of PAN-PyAMI was uniformly active for adsorption of lead at 1st adsorption cycle.

ATR-FTIR technique was used to check the availability of PyAMI on PAN-nfs after each regeneration cycle. Figure 6.15 is the ATR-FTIR spectral of PAN-PyAMI as made and reuse after several regeneration cycles. The results show that the peaks from the ligand started to decrease in intensity after the first regeneration using 0.1 M EDTA (1st regeneration).
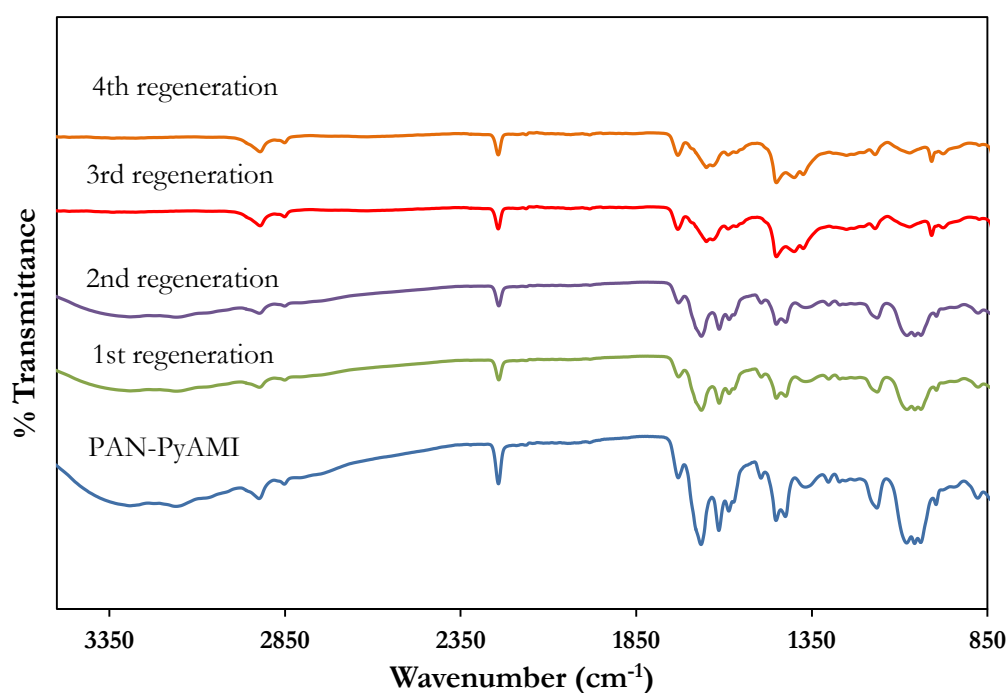
Figure 6.15: ATR-FTIR spectra of regenerated PAN-PyAMI using 0.1 M EDTA.

The peaks further decreased as the number of regeneration cycles increased from 2 to 4. After the 4th regeneration, the peaks attributed to PAN-PyAMI such 1654 cm^{-1} (C=N), 1605 cm^{-1} (N-H bending vibration) and 968 cm^{-1} (N-O) have virtually disappeared. From the SEM-EDS and the ATR-FTIR results, it could be concluded that PAN-PyAMI could not be reused more than 4 times after being regenerated with 0.1 M EDTA because of the loss of adsorption active sites which leads to reduction in adsorption capacities.

6.3 Chapter summary

The findings from this chapter have proven that immobilising the functional ligand PyAMI on PAN-nfs could be used to adsorb Pb^{2+} from an aqueous solution. The maximum adsorption capacity of 21% could be achieved at pH 4.9 with an initial concentration of 150 mg/L and contact time of 80 minutes. At these conditions, the initial material, PAN-nfs had a poor adsorption capacity of 8%. The experimental data were fitted with the Langmuir isotherm, indicating that the monolayer adsorption of Pb^{2+} occurred on homogeneous surface of PAN-PyAMI and the kinetic rate could best be described as pseudo second-order. PAN-PyAMI could be regenerated with 0.1 M EDTA and be reused. However, from ATR-FTIR results, PAN-PyAMI could only be regenerated 3 times before the ligands were weakened from the nanofibres due to their instability.

CHAPTER SEVEN

7 Introduction

This chapter presents the conclusion of this research including the answers to the research questions in chapter one. The chapter also includes the novelty of this research and the recommendations for further studies. So far, this research has reported the production of two polymer nanofibres which are PAN-nfs and PA6-nfs via electrospinning process. The two polymer nanofibres were characterised using HRSEM, TEM, ATR-FTIR, TGA and BET techniques. The two polymer nanofibres were respectively combined with PET track-etched membrane coated with TiO_2 (PET-TM) through electrospinning process to form their respective composite nanofibre track-etched membranes, PET-TMPAN and PET-TMPA6. The composite nanofibres track-etched membranes were characterised using HRSEM analysis. Thereafter, PAN-nfs, PA6-nfs, PET-TM, PET-TMPAN and PET-TMPA6 were used for filtration of RD from solution. Furthermore, this research also reported the immobilisation of a ligand on PAN-nfs. The synthesised ligand, PyAMI was characterised using NMR, ATR-FTIR and TGA techniques. After the immobilisation reaction, the resultant PAN-PyAMI was characterised using HRSEM, TEM, ATR-FTIR, BET, XRD and TGA analysis. Thereafter, the functionalised PAN-PyAMI was used to remove Pb^{2+} from water. PAN-PyAMI was regenerated using EDTA but could not be regenerated using HNO_3.

7.1 Conclusion

From this study, all the membranes reported, PAN-nfs, PA6-nfs, PET-TM, PET-TMPAN and PET-TMPA6 were able to remove RD from solution in a continuous mode. The parameters such as the effect of initial concentration, initial pH and flow rate were studied. The results showed that the effect of initial pH played the most important role in the adsorption of RD as the removal was greatly increased as the initial pH increased.

http://etd.uwc.ac.za/

At initial concentration of 10 mg/L of RD, initial pH of 10 and at flow rate of 1 mL/min, using 0.0026 g with 12 mm diameter of each membrane, PAN-TMPAN gave the best RD removal. At these conditions, PET-TMPAN removed 91.27% of RD, PET-TMPA6, 70.66%, PAN-nfs, 65.97%, PA6-nfs, 36.80% and PET-TM 24.53%.

Again, PAN-PyAMI and the pristine PAN-nfs were used for adsorption of Pb^{2+} in batch experiment with investigating parameters of the effect of initial pH, initial concentration, and the contact time. The effect of initial pH played the most important role in adsorption of Pb^{2+} as the removal was greatly increased as pH increased. PAN-PyAMI performed better when compared to PAN-nfs with optimum adsorption conditions of initial pH of 4.9, initial concentration 200 mg/L, weight of adsorbent 0.1 g and contact time 1 hour. The maximum adsorption capacity of PAN-PyAMI for Pb^{2+} was 4.7 mg/g or 22.5%, while PAN-nfs gave 1.54 mg/g or 8%.

7.1.1   Consideration of research questions

The research questions of this study mentioned in chapter one were answered as follow:

Question 1: Can PAN and PA6 nanofibres be combined with PET track-etched membranes through the electrospinning process?

> One of the aims of this research is to enhance the removal capacity of nanofibres and track-etched membrane by synergising the two materials together. The PAN solution in DMF and PA6 solution in formic acid at optimum concentrations of 8 wt% and 14 wt% respectively were combined with TiO_2 coated-PET-TM through the electrospinning process to form composite nanofibre track-etched membranes. The combination was possible because PET-TM was made conductive as a result of being coated with TiO_2. Therefore, PET-TM could serve as nanofibre collector instead of conventional Al foil.

Question 2: Can PA6-nfs and PAN-nfs remove rhodamine 6G from aqueous solution?

> The electrospun PAN-nfs or PA6-nfs was used as membrane in a continuous adsorption-filtration process of RD solution. The concentrations of the RD effluent as analysed using UV-vis showed significant reduction when compared to the feed concentration. The removal was attributed to the mesoporous nature of the nanofibres which could interact with the dye cations.

Question 3: Can composite nanofibre track-etched membranes remove rhodamine 6G from aqueous solutions?

> From this research, continuous adsorption-filtration experiments showed that PET-TMPAN or PET-TMPA6 removed RD from solution with a greater removal efficiency when compared to the individual constituent materials (nanofibres and PET track-etched membrane). This is due to the synergetic performance of the nanofibres and the track-etched membrane.

Question 4: Can 2-pyridine amidoxime ligand moieties be chemically immobilised on the surface of PAN nanofibres?

> The synthesised PyAMI ligand was chemically immobilised on PAN-nfs by reacting PyAMI and PAN-nfs together in water at 60^0C for 1 hour with $AlCl_3.H_2O$ as catalyst. ATR-FTIR analysis showed the presence of peaks attributed to PyAMI on the newly produced affinity membrane PAN-PyAMI. The reaction proceeded via electrophilic assistance using $AlCl_3.6H_2O$, generating carbocation on PAN-nfs which is susceptible to nucleophilic attack from the ligand PyAMI.

Question 5: Can PAN-PyAMI adsorb Pb^{2+} better than PAN-nfs?

> The batch adsorption experiments showed that the immobilisation of PyAMI on PAN-nfs increased the adsorption capacity of PAN-nfs whereas the pristine PAN-nfs alone had a poor adsorption capacity. PAN-nfs has poor adsorption capacities because of lack of functional groups on it. However,

PAN-PyAMI adsorption capacity was enhanced as a result of chelating property of PyAMI on it.

Question 6: Can PAN-PyAMI be regenerated after Pb^{2+} adsorption?

PAN-PyAMI could be regenerated using 0.1 M EDTA. However, the regeneration could only be done three times before the ligand bonds weakened and become unstable. This led to reduction in the adsorption capacity of PAN-PyAMI. PAN-PyAMI could not be regenerated in strong acids such as HNO_3 because of the instability of the organic ligand in acid.

7.2 Novelty

This research is reporting the use of electrospinning process to combine nanofibres and track-etched membrane to produce composite nanofibre track-etched membranes for the first time. The use of track-etched membrane as collector during electrospinning is also unique to this research. The adsorption results of the composite membranes have shown that ultrafast nano-filtration membrane has been made. In the same vein, this research has been able to contribute new knowledge to the use of nanofibres as supports; the immobilisation of 2-pyridine amidoxime on nanofibres has not been previously studied. Electrospun PAN-nfs was used as support for PyAMI ligands to produce new adsorptive membrane, PAN-PyAMI.

7.3 Recommendations

This research recommends the up scaling of the production of the composite nanofibre track-etched membrane. Further studies should be carried out on the use of these composite membranes for removal of other pollutants such as the micro organic pollutants. This study has opened another avenue for separation of toxic metals; therefore, further research should be carried on the immobilisation of ligands on nanofibres for adsorption and metal separation purposes. The stability of the affinity membrane should be looked into in order to overcome the instability in acids.

REFERENCES

Adak, A., Bandyopadhyay, M. and Pal, A. (2005). Removal of crystal violet dye from wastewater by surfactant-modified alumina, *Separation and Purification Technology*, Vol. 44, pp. 139-144.

Adomaviciute, E. and Rimvydas, M. (2007). The influence of applied voltage on poly (vinyl alcohol) (PVA) nanofibre diameter, *Fibers and Textile in Eastern Europe*, Vol. 15, pp. 64-65.

Aguedach, A., Brosillon, S., Morvan, J. and Lhadi, E.K. (2005). Photocatalytic degradation of azo-dyes reactive black 5 and reactive yellow 145 in water over a newly deposited titanium dioxide, *Applied Catalysis B*, Vol. 57, pp. 55-62.

Akcay, H., Oguz, A. and Karapire, C. (2003). Study of heavy metal pollution and speciation in Buyak Menderes and Gediz river sediments, *Water Research*, Vol. 37, No. 4, pp. 813-822.
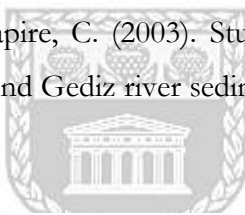
Akcil, A. and Koldas, S. (2006). Acid Mine Drainage (AMD): causes, treatment and case studies, *Journal of Cleaner Production*, Vol. 14, pp. 1139-1145.

Al-Bastaki, N. (2004). Removal of methyl orange dye and Na_2SO_4 salt from synthetic waste water using reverse osmosis, *Chemical Engineering Process*, Vol. 43, pp. 1561-1567.

Al-Degs, Y., Khraisheh, M.A.M., Allen, S.J. and Ahmad, M.N.A. (2001). Sorption behavior of cationic and anionic dyes from aqueous solution on different types of activated carbons, *Separation Science and Technology*, Vol. 36, pp. 91-102.

Alexander, F. and McKay, G. (1977). Kinetics of removal of basic dye from effluent using silica – 1, *Chemical Engineering*, London, pp. 243-246.

Allingham, M.M., Cullen, J.M., Giles, C.H., Jain, S.K. and Woods, J.S. (1958). Adsorption at inorganic surfaces. II. Adsorption of dyes and related compounds by silica, *Journal of Applied Chemistry*, Vol. 8, pp. 108-116.

References

Al-Malack, M.H. and Anderson, G.K. (1997). Use of crossflow microfiltration in wastewater treatment, *Water Resources*, Vol. 31, pp. 3064-3072.

Alpat, S.K., Ozbayrak, O., Alpat, S. and Akcay, H. (2008). The adsorption kinetics and removal of cationic dye, Toluidine Blue O, from aqueous solution with Turkish zeolite, *Journal of Hazardous Materials*, Vol. 151, pp. 213-220.

Anirudhan, T., Jalajamony, S. and Suchithra, P. (2009). Improved performance of a cellulose-based anion exchanger with tertiary amine functionality for the adsorption of chromium (VI) from aqueous solutions, *Colloids and Surfaces*, Vol. 335, pp. 107-113.

Apel, P. Y. (2001). Track etching technique in membrane technology, *Radiation Measurements*, Vol. 34, pp. 559-566.

Apel, P.Y. (2013). Track-etching at Flerov Laboratory of Nuclear Reactions, Joint Institute for Nuclear Research, Moscow Region, *Russia Encyclopedia of Membrane Science and Technology*, Wiley & Sons Incorporation.

Argun, M.E. and Dursun, S. (2008). A new approach to modification of natural adsorbent for heavy metal adsorption, *Bioresource Technology*, Vol. 99, No. 7, pp. 2516-2527.

Armitage, P.D., Bowes, M.J. and Vincent, H.M. (2007). Long-term changes in macroinvertebrate communities of a heavy metal polluted stream: the river Nent (Cumbria, UK) after 28 years, *River Research and Applications*, Vol. 23, No. 9, pp. 997-1015.

Astheimer, L., Schenk, H.J., Witte, E.G. and Schwochau, K. (1983). Development of sorbent for the recovery of uranium from seawater, Part 2. The accumulation of uranium from seawater by resins containing amidoxime and imidoxime groups, *Separation Science Technology*, Vol. 18, pp. 307-339.

Aussawasathien, D., Sahasithiwat, S., Menbangpung, L. and Teerawattananon, C. (2011). Poly(o-anisidine)–polystyrene composite fibers via electrospinning process:

References

Surface morphology and chemical vapor sensing, *Sensors and Actuators B*, Vol. 151, pp. 341-350.

Avlonitis, S.A., Poulios, I., Sotiriou, D., Pappas, M. and Moutesidis, K. (2008). Simulated cotton dye effluents treatment and reuse by nanofiltration, *Desalination*, Vol. 221, pp. 259-267.

Babu, B.R., Parande, A.K., Raghu, S. and Kumar, T. P. (2007). Cotton textile processing: Waste generation and effluent treatment, *Journal of Cotton Science*, Vol. 11, pp. 141-153.

Bae, J.S. and Freeman, H.S. (2007). Aquatic toxicity evaluation of new direct dyes to the Daphnia magna, *Dyes Pigments*, Vol. 73, pp. 81-85.

Bagheri, B., Abdouss, M., Aslzadeh, M. and Shoushtari, A. (2010). Efficient Removal of Cr^{3+}, Pb^{2+} and Hg^{2+} ions from industrial effluents by hydrolyzed/thioamidated polyacrylonitrile fibres, *Iranian Polymer Journal*, Vol. 19, No. 12, pp. 911-925.

Bai, Y., Wang, C., Lun, N., Wang, Y., Yu, M. and Zhu, B. (2006). HRTEM microstructures of PAN precursor fibers, *Carbon*, Vol. 44, pp. 1773-1778.

Baji, A., Mai, Y., Wong, S., Abtahi, M. and Chen, P. (2010). Electrospinning of polymer nanofibers: Effects on oriented morphology, structures and tensile properties, *Composites Science and Technology*, Vol. 70, pp. 703-718.

Bandala, E.R., Pelaez, M.A., Garcia-Lopez, A.J., Salgado, M.d.J. and Moeller, G. (2008). Photocatalytic decolourisation of synthetic and real textile wastewater containing benzidine-based azo dyes, *Chemical Engineering Process*, Vol. 47, pp. 169-176.

Bansal, R.C. and Goyal, M. (2005). Activated carbon adsorption, *Taylor & Francis Group*, Boca Raton.

Barakat, M.A. (2011). New trends in removing heavy metals from industrial wastewater, *Arabian Journal of Chemistry*, Vol. 4, pp. 361-377.

References

Barnes, M., Gerson, A., Kumar, S. and Hwang, N. (2004). The mechanism of TiO_2 deposition by direct current magnetron reactive Sputtering, *Thin Solid Films*, Vol. 446, pp. 29–36.

Barnes, M.C., Kumar, S., Green, L., Hwang, N. and Gerson, A.R. (2005). The mechanism of low temperature deposition of crystalline anatase by reactive DC magnetron sputtering, *Surface & Coatings Technology*, Vol. 190, pp. 321– 330.

Barragan, B.E., Costa, C. and Carmen-Marquez, M. (2007). Biodegradation of azo dyes by bacteria inoculated on solid media, *Dyes and Pigments*, Vol. 75, pp. 73-81.

Behnajady, M.A., Modirshahla, N. and Hamzavi, R. (2006). Kinetic study on photocatalytic degradation of C.I. Acid Yellow 23 by ZnO photocatalyst, *Journal of Hazardous Materials*, Vol. 133, pp. 226-232.

Bernasek, E. (1957). Pyridineamidoximes, *Journal of Organic Chemistry,* Vol. 6208, pp. 1263.

Bhardwaj, N. and Kindu, S. (2010). Electrospinning: A fascinating fiber fabrication technique, *Biotechnology Advances*, Vol. 28, pp. 325-347.

Bhattacharyya, K.G. and Sarma, A. (2003). Adsorption characteristics of the dye, Brilliant Green, on Neem leaf powder, *Dyes Pigments*, Vol. 57, pp. 211-222.

Bilba, D., Bejan, D. and Tofan, L. (1998). Chelating Sorbents in Inorganic Chemical Analysis, *Croatica Chemica Acta*, Vol. 71, No.1, pp. 155-178.

Bilba, N., Bilba, D. and Moroi, G. (2004). Synthesis of a polyacrylamidoxime chelating fiber and its efficiency in the retention of palladium ions, *Journal of Applied Polymer Science*, Vol. 92, pp. 3730-3735.

Bode-Aluko, C.A., Pereao, O., Ndayambaje, G. and Petrik, L. (2017a). Adsorption of Toxic Metals on Modified Polyacrylonitrile Nanofibres: A Review, *Water, Air and Soil Pollution*, 228:35 DOI 10.1007/s11270-016-3222-3.

Bode-Aluko, C.A., Pereao, O., Fatoba, O. and Petrik, L. (2017b). Surface-modified polyacrylonitrile nanofibres as supports, *Polymer Bulletin*, Vol. 74, pp. 2431-2442.

References

Bradshaw, J.S., Krakowiak, E.K., Tarbet, B.J., Bruening, L.R., Biernat, J.F., Bochenska, M., Reed Izatt, R.M. and Christensen, J.J. (1989). Silica gel-bound aza-crowns for the selective removal and concentration of metal ions, *Pure and Applied Chemistry*, Vol. 61, No. 9, pp. 1619-1624.

Brown, D. and Hamburger, B. (1987). The degradation of dye stuffs. Part III. Investigations of their ultimate degradability, *Chemosphere*, Vol. 16, pp. 1539-1553.

Brown, D. and Laboureur, P. (1983). The aerobic biodegradability of primary aromatic amines, *Chemosphere*, Vol. 12, pp. 405-414.

Brunauer, S., Emmett, P. H. and Teller, E. J. (1938). Adsorption of gases in multimolecular layers, *Journal of the American Chemical Society*, Vol. 60, No. 2, pp. 309-319.

Buchko, C.J., Chen, L.C., Shen, Y. and Martin, D.C. (1999). Processing and microstructural characterization of porous biocompatible protein polymer thin films, *Polymer*, Vol. 40, pp. 7397-7407.

Casper, C.L., Stephens, J.S., Tassi, N.G., Chase, D.B. and Rabolt, J.F. (2004). Controlling surface morphology of electrospun polystyrene fibers: effect of humidity and molecular weight in the electrospinning process, *Macromolecules*, Vol. 37, No. 2, pp. 573-578.

Chakraborty, S., Purkait, M.K., Gupta, S., De, S. and Basu, J. K. (2003). Nanofiltration of textile plant effluent for color removal and reduction in COD, *Separation and Purification Technology*, Vol. 31, pp. 41-151.

Chaudhary, B. and Farrell, J. (2014). Preparation and Characterization of Homopolymer Polyacrylonitrile-Based Fibrous Sorbents for Arsenic Removal, *Environmental engineering science*, Vol. 31, No. 11, pp. 1-9.

Chen, G. (2004). Electrochemical technologies in wastewater treatment, *Separation and Purification Technology*, Vol. 38, No. 1, pp. 11-41.

References

Chen, J., Hong, L., Wu, S. and Wang, L. (2002). Elucidation of interactions between metal ions and Ca-alginate-based ion-exchange resin by spectroscopic analysis and modeling simulation, *Langmuir*, Vol. 18, No. 24, pp. 9413-9421.

Chen, J.P., Qu, R., Zhang, Y., Sun, C., Wang, C., Ji, C., Yin, P., Chen, H. and Niu, Y. (2012). Preparation of silica gel supported amidoxime adsorbents for selective adsorption of Hg(II) from aqueous solution, *Chemical Engineering Journal*, Vol. 209, pp. 235-244.

Chen, M., Wang, C., Fang, W., Wang, J., Zhang, W., Jin, G. and Diao, G. (2013). Electrospinning of calixarene-functionalized polyacrylonitrile nanofiber membranes and application as an adsorbent and catalyst support, *Langmuir*, Vol. 29, pp. 11858-11867.

Chen, Z., Feng, X., Han, D., Wang, L., Cao, W. and Shao, L. (2014). Preparation of Aminated Polyacrylonitrile Porous Fiber Mat and Its Application for Cr(VI) Ion Removal, *Fibers and Polymers*, Vol. 15, No.7, pp. 1364-1368.

Cheremisinoff, N.P. (2002). Handbook of water and wastewater treatment technologies, *Butterworth-Heinemann*, Boston.

Chew, S.Y., Hufnagel, T.C., Lim, C.T. and Leong, K.W. (2006). Mechanical properties of single electrospun drug-encapsulated nanofibres, *Nanotechnology*, Vol. 17, pp. 3880-3891.

Chi, F., Hu, S., Xiong, J. and Wang, X. (2013). Adsorption behavior of uranium on polyvinyl alcohol-*g*-amidoxime: Physicochemical properties, kinetic and thermodynamic aspects, *Science China Chemistry*, Vol. 56, No. 111, pp. 1495–1503.

Choi, S., Choi, M., Park, Y., Lee, K. and Kang, H. (2003). Adsorption of uranium ions by resins with amidoxime and amidoxime/carboxyl group prepared by radiation-induced polymerization, *Radiation Physics and Chemistry*, Vol. 67, pp. 387-390.

Christie, R.M. (2007). Environmental aspects of textile dyeing, *Woodhead, Boca Raton*, Cambridge.

References

Chronakis, I. S. (2005). Novel nanocomposites and nanoceramics based on polymer nanofibres using electrospinning process—A review, *Journal of Materials Processing Technology*, Vol. 167, pp. 283-293.

Chu, Y., Tseng, C., Hung, K., Wang, C. and Chen, C. (2005). Surface Modification of Polyacrylonitrile Fibers and their Application in the Preparation of Silver Nanoparticles, *Journal of Inorganic and Organometallic Polymers and Materials*, Vol. 15, No. 3, pp. 309-317.

Ciardelli, G. and Ranieri, N. (2001). The treatment and reuse of wastewater in the textile industry by means of ozonation and electroflocculation, *Water Resources*, Vol. 35, pp. 567-572.

Coskun, R., Yigitoglu, M. and Sacak, M. (2000). Adsorption behavior of copper(II) ion from aqueous solution on methacrylic acid-grafted poly(ethylene terephthalate) fibers. *Journal of Applied Polymer Science*, Vol. 75, pp. 766-772.

Crini, G. (2005). Recent developments in polysaccharide-based materials used as adsorbents in wastewater treatment, *Progress in Polymer Science*, Vol. 30, pp. 38-70.

Dai, H.Q., Gong, J., Kim, H. and Lee, D. (2002). A novel method for preparing ultra-fine alumina-borate oxide fibers via an electrospinning technique, *Nanotechnology*, Vol. 13, No. 5, pp. 674-677.

Dassenakis, M., Scoullos, M., Foufa, E., Krasakopoulou, E., Pavlidou, A. and Kloukiniotou, M. (1998). Effects of multiple source pollution on a small Mediterranean river, *Applied Geochemistry*, Vol. 13, No. 2, pp. 197-211.

Deitzel, J.M, Kosik, W., McKnight, S.H, Ten, N.C.B., Desimone, J.M. and Crette, S. (2002). Electrospinning of polymer nanofibers with specific surface chemistry, *Polymer*, Vol. 43, pp. 1025-1029.

Deitzel, J.M., Kleinmeyer, J., Harris, D. and Tan, N.C.B. (2001). The effect of processing variables on the morphology of electrospun nanofibers and textiles, *Polymer*, Vol. 42, pp. 261-272.

References

Delee, W., O'Neill, C., Hawkes, F.R. and Pinheiro, H.M. (1998). Anaerobic treatment of textile effluents: a review, *Journal of Chemical Technology and Biotechnology*, Vol. 73, pp. 323-335.

Delval, F., Crini, G., Bertini, S., Filiatre, C. and Torri, G. (2005). Preparation, characterization and sorption properties of crosslinked starch-based exchangers, *Carbohydrate Polymer*, Vol. 60, pp. 67-75.

Demir, M.M., Yilgor, I., Yilgor, E. and Erman, B. (2002). Electrospinning of polyurethane fibers, *Polymer*, Vol. 43, pp. 3303-3309.

Deng, S. and Bai, R. (2003) Aminated Polyacrylonitrile Fibers for Humic Acid Adsorption: Behaviors and Mechanisms, *Environmental science and technology*, Vol. 37, pp. 5799-5805.

Deng, S., and Bai, R. (2004). Removal of trivalent and hexavalent chromium with aminated polyacrylonitrile fibers: performance and mechanisms, *Water Resources*, Vol. 38, pp. 2424.

Deng, S., Bai, R. and Chen J. (2003b). Behaviors and mechanisms of copper adsorption on hydrolyzed polyacrylonitrile fibers, *Journal of Colloid and Interface Science*, Vol. 260, pp. 265-272.

Deng, S., Bai, R. and Chen, J. (2003a). Aminated polyacrylonitrile fibers for lead and copper removal, *Langmuir*, Vol. 19, pp. 5058-5064.

Deniseger, J., Erickson, L., Austin, A., Roch, M. and Clark, M. (1990). The effects of decreasing heavy metal concentrations on the biota of Buttle Lake, Vancouver Island, British Columbia, *Water Research*, Vol. 24, No. 4, pp. 403-416.

Department of Water Affairs (2010). Assessment of the Ultimate Potential and Future Marginal Costs of water resources in South Africa. Project completed by BKS, Pretoria.

Dey, S. and Islam, A. (2015). A Review on textile wastewater characterization in Bangladesh, *Resources and Environment*, Vol. 5, No. 1, pp. 15-44.

References

Ding, B., Kim, H.Y., Lee, S.C., Shao, C.L., Lee, D.R. and Park, S.J. (2002). Preparation and characterization of a nanoscale poly (vinyl alcohol) fiber aggregate produced by an electrospinning Method, *Journal of Polymer Science B, Polymer Physics*, Vol. 40, pp. 1261-1268.

Ding, B., Kimura, E., Sato, T., Fujita, S. and Shiratori, S. (2004). Fabrication of blend biodegradable nanofibrous nonwoven mats via multi-jet electrospinning, *Polymer*, Vol. 45, pp. 1895-1802.

Ding, B., Li, C., Miyauchi Y., Kuwaki O. and Shiratore, S. (2006). Formation of novel 2D polymer nanowebs via electrospinning, *Nanotechnology*, Vol. 17, No.15, pp. 3685-3691.

Dogan, D. and Turkdemir, H. (2005). Electrochemical oxidation of textile dye indigo, *Journal of Chemical Technology and Biotechnology*, Vol. 80, pp. 916-923.

Dogan, M., Abak, H. and Alkan, M. (2009). Adsorption of methylene blue onto hazelnut shell: Kinetics, mechanism and activation parameters, *Journal of Hazardous Materials*, Vol. 164, pp. 172–181.

dos Santos, A.B., Cervantes, F.J. and van Lier, J.B. (2007). Review paper on current technologies for decolourisation of textile wastewaters: perspectives for anaerobic biotechnology, *Bioresource Technology*, Vol. 98, pp. 2369-2385.

Doshi, J. and Reneker, D.H. (1995). Electrospinning process and applications of electrospun fibers, *Journal of Electrostatics*, Vol. 35, pp. 151-160.

Drew, C., Wang, X., Senecal, K., Schreuder-Gibson, H., He, J., Kumar, J. and Samuelson, L.A. (2002). Electrospun photovoltaic cells, *Journal of Macromolecular Science, Pure and Applied Chemistry*, Vol. 39, pp. 1085-1094.

Dror, Y., Salalha, W., Khalfin, R.L., Cohen, Y., Yarin, A.L. and Zussman, E. (2003). Carbon nanotubes embedded in oriented polymer nanofibers by electrospinning, *Langmuir*, Vol. 19, pp. 7012-7020.

References

Duan, B., Dong, C., Yuan, X. and Yao, K. (2004). Electrospinning of chitosan solutions in acetic acid with poly(ethylene oxide), *Journal of biomaterial Science, Polymer Edition*, Vol. 15, pp. 797-811.

Egawa, H. and Harada, H. (1979). Recovery of Uranium from Seawater by Using Chelating Resins Containing Amidoxime Groups, *Nippon Kagaku Kaishi*, 958-959.

Egawa, H., Nakayama, M., Nonaaka, T., Yamamoto, H. and Uemura, K. (1987). Recovery of uranium from seawater. V. Preparation and properties of the macroreticular chelating resins containing amidoxime and other functional groups, *Journal of Applied Polymer Science*, Vol. 34, pp. 1557–1575.

Egawa, H., Nonaka, T. and Nakayama, M. (1988). Influence of Crosslinking and Porosity on the Uranium Adsorption of Macroreticular Chelating Resin Containing Amidoxime Groups, *Journal of Macromolecular* Science, *Chemistry,* Vol. 25, pp. 1407-1425.

Eldridge, D.S., Crawford, R.J. and Harding, I.H. (2015). The role of metal ion-ligand interactions during divalent metal ion adsorption, *Journal of Colloid and Interface Science*, Vol. 454, pp. 20–26.

Elzatahry, A. (2014). Polyacrylonitrile Electrospun Nanofiber as a Template to Prepare NiO Nanostructure Electrocatalyst, *International Journal of Electrochemical Science*, Vol. 9, pp. 22-31.

Fallahi, D., Rafizadeh, M., Mohammadi, N. and Vahidi, B. (2008). Effect of applied voltage on jet electric current and flow rate in electrospinning of polyacrylonitrile solutions, *Polymer International*, Vol. 57, pp. 1363-1368.

Faouzi, A.M., Nasr, B. and Abdellatif, G. (2007). Electrochemical degradation of anthraquinone dye Alizarin Red S by anodic oxidation on boron-doped diamond, *Dyes Pigments*, Vol. 73, pp. 86-89.

References

Feng, Q., Wang, X., Wei, A., Wei, Q., Hou, D., Luo, W., Liu, X. and Wang, Z. (2011). Surface Modified Polyacrylonitrile Nanofibers and Application for Metal Ions Chelation, *Fibers and Polymers*, Vol. 12, pp. 1025-1029.

Fennessey, S.F. and Farris, R.J. (2008). Fabrication of aligned and molecularly oriented electrospun polyacrylonitrile nanofibers and the mechanical behavior of their twisted yarns, *Polymer*, Vol. 45, pp. 4217-4225.

Ferain, E. and Legras, R. (2003). Track-etch templates designed for micro- and nano-fabrication, *Nuclear Instruments and Methods in Physics Research B*, Vol. 208, pp. 115-122.

Fergusson, J.E. (1990). The Heavy Elements: Chemistry, Environmental Impact and Health effects, *Oxford Pergamon Press*, pp. 515-550.

Fischer-Colbrie, G., Matama, T., Heumann, S., Martinkova, L., Paulo, A. and Guebitz, G. (2007). Surface hydrolysis of polyacrylonitrile with nitrile hydrolyzing enzymes from *Micrococcus luteus* BST20, *Journal of Biotechnology*, Vol. 129, pp. 62-68.

Fleischer, R.L., Price, P.B. and Walker, R.M. (1975). Nuclear Tracks in Solids; Principles and Applications, *University of California Press*, Berkeley.

Flerov, G.N., Apel, P.Y., Didyk, A.Y., Kuznetsov, V.I. and Oganessian, R.T. (1989). The use of heavy ion accelerators for the production of track membranes, *Atlas Energy (USSR)*, Vol. 67, pp. 274-280.

Fong, H., Chun, I. and Reneker, D.H. (1999). Beaded nanofibers formed during electrospinning, *Polymer*, Vol. 40, pp. 4585-4592.

Forgacs, E., Cserhati, T. and Oros, G. (2004). Removal of synthetic dyes from wastewaters: a review, *Environmental International*, Vol. 30, pp. 953-971.

Formhals, A. (1934). Process and apparatus preparing artificial threads, US Patent, 1-975, 504.

Fouad, H., Elsarnagawy, T., Almajhdi, F.N. and Khalil, K.A. (2013). Preparation and in-vitro thermo-mechanical characterization of electrospun PLGA nanofibers for

References

soft and hard tissue replacement, *International Journal of Electrochemical Science*, Vol. 8, pp. 2293-2304.

Frahn, J., Malsch, G., Matuschewski, H., Schedler, U. and Schwarz, H. (2004). Separation of aromatic/aliphatic hydrocarbons by photo-modified poly(acrylonitrile) membranes, *Journal of Membrane Science*, Vol. 234, No. 1-2, pp. 55-65.

Freger, V., Arnot, T.C. and Howell, J.A. (2000). Separation of concentrated organic/inorganic salt mixtures by nanofiltration, *Journal of Membrane Science*, Vol. 178, pp. 185-193.

Frenot, A. and Chronakis, I.S. (2003). Polymer nanofibers assembled by electrospinning, *Current Opinion in Colloid and Interface Science*, Vol. 8, pp. 64-75.

Frijters, C.T.M., Vos, R.H., Scheffer, G. and Mulder, R. (2006). Decolorizing and detoxifying textile wastewater, containing both soluble and insoluble dyes, in a full scale combined anaerobic/aerobic system, *Water Resources*, Vol. 40, pp. 1249-1257.

Fu, F. and Viraraghavan, T. (2001). Fungal decolorization of dye wastewaters: a review, *Bioresource Technology*, Vol. 79, pp. 51-62.

Fu, F. and Wang, Q. (2011). Removal of heavy metal ions from wastewaters: A review, *Journal of Environmental Management*, Vol. 92, pp. 407-418.

Gashti, M.P., Navid, M. Y. and Rahimi, M.H. (2012). Coating of Macroemulsion and Microemulsion Silicones on Poly(ethylene terephthalate) Fibers: Evaluation of the Thermal Properties and Flammability, *Journal of Applied Polymer Science*, Vol. 125, pp. 1430–1438.

Gautam, S., Dinda, A.K. and Mishra, N.C. (2013). Fabrication and characterization of PCL/gelatin composite nanofibrous scaffold for tissue engineering applications by electrospinning method, *Materials Science and Engineering: C*, Vol. 33, No.3, pp. 1228-1235.

References

Gaylord, N.G. and Piatzer, N.A. (1975). Copolymer, polymer blends, and composites. In: Advances in chemistry series, *American Chemical Society*, Vol. 142, p. 76.

Geng, X., Kwon, O.H. and Jang, J. (2005). Electrospinning of chitosan dissolved in concentrated acetic acid solution, *Biomaterials*, Vol. 26, pp. 5427-5432.

Ghayeni, S.B., Beatson, P.J., Schneider, R.P. and Fane, A.G. (1998). Water reclamation from municipal wastewater using combined microfiltration-reverse osmosis (MERO): Preliminary performance data and microbiological aspects of system operation, *Desalination*, Vol. 116, pp. 65-80.

Ghorai, T.K., Dhak, D., Biswas, S.K., Dalai, S. and Pramanik, P. (2007). Photocatalytic oxidation of organic dyes by nano-sized metal molybdate incorporated titanium dioxide (MxMoTi1O6) (MxNi, Cu, Zn) photocatalysts, *Journal of Molecular Catalysis A: Chemical*, Vol. 273, pp. 224-229.

Gibson, P.W, Schreuder-Gibson, H.L. and Revin, D. (1999). Electrospun fiber mats: transport properties, *AIChE Journal*, Vol. 45, pp. 190-195.

Gibson, P.W., Kendrick, C., Rivin, D., Charmchi, M. and Sicuranza, L. (1995). An automated water vapor diffusion test method for fabrics, laminates, and films, *Journal of Coated Fabrics*, Vol. 24, pp. 322.

Gopal, R., Kaur, S., Feng, C.Y., Chan, C., Ramakrishna, S., Tabe, S. and Matsuura, T. (2007). Electrospun nanofibrous polysulfone membranes as pre-filters: particulate removal, *Journal of Membrane Science*, Vol. 289, pp. 210-219.

Gopal, R., Kaur, S., Ma, Z., Chan, C., Ramakrishna, S. and Matsuura, T. (2006). Electrospun nanofibrous filtration membrane, *Journal of Membrane Science*, Vol. 281, pp. 581-586.

Gorden, A.E., Xu, J., Raymond, K.N. and Durbin, P. (2003). Rational design of sequestering agents for plutonium and other actinides, *Chemical reviews,* Vol. 103, No. 11, pp. 4207-4282.

References

Gordon, P.F. and Gregory, P. (1983). Organic Chemistry in Colour, *Springer*, Berlin.

Guerrini, L., Brancifortia, M., Canovab, T. and Bretas, R.E. (2009). Electrospinning and Characterization of Polyamide 66 Nanofibers With Different Molecular Weights, *Materials Research*, Vol. 12, No. 2, pp. 181-190.

Gupta, B., Deep, A. and Malik, P. (2001). Extraction and recovery of cadmium using Cyanex 923, *Hydrometallurgy,* Vol. 61, No. 1, pp. 65-71.

Gupta, M., Gupta, B., Oppermann, W. and Hardtmann, G. (2004). Surface Modification of Polyacrylonitrile Staple Fibers via Alkaline Hydrolysis for Superabsorbent Applications, *Journal of Applied Polymer Science*, Vol. 91, pp. 3127-3133.

Gupta, V.K. and Suhas, (2009). Application of low-cost adsorbents for dye removal – A review, *Journal of Environmental Management*, Vol. 90, pp. 2313-2342.

Gupta, V.K., Jain, R. and Varshney, S. (2007). Electrochemical removal of the hazardous dye Reactofix Red 3 BFN from industrial effluents, *Journal of Colloid Interface Science*, Vol. 312, pp. 292-296.

Hage, R. and Lienke, A. (2006). Applications of transition-metal catalysts to textile and wood-pulp bleaching, *Angewandte Chemie, International Edition*, Vol. 45, pp. 206-222.

Haghi, A.K. and Akbari, M. (2007). Trends in electrospinning of natural nanofibres, *Physica Status Solidi*, Vol. 204, pp. 1830-1834.

Hai, F.I., Yamamoto, K. and Fukushi, K. (2007). Hybrid treatment systems for dye wastewater, *Critical Reviews in Environmental Science and Technology*, Vol. 37, pp. 315-377.

Hajra, M.G., Mehta, K. and Chase, G.G. (2003). Effects of humidity, temperature, and nanofibers on drop coalescence in glass fiber media, *Separation and Purification Technology*, Vol. 30, pp. 79-88.

Hatch, K.L. and Maibach, H.I. (1999). Dyes as contact allergens: a comprehensive record, *Textile Chemistry Colour*, Vol. 1, pp. 53-59.

References

He, F., Chen, G., Yu, Y., Hao, S., Zhou, Y. and Zheng, Y. (2014). Facile approach to synthesize g-PAN/g-C3N4 composites with enhanced photocatalytic H$_2$ evolution activity, Applied Materials and Interfaces, Vol. 6, pp. 7171-7179.

Heikkilä, P. and Harlin, A. (2008). Parameter study of electrospinning of polyamide-6, *European Polymer Journal*, Vol. 44, pp. 3067-3079.

Hochart, F., De-Jaeger, R. and Levalois-Grutzmacher, J. (2003). Graft-polymerization of a hydrophobic monomer onto PAN textile by low-pressure plasma treatments, *Surface and Coating Technology*, Vol. 165, pp. 201-210.

Hohman, M.M., Shin, M., Rutledge, G. and Brenner, M.P. (2001). Electrospinning and electrically forced jets. II. Applications, *Physics of Fluids*, Vol. 13, pp. 2221-2236.

Hong, G., Li, X., Shen, L., Wang, M., Wang, C., Yu, X. and Wang X. (2015). High recovery of lead ions from aminated polyacrylonitrile nanofibrous affinity membranes with micro/nano structure, *Journal of Hazardous Materials*, Vol. 295, pp. 161-169.

Hong, Q., Hardcastle, J.L., McKeown, R.A.J., Marken, F. and Compton, R.G. (1999). The 20 kHz sonochemical degradation of trace cyanide and dye stuffs in aqueous media, *New Journal of Chemistry*, Vol. 23, pp. 845-849.

Horzum, N., Shahwan, T., Parlak, O. and Demir, M. (2012). Synthesis of amidoximated polyacrilonitrile fibers and its application for sorption of aqueous uranyl ions under continues flow, *Chemical Engineering Journal*, Vol. 213, pp. 41-49.

Huang, F., Xu, Y., Liao, S., Yang, D., Hsieh, Y. and Wei, Q. (2013). Preparation of Amidoxime Polyacrylonitrile Chelating Nanofibers and Their Application for Adsorption of Metal Ions, *Materials*, Vol. 6, pp. 969-980.

Huang, L., Apkarian, R.P. and Chaikof, E.L. (2001). High-Resolution analysis of engineered type I collagen nanofibers by electron microscopy, *Scanning*, Vol. 23, pp. 372-375.

References

Huang, L., McMillan, R.A., Apkarian, R.P., Pourdeyhimi, B., Conticello, V.P. and Chaikof, E.L. (2000). Generation of synthetic elastin-mimetic small diameter fibers and fiber networks, *Macromolecules*, Vol. 33, No. 8, pp. 2989-2997.

Huang, Z., Zhang, Y., Kotaki, M. and Ramakrishna, S. (2003). A review on polymer nanofibers by electrospinning and their applications in nanocomposites, *Composite Science and Technology*, Vol. 63, pp. 2223-2253.

Huang, Z.M., Zhang, Y.Z., Ramakrishna, S. and Lim, C.T. (2004). Electrospinning and mechanical characterization of gelatin nanofibres, *Polymer*, Vol. 45, pp. 5361-5368.

Hubicki, Z. and Kołodyńska, D. (2012). Selective Removal of Heavy Ions from waters and Waste Waters Using Ion Exchange, Licensee InTech (http://creativecommons.org/licenses/by/3.0).

Hunger, K. (2003). Industrial Dyes: Chemistry, Properties and Applications, *Wiley-VCH Weinheim*, Cambridge.

Husain, Q. (2006). Potential applications of the oxidoreductive enzymes in the decolorization and detoxification of textile and other synthetic dyes from polluted water: a review, *Critical Reviews in Biotechnology*, Vol. 26, pp. 201-221.

Im, J., Kim, M. and Lee, Y. (2008). Preparation of PAN-based electrospun nanofiber webs containing TiO_2 for photocatalytic degradation, *Materials Letters*, Vol. 62, pp. 3652-3655.

Imamura, K., Ikeda, E., Nagayasu, T., Sakiyama, T. and Nakanishi, K. (2002). Adsorption behavior of methylene blue and its congeners on a stainless steel surface, *Journal of Colloid Interface Science*, Vol. 245, pp. 50-57.

Inai, R., Kotaki, M. and Ramakrishna, S. (2005). Structure and properties of electrospun PLLA single nanofibres, *Nanotechnology*, Vol. 16, pp. 208-213.

Ishimura, F. and Seijo, H. (1991). Immobilization of penicillin acylase using porous polyacrylonitrile fibres, *Journal of Fermentation Bioengineering*, Vol. 17, pp. 140-143.

References

Ishtchenko, V., Huddersman, K. and Vitkovskaya, R. (2003). Production of a modified PAN fibrous catalyst and its optimisation towards the decomposition of hydrogen peroxide, *Applied Catalysis*, Vol. 242, pp. 123-137.

Islam, M.S., Ahmed, M.K., Raknuzzaman, M., Habibullah-Al-Mamun, M. and Islam, M.K. (2015). Heavy metal pollution in surface water and sediment: A preliminary assessment of an urban river in a developing country, *Ecological Indicators*, Vol. 48, pp. 282-291.

Iwata, M., Adachi, T., Tomidokoro, M., Ohta, M. and Kobayashi, T. (2003). Hybrid sol–gel membranes of polyacrylonitrile–tetraethoxysilane composites for gas permselectivity, *Journal of Applied Polymer Science*, Vol. 88, No. 7, pp. 1752-1759.

Jaeger, R., Schonherr, H. and Vancso, G.J. (1996). Chain packing in electrospun poly(ethylene oxide) visualized by atomic force microscopy, *Macromolecules*, Vol. 29, pp. 7634-7636.

Jain, S., Chattopadhyay, S., Jackeray, R. and Singh, H. (2009). Surface modification of polyacrylonitrile fiber for immobilization of antibodies and detection of analyte, *Analytica Chimica Acta*, Vol. 654, pp. 103-110.

Jal, P.K., Patel, S. and Mishra, B.K. (2004). Chemical modification of silica surface by immobilization of functional groups for extractive concentration of metal ions, *Talanta*, Vol. 62, pp. 1005–1028.

Jarusuwannapoom, T., Hongroijanawiwat, W., Jitjaicham, S., Wannatong, L., Nithitanakul, M., Pattamaprom, C., Koombhongse, P., Rangkupan, R. and Supaphol, P. (2005). Effect of solvents on electro-spinnability of polystyrene solutions and morphological appearance of resulting electrospun polystyrene fibers, *European Polymer Journal*, Vol. 41, pp. 409-421.

Ji, L., Medford, A. and Zhang, X. (2009). Electrospun polyacrylonitrile/zinc chloride composite nanofibers and their response to hydrogen sulfide, *Polymer*, Vol. 50, pp. 605-612.

References

Jia, Z. and Du, S. (2006). Grafting of casein onto polyacrilonitrile fiber for surface modification, *Fibers and Polymers*, Vol. 7, pp. 235-240.

Jia, Z. and Yang, Y. (2007). Surface modification of polyacrylonitrile (PAN) fibers by grafting of natural polymer—soybean protein (SP), *Polymer Bulletins*, Vol. 59, pp. 13-23.

Jin, L. and Bai, R. (2002). Mechanisms of lead adsorption on chitosan/PVA hydrogel beads, *Langmiur*, Vol.18, pp. 9765-9770.

Jin, X.C., Liu, G.Q., Xu, Z.H. and Tao, W.Y. (2007). Decolorization of a dye industry effluent by Aspergillus fumigatus XC6, *Applied Microbiology and Biotechnology*, Vol. 74, pp. 239-243.

Jing, L., Shim, K., Toe, C.Y, Fang, T., Zhao, C., Amal, R., Sun, K., Kim, J.H. and Ng, Y.H. (2016). Electrospun Polyacrylonitrile−Ionic Liquid Nanofibers for Superior PM2.5 Capture Capacity, *ACS Applied Material Interfaces*, Vol. 8, pp. 7030-7036.

Jun, Z., Hou, H., Schaper, A., Wendorff, J.H. and Greiner, A. (2003). Poly-L-lactide nanofibers by electrospinning — influence of solution viscosity and electrical conductivity on fiber diameter and fiber morphology, *e-Polymer*, Vol. 9, pp. 1-9.

Kago, T., Goto, A., Kusakabe, K. and Morooka, S. (1992). Preparation and Performance of Amidoxime Fiber Adsorbents for Recovery of Uranium from Seawater, *Industrial and Engineering Chemistry Research*, Vol. 31, pp. 204-209.

Kampalanonwat, P. and Supaphol, P. (2014). The Study of Competitive Adsorption of Heavy Metal Ions from Aqueous Solution by Aminated Polyacrylonitrile Nanofiber Mats11th Eco-Energy and Materials Science and Engineering (11th EMSES), *Energy Procedia*, Vol. 56, pp. 142 – 151.

Kampalanonwat, P. and Supaphol, P. (2010). Preparation and Adsorption Behavior of Aminated Electrospun Polyacrilonitrile Nanofiber Mats for Heavy Metal Ion Removal, *Applied materials and interphases*, Vol. 2, No.12, pp. 3619-3627.

References

Kampalanonwat, P. and Supaphol, P. (2011). Preparation of Hydrolyzed Electrospun Polyacrylonitrile Fiber Mats as Chelating Substrates: A Case Study on Copper(II) Ions, *Industrial and Engineering Chemistry Research*, Vol. 50, pp. 11912-11921.

Kansal, S.K., Singh, M. and Sud, D. (2007). Studies on photodegradation of two commercial dyes in aqueous phase using different photocatalysts, *Journal of Hazardous Materials*, Vol. 141, pp. 581-590.

Khezami, L. and Capart, R. (2005). Removal of chromium(VI) from aqueous solution by activated carbons: kinetic and equilibrium studies, *Journal of Hazardous Materials*, Vol. 123, pp. 223-231.

Khil, M.S., Cha, D.I., Kim, H.Y., Kim, I.S. and Bhattarai, N. (2003). Electrospun nanofibrous polyurethane membrane as wound dressing, *Journal Biomedical Materials Research B*, Vol. 67, pp. 675-679.

Ki, C.S., Baek, D.H., Gang, K.D., Lee, K.H., Um, I.C. and Park, Y.H. (2005). Characterization of gelatin nanofiber prepared from gelatin-formic acid solution, *Polymer*, Vol. 46, pp. 5094-5102.

Kidoaki, S., Kwon, I.K. and Matsuda, T. (2005). Mesoscopic spatial designs of nano and microfiber meshes for tissue-engineering matrix and scaffold based on newly devised multilayering and mixing electrospinning techniques, *Biomaterials*, Vol. 26, pp. 37-46.

Kim, H.S., Kim, K., Jin, H.J. and Chin, I.J. (2005a). Morphological characterization of electrospun nano-fibrous membranes of biodegradable poly(L-lactide) and poly(lactideco- glycolide), *Macromolecular Symposia*, Vol. 224, pp. 145-54.

Kim, J.S. and Lee, D.S. (2000). Thermal properties of electrospun polyesters, *Polymer Journal*, Vol. 32, No. 7, pp. 616-618.

Kim, J.S. and Reneker, D.H. (1999). Mechanical properties of composites usingnultrafine electrospun fibers, sites, *Polymer Composite*, Vol. 20, pp. 124-131.

References

Kim, S.J., Lee, C.K. and Kim, S.I. (2005b). Effect of ionic salts on the processing of poly (2-acrylamido-2-methyl-1-propane sulfonic acid) nanofibres, *Journal of Applied Polymer Science*, Vol. 96, pp. 1388-1393.

Kisku, G.C., Pandey, P., Negi, M.P.S. and Misra, V. (2011). Uptake and accumulation of potentially toxic metals (Zn, Cu and Pb) in soils and plants of the Durgapur Industrial Belt, *Journal of Environmental Biology*, Vol. 32, No. 6, pp. 831-838.

Ko, F.K. (2006). Nanofiber technology in nanotubes and nanofibers (advanced materials). Yury Gogotsi, editor, *Taylor and Francis Group LLC.*

Ko, Y., Choi, U., Park, Y. and Woo, J. (2004). Fourier Transform Infrared Spectroscopy Study of the Effect of pH on Anion and Cation Adsorption onto Poly(acryloamidinodiethylenediamine), *Journal of Polymer Science: Part A: Polymer Chemistry*, Vol. 42, pp. 2010-2018.

Kobuke, Y., Aoki, T., Tanaka, H., Tabushi, I., Kamaishi, T. and Hagiwara, I. (1990). Recovery of Uranium from Seawater by Composite Fiber Adsorbent, *Industrial and Engineering Chemistry Research*, Vol. 29, pp. 1662-1668.

Koombhongse, S., Liu, W. and Reneker, D.H. (2001). Flat ribbons and other shapes by electrospinning, *Journal of Polymer Science-Polymer Physics*, Vol. 39, pp. 2598-2606.

Korobeinyk, A.V., Whitby, R.L. and Mikhalovsky, S.V. (2012). High temperature oxidative resistance of polyacrylonitrile-methylmethacrylate copolymer powder converting to a carbonized monolith, *European Polymer Journal*, Vol. 48, 97–104.

Kurniawan, T., Chan, G., Lo, W. and Babel, S. (2006). Physicochemical treatment techniques for wastewater laden with heavy metals, *Chemical Engineering Journal*, Vol. 118, pp. 83-98.

Lacour, S., Bollinger, J., Serpaud, B., Chantron, P. and Arcos, R. (2001). Removal of heavy metals in industrial waste waters by ion-exchanger grafted textiles, *Analytica Chimica Act*, Vol. 16, pp. 899-905.

References

Lawrence, N.D., Perera, J.M., Iyer, M., Hickey, M.W. and Stevens, G.W. (2006). The Use of Streaming Potential Measurements to Study the Fouling and Cleaning of Ultrafiltration Membranes, *Separation and Purification Technology*, Vol. 48, pp. 106-112.

Lee, J.S., Choi, K.H., Ghim, H.D., Kim, S.S., Chun, D.H. and Kim, H.Y. (2004). Role of molecular weight of a tactic poly (vinyl alcohol) (PVA) in the structure and properties of PVA nanofabric prepared by electrospinning, *Journal of Applied Polymer Science*, Vol. 93, pp. 1638-1646.

Lee, J.W., Choi, S.P., Thiruvenkatachari, R., Shim, W.G. and Moon, H. (2006). Evaluation of the performance of adsorption and coagulation processes for the maximum removal of reactive dyes, *Dyes Pigments*, Vol. 69, pp. 196-203.

Lee, S., Ku, B.C., Wang, X., Samuelson, L.A. and Kumar, J. (2002). Design, synthesis and electrospinning of a novel fluorescent polymer for optical sensor applications, *Material Research Society Symposium Proceedings*, Vol. 708, pp. 403-408.

Leiriao, P., Fonseca, L., Taipa, M., Cabral, J. and Mateus, M. (2003). Horseradish Peroxidase Immobilized Through Its Carboxylic Groups onto a Polyacrylonitrile Membrane, *Applied Biochemistry and Biotechnology*, Vol. 110, pp. 1-10.

LeVan, M.D., Carta, G., Yon, C.M., Perry, R.H., Green, D.W. and Maloney, J.O. (1997). Adsorption and Ion Exchange, *Perry's chemical engineers' handbook, McGraw-Hill*, seventh ed., New York.

Li, D. and Xia, Y. (2004). Electrospinning of nanofibers: reinventing the wheel, *Advance Materials*, Vol. 16, pp. 1151-1170.

Li, D., Wang, Y. and Xia, Y. (2004). Electrospinning nanofibers as uniaxially aligned arrays and layerby-layer stacked films, *Advance Materials*, Vol. 16, pp. 361–366.

Li, W.J., Laurencin, C.T., Caterson, E.J., Tuan, R.S. and Ko, F.K. (2002). Electrospun nanofibrous structure: A novel scaffold for tissue engineering, *Journal of Biomedical Materials Research*, Vol. 60, No.4, pp. 613–621.

References

Li, Z., Huang, H., Shang, T., Yang, F., Zheng, W., Wang, C. and Manohar, S. (2006). Facile synthesis of single-crystal and controllable sized silver nanoparticles on the surfaces of polyacrylonitrile nanofibres, *Nanotechnology*, Vol. 17, pp. 917-920.

Liang, Y., Ji, L., Guo, B., Lin, Z., Yao, Y. and Li, Y. (2011). Preparation and electrochemical characterization of ionic conducting lithium lanthanum titanate oxide/polyacrylonitrile submicron composite fiber-based lithium-ion battery separators, *Journal of Power Sources*, Vol. 196, pp. 436-441.

Lin, S.H. and Peng, C.F. (1994). Treatment of textile wastewater by electrochemical method, *Water Resources*, Vol. 28, pp. 277-282.

Liu, C.H., Wu, J.S., Chiu, H.C., Suen, S.Y. and Chu, K.H. (2007). Removal of anionic reactive dyes from water using anion exchange membranes as adsorbers, *Water Resources*, Vol. 41, pp. 1491-1500.

Liu, H., Kameoka, J., Czaplewski, D.A. and Craighead, H.G. (2004). Polymeric nanowire chemical sensor, *Nano Letter*, Vol. 4, pp. 671-675.

Liu, H.Q. and Hsieh, Y.L. (2002). Ultrafine fibrous cellulose membranes from electrospinning of cellulose acetate, *Journal of Polymer Science Part B Polymer Physics*, Vol. 40, pp. 2119-2129.

Liu, R., Li, Y. and Tang, H. (1999). Application of the Modified Polyacrylonitrile Fiber with Amino-Carboxyl-Tetrazine Groups for the Preconcentration of Trace Heavy Metal Ions, *Journal of Applied Polymer Science*, Vol. 74, 2631-2636.

Liu, W., Wang, M., Xing, Z., Qi, Y. and Wu, G. (2012). Radiation-induced crosslinking of polyacrylonitrile fibers and the subsequent regulative effect on the peroxidation process, *Radiation Physics and Chemistry*, Vol. 81, pp. 622–627.

Lohokare, H., Kumbharkar, S., Bhole Y. and Kharul, U. (2006). Surface Modification of Polyacrylonitrile Based Ultrafiltration Membrane, *Journal of Applied Polymer Science*, Vol. 101, 4378-4385.

References

Lohokare, H., Muthu, M., Agarwal, G. and Kharul, U. (2008). Effective arsenic removal using polyacrylonitrile-based ultrafiltration (UF) membrane, *Journal Membrane Science*, Vol. 320, pp. 159-166.

Lu, J.W., Zhang, Z.P., Ren, X.Z., Chen, Y.Z., Yu, J. and Guo, Z.X. (2008). High-elongation fiber mats by electrospinning of polyoxymethylene, *Macromolecules*, Vol. 41, pp. 3762-3764.

Lueck, H.B., Matthes, H., Gemende, B., Heinrich, B., Pfestorf, W., Seidel, W. and Turuc, S. (1990). Production of particle-track membranes by means of a 5 MeV tandem accelerator, *Nuclear Instruments and Methods B*, Vol. 50, pp. 395-400.

Lyons, J. and Ko, F. (2005). Melt electrospinning of polymers: a review, *Polymer News*, Vol. 30, pp. 1 -9.

Lyons, J., Li, C. and Ko, F. (2004). Melt-electrospinning part I: processing parameters and geometric properties, *Polymer*, Vol. 45, pp. 7597-7603.

Ma, X.J., Li, Y.F., Ye, Z.F., Yang, L.Q., Zhou, L.C. and Wang, L.Y. (2011). Novel chelating resin with cyanoguanidine group: useful recyclable materials for Hg(II) removal in aqueous environment, *Journal of Hazardous Materials*, Vol. 185, pp. 1348-1354.

Machenbach, I. (1998). Membrane technology for dye house effluent treatment, *Membrane Technology*, Vol. 58, pp. 7-10.

Madrakian, T., Afkhami, A. and Mousavi, A. (2007). Spectrophotometric determination of trace amounts of uranium (VI) in water samples after mixed micelle-mediated extraction, *Talanta,* Vol. 71, No. 2, pp. 610-614.

Marcucci, M., Nosenzo, G., Capannelli, G., Ciabatti, I., Corrieri, D. and Ciardelli, G. (2001). Treatment and reuse of textile effluents based on new ultrafiltration and other membrane technologies, *Desalination*, Vol. 138, pp. 75-82.

Matheyarasu, R., Seshadri, B., Bolan N. and Naidu, R. (2015). Impacts of Abattoir Waste-Water Irrigation on Soil Fertility and Productivity, Irrigation and Drainage -

References

Sustainable Strategies and Systems, Dr. Muhammad Salik Javaid (Ed.), InTech, DOI: 10.5772/59312.

Mckee, M.G., Wilkes, G.L., Colby, R.H. and Long, T.E. (2004). Correlations of solution rheology with electrospun fiber formation of linear and branched polyesters, *Macromolecules*, Vol. 37, pp. 1760.

Meena, A.K., Kadirvelu, K., Mishra, G.K., Rajagopal, C. and Nagar, P.N. (2008). Adsorptive removal of heavy metals from aqueous solution by treated sawdust (Acacia arabica), *Journal of Hazardous Materials*, Vol. 150, No. 3, pp. 604-611.

Megelski, S., Stephens, J.S., Chase, D.B. and Rabolt, J.F. (2002). Micro- and nanostructured surface morphology on electrospun polymer fibers, *Macromolecules*, Vol. 35, No. 22, pp. 8456-8466.

Mei, Y., Yao, C., Fan, K. and Li, X. (2012). Surface modification of polyacrylonitrile nanofibrous membranes with superior antibacterial and easy-cleaning properties through hydrophilic flexible spacers, *Journal of Membrane Science*, Vol. 417-418, pp. 20-27.

Meric, S., Kaptan, D. and Tunay, C. (2003). Removal of color and COD from a mixture of four reactive azo dyes using Fenton oxidation process, *Journal of Environmental Science and Health Part A*, Vol. 38, pp. 2241-2250.

Mignani, M., Nosenzo, G. and Gualdi, A. (1999). Innovative ultrafiltration for wastewater reuse, *Desalination*, Vol. 124, pp. 287-292.

Mishra, A., Bajpai, M. and Pandey, S. (2006). Removal of dyes by biodegradable flocculants: a lab scale investigation, *Separation Science and Technology*, Vol. 41, pp. 583-593.

Mit-Uppatham, C., Nithitanakul, M., and Supaphol, P. (2004). Ultrafine electrospun polyamide-6 fibers: effect of solution conditions on morphology and average fiber diameter, *Macromolecular Chemistry and Physics*, Vol. 205, pp. 2327-2338.

References

Morooka, S., Kato, T., Inada, M., Kago, T. and Kusakabe, K. (1991). Modeling of an Adsorption Unit Packed with Amidoxime Fiber Balls for the Recovery of Uranium from Seawater, *Industrial and Engineering Chemistry Research*, Vol., 30, pp. 190-196.

Musale, D. and Kulkarni, S. (1997). Relative rates of protein transmission through poly(acrylonitrile) based ultrafiltration membranes, *Journal of Membrane Science*, Vol. 136, pp. 13-23.

Musyoka, S., Ngila, C., Moodley, B., Kindness, A., Petrik, L. and Greyling, C. (2011). Oxolane-2,5-dione modified electrospun cellulose nanofibers for heavy metals Adsorption, *Journal of Hazardous Materials*, Vol. 192, pp. 922– 927.

Namasivayam, C. and Kadirvelu, K. (1999). Uptake of mercury (II) from wastewater by activated carbon from unwanted agricultural solid by-product: coirpith, *Carbon* Vol. 37, pp. 79-84.

Namboodri, C.G. and Walsh, W.K. (1996). UV light/H_2O_2 system for decolorizing spent reactive dye-bath wastewater, *America Dyestuff Report*, Vol. 85, pp. 27-36.

Naraghi, M., Chasiotis, I., Kahn, H., Wen, Y. and Dzenis, Y. (2007). Novel method for mechanical characterization of polymeric nanofibres, *Review of Scientific Instruments*, Vol. 78, pp. 1-7.

Naseem, R. and Tahir, S.S. (2001). Removal of Pb(II) from aqueous solution by using bentonite as an adsorbent, *Water Resources*, Vol. 35, pp. 3982-3986.

Nataraj, S., Yang, K. and Aminabhavi, T. (2012). Polyacrylonitrile-based nanofibers—A state-of-the-art review, *Progress in polymer science*, Vol. 37, pp. 487-513.

Ndayambaje, G., Laatikainen, K., Laatikainen, M., Beukes, E., Fatoba, O., Van der Walt, N., Petrik, L. and Sainio, T. (2016). Adsorption of nickel(II) on polyacrylonitrile nanofiber modified with 2-(20-pyridyl)imidazole, *Chemical Engineering Journal*, Vol. 284, pp. 1106-1116.

References

Neghlani, P., Rafizadeh, M. and Taroni, F. (2011). Preparation of aminated-polyacrilonitrile nanofiber membranes for the adsorption of metal ions: Comparison with microfibers, *Journal of Hazardous Materials*, Vol. 186, pp. 182-189.

Nesteronok, P. and Soldatov, V. (2012). Acid-base properties of ion exchangers (IV) Synthesis and potentiometric analysis of polyampholytes on the base of polyacrilonitrile fibers, *Solvent Extraction and Ion Exchange*, Vol. 30, pp. 414-422.

Nilchi, A., Babalou, A.A. and Rafiee, R. (2008a). Adsorption properties of amidoxime resins for separation of metal ions from aqueous systems, *Reactive and Functional Polymer*, Vol. 68, pp. 1665-1670.

Nilchi, A., Rafiee, R. and Babalou, A. A. (2008b). Adsorption Behavior of Metal Ions by Amidoxime Chelating Resins, *Macromolecular Symposia*, Vol. 274, pp. 101–108.

Nirmala, R., Navamathavan, R., Park, S. and Kim, H.Y. (2014). Recent Progress on the Fabrication of Ultrafine Polyamide-6 Based Nanofibers Via Electro- spinning: A Topical Review, *Nano-Micro Letters*, Vol. 6, No. 2, pp. 89-107.

Nirmala, R., Panth, H.R., Yi, C., Nam, K.T, Park, S., Kim, H.Y. and Navamathavan, R. (2010). Effect of Solvents on High Aspect Ratio Polyamide-6 Nanofibers *via* Electrospinning, *Macromolecular Research*, Vol. 18, No. 8, pp. 759-765.

Norris, I.D, Shaker, M.M., Ko, F.K. and Macdiarmid, A.G. (2000). Electrostatic fabrication of ultrafine conducting fibers: polyaniline/polyethylene oxide blends, *Synthetic Metals*, Vol. 114, No. 2, pp. 109-114.

Nur, H., Manan, A.F.N.A., Wei, L.K., Muhid, M.N.M. and Hamdan, H. (2005). Simultaneous adsorption of a mixture of paraquat and dye by NaY zeolite covered with alkylsilane, *Journal of Hazardous Materials*, Vol. 117, pp. 35-40.

Oliveira, F.H., Osugi, M.E., Paschoal, F.M.M., Profeti, D., Olivi, P. and Zanoni, M.V.B. (2007). Electrochemical oxidation of an acid dye by active chlorine generated using Ti/Sn, Ir/O(2) electrodes, *Journal of Applied Electrochemistry*, Vol. 37, pp. 583-592.

References

Omura, T. (1994). Design of chlorine-fast reactive dyes and degradation of amino containing azo dyes by sodium-hypochlorite, *Dyes Pigments*, Vol. 26, pp. 33-50.

Papageorgiou, G., Tsanaktsis, V. and Bikiaris, D. (2014). Synthesis of poly(ethylene furandicarboxylate) polyester using monomers derived from renewable resources: thermal behavior comparison with PET and PEN, *Physical Chemistry Chemical Physics*, Vol. 16, pp. 7946-7958.

Pekel, N., Sahiner, N. and Guven, O. (2000). Development of new chelating hydrogels based on N-vinyl imidazole and acrylonitrile, *Radiation Physics and Chemistry*, Vol. 59, pp. 485-491.

Pelekani, C. and Snoeyink, V.L. (2000). Competitive adsorption between Atrazine and Methylene Blue on activated carbon: the importance of pore size distribution, *Carbon*, Vol. 38, pp. 1423-1436.

Peppas, A., Komnitsas, K. and Halikia, I. (2000). Use of organic covers for acid mine drainage control, *Minerals Engineering*, Vol. 13, pp. 563-574.

Pereao, O. K., Bode-Aluko, C., Ndayambaje, G., Fatoba, O. and Petrik, L. F. (2016). Electrospinning: Polymer Nanofibre Adsorbent Applications for Metal Ion Removal, *Journal of Polymer and Environment*, DOI 10.1007/s10924-016-0896-y.

Perkins, W.S., Walsh, W.K., Reed, I.E. and Namboodri, C.G. (1996). A demonstration of reuse of spent dyebath water following color removal with ozone, *Textile Chemistry Colour*, Vol. 28, pp. 31-37.

Pham, Q., Sharma, U. and Mikos, A. (2006). Electrospinning of polymeric nanofibers for tissue engineering applications: a review, *Tissue Engineering*, Vol. 12, pp. 1197-1211.

Powell, K.J., Brown, P.L., Byrne, R.H., Gajda, T., Hefter, G., Leuz, A.K., Sjoberg, S. and Wanner, H. (2009). Chemical speciation of environmentally significant metals with inorganic ligands. Part 3: the Pb^{2+}, OH^-, Cl^-, CO_3^{2-}, SO_4^{2-}, and PO_4^{3-} systems (IUPAC technical report), *Pure and Applied Chemistry*, Vol. 81, pp. 2425–2476.

References

Pramoda, K.P., Liu, T., Liu, Z., He, C. and Sue, H. (2003). Thermal degradation behavior of polyamide 6/clay nanocomposites, *Polymer Degradation and Stability*, Vol. 81, pp. 47–56.

Raeesi, F., Nouri, M. and Haghi, A.K. (2009). Electrospinning of polyaniline-polyacrylonitrile blend Nanofibres, *e-Polymers*, Vol. 114, pp. 1-13.

Raghu, S. and Ahmed-Basha, C. (2007). Chemical or electrochemical techniques, followed by ion exchange, for recycle of textile dye wastewater, *Journal of Hazardous Materials*, Vol. 149, pp. 324-330.

Rai, H.S., Bhattacharyya, M.S., Singh, J., Bansal, T.K., Vats, P. and Banerjee, U.C. (2005). Removal of dyes from the effluent of textile and dyestuff manufacturing industry: a review of emerging techniques with reference to biological treatment, *Critical Reviews in Environmental Science and Technology*, Vol. 35, pp. 219-238.

Ramakrishna, S., Fujihara, K., Teo, W.E., Lim, T.C. and Ma, Z. (2005). An introduction to electrospinning and nanofibres, *World Scientific*, Singapore.

Reneker, D.H., Yarin, A.L., Fong, H. and Koombhongse, S. (2000). Bending instability of electrically charged liquid jets of polymer solutions in electrospinning, *Journal of Applied Physics*, Vol. 87, pp. 4531-4547.

Robinson, T., McMullan, G., Marchant, R. and Nigam, P. (2001). Remediation of dyes in textile effluent: a critical review on current treatment technologies with a proposed alternative, *Bioresource Technology*, Vol. 77, pp. 247-255.

Rodríguez, A.M., Gómez-Límón, D. and Alguacil, F.J. (2005). Liquid–liquid extraction of cadmium (II) by Cyanex 923 and its application to a solid-supported liquid membrane system, *Journal of Chemical Technology and Biotechnology*, Vol. 80, No. 9, pp. 967-972.

Rosner, T. (1999). The environmental impact of seepage from gold mine tailings dams near Johannesburg, South Africa, Phd Thesis University of Pretoria.

References

Rossignol, N.J., Jaouen, P., Robert, J.M. and Quéméneur, F. (2000). Production of exocellular pigment by the marine diatom *Haslea ostrearia* Simonsen in a photobioreactor equipped with immersed ultrafiltration membranes, *Biotechnology*, Vol. 73, pp. 197-200.

Rossouw, A., Artoshina, O. V., Nechaev, A. N., Apel, P. Y., Petrik, L., Perold, W. J. and Pineda-Vargas, C. A. (2015). Stable Ion Beam Analysis (RBS and PIXE) Study of Photocatalytic Track-Etched Membranes. Exotic Nuclei (IASEN-2013) - Proceedings of the First International African Symposium on Exotic Nuclei. Edited by Erastovich, P.P. et al., *World Scientific Publishing Co. Pte. Ltd.*, pp. 591-596.

Rothman, J.E. and Orci, L. (1990). Movement of proteins through the Golgi stack: a molecular dissection of vesicular transport, *FASEB Journal*, Vol. 4, pp. 1460-1468.

Ryu, Y.J., Kim, H.Y., Lee, K.H., Park, H.C. and Lee, D.R. (2003). Transport properties of electrospun nylon 6 nonwoven mats, *European Polymer Journal*, Vol. 39, pp. 1883.

Saeed, K., Haider, S., Oh, T. and Park, S. (2008). Preparation of amidoxime-modified polyacrylonitrile (PAN-oxime) nanofibres and their applications to metal ions adsorption, *Journal of Membrane Science*, Vol. 322, pp. 400-405.

Saeed, K., Park, S. and Oh, T. (2011). Preparation of Hydrazine-Modified Polyacrylonitrile Nanofibers for the Extraction of Metal Ions from Aqueous Media, *Journal of Applied Polymer Science*, Vol. 121, pp. 869-873.

Safi, I. (2000). Recent aspects concerning DC reactive magnetron sputtering of thin films: a review, *Surface and Coatings Technology*, Vol. 127, pp. 203-219.

Saini, G.S.S., Kaur, S., Tripathia, S.K., Mahajan, C.G., Thanga, H.H. and Verma, A.L. (2005). Spectroscopic studies of rhodamine 6G dispersed in polymethylcyanoacrylate, *Spectrochimica Acta Part A*, Vol. 61, pp. 653–658.

Salgın, S., Takac, S. and Zdamar, T.H. (2006). Effect of ionic environments on the adsorption and diffusion characteristics of serine alkaline protease enzyme in

References

polyethersulfone ultrafiltration membranes, *Journal of Colloid and Interface Science*, Vol. 299, pp. 806-814.

Sang, Y. and Sung, H. (2003). Preparation and characterization of polypropylene/silver nanocomposite fibers, *Polymer international*, Vol. 52, pp. 1053-1057.

Sanguineti, G., Le, H.V. and Ganem, B. (2011). Studies on the synthesis of amidoximes from nitroalkanes, *Tetrahedron*, Vol. 67, pp. 10208-10211.

Sani, R. and Banerjee, U. (1999). Decolorization of acid green 20, a textile dye, by the white rot fungus Phanerochaete chrysosporium, *Advances in Environmental Research*, Vol. 2, pp. 485-490.

Saurer management AG, (2004). The Fiber Year 2003, *The Saurer Group*, Winterthur, Switzerland.

Schreuder-Gibson, H.L, Gibson, P., Senecal, K., Sennett, M., Walker, J. and Yeomans, W. (2002). Protective textile materials based on electrospun nanofibres, *Journal of Advanced Materials*, Vol. 34, No. 3, pp. 44-55.

Schreuder-Gibson, H.L. and Gibson, P. (2002). Transport properties of electrospun nonwoven membranes, *International Nonwoven Journal*, Vol. 11, No.2, pp. 21-26.

Senturk, B.B, Ozdes, D. and Duran, C. (2010). Biosorption of Rhodamine 6G from aqueous solutions onto almond shell (Prunus dulcis) as a low cost biosorbent, *Desalination*, Vol. 252, pp. 81–87.

Sergent-Engelen, T., Halleux, C., Ferain, E., Hanot, H., Legras, R. and Schneider, Y.J. (1990). Improved cultivation of polarized animal cells on culture inserts with new transparent PETP or polycarbonate microporous membranes, *Biotechnology Techniques*, Vol. 4, pp. 89-94.

Shah, M. (2014). Effective Treatment Systems for Azo Dye Degradation: A Joint Venture between Physico-Chemical & Microbiological Process, *International Journal of Environmental Bioremediation & Biodegradation*, Vol. 2, No. 5, pp. 231-242.

References

Shenoy, S.L., Bates, W.D., Frisch, H.L. and Wnek, G.E. (2005). Role of chain entanglements on fiber formation during electrospinning of polymer solutions: good solvent, non-specific polymer-polymer interaction limit, *Polymer*, Vol. 46, No. 10, pp. 3372-3384.

Sherrington, D.C. (1998). Preparation, structure and morphology of polymer supports, *Chemical Communications,* pp. 2275-2286.

Shi, B.Y., Li, G.H., Wang, D.S., Feng, C.H. and Tang, H.X. (2007). Removal of direct dyes by coagulation: the performance of preformed polymeric aluminum species, *Journal of Hazardous Materials*, Vol. 143, pp. 567-574.

Shi, T., Wang, Z., Liu, Y., Jia, S. and Du, C. (2009). Removal of hexavalent chromium from aqueous solutions by D301, D314 and D354 anion-exchange resins, *Journal Hazardous Materials*, Vol. 161, pp. 900-906.

Shields, K.J., Beckman, M.J. and Bowlin, G.L. (2004). Mechanical properties and cellular proliferation of electrospun collagen type II, *Tissue Engineering*, Vol. 10, pp. 1510-1517.

Shin, D., Ko, Y., Choi, U. and Kim, W. (2004). Design of high efficiency chelate fibers with an amine group to remove heavy metal ions and pH-related FT-IR analysis, *Industrial Engineering Chemical Resource*, Vol. 43, pp. 2060-2066.

Shoushtari, A., Zargaran, M. and Abdouss, M. (2006). Preparation and characterization of high efficiency ion-exchange crosslinked acrylic fibers, *Journal of Applied Polymer Science,* Vol. 101, pp. 2202-2209.

Sill, T.J. and Recum, H.A.V. (2008). Electrospinning: applications in drug delivery and tissue engineering, *Biomaterials*, Vol. 29, pp. 1989-2006.

Simon, Y.W.S., Lutfor, M.R., Arshad, S.E., Loumie, S.N. and Baba, M. (2011). Synthesis and characterization of poly(hydroxamic acid)-poly (amidoxime) chelating ligands from polymer-grafted acacia cellulose, *Journal of Applied Polymer Science*, Vol. 124, pp. 4443–4451.

References

Sin, S.N., Chua, H., Lo, W. and Ng, L.M. (2001). Assessment of heavy metal cations in sediments of Shing Mun River, Hong Kong, *Environment International*, Vol. 26, No. 5-6, pp. 297-301.

Soltanzadeh, M., Kiani, G. and Khataee, A. (2013). Adsorptive Capacity of Polyacrylonitrile Modified with Triethylenetetramine for Removal of Copper and Cadmium Ions from Aqueous Solutions, *Environmental Progress and Sustainable Energy*, 00:1-9.

Sostar-Turk, S., Simonic, M. and Petrinic, I. (2005). Wastewater treatment after reactive printing, *Dyes Pigments*, Vol. 64, pp. 147-152.

Srinivasan, G. and Reneker, D.H. (1995). Structure and morphology of smalldiameter electrospun aramid fibers, *Polymer International*, Vol. 36, No. 2, pp. 195-201.

Stankus, J.J., Guan, J., Fujimoto, K. and Wagner, W.R. (2006). Microintegrating smooth muscle cells into a biodegradable, elastomeric fiber matrix, *Biomaterials*, Vol.27, pp. 735-744.

Stillwell, C.R. (1996). Characterization of pore structure in filter cartridges, *Advance Filtration and Separation Technology*, Vol. 10, pp. 151-156.

Stolz, A. (2001). Basic and applied aspects in the microbial degradation of azo dyes, *Applied Microbiology and Biotechnology*, Vol. 56, pp. 69-80.

Subbiah, T., Bhat, G.S., Tock, R.W., Parameswaran, S. and Ramkumar, S.S. (2005). Electrospinning of nanofibers, *Journal of Applied Polymer Science*, Vol. 96, pp. 557-569.

Sukigara, S., Gandhi, M., Ayutsede, J., Micklus, M. and Ko, F. (2003). Regeneration of Bombyx mori silk by electrospinning—part 1: processing parameters and geometric properties, *Polymer*, Vol. 44, pp. 5721-5727.

Sundaray, B., Subramanian, V., Natarajan, T.S., Xiang, R.Z., Chang, C.C. and Fann, W.S. (2004). Electrospinning of continuous aligned polymer fibers, *Applied Physics Letter*, Vol. 84, pp. 1222-1224.

References

Supaphol, P., Mit-Uppatham, C. and Nithitanakul, M. (2005). Ultrafine electrospun polyamide-6 fibres: effect of emitting electrode polarity on morphology and average fibre diameter, *Journal Polymer Science B, Polymer Physics*, Vol. 43, No. 24, pp. 3699-3712.

Sutasinpromprae, J., Jitjaicham, S., Nithitanakul, M., Meechaisue, C. and Supaphol, P. (2006). Preparation and characterization of ultrafine electrospun polyacrylonitrile fibers and their subsequent pyrolysis to carbon fibers, *Polymer International*, Vol. 55, pp. 825-833.

Sylwester, E., Hudson, E. and Allen, P. (2000). The structure of uranium(VI) sorption complexes on silica, alumina, and montmorillonite, *Geochimica et Cosmochimica Acta* , Vol. 64, pp. 2431-2438.

Tahaei, P., Abdouss, M., Edrissi, M., Shoushtari, A. and Zargaran, M. (2008). Preparation of chelating fibrous polymer by different diamines and study on their physical and chemical properties, *Materials-Werkstofftec*, Vol. 39, pp. 839-844.

Takeda, T., Saito, K., Uezu, K., Furusaki, S., Sugo, T. and Okamoto, J. (1991). Adsorption and Elution in Hollow-Fiber-Packed Bed for Recovery of Uranium from Seawater, *Industrial and Engineering Chemistry Research*, Vol. 30, pp. 185-190.

Tan, E.P.S., Ng, S.Y. and Lim, C.T. (2005b). Tensile testing of a single ultrafine polymeric fiber, *Biomaterials*, Vol. 26, pp. 1453-1456.

Tan, S.H., Inai, R., Kotaki, M. and Ramakrishna S. (2005a). Systematic parameter study for ultra-fine fiber fabrication via electrospinning process, *Polymer*, Vol. 46, pp. 6128-6134.

Taylor, G. (1969). Electrically driven jets, *Proceedings of the Royal Society of London, Series A*, Vol. 313, pp. 453-475.

Teo, W.E. and Ramakrishna, S. (2006). A review on electrospinning design and nanofibre assemblies, *Nanotechnology*, Vol. 17, pp. 89-106.

Theron, S.A., Yarin, A.L., Zussman, E. and Kroll, E. (2005). Multiple jets in electrospinning: experiment and modeling, *Polymer*, Vol. 46, pp. 2889-2899.

References

Thomas, M., Valette, P., Mausset, A. and Dejardin, P. (2000). High molecular weight kininogen adsorption on hemodialysis membranes: Influence of pH and relationship with contact phase activation of blood plasma. Influence of pre-treatment with poly(ethyleneimine), *International Journal of Artificial Organs*, Vol. 23, pp. 20-26.

Tian, G., Wang, J., Shen, Y. and Rao, L. (2005). Extraction of strontium from HLLW using N, N, N', N'-tetraisobutyl 3-oxa-glutaramide, *Solvent extraction and ion exchange,* Vol. 23, No. 4, pp. 519-528.

Tijani, J.O., Fatoba, O.O., Madzivire, G. and Petrik, L.F. (2014). A Review of Combined Advanced Oxidation Technologies for the Removal of Organic Pollutants from Water, *Water, Air and Soil Pollution*, Vol. 225:2102.

Tong, S., von Schirnding, Y. and Prapamontol, T. (2000). Environmental lead exposure: a public health problem of global dimensions, *Bulletin of the World Health Organization*, Vol. 78, No. 9.

Topolska, K., Sawicka-Kapusta, K. and Cieslik, E. (2004). The effect of contamination of the Krakow region on heavy metals content in the organs of bank voles (Cleithrionomys glareolus, Schreber, 1780), *Polish Journal of Environmental Studies*, Vol. 13, pp. 103-109.

Treffry-Goatley, K., Buckley, C.A. and Groves, G.R. (1983). Reverse osmosis treatment and reuse of textile dye house effluents, *Desalination*, Vol. 47, pp. 313-320.

Tsou, S., Lin, H., Cheng, P., Huang, C., Wuc, J. and Wang, C. (2013). Rheological aspect on electrospinning of polyamide 6 solutions, *European Polymer Journal*, Vol. 49, pp. 3619-3629.

Tutu, H., McCarthy, T.S. and Cukrowska, E.M. (2008). The chemical characteristics of acid mine drainage with particular reference to sources, distribution and remediation: The Witwatersrand Basin, South Africa as a case study, *Applied Geochemistry*, Vol. 23, No. 12, pp. 3666-3684.

References

Tuzen, M., Uluozlu, O.D., Usta, C. and Soylak, M. (2007). Biosorption of copper(II), lead(II), iron(III) and cobalt(II) on Bacillus sphaericus-loaded Diaion SP-850 resin, *Analytica Chimica Acta*, Vol. 581, pp. 241-246.

Uddin, T., Islam, A., Mahmud, S. and Rukanuzzaman, M. (2009). Adsorptive removal of methylene blue by tea waste, *Journal of Hazardous Materials*, Vol. 164, pp. 53–60.

Ulbricht, M., Oechel, A., Lehmann, C., Tomaschewski, G. and Hicke, H. (1995). Gas-phase photoinduced graft polymerization of acrylic acid onto polyacrilonitrile ultrafiltration membranes, *Journal of Applied Polymer Science*, Vol. 55, pp. 1707-1723.

Valette, P., Thomas, M. and DeHjardin, P. (1999). Adsorption of low molecular weight proteins to hemodialysis membranes: experimental results and simulations, *Biomaterials*, Vol. 20, pp. 1621-1634.

Verreck, G., Chun, I., Peeters, J., Rosenblatt, J. and Brewster, M.E. (2003). Preparation and characterization of nanofibers containing amorphous drug dispersions generated by electrostatic spinning, *Pharmaceutical Research*, Vol. 20, pp. 810-817.
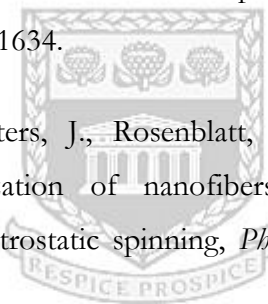
Vilensky, A.I. and Tolstikhina, A.L. (1999). Etching of tracks of accelerated heavy ions in poly(ethylene terephthalate) and some physicochemical properties of track membranes, *Russian Chemical Bulletin*, Vol. 48, No. 6, pp. 1100-1103.

Vitkovskaya, R., Rumynskaya, I., Romanova, E. and Tereshchenko, L. (2003). Fibre catalyst from modified polyacrilonitrile fibres, *Fibre chemistry*, Vol. 35, No. 3, pp. 202-207.

Walker, G.M. and Weatherley, L.R. (1999). Kinetics of acid dye adsorption on GAC, *Water Resources*, Vol. 33, pp. 1895-1899.

Walsh, G.E., Bahner, L.H. and Horning, W.B. (1980). Toxicity of textile mill effluents to freshwater and estuarine algae, crustaceans and fishes, *Environmental Pollution, A*, Vol. 21, pp. 169-179.

References

Wan, Y., He, J., Wu, Y. and Yu, J. (2006). Vibrorheological effect on electrospun polyacrylonitrile (PAN) nanofibres, *Material Letters*, Vol. 60, pp. 3296-3300.

Wang, C., Wang, L., Zhu, X., Wang, Y. and Xue, J. (2012a). Low-voltage electroosmotic pumps fabricated from track-etched polymer membranes, *The Royal Society of Chemistry*, Vol. 12, pp. 1710-1716.

Wang, J., Luo, C., Qi, G., Pan, K. and Cao, B. (2014). Mechanism study of selective heavy metal ion removal with polypyrrole-functionalized polyacrylonitrile nanofiber mats, *Applied Surface Science*, Vol. 316, pp. 245-250.

Wang, J., Lv, X., Zhao, L. and Li, J. (2011). Removal of Chromium from Electroplating Wastewater by Aminated Polyacrylonitrile Fibers, *Environmental engineering science*, Vol. 28, No. 8, pp. 585-589.

Wang, J., Yue, Z., Ince, J. and Economy, J. (2006). Preparation of nanofiltration membranes from polyacrilonitrile ultrafiltration membranes, *Journal of Membrane Science*, Vol. 286, pp. 333-341.

Wang, S. (2008). A Comparative study of Fenton and Fenton-like reaction kinetics in decolourisation of wastewater, *Dyes Pigments*, Vol. 76, pp. 714-720.

Wang, S. and Ariyanto, E. (2007). Competitive adsorption of malachite green and Pb ions on natural zeolite, *Journal of Colloid and Interface Science*, Vol. 314, pp. 25-31.

Wang, X. Chen, X. Yoon, K. Fang, D. Hsiao, B.S. and Chu, B. (2005). High flux filtration medium based on nanofibrous substrate with hydrophilic nanocomposite coating, *Environmental and Science Technology*, Vol. 39, pp. 7684-7691.

Wang, X.Y, Lee, S.H., Drew, C., Senecal, K.J., Kumar, J. and Samuelson, LA. (2002). Highly sensitive optical sensors using electrospun polymeric nanofibrous membranes, *Materials Research Society Symposium Proceedings*, Vol. 708, pp. 397-402.

Wang, Y., Ma, X., Li Y., Li, X., Yang, L., Ji, L. and He, Y. (2012b). Preparation of a novel chelating resin containing amidoxime–guanidine group and its recovery

References

properties for silver ions in aqueous solution, *Chemical Engineering Journal*, Vol. 209, pp. 394-400.

Wang, Z., Wan, L. and Xu, Z. (2007). Surface engineering of polyacrylonitrile-based asymmetric membranes towards biomedical applications: An overview, *Journal of Membrane Science*, Vol. 304, pp. 8-23.

Wannatong, L., Sirivat, A. and Supaphol, P. (2004). Effects of solvents on electrospun polymeric fibers: preliminary study on polystyrene, *Polymer International*, Vol. 53, pp. 1851-2004.

Watters, J.C., Biagtan, E. and Sener, O. (1991). Ultrafiltration of textile plant effluent, *Separation science and Technology*, Vol. 26, pp. 1295-1313.

Wen, B. and Shan, X. (2002). Improved immobilization of 8-hydroxyquinoline on polyacrylonitrile fiber and application of the material to the determination of trace metals in seawater by inductively coupled plasma mass spectrometry, *Analytical and Bioanalytical Chemistry*, Vol. 374, pp. 948-954.

Winde, F. (2006). Challenges for sustainable water use in dolomitic mining regions of South Africa- A case study of Uranium pollution Part 1: Sources and pathways, *Physical Geography*, Vol. 27, No. 4, pp. 333-347.

Winde, F. and Sandham, L. (2004). Uranium pollution in South Africa streams. An overview of the situation on gold mining area of the Witwatersrand, *Geojournal Kluiver Academic publishers*, Vol. 61, pp. 131-149.

Wong, S.C, Baji, A. and Leng, S.W. (2008). Effect of fiber diameter on tensile properties of electrospun poly(å-caprolactone), *Polymer*, Vol. 21, pp. 4713-22.

Wu, J., Doan, H. and Upreti, S. (2008a). Decolorization of aqueous textile reactive dye by ozone, *Chemical Engineering Journal*, Vol. 142, pp. 156-160.

Wu, J.S., Liu, C.H., Chu, K.H. and Suen, S.Y., (2008b). Removal of cationic dye methyl violet 2B from water by cation exchange membranes, *Journal of Membrane Science*, Vol. 309, pp. 239-245.

References

Xu, B., Wang, X. and Lu, Y. (2006). Surface modification of polyacrylonitrile-based carbon fiber and its interaction with imide, *Applied Surface Science*, Vol. 253, pp. 2695-2701.

Xu, C.Y., Inai, R., Kotaki, M. and Ramakrishna, S. (2004). Aligned biodegradable nanofibrous structure: a potential scaffold for blood vessel engineering, *Biomaterials*, Vol. 25, pp. 877-886.

Yang, S., Chen, S., Chang, Y., Cao, A., Liu, Y. and Wang, H. (2011). Removal of methylene blue from aqueous solution by graphene oxide, *Journal of Colloid and Interface Science*, Vol. 359, pp. 24–29.

Yee, W.A,, Nguyen, A.G., Lee, P.S., Kotaki, M., Liu, Y. and Tan, B.T. (2008). Stress-induced structural changes in electrospun polyvinylidene difluoride nanofibers collected using a modified rotating disk, *Polymer*, Vol. 49, pp. 4196-4203.

Yin, C. (2010). Emerging usage of plant-based coagulants for water and wastewater treatment, *Process Biochemistry*, Vol. 45, No. 9, pp. 1437-1444.

Yordem, O.S, Papila, M. and Menceloğlu, Y.Z. (2008). Effects of electrospinning parameters on polyacrylonitrile nanofiber diameter: an investigation by response surface methodology, *Materials and Design*, Vol. 29, pp. 34–44.

Yu, J., Fridrikh, S. and Rutledge, G. (2006). The role of elasticity in the formation of electrospun fibers, *Polymer*, Vol. 47, pp. 4789-4797.

Yu, X., Xiang, H., Long, Y., Zhao, N., Zhang, X. and Xu, J. (2010). Preparation of porous polyacrylonitrile fibers by electrospinning a ternary system of PAN/DMF/H_2O, *Materials Letters*, Vol. 64, pp. 2407-2409.

Yue, Q.Y., Gao, B.Y., Wang, Y., Zhang, H., Sun, X., Wang, S.G. and Gu, R.R. (2008). Synthesis of polyamine flocculants and their potential use in treating dye wastewater, *Journal of Hazardous Material*, Vol. 152, pp. 221-227.

References

Yun, K., Hogan Jr., C., Matsubayashi, Y., Kawabe, M., Iskandar, F. and Okuyama, K. (2007). Nanoparticle filtration by electrospun polymer fibers, *Chemical Engineering Science*, Vol. 62, pp. 4751-4759.

Yusof, N. and Ismail, A. (2012). Post spinning and pyrolysis processes of polyacrylonitrile (PAN)-based carbon fiber and activated carbon fiber: A review, *Journal of Analytical and Applied Pyrolysis*, Vol. 93, pp. 1-13.

Yuya, P.A., Wen, Y., Turner, J.A., Dzenis, Y.A. and Li, Z. (2007). Determination of Young's modulus of individual electrospun nanofibers by microcantilever vibration method, *Applied Physics Letters*, Vol. 90, pp. 1-3.

Zarkoob, S., Eby, R.K., Reneker, D.H., Hudson, S.D., Ertley, D. and Adams, W.W. (2004). Structure and morphology of electrospun silk nanofibres, *Polymer*, Vol. 11, pp. 3973-3977.

Zhang, A., Uchiyama, G. and Asakura, T. (2005a). pH Effect on the uranium adsorption from seawater by a macroporous fibrous polymeric material containing amidoxime chelating functional group, *Reactive & Functional Polymers*, Vol. 63, pp. 143-153.

Zhang, C., Li, X., Bian, X., Zheng, T. and Wang, C. (2012). Polyacrylonitrile/manganese acetate composite nanofibers and their catalysis performance on chromium (VI) reduction by oxalic acid, *Journal of Hazardous Materials*, Vol. 229-230, pp. 439-445.

Zhang, C., Yuan, X., Wu, L., Han, Y. and Sheng, J. (2005b). Study on morphology of electrospun poly (vinyl alcohol) mats, *European Polymer Journal*, Vol. 41, pp. 423-432.

Zhang, G., Song, X., Li, J., Ji, S. and Liu, Z. (2010a). Single-side hydrolysis of hollow fiber polyacrylonitrile membrane by an interfacial hydrolysis of a solvent-impregnated membrane, *Journal of Membrane Science*, Vol. 350, pp. 211-216.

References

Zhang, H., Nie, H., Li, S., White, C. and Zhu, L. (2009). Crosslinking of electrospun polyacrylonitrile/hydroxyethyl cellulose composite nanofibres, *Materials Letters*, Vol. 63, pp. 1199-1202.

Zhang, H., Nie, H., Yu, D., Wu, C., Zhang, Y., White, C. and Zhu, L. (2010b). Surface modification of electrospun polyacrylonitrile nanofiber towards developing an affinity membrane for bromelain adsorption, *Desalination*, Vol. 256, pp. 141-147.

Zhang, L., Luo, J., Menkhaus, T., Varadaraju, H., Sun, Y. and Fong, H. (2011). Antimicrobial nano-fibrous membranes developed from electrospun polyacrylonitrile nanofibres, *Journal of Membrane Science*, Vol. 369, pp. 499-505.

Zhang, P., Wang, Q., Zhang, J., Li, G. and Wei, Q. (2014). Preparation of Amidoxime-modified Polyacrylonitrile Nanofibers Immobilized with Laccase for Dye Degradation, *Fibers and Polymers*, Vol. 15, No.1, pp. 30-34.

Zhang, W., Li, Y., Zhu, S. and Wang, F. (2003a). Surface modification of TiO_2 film by iron doping using reactive magnetron sputtering, *Chemical Physics Letters*, Vol. 373, pp. 333–337.

Zhao, Y., He, X., Li, J., Gao, X. and Jia J. (2012). Porous CuO/SnO_2 composite nanofibers fabricated by electrospinning and their H_2S sensing properties, *Sensors and Actuator B: Chemical*, Vol. 165, pp. 82-87.

Zhao, Z., Li, J., Wang, D. and Chen, C. (2005). Nanofiltration membrane prepared from polyacrylonitrile ultrafiltration membrane by low-temperature plasma: 4. grafting of N-vinylpyrrolidone in aqueous solution, *Desalination*, Vol. 184, pp. 37-44.

Zhao, Z., Li, J., Zhang, D. and Chen, C. (2004). Nanofiltration membrane prepared from polyacrylonitrile ultrafiltration membrane by low-temperature plasma I. Graft of acrylic acid in gas, *Journal of Membrane Science*, Vol. 232, pp. 1-8.

Zhenbang, H., Yongchun, D. and Siming, D. (2010). Comparative study on the mechanical and thermal properties of two different modified PAN fibers and their Fe complexes, *Materials and Design*, Vol. 31, pp. 2784-2789.

References

Zheng, S.K., Xiang, G., Wang, T.M., Pan, F., Wang, C. and Hao, W.C. (2004). Photocatalytic activity studies of TiO_2 thin films prepared by r.f. magnetron reactive sputtering, *Vacuum*, Vol. 72, pp. 79–84.

Zhou, Y., Liang, Z. and Wang, Y. (2008). Decolorization and COD removal of secondary yeast wastewater effluents by coagulation using aluminum sulfate, *Desalination*, Vol. 225, pp. 301-311.

Zhu, Z., Feng, X. and Penlidis, A. (2007). Layer-by-layer self-assembled polyelectrolyte membranes for solvent dehydration by pervaporation, *Materials Science Engineering C*, Vol. 27, pp. 612-619.

Zimmerman, J., Mark, H.F. and Bikales, N.M. (1988). In: Encyclopedia of polymer science and engineering, New York: *Wiley*, Vol. 6, p. 802-839.

Zong, X., Kim, K., Fang, D., Ran, S., Hsiao, B.S. and Chu, B. (2002). Structure and process relationship of electrospun bioadsorbable nanofiber membrane, *Polymer*, Vol. 43, pp. 4403-4412.

Zuo, W.W., Zhu, M.F., Yang, W., Yu, H., Chen, Y.M. and Zhang, Y. (2005). Experimental study on relationship between jet instability and formation of beaded fibers during electrospinning, *Polymer Engineering and Science*, Vol. 45, pp. 704-709.

Zussman, E., Burman, M., Yarin, A.L., Khalfin, R. and Cohen, Y. (2006). Tensile deformation of electrospun nylon-6, 6 nanofibers, *Journal of Polymer Science Part B: Polymer Physics*, Vol. 44, pp. 1482-1489.

Zuwei, M., Kotaki, M. and Ramakrishna, S. (2005). Electrospun cellulose nanofiber as affinity membrane, *Journal of Membrane Science*, Vol. 265, pp. 115-123.
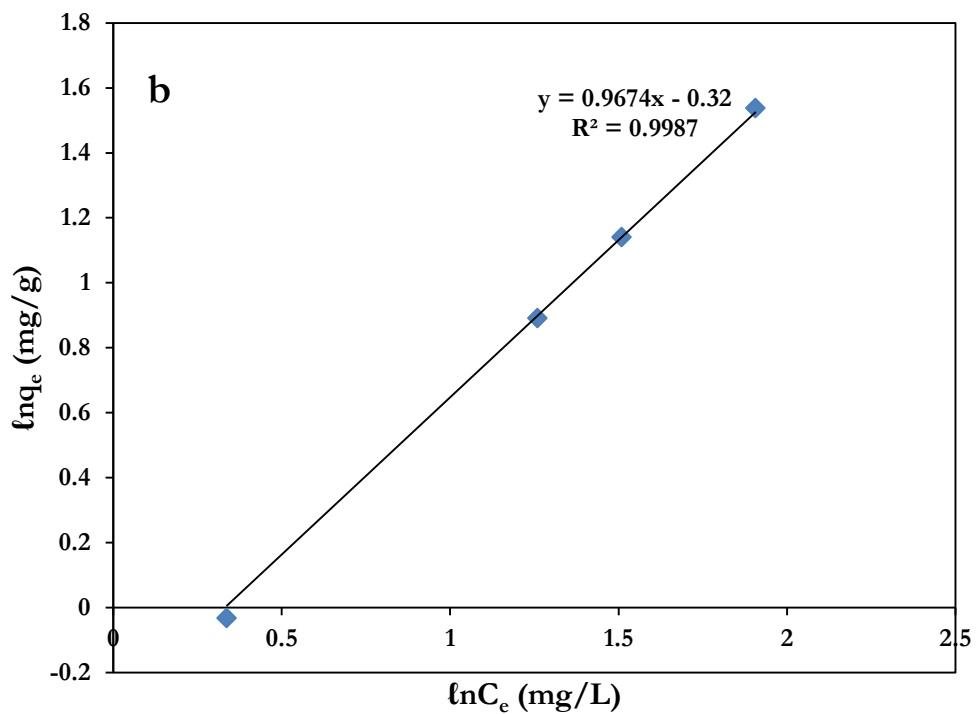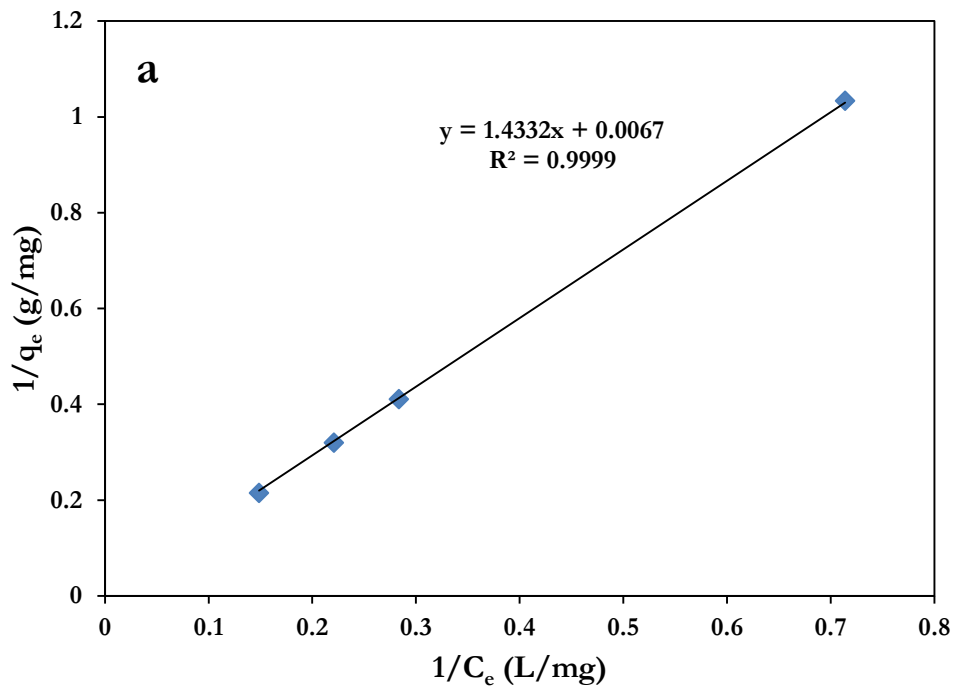
Appendix A: (a) Linearised graph of Langmuir isotherm and (b) linearised graph of Freundlich isotherm for the adsorption of RD onto PET-TMPAN.
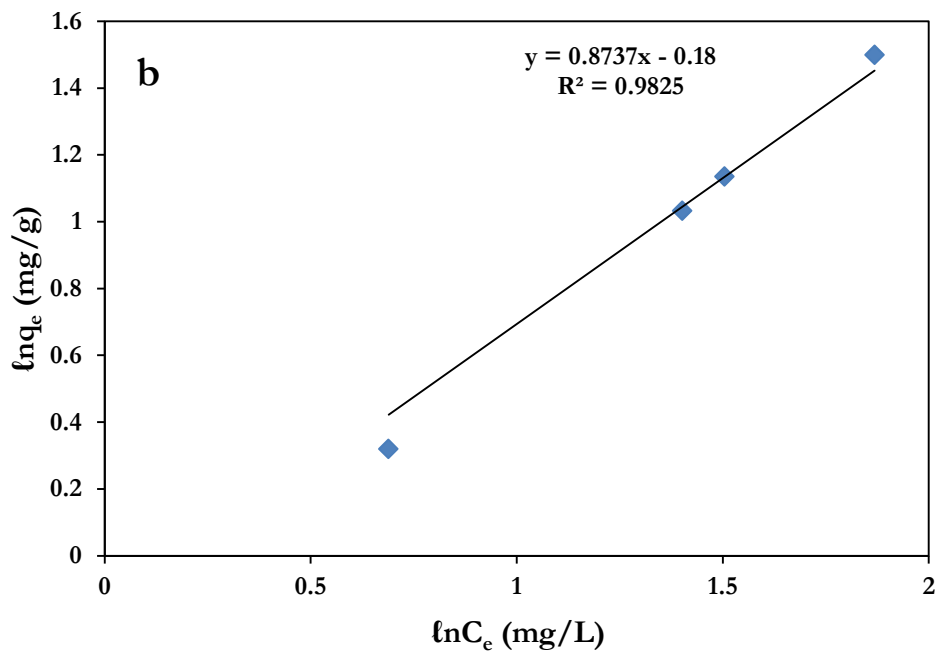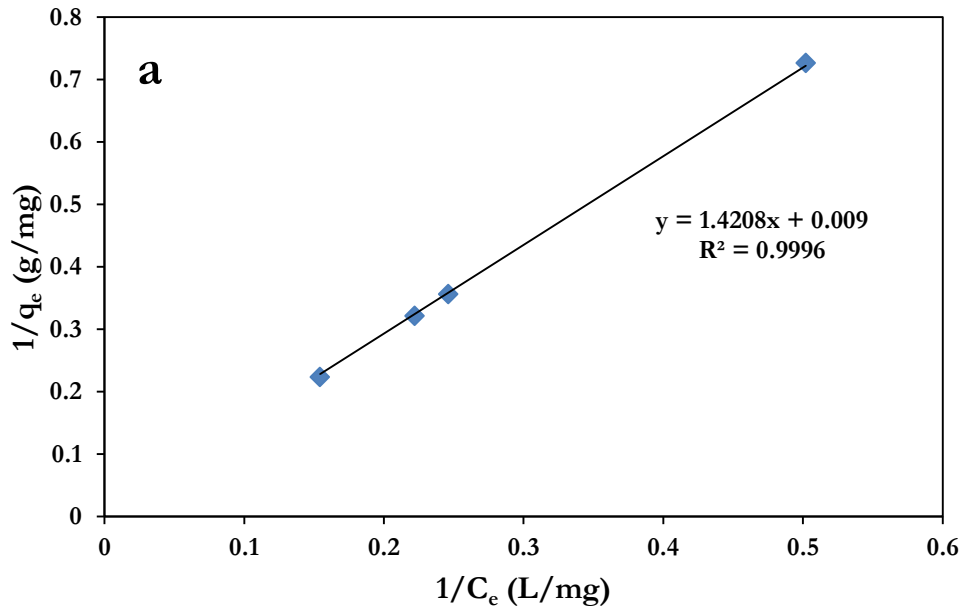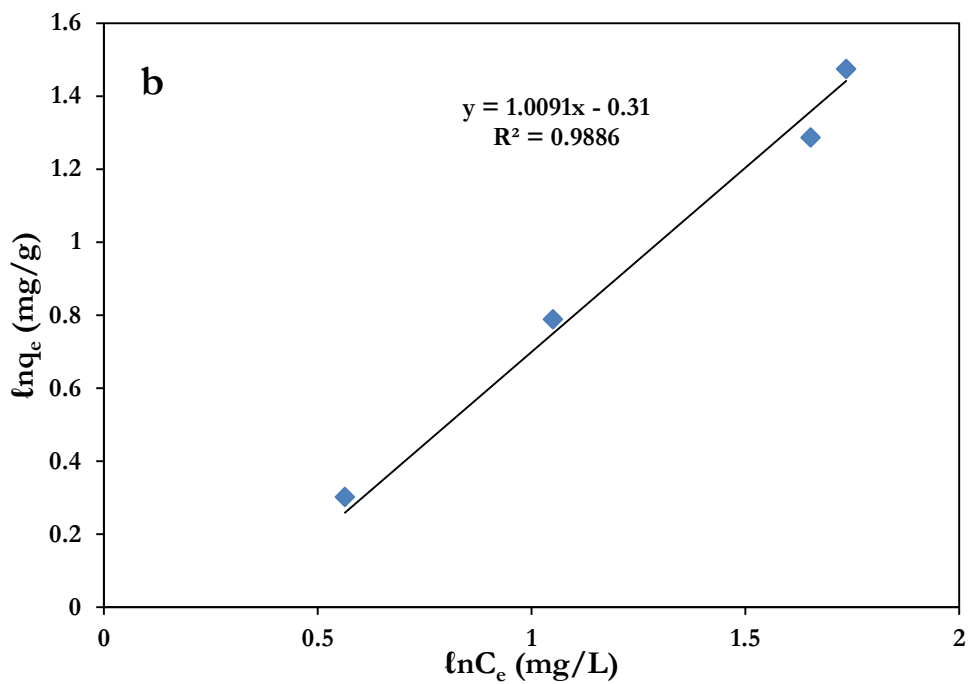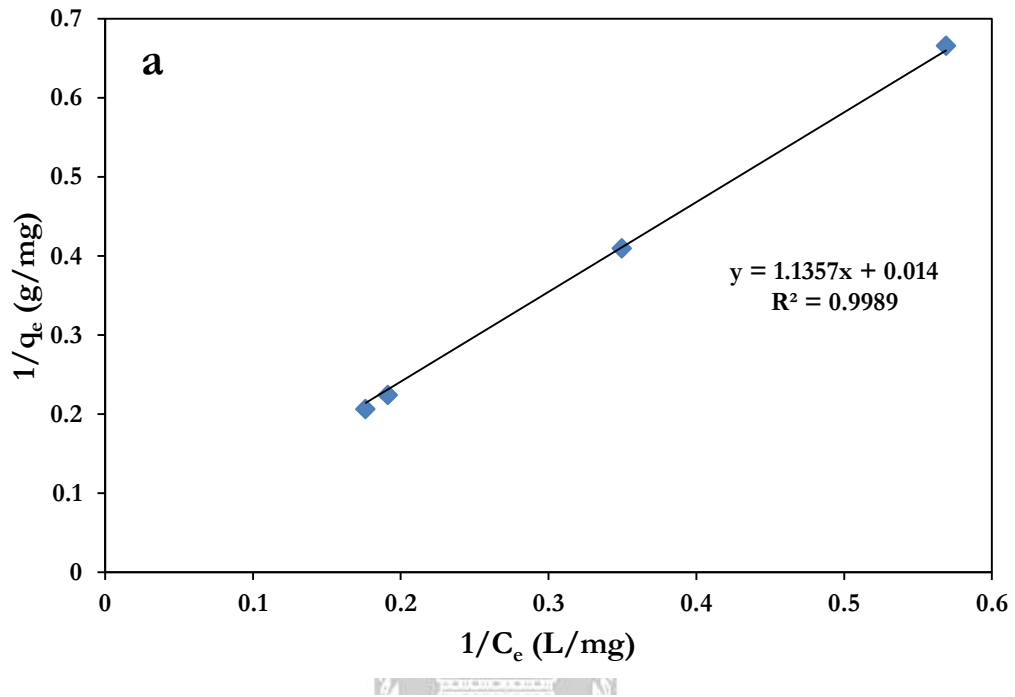
Appendix B: (a) Linearised graph of Langmuir isotherm and (b) linearised graph of Freundlich isotherm for the adsorption of RD onto PET-TMPA6.
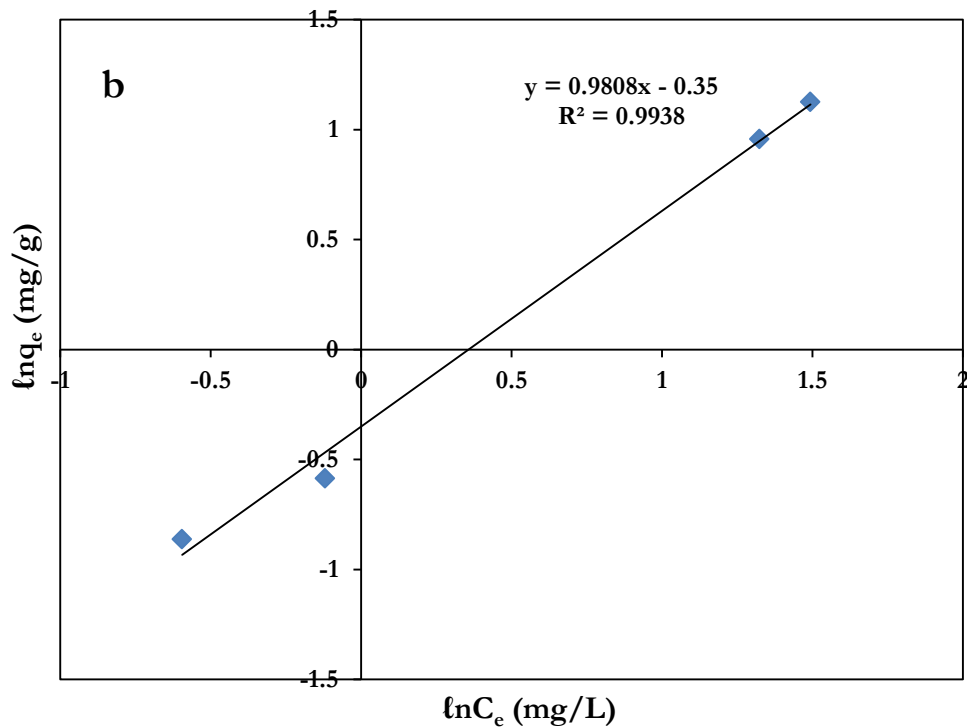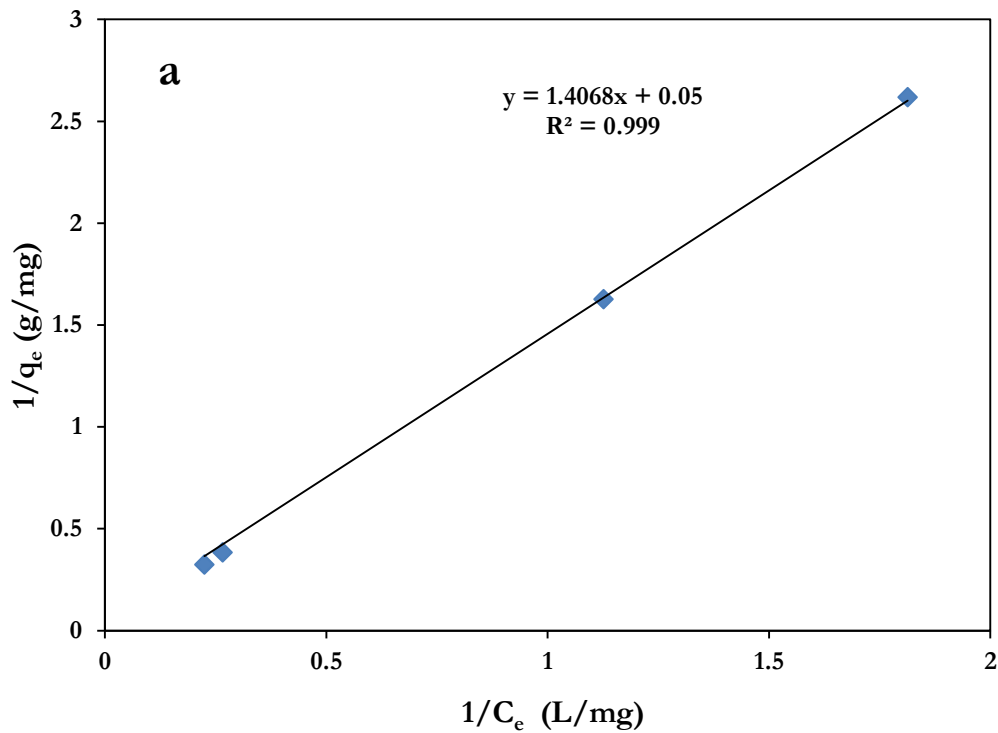
Appendices

Appendix C: (a) Linearised graph of Langmuir isotherm and (b) linearised graph of Freundlich isotherm for the adsorption of RD onto PAN-nfs.
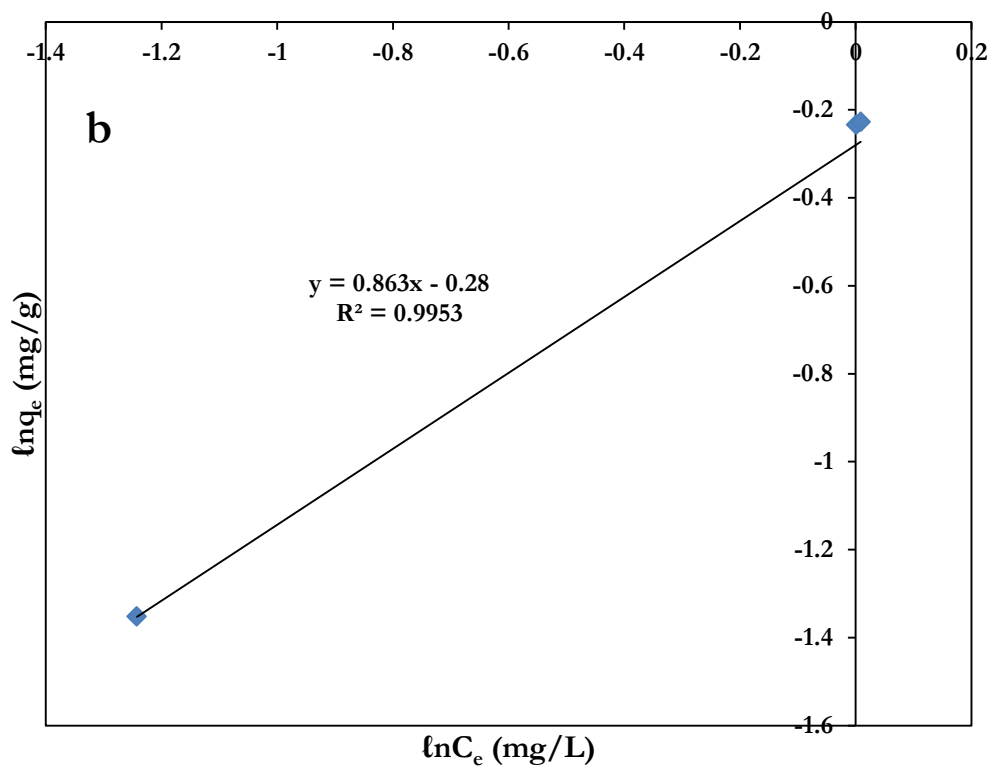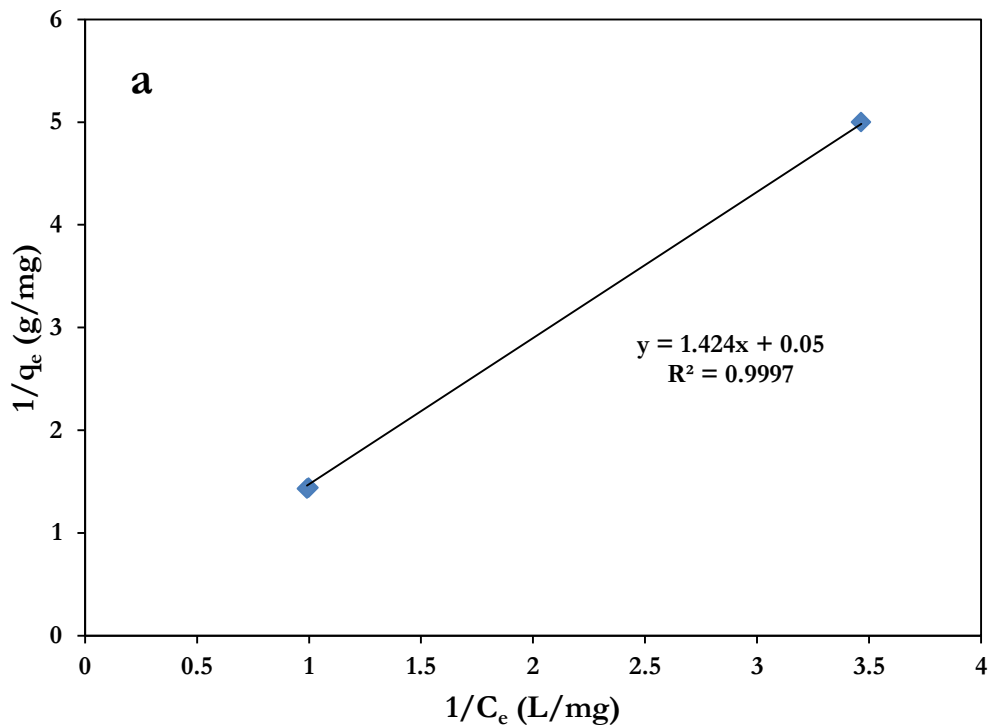
Appendix D: (a) Linearised graph of Langmuir isotherm and **(b)** linearised graph of Freundlich isotherm for the adsorption of RD onto PA6-nfs.

Appendix E: (a) Linearised graph of Langmuir isotherm and (b) linearised graph of Freundlich isotherm for the adsorption of RD onto PET-TM.

y = 1.424x + 0.05
R² = 0.9997

y = 0.863x - 0.28
R² = 0.9953

Appendices

Appendix F: (a) Linearised graph of Langmuir isotherm and (b) linearised graph of Freundlich isotherm for the adsorption of Pb^{2+} onto PAN-PyAMI.

250